# A Stochastic Framework for Soil-Structure Interaction and Constitutive Modelling

by

Julien Chaperon

A thesis

presented to the University of Waterloo

in fulfillment of the

thesis requirement for the degree of

Master of Applied Science

in

Civil Engineering

Waterloo, Ontario, Canada, 2019

# AUTHOR'S DECLARATION

I hereby declare that I am the sole author of this thesis. This is a true copy of the thesis, including any required final revisions, as accepted by examiners.

I understand that my thesis may be made electronically available to the public.

# ABSTRACT

A stochastic framework for soil-structure interaction and constitutive modelling is investigated in this thesis and developed to account for uncertainties in material properties and loading conditions.

The development of a one-dimensional Stochastic Finite Element Method (SFEM) for foundation problems is used as a starting point to describe the statistical behaviour of shallow and deep foundations at a local scale, where spatial variability exists. The Winkler model is adopted, and three sets of loading and boundary conditions are analyzed. A 1-D *Karhunen-Loeve* (KL) expansion is used to propagate the uncertainties in the material properties or loading conditions of each case. An exponential covariance structure is assumed for its applications in geophysics and in earthquake engineering. A different series representation known as the Polynomial Chaos expansion (PCE) is used to represent the random response since the covariance structure of the response is not known a priori. The method is combined with the Finite Element method (FEM) and used to solve three foundation problems. The accuracy and computational efficiency of the methodology for different orders of expansion is then compared with the *Monte Carlo* method.

Thereafter, a similar problem is tackled for random inputs with a 2-D random field. A 2-D *Karhunen-Loeve* expansion is used and incorporated in the analytical solution of a 2-parameter continuum pile. Because of the analytical nature of the solution, and due to the

non-linearity that arises as a result of the spectral decomposition of the soil properties, the representation of the response using the PCE is dropped to give way to an iterative solution. The results of the mean response for two examples taken from Basu and Salgado, 2008 are presented and compared to the deterministic solution.

The uncertainties in material properties and loading conditions are then propagated at the constitutive level. A new methodology, the Fokker-Plank-Kolmogorov equation (FPKE), is adopted. The FPKE transforms the stochastic continuity equation of non-linear constitutive laws to second order linear deterministic partial differential equations. The one-dimensional development of the FPKE is undertaken and validated for a linear elastic shear model and linear elastic-plastic *Von Mises* model. Finally, the FPKE is extended to a three-dimensional framework and validated for a 3-D linear elastic model.

# ACKNOWLEDGEMENTS

First and foremost, I would like to thank Professor Dipanjan Basu for his guidance and support in this research work. Such an incredible amount of faith is seldom put in fresh graduates and I am extremely grateful to have been the recipient of so much faith.

I thank Professor Zoran Miskovic, for teaching me the basic concepts of stochastic processes and helping me with my research work. I also thank Professor Edward Vsrcay, who has introduced me to functional analysis and helped me in the best of his capabilities. I would also like to acknowledge Professor Clifford Butcher's teaching and guidance. He taught me how to create user material subroutines and his course on advanced stress analysis has served as the foundation for the work on constitutive laws presented in this thesis.

I would also like to thank Ryan Barrage, a friend and an incredible Teachers Assistant, for his help with the mathematical proofs and theorems covered in this thesis. His insightful comments have proved really helpful.

I also appreciate the help of Chakshu Shah, my dearest friend and partner, who has helped me format this entire thesis. She has been with me since the beginning of this journey and is the one person who has truly witnessed me go through all the trials and tribulations of this Masters degree.

I would also like to thank my undergraduate friends from the Civil Class, and my friends from the University of Waterloo, Dubai Campus, they will recognize themselves. To my colleagues in the Civil Engineering Department and my brother, a special thank you.

Finally, I would like to thank my parents without whom I would not have made it this far. They have been a constant source of support, mental and of course financial. They are my biggest source of inspiration and are the reason I always strive for excellence. I dedicate this thesis to them with the hope that I can make them a little prouder than they already are.

# TABLE OF CONTENTS

# LIST OF FIGURES

# LIST OF TABLES

# CHAPTER 1.

# STOCHASTICITY IN SOIL-STRUCTURE SYSTEMS

## 1.1 Introduction

The literature pertaining to uncertainty in Geotechnical Engineering is one, which is filled with platitudes. Perhaps the most unforgiving among them is the fact that in order to fully ascertain the soil properties at a particular site, it would have to be excavated in its entirety. However, there would no longer be anything to rest a structure on (Fenton, 1999). The inherent variability that exists in soil properties is largely due to the unique attributes that every individual soil particle (for instance their shape, origin, or history) possesses. In addition to its intrinsic variability, two major sources that contribute to its heterogeneity are measurement errors and transformation uncertainties (Phoon and Kulhawy, 1999).

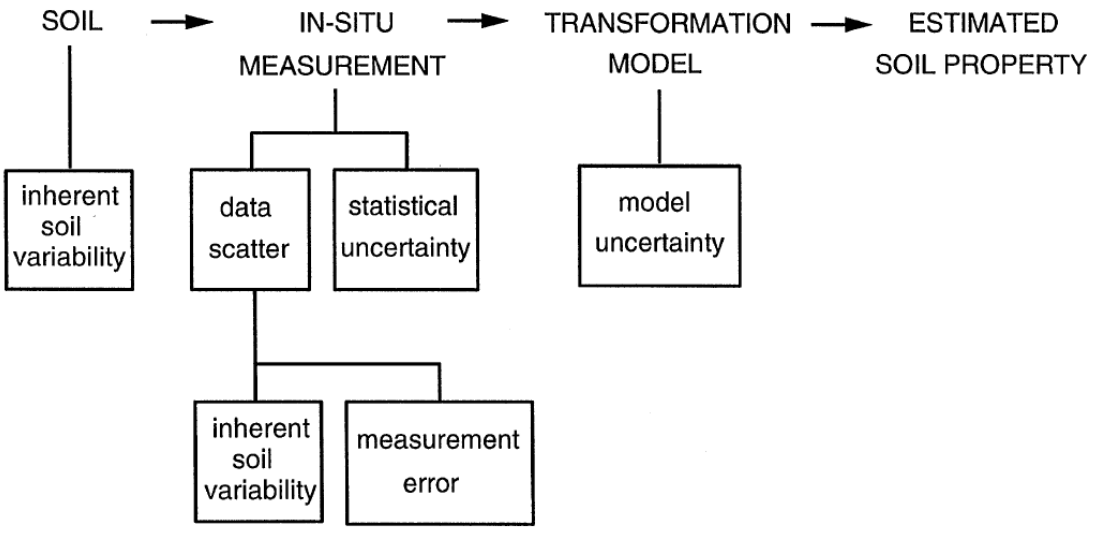


**Figure 1.1: Uncertainty in soil property estimates (source: Kulhawy 1992, p.101)**

Moreover, this heterogeneity presents itself at various scales of description. We can break down the scale of variation into two parts: A large scale where the soil properties are considered piece-wise homogeneous and a smaller scale, where the soil properties are spatially random (Sudret, 2014) The former depicts well-defined soil strata where within each layer the mean soil properties can be reported. In the second case, because of the unique attributes of each particle, additional information such as the correlation structure of the soil is required.

The limitations of deterministic designs given the scarcity of available data create the need for methods amenable to the intrinsic randomness of soil. More importantly, there is a need to cater for the scale effects mentioned earlier. Scaling effects include, but are not limited to, problems with aliasing. As a result, early studies on the problem of geotechnical variability were mostly focused on the characterization of soil heterogeneity and the modelling of random fields (Vanmarcke, 1983; Jaska et al., 1997). Since the development of mathematical techniques such as geostatistics and random field theory, the emphasis has shifted towards advanced numerical methods that simulate the highly nonlinear properties of soil and provide insights in the response of soil-structure systems.

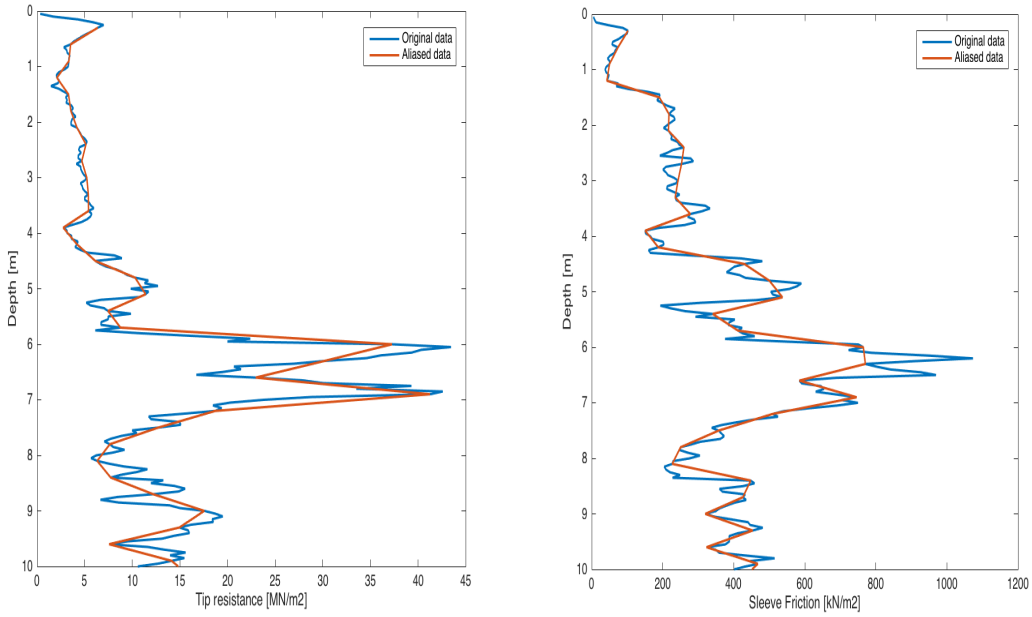


**Figure 1.2: Example of aliasing in CPT data. a) Tip resistance. b) Sleeve friction (Source: Data from USGS**

Geotechnical problems as we know them are for the most part presented as deterministic problems with the issue of uncertainty being circumvented by means of reliability factors. However in design, those factors give little if any information about the nature of the process being investigated. They are empirical in nature and thus fail to describe the fundamental behaviour of the system. With the increasing demand for sound reliability-based design, more realistic and robust probabilistic analyses of soil models are desirable.

## 1.2 Context of the Study

Beset with statistical uncertainties, the probabilistic treatment of soil has been the focus of researchers for a long time (Vanmarcke ,1977; Baecher and Ingra, 1981; Fenton, 1999; Rackwitz, 2001; Popescu, 2005). Recently, with the significant increase in computational

power and the advancement of numerical analysis, more realistic soil models, which take into account the spatial variability of the material, have received more attention. The development of various methods dealing with the intrinsic randomness of soil has also enabled the considerable progress of risk and reliability assessment of geotechnical projects. In this section, we will review the contributions of several researchers in identifying and estimating random soil properties along with the mathematical tools developed to propagate these uncertainties throughout different soil models. We refer to the task of estimating and identifying random properties as being of descriptive nature while referring to the propagation of uncertainties as being of inferential nature.

In the practice of geotechnical engineering, like in many other engineering disciplines, field tests and laboratory tests are essential for reliable and economical designs. However, there can only be so much data gathered to characterize a site. Therefore some degree of uncertainty will always subsist. The objective of descriptive techniques is to best describe the data available to minimize any risks of the design failing. A common descriptive technique for the analysis of a data set is the use of a regression with a best-fit polynomial to interpolate the data. However, a regressive analysis only provides the trend function and the residuals are often assumed uncorrelated. Such an assumption does not hold for geological data when field tests are carried out in the vicinity of each other.

In order to better understand the behaviour of the random soil properties, its correlation structure is required. This structure can be obtained from the autocovariance function of the residuals off the trend. A well-known method for the estimation of the autocovariance

function is the method of moments. The method of moments is quite straightforward but suffers from accuracy when the sample size is small. A lesser-known method is the Maximum Likelihood technique (ML) applied to field data (DeGroot & Baecher 1993). DeGroot and Baecher showed the method could estimate the spatial trends, measurement of noise and the autocovariance structure about spatial trends and be in good agreement with asymptotic theory (large sample theory) despite smaller sample sizes.

The idea that soil could be modeled as a random field paved the way to numerous researches, not only in the development of descriptive techniques but also in the development of inferential statistics to simulate soil properties at different sites. In fact, the work done to capture the many disparate sources of uncertainties fostered the research on inferential statistics for the purpose of extrapolating soil properties to sites, which lacked data for meaningful statistical analyses. The study on the characterization of geotechnical variability done by Phoon and Kulhawy (Phoon and Kulhawy 1999) formalized the output of descriptive techniques in the form of the coefficient of variation (COV) and scale of fluctuation, which provided a starting point for the propagation of uncertainties at different locations.

One very popular and powerful method that introduces uncertainty in soil models is the *Monte Carlo* simulation method. *Monte Carlo* simulations are based on repeated random sampling and the law of large numbers to solve any problem having a probabilistic interpretation (Wikipedia Monte Carlo method). While *Monte Carlo* simulations are typically used to model random variables, with the use of auto-regressive filters or local

average subdivision, they can effectively be used to model random fields (Griffiths et al., 2002; Fenton and Griffiths, 2002; Fenton and Vanmarcke, 1990). Although easy to use, the *Monte Carlo* method has one main downside, which is its computational efficiency (in particular for large-scale probabilistic simulations).

As we journey into the random field modelling of soil, we differentiate the methodologies developed with respect to the results that they produce (Sudret and Der Kiureghian 2000). We classify these methods in three categories, namely perturbation methods, structural reliability methods and stochastic finite element methods. In the first category, the aim is to obtain the first two statistical moments (mean, variance and correlation coefficients) of the response. This is accomplished by representing the properties of the soil using a Taylor series expansion about the mean values of the random functions (Baecher and Ingra, 1981; Phoon et al., 1990). In the second class of approaches, the focus is on evaluating the probability of failure of the system. A prescribed threshold known as a limit state function is defined based upon which failure can be interpreted. In geotechnical engineering, methods like FOSM (first-order second-moment methods) have been employed by researchers (Phoon et al., 1990; Mellah et al., 2000; Eloseily et al 2002). Finally the last category, stochastic finite element methods developed by Ghanem and Spanos in 1991 (Ghanem and Spanos, 1991) consist of representing the soil properties over a discretized domain using a series expansion similar to the perturbation method and expanding the response of the system in its random inputs onto a basis of the probability space known as the Polynomial Chaos basis.

Each of the methodologies described above have successfully been implemented in the probabilistic treatment of soil and have proven viable in their own respect. However, aside from the *Monte Carlo* method, only the use of the stochastic finite element method has been applied to nonlinear constitutive laws. Since it is well known that soil exhibits non-linear elastic and elasto-plastic behaviour, the need for a mathematical framework that accounts for this nonlinearity without the limitations of the *Monte Carlo* method was imperative. It was not until very recently with the work of Kallol (Kallol et al, 2007) that the latter could be incorporated in probabilistic models of soil. This was made possible through the contributions of M.L Kavvass who developed the Eulerian-Lagrangian Fokker-Plank equation for the ensemble average of hydrologic processes. (Kavvas 2003). It is the work of Ghanem and Spanos on the stochastic finite element method and that of Kallol and Kavvass on probabilistic constitutive rate equations that inspired the current research.

## 1.3 Motivation for the Study

The motivation for the work presented in this thesis is threefold: Firstly, there is a need for a better framework which accounts for the variability of soil properties and this can only be accomplished through the study of soil-structure interaction as a stochastic process and by taking the nonlinear behaviour of soil into consideration. Secondly, it is compelling to capitalize on the progress of computers' processing power while refraining from computationally expensive methods such as the *Monte Carlo* method. Finally, this research is motivated by the fundamental question of how impactful the elasto-plastic behaviour of soil is on the degree of uncertainty of the system.

## 1.4 Scope of the Study

This thesis is comprised of six chapters with the bulk of the author's technical (original) work spanning chapter three to five. The first two chapters serve as premise to the current research and the last chapter offers concluding remarks to the study undertaken in this thesis.

Chapter 1 provides a review of the literature by dissecting the work done by previous researchers in the identification and estimation of uncertainty in soil properties and their propagation in complex soil models. It also provides the motivation and the scope of the study.

Chapter 2 introduces the reader to the mathematical concepts and formulations used throughout this thesis. It contains a review of random variables and stochastic processes. It also introduces the reader to some basic continuum mechanics, and touches on the subject of elasticity and plasticity, which is used in subsequent sections of this thesis.

The third chapter entails the development of the stochastic finite element method in one-dimension with numerical examples in geotechnical problems. The chapter begins with the representation of random fields using the *Karhunen-Loeve* expansion and its incorporation in the classical finite element formulation. This is known as a spectral approach. In subsequent sections, the construction of the Polynomial Chaos basis is illustrated and applied to represent the response function.

The fourth chapter makes use of the *Karhunen-Loeve* expansion introduced in the third chapter, and extends it to a two-dimensional random field. The latter is then used in the stochastic analysis of a two-parameter continuum pile model.

Chapter 5 presents the derivation of the Eulerian-Lagrangian Fokker-Plank equation and the development of the probabilistic elastic-plastic constitutive equation in one and three dimensions respectively. Subsequent sections of the chapter provide numerical examples and validations for one-dimensional elastic and elastic-plastic constitutive models. A numerical example is also given for a three-dimension elastic constitutive model.

Chapter 6 probes into future studies and, as mentioned previously, provides a conclusion to the research undertaken.

# CHAPTER 2.

# FUNDAMENTALS

## 2.1 Introduction

In this chapter, the reader is introduced to the fundamental mathematical concepts and formulations used throughout this thesis. The materials presented in the subsequent sections of this chapter have been curated to offer the reader with the basic tools to understand and reproduce the results of analyses carried out in later chapters. This chapter is by no means complete in terms of the larger spectrum of mathematical theories involved in the current study. The concepts pertaining to random variables and stochastic processes depicted in this chapter were borrowed from the "Stochastic Processes in the Physical Sciences" course notes authored by Professor Zoran Miskovic (Miskobic, Z, 2015) and concepts relating to continuum mechanics and elastic-plastic materials were borrowed from the "Mechanics of Continua" course notes authored by Professor Michael Worswick (Worswick, M, n.d) with some excerpts obtained from Professor Cliff Butcher's lecture notes (Butcher, C, n.d).

## 2.2 Review of Random Variables

### 2.2.1 Basic definitions

We start by providing some basic definitions pertinent to the following section:

*Probabilistic experiment*: An experiment which is specified by its outcomes $\omega \in \Omega$ ($\Omega$ is the set of all possible outcomes) and by a distribution of probabilities $P\{\varepsilon\}$ of occurrence of various events (denoted by $\varepsilon$) $\varepsilon \subseteq \Omega$.

*Sample space*: The *sample space* $\Omega$ is the set of all possible outcomes.

*Probabilistic event*: An *event* ε is a realization of an outcome.

*Random variable*: A *random variable* (*rv*) is a function $X : \Omega \mapsto \mathbb{R}$ which assigns a numerical value $X(\omega)$ to each outcome $\omega$, i.e $X : \omega \mapsto X(\omega)$.

### 2.2.2 Probability distribution functions

Given a *rv X*, the *cumulative distribution function* (*cdf*) $F_X : \mathbb{R} \mapsto \mathbb{R}$ is defined by

$$F_X(x) = P\{X \leq x\} \tag{2.1}$$

where $\{X \leq x\}$ is an event such that random variable $X$ takes a value less than or equal to $x$. This event can be mathematically represented as $\{\omega \in \Omega : X(\omega) \leq x\}$.

The *cumulative distribution function* $F_X$ has the following properties:

- $F_X$ is a non-decreasing and bounded function of $x \in \mathbb{R}$, such that $F_X(-\infty) = 0$ and $F_x(+\infty) = 1$. This implies:

$$P\{x_1 \leq X \leq x_2\} = F_X(x_2) - F_X(x_1) \tag{2.2}$$

- $F_X(x)$ is continuous from the right, $F_X(x+0) = F_X(x)$, whereas from the left we have $F_X(x) - F_X(x-0) = P\{X = x\}$.
- $X$ can be discrete, continuous, or a combination of both. If $X$ is discrete, it has a *probability mass function* (*pmf*), as a result $F_X$ is a staircase function of $x$ with jumps $p_n$ at points $x_n$.

$$p_n = P\{X = x_n\} = F_X(x_n) - F_X(x_n - 0) \geq 0 \tag{2.3}$$

- If $X$ is continuous, then $F_X$ can be written as integral as follows:

$$F_X(x) = \int_{-\infty}^{x} f_X(x')dx' \tag{2.4}$$

Which brings us to the *probability density function (pdf)*, some integrable (in the Riemann sense) function on $\mathbb{R}$.

The *probability density function* $f_X$ has the following properties:

- If $f_X$ is piecewise continuous, then taking the limit $\Delta x \to 0^+$ gives:

$$P\{x \leq X \leq x + \Delta x\} \equiv F_X(x + \Delta x) - F_X(x) = \int_{x}^{x+\Delta x} f_X(x')dx' \tag{2.5}$$

- This implies that $F_X(x)$ is a continuous and piecewise differentiable function, such that

$$\frac{dF_X(x)}{dx} = f_X(x) \tag{2.6}$$

- When $X$ is a continuous *rv*, then $P\{X = x\} = 0$, and for infinitesimally small $dx$ we have:

$$P\{x \leq X \leq x + dx\} = f_X(x)dx \tag{2.7}$$

- Because of the properties of $F_X$, $f_X$ is non-negative ($f_X \geq 0$) and the following is true:

$$\int_{-\infty}^{+\infty} f_X(x)dx = 1 \tag{2.8}$$

We now want to know what happens to the *probability density function* $f_X$ when $X$ is a discrete *rv*. Since $F_X$ is not continuous when $X$ is discrete, $f_X$ does not exist in the sense of ordinary functions. However, we can use the *Stieltjes integral* to bypass this issue. Before proceeding, the reader is encouraged to refer to APPENDIX A for a brief review of the *Stieltjes Integral*.

- When $X$ is a discrete *rv*, then we can use *the Stieltjes integral* and write the *cdf* as follows:

$$F_X(x) = \int_{-\infty}^{x} dF_X(x') \tag{2.9}$$

In the above representation of the *cdf*, we can think of the integrand as being the product $f_X(x).dx$ in which case we would need to use the Dirac delta function to write $f_X(x)$ since it does not exist in the sense of ordinary functions.

$$f_X(x) = \sum_n p_n \delta(x - x_n) \tag{2.10}$$

The Dirac delta function also comes in handy to represent a sure, or deterministic, variable $X$ which takes a 'sharp" value $x_0$, such that

$$P\{X = x_0\} = 1 \tag{2.11}$$

so that we can express its *pdf* as:

$$f_X(x) = \delta(x - x_0) \tag{2.12}$$

For example we can represent the stress on a body whose material properties are random as a random process. However at time $t = 0$, before the body experiences any deformation (IC: Initial Condition), the stress is a "sure" variable and can be represented using the Dirac delta function. Alternatively, when dealing with numerical solutions, one can approximate the Dirac delta function using a normal distribution with infinitesimal variance such as to avoid dealing with infinity in the solution.

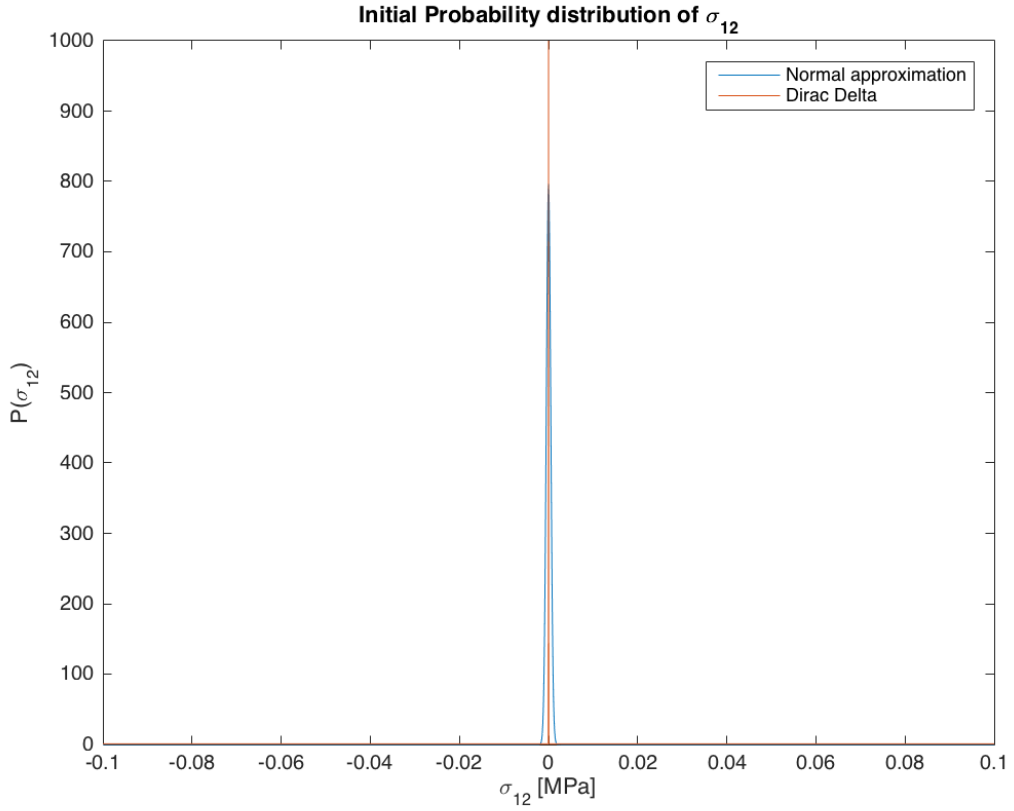


**Figure 2.1: PDF of Initial stress evaluated by the Dirac Delta and approximated by a Gaussian function**

### 2.2.3 Examples of random variables

In this section, we illustrate examples of random variables for discrete and continuous cases respectively by providing geotechnical engineering applications where applicable.

Examples of discrete rv:

1. Binomial

   For a *random variable* to be modeled as a Binomial *rv*, the following assumptions must hold:

   i. There can only be two outcomes (success or failure) from the random experiment (trial).
   ii. The probability of success is the same for each trial.
   iii. The outcome of each trial is independent from each other.
   iv. The number of trials to be conducted is finite.

   For an experiment with *probability of success p* in each trial, and *N* number of trials, the probability of getting n number of successes among *N* trials is given by the *probability mass function (pmf):*

$$p_n = \binom{N}{n} p^n (1-p)^{N-n} \qquad \text{for n = 0,1,…,N} \qquad (2.13)$$

   Example:

   The number of boulders encountered during a soil boring. There are only two outcomes, either there is a boulder or not, both independent from each other (Maity, R, n.d).

2. Geometric

For a geometric *rv*, the same assumptions for a Binomial distribution hold with the exception that this time we are looking at the probability that the first success occurs on the $n^{th}$ trial. This probability is given by the *pmf*:

$$p_n = (1-p)^{n-1} p \qquad \text{for n = 0,1,2,…,} \tag{2.14}$$

Example:

The probability that a structure fails due to the design earthquake intensity being exceeded for the first time on the third year after the structure is built.

3. Poisson

For a discrete *rv* to be modeled as a Poisson process, the following assumptions must hold true:

i. A probabilistic event can occur at any point in time or space.

ii. The number of occurrences of that event in a given time or space interval must be independent from another event in any other non-overlapping time or space intervals.

iii. The probability of occurrence of an event in a small interval $\Delta t$ is given by $\lambda \Delta t$, where $\lambda$ is defined as the mean rate of occurrence of the event.

iv. The probability of more than one occurrence of an event in the small interval $\Delta t$ is negligible.

The probability of n occurrences in time t is given by the *pmf*:

$$p_n = e^{-\lambda t}\frac{(\lambda t)^n}{n!} \qquad \text{for n = 0,1,2,…} \tag{2.15}$$

Example:

- The number of earthquakes within a given period
- The number of occurrences of boulders within a soil mass

Examples of continuous *rv*:

1. Uniform

   If a *random variable X* is uniformly distributed over the interval *[a, b]*, then it has *probability density function (pdf):*

$$f_X(x) = \begin{cases} \dfrac{1}{b-a}, & a \le x \le b \\ 0, & \textit{Otherwise} \end{cases} \tag{2.16}$$

   Uniform random variables are not common in geotechnical engineering but one can imagine an example where given an interval, the probability of occurrence within that interval is the same for any other occurrences similar to the results of a tossed die.

2. Exponential

   An exponential *rv* is characterized by the strictly positive parameter $\lambda$ *($\lambda$>0)* analogous to the mean rate occurrence $\lambda$ in a Poisson process. An exponentially distributed *rv X* has the following *pdf*:

$$f_X(t) = \begin{cases} \lambda e^{-\lambda t}, & t \ge 0 \\ 0, & \textit{Otherwise} \end{cases} \tag{2.17}$$

Example:

In geotechnical engineering as in other engineering disciplines, exponential rvs are extensively used to model the lifetimes of systems.

3. Normal (Gaussian)

Normal or Gaussian random variables are the most commonly encountered *rv*s in any discipline, thus earning their name. This is mostly a result of the central limit theorem, which establishes that when a large number of independent random variables are added, their properly normalized sum tends toward a normal distribution (Wikipedia Central Limit Theorem). A normal *rv* is characterized by its mean value, $\mu$ and standard deviation, $\sigma$ and has the following *pdf*:

$$f_X(x) = \frac{1}{\sigma\sqrt{2\pi}} \exp\left( -\frac{(x-\mu)^2}{2\sigma^2} \right) \qquad \text{for } x \in \mathbb{R} \tag{2.18}$$

Example:

Most of the examples presented in this thesis are based on the assumptions that our random variable is normally distributed. For instance, we can postulate that the shear modulus of a soil at a specific depth is normally distributed.

### 2.2.4 Multi-dimensional random variables

A multi-dimensional random variable $\boldsymbol{X}: \Omega \mapsto \mathbb{R}^N$, where $\boldsymbol{X} = (X_1, X_2, \ldots, X_N)$, is characterized by the joint *cdf* and *pdf*. The following equation relates the joint *cdf* and *pdf* of a two-dimensional *rv*:

$$F_{XY}(x,y) = P\{X \le x \cap Y \le y\} = \int_{-\infty}^{x+0} \int_{-\infty}^{y+0} f_{XY}(x',y')dy'dx' \tag{2.19}$$

if we now let $X$ and $Y$ be jointly continuous, we have the following:

$$f_{XY}(x,y) = \frac{\partial^2 F_{XY}(x,y)}{\partial x \partial y} \tag{2.20}$$

and

$$P\{x \le X \le x+dx \cap y \le Y \le y+dy\} = f_{XY}(x,y)dxdy \tag{2.21}$$

Let us now assume that $X$ and $Y$ are independent. Two *rv*'s $X$ and $Y$ are said to be independent *if and only if (iff)* $f_{XY}(x,y) = f_X(x)f_Y(y)$.

Alternatively, if $X$ and $Y$ are dependent, we require their conditional *cdf* and *pdf*. The conditional *cdf* is given by:

$$F_{X|Y}(x|y) = \frac{\partial F_{XY}(x,y)}{\partial y} \Big/ \frac{dF_Y(y)}{dy} \tag{2.22}$$

We know the definitions of $f_Y(y) = \frac{dF_Y(y)}{dy}$ and $f_{X|Y}(x|y) = \frac{\partial F_{X|Y}(x|y)}{\partial x}$. We can therefore differentiate the above equation with respect to $x$ and substitute our two definitions to obtain the so-called Bayes' relation:

$$f_{X|Y}(x|y) = \frac{f_{XY}(x,y)}{f_Y(y)} \tag{2.23}$$

which can be interpreted as:

$$P\{x \le X \le x+dx | Y = y\} = f_{X|Y}(x|y)dx \tag{2.24}$$

### 2.2.5 Statistical moments

The *average* or *expectation value* of a function $h: \mathbb{R} \mapsto \mathbb{R}$ of a *rv* $X$ (discrete or continuous) with *pdf f* where f employs the Dirac delta definition for the discrete case, is given by:

$$\left\langle h\left(X\right)\right\rangle \equiv E\left[h\left(X\right)\right] = \int_{-\infty}^{+\infty} h\left(x\right) f\left(x\right) dx \tag{2.25}$$

The above definition is also known as the first moment of a function of a random variable. Moments are used in various fields of mathematics as a way to measure the shape of a function. In mechanics, the reader should be familiar with the zeroth moment of a general body or its total mass. The ratio of the first moment of a general body to its total mass on the other hand gives the center of mass, and the second moment is the rotational inertia.

In statistics, the first moment of a random variable as mentioned before is the mean. The second moment is the variance and the third and fourth moments are the skewness and kurtosis respectively. We represent the $m$-th moment of a random variable $X$ as follows:

$$\left\langle X^m \right\rangle \equiv \mu_m = \int_{-\infty}^{+\infty} \left(x - c\right)^m f\left(x\right) dx \tag{2.26}$$

In the above expression, $c$ is a value about which the moment is calculated[1].

We now define the variance of $X$ as:

[1] It should be noted that statistical moments can be calculated about different values c, and in statistics we are mostly interested in raw moments (c = 0) and central moments (c = <X>). The mean of X is the first raw moment, and the variance of X is the second central moment. Skewness and kurtosis are also central moments but normalized with respect to the standard deviation raised to the power of their respective moment order ($\sigma^m$).

$$\sigma^2 \equiv Var\left[X\right] \equiv \left\langle \left\langle X^2 \right\rangle \right\rangle = \left\langle \left(X - \left\langle X \right\rangle\right)^2 \right\rangle = \left\langle X^2 \right\rangle - \left\langle X \right\rangle^2 = \mu_2 - \mu^2 \tag{2.27}$$

and the standard deviation as:

$$\sigma = \sqrt{Var\left[X\right]} \tag{2.28}$$

In addition, some useful properties of the above operations are provided below:

1. $E\left[X+Y\right] = E\left[X\right] + E\left[Y\right] \equiv \left\langle X+Y \right\rangle = \left\langle X \right\rangle + \left\langle Y \right\rangle$ (2.29-a)
2. $E\left[cX\right] = c \cdot E\left[X\right] \equiv \left\langle cX \right\rangle = c\left\langle X \right\rangle$ c = const (2.29-b)
3. $Var\left[X+c\right] = Var\left[X\right]$ c = const (2.29-c)
4. $Var\left[cX\right] = c^2 Var\left[X\right]$ c = const (2.29-d)

Of interest also is the *moment generating function*[2], $G : \mathbb{R} \mapsto \mathbb{R}$ of the *rv X*. The moment generating function, as suggested by its name is used to obtain higher order moments. *G* is defined by:

$$G\left(k\right) = \left\langle \exp\left(ikX\right) \right\rangle \tag{2.30}$$

and can be expanded using an infinite series as follows:

$$G\left(k\right) = \sum_{m=0}^{+\infty} \frac{\left(ik\right)^m}{m!} \mu_m \tag{2.31}$$

As a result, the *m*-th statistical moment can be found using the following equation:

---

[2] G(k) is the fourier transform of the pdf f(x), so that : $f\left(x\right) = \left(2\pi\right)^{-1} \int_{-\infty}^{+\infty} e^{-ikx} G\left(k\right) dk$

$$\mu_m = i^{-m} \left. \frac{d^m G(k)}{dk^m} \right|_{k=0} \tag{2.32}$$

An alternative to moments in statistics is *cumulants* $\kappa_m$. One can use moments to determine *cumulants* or vice versa. Once more the *moment generating function, G* is used to define the *cumulants* $\kappa_m$ of *X* via the expansion:

$$\ln G(k) = \sum_{m=1}^{+\infty} \frac{(ik)^m}{m!} \kappa_m \tag{2.33}$$

For a multi-dimensional *rv* $\boldsymbol{X} = (X_1, X_{2,\ldots,} X_N)$, the *moment generating function, G* is given by:

$$G_N(\underset{\sim}{k}) \equiv G_N(k_1,\ldots,k_N) = \left\langle \exp\left(i\underset{\sim}{k}\underset{\sim}{X}\right) \right\rangle = \int \ldots \int e^{i\underset{\sim}{k}\underset{\sim}{x}} f_N(\underset{\sim}{x}) d^N x \tag{2.34}$$

where the *pdf* $f_N(\boldsymbol{x}) \equiv f_N(x_1,\ldots,x_N)$.

We can then find the first and second moments of $\boldsymbol{X}$ as follows:

$$\langle X_n \rangle = \int \ldots \int x_n f_N(\underset{\sim}{x}) d^N \underset{\sim}{x} = -i \left. \frac{\partial G_N(\underset{\sim}{k})}{\partial k_n} \right|_{\underset{\sim}{k}=0} \tag{2.35-a}$$

$$\langle X_m X_n \rangle = \int \ldots \int x_m x_n f_N(\underset{\sim}{x}) d^N \underset{\sim}{x} = -\left. \frac{\partial^2 G_N(\underset{\sim}{k})}{\partial k_m \partial k_n} \right|_{\underset{\sim}{k}=0} \quad \text{for } 1 \le \text{m, n} \le \text{N} \tag{2.35-b}$$

$$\langle\langle X_m X_n \rangle\rangle \equiv \langle X_m, X_n \rangle \equiv Cov[X_m, X_n] = \langle (X_m - \langle X_m \rangle)(X_n - \langle X_n \rangle) \rangle = \langle X_m X_n \rangle - \langle X_m \rangle \langle X_n \rangle \tag{2.35-c}$$

where the second central moment (last definition above) form the *covariance* matrix.

With the above definitions, we can now talk about correlation and independence. We say that two *rv*'s are *uncorrelated iff* $\langle\langle XY \rangle\rangle = 0$. It then naturally follows that two *rv*'s that are *uncorrelated* are *independent*. The assumption that *rv*'s or stochastic processes are *independent* will be prominent in this thesis since independent *rv*'s have neat properties which simplify a lot of the algebraic manipulations performed in later sections. Below are some useful properties of independent *rv*'s.

1. $E[XY] = E[X]E[Y] \equiv \langle XY \rangle = \langle X \rangle \langle Y \rangle$ (2.36-a)

2. $Var[X+Y] = Var[X] + Var[Y]$ (2.36-b)

Let the *rv Y* be the sum of *N* mutually uncorrelated and independent *rv*'s $X_n$, then

3. $\langle Y \rangle = \sum_{n=1}^{N} \langle X_n \rangle$ (2.36-c)

4. $\langle\langle Y^2 \rangle\rangle = \sum_{n=1}^{N} \langle\langle X_n^2 \rangle\rangle$ (2.36-d)

5. $G_Y(k) = \prod_{n=1}^{N} G_{X_n}(k)$ (2.36-e)

## 2.3 Basic Concepts of Stochastic Processes

### 2.3.1 Basic definitions

In line with the previous section, we start with some basic definitions to ease the reader into the topic.

<u>*Stochastic process*</u>: A *stochastic process* (*sp*) is a function of two variables *X(ω,t),* where *ω* is the outcome of a *probabilistic experiment* $\omega \in \Omega$, and *t* is a variable of known value $t \in \mathbb{R}$, often time or space.

A *sp* can also be thought of as an *ensemble or family* of functions $X_\omega(t)$, one for each *outcome ω*. In a way, a *sp* is a collection of *rv*'s which fall in a range known as states of the *sp* dictated by the distribution of probabilities $P\{\omega \in \varepsilon\}$ for various events $\varepsilon \subseteq \Omega$. For instance, we can think of the diameter of a sewing thread along its length to be a sp due to very small fluctuations or errors made by the machine as it spins the fibers into a single yarn. In the example of the thread, the random variable is the diameter, and the "sure" variable is the length along which the diameter is random.

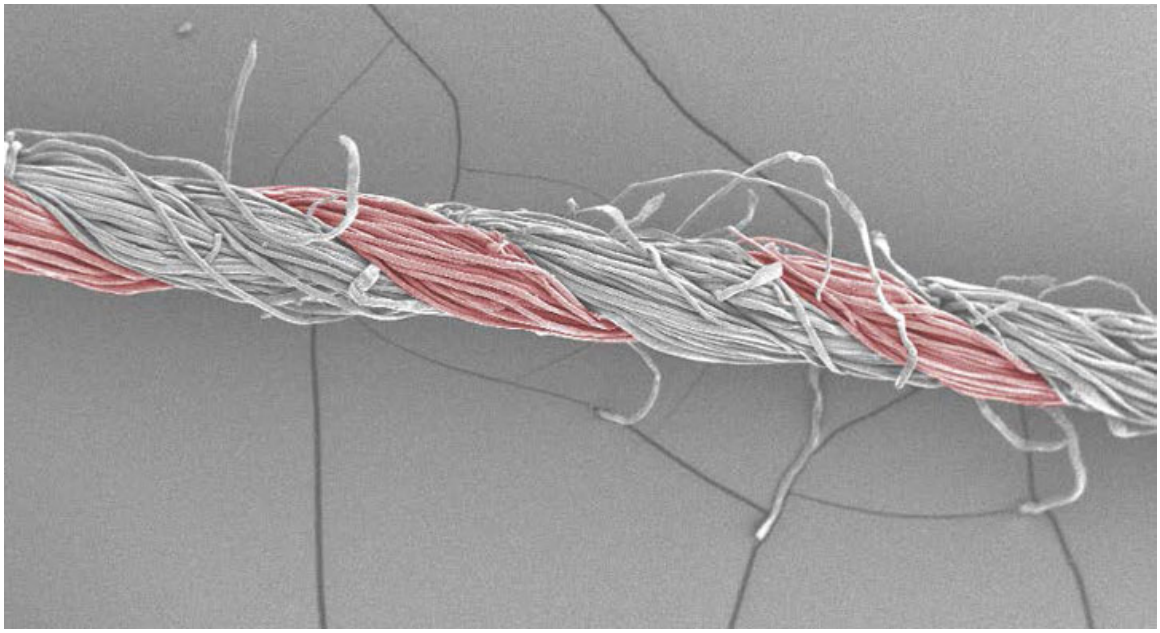

**Figure 2.2: Electron microscope image of cotton sewing thread (Source: P Warren, R Ball, and R Goldstein/Phys. Rec. Lett.)**

In soil, we can conceptualize some properties such as the shear modulus to be a stochastic process. This is based on the assumption that the shear modulus is spatially random.

*Statistical ensemble:* A *statistical ensemble (ensemble*) can be thought of as the set of all possible states that a system could be in. In other words, a statistical ensemble is a probability distribution for the state of the system (Gibbs, J, 2015).

*Realization*: A *realization* of a stochastic process is the function $X_\omega(t)$ when $\omega$ is fixed. It is also known as a *sample function*.

### 2.3.2 Probability distributions

Similar to a *random variable*, we define the *cdf* of a *sp X(t)* as:

$$F_X\left(x,t\right)=P\left\{X\left(t\right)\leq x\right\} \tag{2.37}$$

where the only difference with a *rv* is the added dimension of the "sure" variable *t*.

The relationship between the *cdf* of a continuous-state *sp* and its *pdf* is given by:

$$F_X\left(x,t\right)=\int_{-\infty}^{x+0} f_X\left(x',t\right)dx' \tag{2.38}$$

We can now define the *pdf* of continuous-state or discrete-state *sp* as:

$$f_X\left(x,t\right)=\frac{\partial F_X\left(x,t\right)}{\partial x} \tag{2.39}$$

It goes without saying that in the case of a discrete-state *sp*, special care should be taken by using the Dirac delta function. The Dirac delta function can once more be used to

represent a deterministic *sp* i.e a known function of t for example $X(t) = \phi(t)$. Then the *pdf* reads:

$$f_X\left(x,t\right)=\delta\left(x-\phi\left(t\right)\right) \tag{2.40}$$

Let us now introduce multi-dimensional *sp*'s. The n[th] order *cdf* of $X(t)$ with $t \in I$ is defined by the joint *cdf* of *n rv*'s $X(t_1), X(t_2),\ldots,X(t_n)$ where *t* is chosen arbitrarily from a *closed interval I*.

$$F_n\left(x_1,t_1;x_2,t_2;\ldots;x_n,t_n\right)=P\left\{X\left(t_1\right)\le x_1,X\left(t_2\right)\le x_2,\ldots,X\left(t_n\right)\le x_n\right\} \tag{2.41}$$

The $n^{th}$ order pdf of the multi-dimensional *sp* $X(t)$ is defined by:

$$f_n\left(x_1,t_1;x_2,t_2;\ldots;x_n,t_n\right)=\frac{\partial^n F_n\left(x_1,t_1;x_2,t_2;\ldots;x_n,t_n\right)}{\partial x_1\,\partial x_2\ldots\partial x_n}\ge 0 \tag{2.42}$$

In addition to the properties of the *cdf* and *pdf* of a *rv*, we note that the *cdf* and *pdf* of multi-dimensional *sp*'s satisfy *symmetry* and *compatibility* conditions.

For the *symmetry* condition, $F_n$ and $f_n$ do not change when two pairs $(x_k, t_k)$ and $(x_l, t_l)$ are interchanged. For example:

$$F_2\left(x_1,t_1;x_2,t_2\right)=F_2\left(x_2,t_2;x_1,t_1\right) \tag{2.43}$$

For the compatibility condition, when the *sp* takes on infinite values, we have the following *cdf*:

$$F_n\left(x_1,t_1;x_2,t_2;\ldots;x_{n-1},t_{n-1};+\infty,t_n\right)=F_{n-1}\left(x_1,t_1;x_2,t_2;\ldots;x_{n-1},t_{n-1}\right) \tag{2.44}$$

such that the *pdf* satisfies *compatibility* as follows:

$$\int_{-\infty}^{+\infty} f_n\left(x_1,t_1;x_2,t_2;\ldots;x_{n-1},t_{n-1};x_n,t_n\right)dx_n = f_{n-1}\left(x_1,t_1;x_2,t_2;\ldots;x_{n-1},t_{n-1}\right) \tag{2.45}$$

### 2.3.3 Statistical moments

We will now define the moments of a *sp X(t)*.

- The mean of a *sp* is given by:

$$\mu(t) \equiv \left\langle X(t) \right\rangle = \int_{-\infty}^{+\infty} x f_1(x,t)\, dx \tag{2.46}$$

- The *auto-correlation function* of a *sp* is given by:

$$B(t_1,t_2) \equiv \left\langle X(t_1) X(t_2) \right\rangle = \int_{-\infty}^{+\infty}\int_{-\infty}^{+\infty} x_1 x_2 f_2(x_1,t_1;x_2,t_2)\, dx_1\, dx_2 \tag{2.47}$$

- The *auto-covariance function* of a *sp* is given by:

$$C(t_1,t_2) \equiv \left\langle \left\langle X(t_1) X(t_2) \right\rangle \right\rangle = \left\langle \left[ X(t_1) - \mu(t_1) \right] \left[ X(t_2) - \mu(t_2) \right] \right\rangle = B(t_1,t_2) - \mu(t_1)\mu(t_2) \tag{2.48}$$

### 2.3.4 Example of stochastic processes

Here we provide some examples of stochastic processes with an emphasis on continuous-state processes only. However before proceeding, a few more definitions are in order.

<u>*Gaussian process*</u>: A *sp* is called a Gaussian or normal *sp*, if its moment generating function for a finite set of points $\{t_1, t_2, \ldots, t_n\}$ and *rv*'s $X(t_1), X(t_2), \ldots, X(t_n)$ is given by:

$$G_n(k_1,t_1;\ldots;k_n,t_n) = \exp\left( i\underset{\sim}{k}^T \underset{\sim}{\bar{x}} - \frac{1}{2}\underset{\sim}{k}^T C \underset{\sim}{k} \right) \tag{2.49}$$

where $\boldsymbol{k}^T = (k_1,\ldots,k_n)$, $\underset{\sim}{\bar{x}}^T = \left( \left\langle X(t_1) \right\rangle, \ldots, \left\langle X(t_n) \right\rangle \right)$ and elements of covariance matrix $C$,

$c_{mn} = \left\langle \left\langle X(t_m) X(t_n) \right\rangle \right\rangle$ all depend on $t_1, t_2, \ldots, t_n$.

<u>*Stationary process*</u>: There are two kinds of stationary processes:

1. <u>*Strict-sense stationary*</u>: A *sp* is strict-sense stationary *iff*

   $F_n\left(x_1,t_1+\tau;x_2,t_2+\tau;\ldots;x_n,t_n+\tau\right)=F_n\left(x_1,t_1;x_2,t_2;\ldots;x_n,t_n\right)$ for any *n,* $\tau$ and set of *t*.

   This implies that $f_1$ is independent of time i.e $f_1(x_1,t_1) = f_1(x_1)$ and $f_2$ depends on the time difference i.e $f_2(x_1,t_1;x_2,t_2)$.

2. <u>*Wide-sense stationary*</u>: A *sp* is called wide-sense stationary *iff* $\mu(t) = \mu = const$ and $B(t_1, t_2) = B(t_2 - t_1) = B(t_1 - t_2)$.

<u>*Homogeneous process*</u>: A non-stationary *sp* can be one of two homogeneous processes or both simultaneously:

1. <u>*Spatially homogeneous*</u>: The transition probability[3] depends on the difference between $x_1$ and $x_2$.

$$f_{1|1}\left(x_2,t_2\middle|x_1,t_1\right)=f_{1|1}\left(x_2-x_1,t_2\middle|0,t_1\right) \tag{2.50}$$

2. <u>*Temporally homogeneous*</u>: The transition probability depends on the time difference.

$$f_{1|1}\left(x_2,t_2\middle|x_1,t_1\right)=f_{1|1}\left(x_2,t_2-t_1\middle|x_1,0\right) \quad \text{for } t_2 > t_1 \tag{2.51}$$

   If a *sp* is homogeneous in time and in space, the transition probability can be written as:

$$f_{1|1}\left(x_2,t_2\middle|x_1,t_1\right)=f_{1|1}\left(x_2-x_1,t_2-t_1\middle|0,0\right) \qquad \text{for } t_2 > t_1 \tag{2.52}$$

---

[3] The transition probability is another name given to the conditional pdf $f_{1|1}(x_2,t_2|x_1,t_1)$ of a sp X(t) which can be obtained using the Bayesian relation: $f_{1|1}\left(x_2,t_2\middle|x_1,t_1\right)=\dfrac{f_2\left(x_2,t_2;x_1,t_1\right)}{f_1\left(x_1,t_1\right)}$

In passing, a non-trivial concept, which should be mentioned, is the *ergodic theorem*. The *ergodic* theorem tells us that the mean $\mu$ of a stationary process can in fact be obtained from only one realization of $X(\omega,t)$ provided that $X(\omega,t)$ is available for a sufficiently long interval of time . This concept is of capital importance in later sections as we assume that soil properties modeled as *sp*'s are in fact *ergodic*. It should be noted nonetheless that this assumption has not formally been checked since the procedures involved are impractical for general *sp*'s.

Stochastic processes can also be classified based on memory

*a)* *Purely random processes*: Purely random processes hold no memory such that their *pdf*'s read:

$$f_n\left(x_1,t_1;x_2,t_2;\ldots;x_n,t_n\right)=f_1\left(x_1,t_1\right)f_1\left(x_2,t_2\right)\ldots f\left(x_n,t_n\right) \qquad (2.53\text{-a})$$

b) *Markov process*: Markov processes depend on the one occurrence at $t_{n-1}$ of the *sp* prior to the present time such that the entire process is defined by $f_1$ and $f_{1|1}$

$$f_{1|n-1}\left(x_n,t_n\middle|x_{n-1},t_{n-1};\ldots;x_1,t_1\right)=f_{1|1}\left(x_n,t_n\middle|x_{n-1},t_{n-1}\right) \qquad (2.53\text{-b})$$

c) *Processes with stationary-independent increments (sii)*: These processes belong to a special class of Markovian processes in which the increments of a *sp* depend on the corresponding time difference.

$$X\left(t_i\right)-X\left(t_{i-1}\right)=\Delta X\left(t_i-t_{i-1}\right) \qquad (2.53\text{-c})$$

*SP*'s with *sii* are homogeneous in both time and space.

We are now ready to look at examples of *continuous-state sp*'s.

a) *Wiener process* (*Wp*) also known as *Wiener-Lévy process*, or *Diffusion process*, or *Brownian motion*.

An *sp* is considered a *Wp iff* the following holds true:

i. X(0) = 0

ii. It has sii

iii. For every t > 0, X(t) ~ N(0,1) i.e X(t) is a normal (Gaussian) *rv* with zero mean and variance t, with first-order *pdf*:

$$f_1\left(x,t\right)=\frac{1}{\sqrt{2\pi t}}e^{-\frac{x^2}{2t}} \tag{2.54}$$

Because a *Wp* has *sii*, it is non-stationary and is homogeneous in time and space. Also noteworthy, is the fact that a *Wp* is Markovian.

b) *Ornstein-Uhlenbeck process* (*OUp*)

A *OUp* has the following properties:

i. It is stationary

ii. It is Markovian

iii. It is Gaussian

The *OUp* is completely defined by the first-order *pdf*:

$$f_1\left(x\right)=\frac{1}{\sqrt{2\pi}}e^{-\frac{x^2}{2}} \tag{2.55-a}$$

and the transition probability for $t_2 > t_1$:

$$f_{1|1}\left(x_2,t_2\middle|x_1,t_1\right)=f_{1|1}\left(x_2,t_2-t_1\middle|x_1,0\right)=\frac{1}{\sqrt{2\pi\left(1-e^{-2\left(t_2-t_1\right)}\right)}}e^{\left[\frac{\left(x_2-x_1e^{-\left(t_2-t_1\right)}\right)^2}{2\left(1-e^{-2\left(t_2-t_1\right)}\right)}\right]} \tag{2.55-b}$$

## 2.4 Rudiments of Stochastic Calculus

### 2.4.1 Convergence of a random sequence

Consider a *random sequence (rs)* $\{X_n\}$, let it be a converging sequence, then we can say that $\{X_n\}$ converges in the *mean square* (*ms*) or it converges *in probability* (*ip*).

Mean-square converging: We say that the *rs* $\{X_n\}$ converges in the *ms* to $X$ if

$$\lim_{n\to\infty}\left\langle \left(X - X_n\right)^2 \right\rangle = 0 \tag{2.56}$$

In probability converging: We say that the *rs* $\{X_n\}$ converges *ip* to $X$ if

$$\lim_{n\to\infty} P\left\{\left|X - X_n\right| \geq \varepsilon\right\} = 0 \tag{2.57}$$

holds for any $\varepsilon > 0$, no matter how small.

A noteworthy implication of the *ms* convergence is the *ip* convergence, which is a result of a theorem that can be proven using the *Chebyshev's inequality* (not provided here).

### 2.4.2 Continuity

The *sp X(t)* is said to be ms continuous if

$$\lim_{h\to 0}\left\langle \left[X\left(t+h\right) - X\left(t\right)\right]^2 \right\rangle = 0 \tag{2.58}$$

Another way to check if *X(t)* is *ms* continuous is through the following theorem:

*If the auto-correlation function $B(t_1,t_2)$ is continuous (in the ordinary sense) at $(t_1,t_2) = (t,t)$, then the sp is ms continuous at t. The proof of the theorem follows from:*

$$\left\langle \left[ X\left(t+h\right)-X\left(t\right) \right]^2 \right\rangle = B\left(t+h,t+h\right)-2B\left(t+h,t\right)+B\left(t,t\right) \tag{2.59}$$

### 2.4.3 Differentiability

The *sp X(t)* is ms differentiable if, given any sequence of (deterministic) numbers $\{h_n\}$ that convergences to zero, the following *rs* converges in the *ms* to a *rv* $\dot{X}\left(t\right)$ called the derivative of *X(t)*.

$$\left\{ \frac{X\left(t+h_n\right)-X\left(t\right)}{h_n} \right\} \tag{2.60}$$

Moreover, $\dot{X}\left(t\right)$ is a *ms* continuous *sp* with its moments given by:

$$\left\langle \dot{X}\left(t\right) \right\rangle = \frac{d}{dt}\left\langle X\left(t\right) \right\rangle \tag{2.61}$$

and

$$\left\langle \dot{X}\left(t_1\right)\dot{X}\left(t_2\right) \right\rangle = \frac{\partial^2 B\left(t_1,t_2\right)}{\partial t_1 \partial t_2} \tag{2.62}$$

### 2.4.4 Integrability

We say that the integral

$$\int_a^b \phi\left(t\right)X\left(t\right)dt \tag{2.63}$$

where $\phi(t)$ is an ordinary (deterministic) function and *X(t)* is a *sp*, exists in the *ms*, *iff* the *rs* of partial sums

$$S_n = \sum_{j=1}^{n} \phi\left(t_j^*\right) X\left(t_j^*\right) \Delta t_j \tag{2.64}$$

where $\Delta t_j \equiv t_j - t_{j-1}$, converges in the *ms* to a unique *rv Y* for any partition

$$a = t_0 < t_1 < \ldots < t_{n-1} < t_n = b \tag{2.65}$$

with $t_{j-1} \leq t^*_j \leq t_j$, and any two numbers *a* and *b*.

### 2.4.5 Fokker-Plank-Kolmogorov Equation (Diffusion Equation)

An account of a diffusion process is the famous Brownian motion investigated by Robert Brown in 1827 (Brown, R, 1828) but originally discovered by Jan IngenHousz in 1785, who too often is not credited for his discovery. Albert Einstein later in 1905 (Einstein, A, 1905) gave the very first quantitative description of Brownian motion. Meanwhile, the same year Albert Einstein published two other papers on completely different topics, one on the Photo-electric Effect and the other on the Special Theory of Relativity. These three papers have influenced many researches across the board of STEM fields, including this research, and have deservedly earned him the Nobel Prize. In 1908, Paul Langevin (Lnagevin, p, 1908) provided a different interpretation of Brownian motion, which idealizes a particle in a "noisy" surrounding medium. Langevin's equation for the position of a particle can be written as follows:

$$\frac{dX\left(t\right)}{dt} = a\left(X\left(t\right),t\right) + b\left(X\left(t\right),t\right)\Gamma\left(t\right) \tag{2.66}$$

where *Γ(t)* is the *Gaussian white noise* (*GWN*), and a and b are known as the drift and diffusion coefficient respectively. From these contributions emerged the work of Kolmogorov (1931) who derived a pair of differential equations known as the Forward-

Kolmogorov Equation and the Backward-Kolmogorov Equation describing the evolution of the probability distribution of a Markov process. Focusing on continuous-time processes, Fokker (1914) and Plank (1917) derived the equivalent differential equation for the evolution of the first-order *pdf* of diffusion with drift. The general form of the Fokker-Plank-Kolmogov (FPK) equation is the second-order PDE of parabolic type given by:

$$\frac{\partial f\left(x,t\right)}{\partial t}=-\frac{\partial}{\partial x}\left[a_1\left(x\right)f\left(x,t\right)\right]+\frac{\partial^2}{\partial x^2}\left[a_2\left(x\right)f\left(x,t\right)\right] \tag{2.67}$$

In the above equation the coefficients $a_1(x)$ and $a_2(x)$ are the drift and diffusion coefficient respectively. Although revolutionary, the papers published by Einstein and Langevin on Brownian motion only observed the phenomenon on "coarse" time scales, which are observation times that are much longer than the auto-correlation times ($10^{-8}s$). It was not until G.E Uhlenbeck and L.S Ornstein in 1930, that Brownian motion was studied at a fine time scale ($10^{-12}s$). In the above equation, we say that t is at the limit of equilibrium with the fine time scale; hence $a_1$ and $a_2$ contain microscopic information. When $a_1(x) = \upsilon_d$ and $a_2(x) = 2D$, the PDE of the diffusion process with drift is satisfied by the *pdf*:

$$f\left(x,t\right)=\frac{1}{2\sqrt{\pi Dt}}\exp\left[-\frac{\left(x-\upsilon_d t\right)^2}{4Dt}\right] \tag{2.68}$$

It is interesting to note the FPKE is deterministic. It can therefore be solved using conventional numerical approximations such as the finite-difference method or the finite-

element method. If we differentiate the FPKE above by making use of the product rule, we obtain:

$$\begin{aligned}\frac{\partial f(x,t)}{\partial t} &= -a_1(x)\frac{\partial f(x,t)}{\partial x} - f(x,t)\frac{\partial a_1(x)}{\partial x} \\ &+ a_2(x)\frac{\partial^2 f(x,t)}{\partial x^2} + 2\frac{\partial f(x,t)}{\partial x}\frac{\partial a_2(x)}{\partial x} + f(x,t)\frac{\partial^2 a_2(x)}{\partial x^2}\end{aligned} \tag{2.69}$$

which when rearranged gives us:

$$\frac{\partial f(x,t)}{\partial t} = f(x,t)\left(\frac{\partial^2 a_2(x)}{\partial x^2} - \frac{\partial a_1(x)}{\partial x}\right) + \frac{\partial f(x,t)}{\partial x}\left(2\frac{\partial a_2(x)}{\partial x} - a_1(x)\right) + \frac{\partial^2 f(x,t)}{\partial x^2}a_2(x) \tag{2.70}$$

We use a simple central difference (finite difference) scheme with a homogeneous discretization of space for good measure.

$$\begin{aligned}\frac{\partial f^i(x,t)}{\partial t} &= f^{(i-1)}(x,t)\left(\frac{a_1^{(i)}(x)}{2\Delta x} + \frac{a_2^{(i)}(x)}{\Delta x^2} - \frac{1}{\Delta x}\frac{\partial a_2^{(i)}}{\partial x}\right) - f^{(i)}(x,t)\left(\frac{\partial a_1^{(i)}}{\partial x} + 2\frac{a_2^{(i)}(x)}{\Delta x^2} - \frac{\partial a_2^{(i)}(x)}{\partial x^2}\right) \\ &+ f^{(i+1)}(x,t)\left(-\frac{a_1^{(i)}(x)}{2\Delta x} + \frac{a_2^{(i)}(x)}{\Delta x^2} + \frac{1}{\Delta x}\frac{\partial a_2^{(i)}}{\partial x}\right)\end{aligned} \tag{2.71}$$

## 2.5 Basic Concepts of Continuum Mechanics

Thus far we have been acquainted with stochastic processes which when investigated at a "fine" time scale, requires the application of "statistical mechanics". Such tools allow us to establish contact with the microscopic world. Looking at the bigger picture, Continuum mechanics, allow us to represent the mechanical behaviour of materials at a macroscopic scale.

### 2.5.1 Soil as a continuum

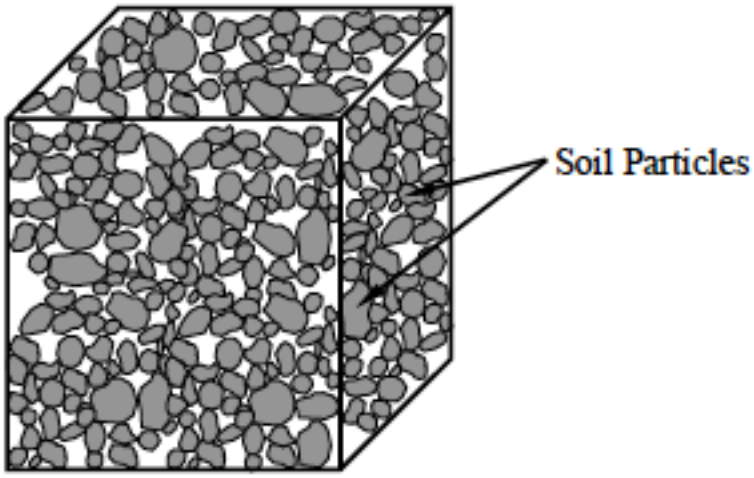


**Figure 2.3 A Representative Elemental Volume (REV) of Soil (Source: Basu, D, 2006)**

Given the size of soil particles, they are clearly discrete in nature, however, if a representative volume is considered, then we can assume the soil to be continuous. This minimum volume within which soil is considered continuous is called the representative elemental volume (*REV*). The definition of a *REV* diverges slightly from that of a continuous volume in its definition of density where conventionally, density in a continuum is defined as:

$$\rho = \lim_{\Delta V \to 0} \frac{\Delta M}{\Delta V} \tag{2.72}$$

while for a *REV*, the following modification was proposed by Davis and Selvadurai in 1996 (Davis and Selvadurai, 1996) about the definition of density:

$$\rho = \lim_{\Delta V \to \Delta V_0} \frac{\Delta M}{\Delta V} \tag{2.73}$$

where $\Delta V_0$ is the *REV*.

A *REV* must respect the following conditions to be applied to soil (Basu, D, 2006):

1. The *REV* must contain a sufficient number of soil particles (thousands) so that it can be representative of the soil properties.
2. The *REV* must be significantly smaller than the volume of soil under consideration.

### 2.5.2 Tensors

In general, a tensor is a mathematical object whose components are characterized by a magnitude and direction and which can be generalized in multiple dimensions. For example, a vector is a first-order tensor. The properties of a tensor are also independent of the reference frame. This is important in the development of invariant tensors. We now illustrate important second-order tensors and operations on them.

*Second-Order Tensor:* A second order tensor simply put is a vector-valued function. It is a function that takes an independent vector as input and returns a dependent vector as output. A second-order tensor can be represented by a 3x3 matrix and has nine components ($3^n$, $n = 2$ for a second-order tensor). A recurring second-order tensor in this thesis is the stress tensor, $\sigma_{ij}$. Due to equilibrium, the stress tensor is given by a symmetric matrix.

$$\sigma_{ij} = \begin{bmatrix} \sigma_{11} & \sigma_{12} & \sigma_{13} \\ \sigma_{21} & \sigma_{22} & \sigma_{23} \\ \sigma_{31} & \sigma_{32} & \sigma_{33} \end{bmatrix} = \begin{bmatrix} \sigma_{11} & \sigma_{21} & \sigma_{31} \\ \sigma_{12} & \sigma_{22} & \sigma_{32} \\ \sigma_{13} & \sigma_{23} & \sigma_{33} \end{bmatrix} = \sigma_{ji} \tag{2.74}$$

where the off-diagonal elements are the shear components and can be interchanged with their mirrored counterparts along the diagonal. The shears are equal to preserve rotational equilibrium.

The index notation used in equation 2.74 is known as Einstein notation. A rule of thumb is that repeated indices are considered "dummy" indices as they vanish to create the summation of tensor elements. The remaining indices are called "free" indices and typically indicate the order of a tensor.

Let $\lambda$ be a scalar and $n_i$ be a vector relating the second-order tensor $\sigma_{ij}$ by the equation:

$$\sigma_{ij} n_j - \lambda n_i = 0 \tag{2.75}$$

We can *factor* the above equation by making use of the *Kronecker delta* as follows:

$$\left(\sigma_{ij} - \lambda \delta_{ij}\right) n_j = 0 \tag{2.76}$$

The *Kronecker delta* can also be used as a *contraction*[4] on the second-order tensor s.t:

$$tr\left(\sigma_{ij}\right) = \sigma_{ij}\delta_{ij} = \sigma_{ii} = \sigma_{11} + \sigma_{22} + \sigma_{33} \tag{2.77}$$

The above operation is also known as the trace of a second-order tensor. When the trace of a stress tensor is taken, the resulting tensor is a scalar known as the hydrostatic pressure (volumetric tensor). If $\sigma_{ij}$ represents the stress state of a saturated soil *REV*, then $tr(\sigma_{ij})$ gives the pore-water pressure acting on the *REV*.

[4] The word contraction is used in the sense that the order of the tensor is lowered

The volumetric stress however does not give us any information about the shear components. We therefore introduce the deviatoric tensor $s_{ij}$, which gives us more information about the deformation.

$$s_{ij} = \sigma_{ij} - \sigma_{hyd} = \sigma_{ij} - \frac{tr(\sigma_{ij})}{3} = \begin{bmatrix} \sigma_{11} - \sigma_{hyd} & \sigma_{12} & \sigma_{13} \\ \sigma_{21} & \sigma_{22} - \sigma_{hyd} & \sigma_{23} \\ \sigma_{13} & \sigma_{23} & \sigma_{33} - \sigma_{hyd} \end{bmatrix} \tag{2.78}$$

We are now interested in the transformation of second-order tensors. The rotation of a point represented by a vector $v_j$, is achieved through the dot product of the transformation matrix $R_{ij}$ with the vector $v_j$.

$$v_i^{'} = R_{ij} v_j \tag{2.79}$$

For a second-order tensor, two transformations are required such that:

$$\sigma_{ij}^{'} = R_{ik} \sigma_{kl} R_{lj} = R \cdot \sigma \cdot R^T \tag{2.80}$$

Up until now, the dot product operation has been employed. We now introduce the reader to the dyad operator ($\otimes$). Unlike a contraction, the dyadic product of two tensors increases the order of the latter. For example, see the dyadic product between two vectors followed by the same operation between two second-order tensors:

$$C_{ij} = A_i \otimes B_j = a_i b_j \tag{2.81-a}$$

$$C_{ijkl} = A_{ij} \otimes B_{kl} = a_{ij} b_{kl} \tag{2.81-b}$$

*Fourth-Order Tensor*: A Fourth-order tensor can be obtained from the dyadic product of two second-order tensors. They are conceptually harder to grasp from a physical point of view but are nonetheless very popular in rate constitutive equations. A famous example

of a fourth order tensor is the fourth-order linear elastic tensor that relates stress to strain via a double contraction as shown in equation 2.82.

$$\sigma_{ij} = L_{ijkl} : \varepsilon_{kl} \tag{2.82}$$

There are eighty-one independent elements each related to the combination of one of nine elements of the stress tensor and one of nine elements of the strain tensor. The fourth-order elastic tensor can be expressed in terms of the elastic modulus *E*, and Poisson's ratio $\upsilon$ as:

$$L^{el} = \lambda\left(\delta \otimes \delta\right) + 2G1^{(4s)} \tag{2.83}$$

where *G* is the shear modulus given by: $G = \frac{E}{2\left(1+\upsilon\right)}$, and *K* is the bulk modulus given by: $K = \frac{E}{3\left(1-2\upsilon\right)}$ with Lame's constant $\lambda = K - 2G/3$.

We also encounter the symmetric part of the fourth-order unit tensor $I^{(4s)}$, which can be obtained by first writing $I^{(4)}$ as:

$$1^{(4)} = \delta_{ik}\delta_{jl} \tag{2.84}$$

and from which the symmetric and anti-symmetric part can be extracted as follows:

$$1^{(4s)} = \frac{1}{2}\left(\delta_{ik}\delta_{jl} + \delta_{il}\delta_{jk}\right) \tag{2.85-a}$$

$$1^{(4a)} = \frac{1}{2}\left(\delta_{ik}\delta_{jl} - \delta_{il}\delta_{jk}\right) \tag{2.85-b}$$

Another useful quantity is the *invariant* of a tensor. *Invariants* are independent from the material frame and are often used throughout continuum mechanics to uniquely define tensors. There are three invariants $I_1$, $I_2$ and $I_3$ enumerated below:

1. $I_1 = tr(\sigma_{ij})$ (2.86-a)
2. $I_2 = \frac{1}{2}[[tr(\sigma_{ij})]^2 - tr(\sigma^2_{ij})]$ (2.86-b)
3. $I_3 = det(\sigma_{ij})$ (2.86-c)

A different set of invariants known as the deviatoric invariants $J_1$, $J_2$ and $J_3$ are also extensively used in continuum mechanics. They are given by:

1. $J_1 = tr(s_{ij}) = 0$ (2.87-a)
2. $J_2 = -\frac{1}{2}s_{ij}s_{ji}$ (2.87-b)
3. $J_3 = det(s_{ij})$ (2.87-c)

The *Von Mises* equivalent stress for instance which we will introduce more formally later is a function of the second deviatoric invariant of stress.

$$\sigma_{eq}^{vm} = \sqrt{\frac{3}{2}s:s} = \sqrt{\frac{3}{2}s_{ij}s_{ji}} = \sqrt{3J_2} \tag{2.88}$$

### 2.5.3 Derivatives of Tensors

The derivative of a scalar function f with a tensor argument $\boldsymbol{A}$ with respect to another tensor in general produces a tensor of equal or higher order. For example, the derivative of a scalar with a second-order tensor produces a second-order tensor. The derivative of

the equivalent stress (a scalar) with respect to stress ($2^{nd}$ order tensor) gives the Normal, which is another second-order tensor.

$$N_{ij} = \frac{\partial \sigma_{eq}}{\partial \sigma_{ij}} = \frac{scalar}{2^{nd} Order} = 2^{nd} Order \tag{2.89}$$

That is equally true for the derivative of a second-order tensor with respect to a second order tensor, which produces a fourth-order tensor.

$$C_{ijkl} = \frac{\partial F\left(A_{ij}\right)}{\partial A_{kl}} = \frac{2^{nd} Order}{2^{nd} Order} = 4^{th} Order \tag{2.90}$$

We now introduce the *Del* operator ($\nabla$), which is defined as:

$$\nabla = \left( \frac{\partial}{\partial x_j} \right) e_j \tag{2.91}$$

And which can be treated as a vector with elements $j = 1,2,3$ and $e_j$ is a basis vector. The *Del* operator is used to define three very important operations known as the *gradient, divergence* and *curl*.

1. The <u>*gradient*</u> of a scalar valued function $\phi$ is the tensorial product of the *Del* operator with $\phi$.

$$\nabla \phi = \frac{\partial \phi}{\partial x_i} e_i = \phi_{,i} e_i \tag{2.92}$$

When applied to a vector *u*, the *gradien*t is given by the dyadic product of the *Del* operator with the vector *u.*

$$\nabla u = \nabla \otimes u = \frac{\partial}{\partial x_i} e_i \otimes u_j e_j = \frac{\partial u_j}{\partial x_i} e_i \otimes e_j \tag{2.93}$$

2. The *divergence* of a tensor is given by the inner product of the *Del* operator with the tensor. In other words, we apply a *contraction* on the *gradient* of the tensor.

$$\nabla \cdot u = \frac{\partial}{\partial x_i} e_i \cdot u_j e_j = \frac{\partial u_j}{\partial x_i} e_i \cdot e_j = u_{j,i} \delta_{ij} = u_{i,i} \tag{2.94}$$

3. The *curl* of a tensor is the *cross product* of the *Del* operator with the tensor:

$$\nabla \times u = \frac{\partial}{\partial x_i} e_i \times u_j e_j = \frac{\partial u_j}{\partial x_i} e_i \times e_j = \varepsilon_{ijk} \frac{\partial u_j}{\partial x_i} e_k \tag{2.95}$$

## 2.6 Elastic-Plastic Materials

With the language of tensors formally introduced, we now cross the final chasm in the understanding of soil as an elastic-plastic material.

Under the action of external loads, an object deforms up to a threshold point known as its yield point. We define the elastic and plastic behaviour of a material based on its yield strength. If the material has not yet yielded, we say that it is in the elastic region and hence behaves as such. On the contrary, if an object has yielded, it behaves as a plastic material.

Elastic deformation is conservative in the sense that the strain energy of the system is recovered upon release of loading. The process is also compressible since the material's volume can change unless its Poisson ratio is 0.5. As a result, an elastic material regains its shape when it is unloaded. On the other hand, plastic deformation is non-conservative.

It is incompressible and since the volume of a plastic material must be conserved, plastic deformation is irreversible.

### 2.6.1 Stress-strain idealizations

To understand plasticity, it is important to first understand three concepts:

1. Yield function
2. Hardening rule
3. Flow rule

A series of idealized stress-strain curves are provided below for the purpose of developing equations pertaining to the concepts listed above. Theses idealizations are also simplifications made to capture the behaviour of materials under certain conditions.

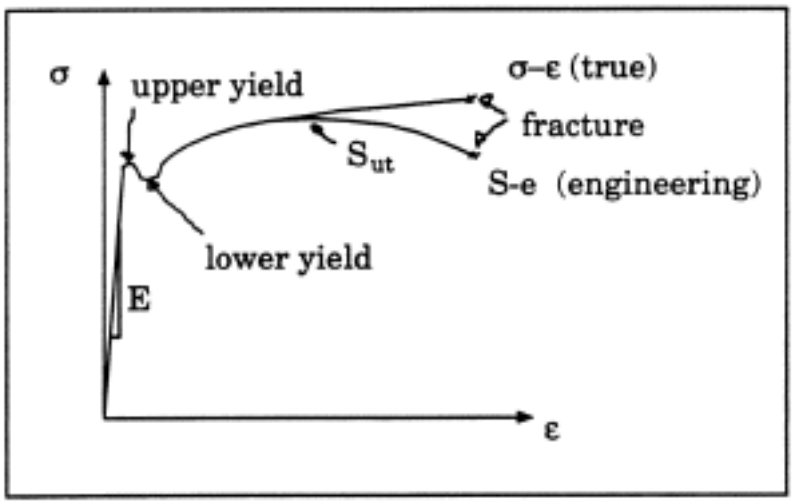


**Figure 2.4: Stress-strain curve of material undergoing a uniaxial tensile test (Source: ME 620 course notes)**

Figure 2.4 shows at which point the above three concepts take place. If we were to look at an object with no elastic deformation, or in other words an object that yields instantaneously, we can idealize the material as *Rigid-Perfectly Plastic* which does not

allow for the development of stress with further deformation or *Rigid-plastic* where the stress is a non-linear function of strain.

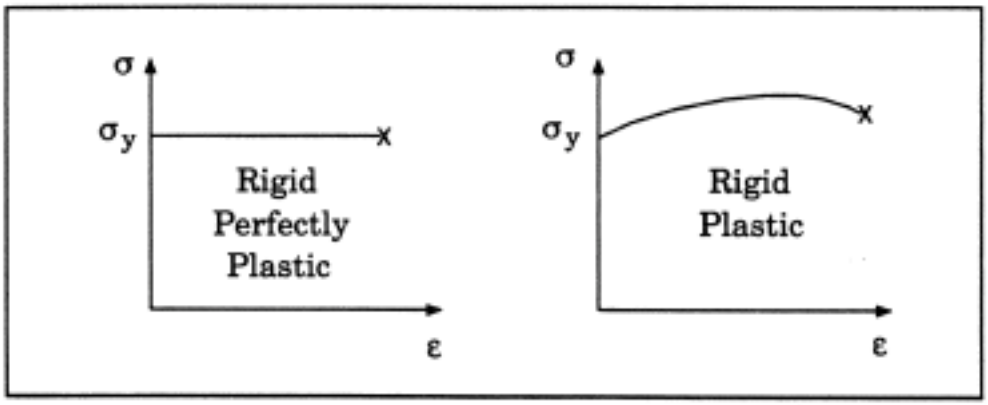


**Figure 2.5: Stress-strain curves for Rigid Perfectly Plastic and Rigid Plastic materials (Source: ME 620 course notes)**

Figure 2.5 can also represent the stress-strain curve of large plastic flow problems. When problems only involve small strains, an *Elastic-Perfectly Plastic* or *Elastic-Plastic* model can be adopted as shown in figure 2.6.

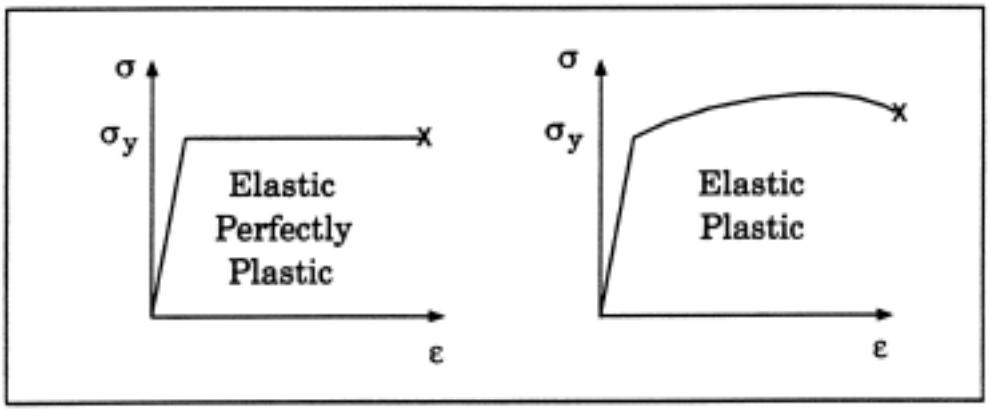


**Figure 2.6: Stress-strain curves for Elastic Perfectly Plastic and Elastic Plastic materials (Source: ME 620 course notes)**

The problems tackled in this thesis are limited to small-strain problems. We therefore turn our attention to the *Elastic-Plastic* model.

### 2.6.2 Yield function

Let us begin by defining a yield criterion. There are a few important theories that are used to define yield criteria, among which we will list only some important ones.

*Maximum Normal Stress Theory*: The *maximum normal stress theory* tells us that yielding occurs when the largest principle stress becomes equal to or greater than the yield stress of the material.

$$\max\left|\sigma_i\right| \geq \left|\sigma_y\right| \qquad \text{i=1,2,3} \tag{2.96}$$

For a two-dimensional stress state, the yield function is given by the contour formed in the σ-space, where a point in the shaded region behaves as an elastic material.

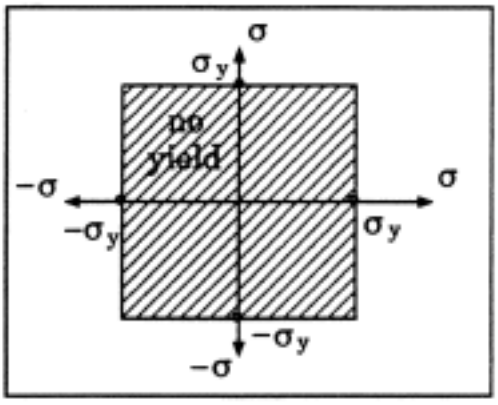


**Figure 2.7: Yield function of Maximum Normal stress Theory (Source: ME 620 course notes)**

*Maximum Shear Stress Theory*: The *maximum shear stress theory* establishes that yielding occurs when the maximum shear stress reaches a value equal or greater to that the maximum shear strength of a material.

$$\left|\tau_{\max}\right| \geq \frac{\sigma_y}{2} \tag{2.97}$$

This criterion is also known as the *Tresca* criterion depicted graphically below:

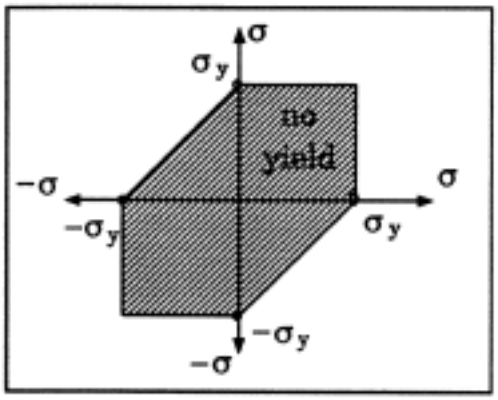


**Figure 2.8: Yield function of Maximum Shear Stress Theory (Tresca) (Source: ME 620 course notes)**

*Shear or Distortion Energy Theory*: The *distortion energy theory* states that a material yields when its distortion energy per unit volume is equal or greater than its distortion energy at yield. The *Von Mises* equivalent stress is an example of the distortion energy theory.

$$\sqrt{\frac{1}{2}\left[\left(\sigma_1-\sigma_2\right)^2+\left(\sigma_2-\sigma_3\right)^2+\left(\sigma_3-\sigma_1\right)^2\right]}=\sqrt{\frac{3}{2}\sigma'_{ij}\sigma'_{ij}}=\sigma_{eff}\geq\sigma_y \qquad (2.98)$$

As shown in the equation 2.98, the equivalent stress is independent of hydrostatic stresses. The yield function is represented graphically in figure 2.9:

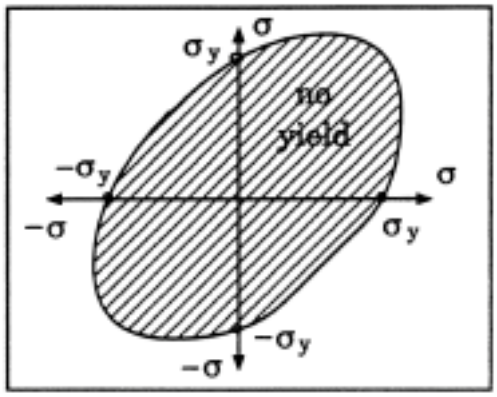

**Figure 2.9: Yield function of Distortion Energy Theory (Von Mises) (Source: ME 620 course notes)**

*Other Yield Functions*: There are many other yield functions, which have been proposed to describe the behaviour of different materials. One class of yield functions that we will focus on in particular are pressure sensitive yield functions suitable for soils. For example the *Mohr-Coulomb* yield function or the *Drucker-Prager* yield function or the Modified Cam-Clay.

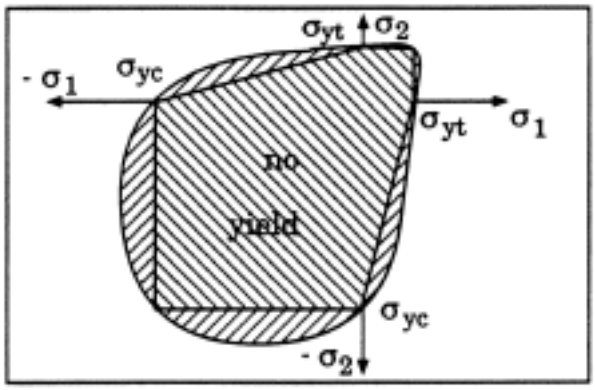


**Figure 2.10: Yield function of pressure sensitive material (Source: ME 620 course notes)**

A yield function is therefore a way to express a yield criterion.

### 2.6.3 Hardening rule

When a material's yield stress increases, we say it hardens. The hardening process causes the contours of the yield function to shift right or to expand as depicted by figure 2.11.

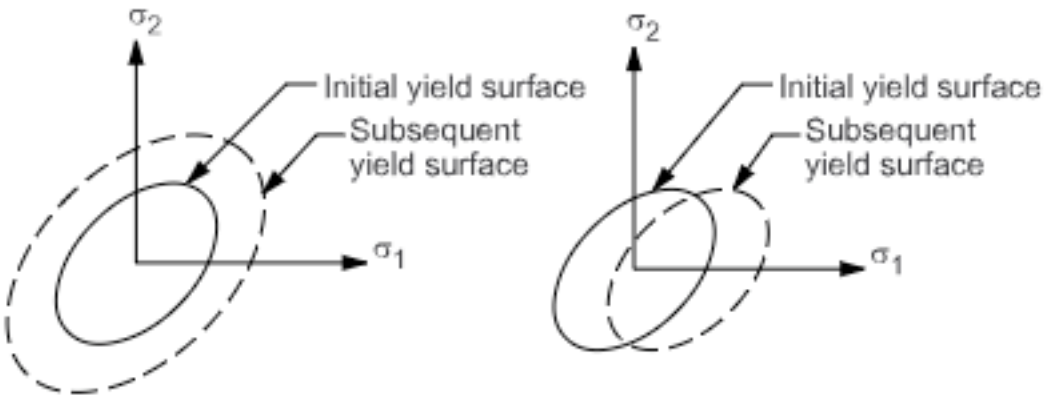


**Figure 2.11: Hardening a)Isotropic hardening, b) Kinematic hardening. (Source: www.sharcnet.ca)**

There are two commonly used hardening rules:

1. *Work hardening*: In *work hardening*, the flow stress is a function of the plastic work done $W^{pl}$.

$$\bar{\sigma} = f\left(W^{pl}\right) \tag{2.99}$$

In one dimension, we have the *total plastic work* done on a body given by:

$$W^{pl} = \int_0^t \bar{\sigma}\dot{\varepsilon}_{pl}\, dt \tag{2.100}$$

2. *Strain hardening*: In *strain hardening*, the flow stress is a function of the "*effective plastic strain*" $\bar{\varepsilon}_{pl}$.

$$\bar{\sigma} = f\left(\bar{\varepsilon}_{pl}\right) \tag{2.101}$$

where $\bar{\varepsilon}_{pl} = \int_0^t \dot{\bar{\varepsilon}}_{pl}\, dt$ and $\dot{\bar{\varepsilon}} = \left[\frac{2}{3}\dot{\varepsilon}_{ij}^{pl}\dot{\varepsilon}_{ij}^{pl}\right]^{\frac{1}{2}}$

### 2.6.4 Flow rule

In Plasticity theory, the plastic flow of a material is used to describe its plastic behaviour. We know that plastic flow occurs along the maximum shear planes. This implies that there exists a relationship between plastic strain increments and the current stress. We can now introduce the functional $g(\sigma_{ij})$ known as *the plastic-potential* which relates the plastic strain increment to the current stress by:

$$d\varepsilon_{ij}^{pl} = \frac{\partial g\left(\sigma_{ij}\right)}{\partial \sigma_{ij}} d\lambda \tag{2.102}$$

where $d\lambda$ is a scalar known as the *plastic multiplier*. There are two assumptions for the Flow rule:

1. *Associated Flow Rule*: When *Associated Flow Rule (AFR)* also known as *normality rule* is assumed, the plastic strain increment vector is normal to the yield surface.

$$d\varepsilon_{ij}^{pl} = \frac{\partial f}{\partial \sigma_{ij}} d\lambda \tag{2.103}$$

2. *Non-Associated Flow Rule*: When *Non-Associated Flow rule* is assumed, then the plastic strain increment vector is normal to the *plastic potential* as in equation 2.102

A graphical representation of the two flow rules is provided in figure 2.12.

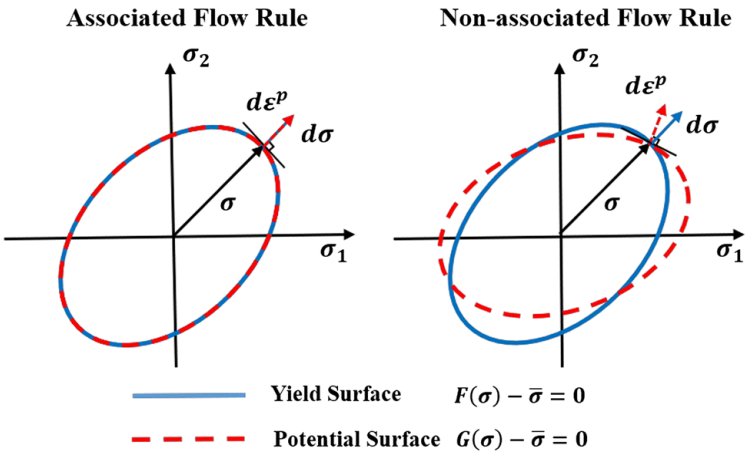


**Figure 2.12: a) Associated Flow Rule b) Non-Associated Flow Rule (Source: ME 620 course notes)**

# CHAPTER 3.

# ONE-DIMENSIONAL STOCHASTIC FINITE ELEMENT METHOD IN FOUNDATION PROBLEMS

## 3.1 Introduction

The problem at hand is that of material heterogeneity and uncertainty in loading conditions. In soil, heterogeneity presents itself in two forms: on a large scale, the soil exhibits similar properties within a region delineated by the soil stratigraphy. The soil properties are then said to be piecewise homogeneous for defined regions or soil layers (Sudret, 2014). On a smaller scale, the soil properties also possess local spatial variability due to the presence of other types of soil grains. Given the unpredictability of geotechnical problems, it becomes clear that the treatment of the latter calls for probabilistic models.

Current norms in the construction industry, more specifically in the limit state design of structures, impose the use of load factors and material strength factors to achieve the desired level of reliability. Load factors account for uncertainties in loading conditions while material strength factors account for variability in the material properties. In the design of geotechnical structures, however, the use of reliability factors induces high-costs. The crude treatment of uncertainties through their amalgamation into reliability factors yields over-conservative designs.

An alternate methodology tailored to problems subject to high levels of uncertainty is therefore necessary. There are numerous methods reported in the literature that are used to analyze systems with uncertainties. The perturbation method was used in the 80s and 90s (Baecher and Ingra, 1981; Phoon et al 1990), then came First/Second order reliability methods (FORM/SORM), which were used to compute the probability of failure of a system with respect to a performance criteria (Ditlevsen and Madsen, 1996). In the late 90s the popular *Monte Carlo* method was adapted for geotechnical problems under the name of Random Finite Element Analysis or RFEM (Griffiths and Fenton, 1999). The RFEM remained mainstream despite being computationally demanding until the emergence of the Stochastic Finite Element Method (SFEM) (Ghanem and Spanos, 1991)

The SFEM is used in this chapter for its performance, where the random soil properties are modeled as random fields using the spectral decomposition of their covariance function and the random response of the soil-structure system is represented using a Polynomial Chaos Expansion as polynomial series in the input variables. Early applications of SFEM in geotechnics can be found in the literature (Ghanem and Brzkala, 1996; Sudret and Der Kiureghian, 2000; Ghiocel and Ghanem, 2002; Clouteau and Lafargue, 2003; Sudret et al, 2004; Sudret et al, 2006; Berveiller et al, 2006).

## 3.2 Analysis

The SFEM is applied to three cases of Winkler foundations. The configuration of each beam is given below.

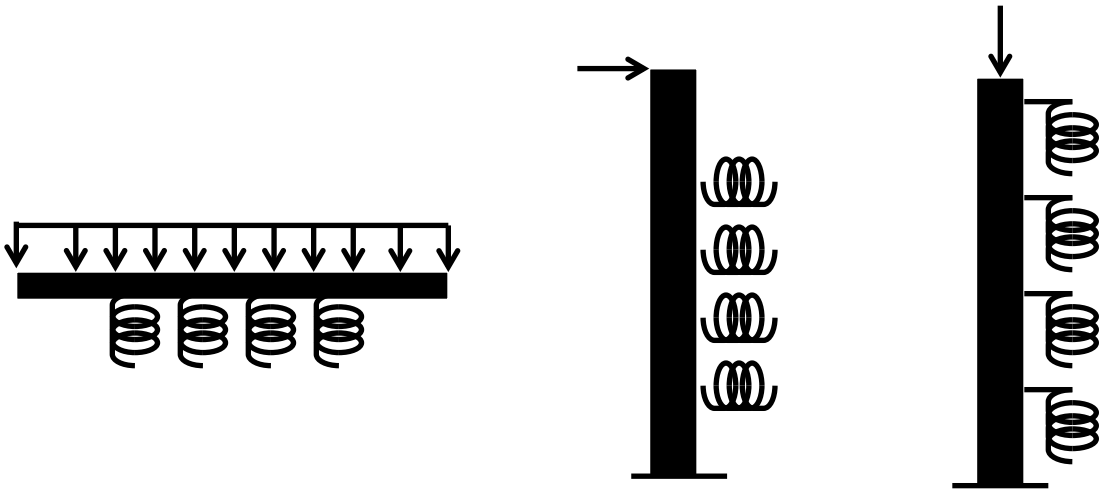

**Figure 3.1: a) Case 1: Uniformly loaded free-end beam on an elastic foundation, b) Case 2: Laterally loaded pile on an elastic foundation, fixed at one end, c) Case 3: Axially loaded pile on an elastic foundation, fixed at one end**

### 3.2.1 Problem Definition

In practice, site-specific index and classification tests are performed on the soil mass to obtain a rough estimate of its mechanical properties. Despite the availability of site-specific data, the range within which soil properties vary remain significant as suggested by the table below (Lee et al, 1983).

**Table 3.1: Typical range for the coefficient of variation of different soil properties a) Lacasse and Nadim (1996), b) Lumb (1974)**

| a) Soil property | Soil type | pdf | Mean | COV (%) |
|---|---|---|---|---|
| Cone resistance | Sandy Clay | LN | - | - |
| | Clay | N/LN | - | - |
| Undrained shear strength | Clay (triaxial) | LN | - | 5-20 |
| | Clay (Index Su) | LN | - | 10-35 |
| | Clayey silt | N | - | 10-30 |
| Ratio $S_u/\sigma'_{v0}$ | Clay | N/LN | - | 5-15 |
| Plastic limit | Clay | N | 0.13-0.23 | 3-20 |
| Liquid limit | Clay | N | 0.30-0.80 | 3-20 |
| Submerged unit weight | All soils | N | 5 - 11 ($kN/m^3$) | 0-10 |
| Friction angle | Sand | N | - | 2-5 |
| Void ratio, porosity, initial void ratio | All soils | N | - | 7-30 |
| Over consolidation ratio | Clay | N/LN | - | 10-35 |
| **b) Soil property** | | | | |
| Density | All soils | | | 5-10 |
| Voids ratio | All soils | | | 15-30 |
| Permebility | All soils | | | 200-300 |
| Compressibility | All soils | | | 25-30 |
| Undrained cohesion (clays) | All soils | | | 20-50 |
| Tangent of angle of shearing resistance (sands) | All soils | | | 5-15 |
| Coefficient of consolidation | All soils | | | 25-50 |

In each of the above cases, the spatially random parameters are identified and defined using a random field. Numerous methods of discretizing random fields exist, among which we will consider the *Karhunen-Loeve (KL)* expansion over the *EOLE* (*Expansion optimal linear estimation*) method and the *OLE* (*Optimal linear estimataion*) method.

### 3.2.2 Random fields

We can interpret the *Karhunen-Loeve* expansion as the representation of a *stochastic process* using an infinite linear combination of orthogonal functions as shown in figure 3.2, similar to the Fourier series representation of a function on a bounded interval as shown in figure 3.3.

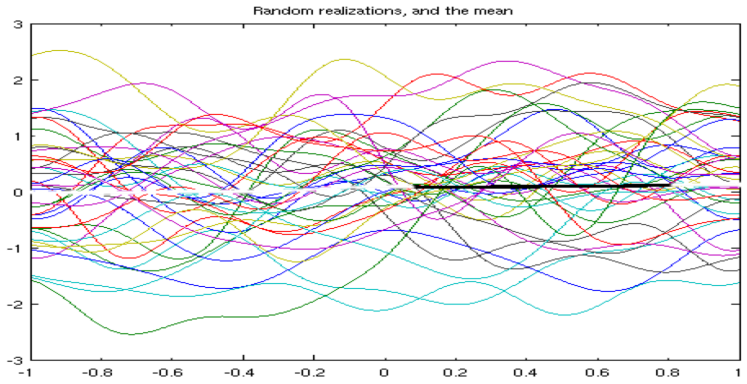


**Figure 3.2: Spectral representation of a stochastic process**

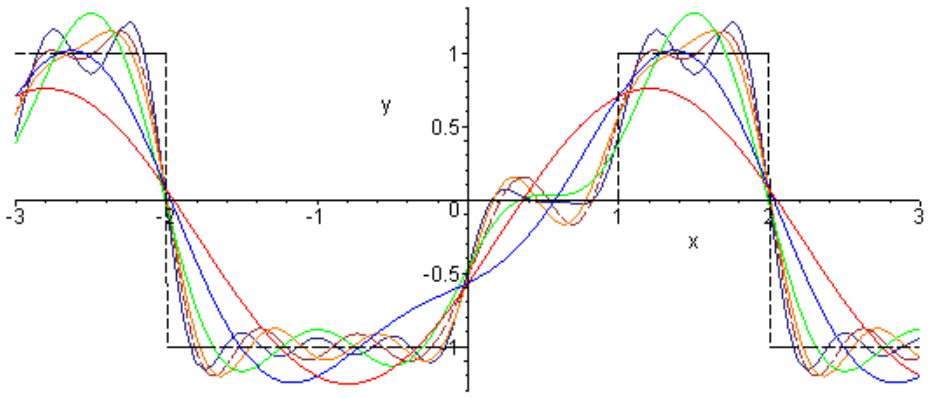


**Figure 3.3: Fourier series representation of a Heaviside function (Source: Maple Worksheets on Fourier series)**

Let $S(x)$ be a random process, a function of position $x$ over the domain $L$. We now introduce $\overline{S}(x)$ as the mean of the random process $S(x)$ and $C(x_1,x_2)$ as the *covariance function* associated with positions $x_1$ and $x_2$. It can be shown that $C(x_1,x_2)$ is *symmetric*, *bounded* and *positive definite*, hence it has spectral decomposition (P.D Spanos, R.Ghanem 1989):

$$C(x_1,x_2)=\sum_{n=0}^{\infty}\lambda_n\phi_n(x_1)\phi_n(x_2) \tag{3.1}$$

Where $\lambda_n$ and $\phi_n$ are the *eigen-values* and *eigen-functions* respectively.

The existence of such a spectral decomposition follows from the *general theorem of Khlinchin (Wierner-Khlinchin)* on the integral representation of the correlation function (see Stationary stochastic process) (Wiener, 1964). This shows that any stationary process can be regarded as the superposition of mutually uncorrelated harmonic oscillations of various frequencies and with random phases and amplitudes.

The *eigen-values* and *eigen-functions* are obtained by solving the integral equation:

$$\int_L C(x_1,x_2)\phi_n(x_1)dx_2=\lambda_n\phi_n(x_1) \tag{3.2}$$

Because of the *symmetry* and *positive-definiteness* (Loeve, 1977) of the *covariance kernel*, the *eigen-functions* form a complete orthogonal set, which satisfies:

$$\int_L \phi_n(x)\phi_m(x)dx=\delta_{nm} \tag{3.3}$$

From the above definitions, we can now write the process $\Delta S(x)$ as follows:

$$S(x) = \bar{S}(x) + \Delta S(x) \tag{3.4}$$

In which $\Delta S(x)$ denotes a process with zero mean and *covariance function C($x_1$,$x_2$)*.

The process $\Delta S(x)$ can be expanded in terms of $\lambda_n$ and $\phi_n$ as follows:

$$\Delta S(x) = \sum_{n=1}^{\infty} t_n \sqrt{\lambda_n} \phi_n(x) \tag{3.5}$$

Where $t_n$ is a random coefficient independent of *x*. We can obtain $t_n$ by multiplying both sides of equation 3.5 by $\Delta S(x_2)$ and by taking the expectation on both sides.

$$C(x_1, x_2) = \langle \Delta S(x_1) \Delta S(x_2) \rangle = \sum_{n=0}^{\infty} \sum_{m=0}^{\infty} \langle t_n t_m \rangle \sqrt{\lambda_n \lambda_m} \phi_n(x_1) \phi_m(x_2) \tag{3.6}$$

Making use of the orthogonal property of the set of *eigen-functions* $\{\phi_n(x)\}$, we multiply the above equation by $\phi_k(x_1)$ and integrate over the domain of the problem.

$$\int_L C(x_1, x_2) \phi_k(x_2) dx_2 = \lambda_k \phi_k(x_1) = \sum_{n=0}^{\infty} \langle t_n t_k \rangle \sqrt{\lambda_n \lambda_k} \phi_n(x_1) \tag{3.7}$$

Once more exploiting the orthogonal property of $\{\phi_n(x)\}$, the following equation is obtained:

$$\lambda_k \int_L \phi_k(x) \phi_l(x) dx = \lambda_k \phi_k(x) = \sum_{n=0}^{\infty} \langle t_n t_k \rangle \sqrt{\lambda_n \lambda_k} \phi_n(x) \tag{3.8}$$

Which can be rewritten as:

$$\lambda_k \delta_{kl} = \sqrt{\lambda_k \lambda_l} \langle t_k t_l \rangle \tag{3.9}$$

From equation 3.9, the correlation of the random coefficient $t_n$ reads:

$$\left\langle t_k t_l \right\rangle = \delta_{kl} \tag{3.10}$$

Hence, the *random process S(x)* can be rewritten as:

$$S(x) = \overline{S}(x) + \sum_{n=1}^{\infty} t_n \sqrt{\lambda_n} \phi_n(x) \tag{3.11}$$

with an explicit equation for $t_n$ given by:

$$t_n = \frac{1}{\sqrt{\lambda_n}} \int_L S(x) \phi_n(x) dx \tag{3.12}$$

The *Karhunen-Loeve* expansion is known to converge in the *mean square* sense for any distribution of $S(x)$. Moreover, if $S(x)$ is a Gaussian process, the series can be shown to be also converging (Loeve, 1977), in which case the vector of random coefficients formed $\{t_n\}$, is a vector of zero-mean uncorrelated Gaussian random variables. The *Wiener* process is an exemplification of such real centered stochastic process. It should be noted that for any distribution of $S(x)$, the probability distribution of $t_n$ can be estimated by using the explicit equation 3.12 and any quadrature technique which uses linear interpolations of values of the integrands at discrete points of the integration interval.

Truncating the expansion at the $M^{th}$ term gives:

$$S(x) = \overline{S}(x) + \sum_{n=1}^{M} t_n \sqrt{\lambda_n} \phi_n(x) \tag{3.13}$$

### 3.2.3 Exponential covariance

We will now apply the orthogonal expansion derived in the previous section to the *exponential covariance function* defined by the following equation:

$$C\left(x,x_2\right)=\sigma_S^2 e^{-c\left|x-x_2\right|} \tag{3.14}$$

Where $\sigma_S$ is the standard deviation of the *random process* and the parameter *c* is related to the *correlation length* in that it is the inverse of the latter. In *Monte Carlo* simulations, the *correlation length* is accounted for through auto-regressive filters. The choice of this *covariance kernel* is rooted in its applications in geophysics and in earthquake engineering as it can be traced back to a first-order Markovian process (Vanmarcke, 1983).

It now becomes a matter of solving the *Fredholm* integral problem below to represent $S\left(x\right)$ into its spectral decomposition.

$$\sigma_S^2\int_{-a}^{+a} e^{-c\left|x-x_2\right|}\phi\left(x_2\right)dx_2=\lambda\phi\left(x\right) \tag{3.15}$$

By making use of the symmetrical properties of the kernel, equation 3.15 can be written as:

$$\sigma_S^2\int_{-a}^{x} e^{-c\left(x'-x_2\right)}\phi\left(x_2\right)dx_2+\sigma_S^2\int_{x}^{+a} e^{c\left(x'-x_2\right)}\phi\left(x_2\right)dx_2=\lambda\phi\left(x'\right) \tag{3.16}$$

We differentiate equation 3.16 with respect to *x'* and rearrange it to obtain:

$$\lambda\phi'\left(x'\right)=-c\sigma_S^2\int_{-a}^{x} e^{-c\left(x'-x_2\right)}\phi\left(x_2\right)dx_2+c\sigma_S^2\int_{x}^{+a} e^{c\left(x'-x_2\right)}\phi\left(x_2\right)dx_2 \tag{3.17}$$

Differentiating once more with respect to *x'*, we obtain:

$$-c\sigma_S^2\frac{d}{dx'}\left(\int_{-a}^{x}e^{-c(x'-x_2)}\phi(x_2)dx_2\right)=-c\sigma_S^2\left(e^{-c(x-x')}\phi(x')-e^{-c(x+a)}\phi(-a)\cdot 0-c\int_{-a}^{x}e^{-c(x-x_2)}\phi(x_2)dx_2\right) \quad (3.18\text{-a})$$

$$c\sigma_S^2\frac{d}{dx'}\left(\int_{x}^{+a}e^{c(x'-x_2)}\phi(x_2)dx_2\right)=c\sigma_S^2\left(e^{c(x-a)}\phi(a)\cdot 0-e^{c(x-x')}\phi(x')+c\int_{x}^{a}e^{c(x-x_2)}\phi(x_2)dx_2\right) \quad (3.18\text{-b})$$

Combining equations 3.18-a and 3.18-b, we obtain:

$$-c\sigma_S^2e^{-c(x'-x)}\phi(x)-c\sigma_S^2e^{c(x'-x)}\phi(x)+\sigma_S^2c^2\left[\int_{-a}^{x}e^{-c(x'-x_2)}\phi(x_2)dx_2+\int_{x}^{a}e^{c(x'-x_2)}\phi(x_2)dx_2\right]=\lambda\phi''(x') \quad (3.19)$$

Letting $x'\to x$ and $\sigma_S^2=1$

$$-2c\phi(x)+c^2\lambda\phi(x)=\lambda\phi''(x) \quad (3.20)$$

Which when rearranged reads:

$$\left(-2c+c^2\lambda_n\right)\phi_n(x)=\lambda_n\phi_n''(x) \quad (3.21)$$

The solution to the differential equation can be found in the work of Van Trees (Van Trees, 1968) on signal detection and estimation. The *eigen-function* and *eigen-va*lue for the *exponential covariance function* reported is:

$$\phi_n(x)=\frac{\cos(\omega_n x)}{\sqrt{a+\dfrac{\sin(2\omega_n a)}{2\omega_n}}} \quad (3.22\text{-a})$$

$$\lambda_n=\frac{2\sigma_S^2c}{\omega_n^2+c^2} \quad (3.22\text{-b})$$

for n odd, and

$$\phi_n^*(x)=\frac{\cos(\omega_n^* x)}{\sqrt{a+\dfrac{\sin(2\omega_n^* a)}{2\omega_n^*}}} \quad (3.23\text{-a})$$

$$\lambda_n = \frac{2\sigma_S^2 c}{\omega_n^{*2} + c^2} \tag{3.23-b}$$

for *n* even.

In which $\omega_n$ and $\omega_n^*$ are solutions to the following transcendental equations:

$$c - \omega_n \tan(\omega_n a) = 0 \tag{3.24-a}$$

$$\omega_n^* + c \tan(\omega_n^* a) = 0 \tag{3.24-b}$$

The figures below show the first four *eigen-functions* for *c = 1* and the dependency of the *eigen-values* on the inverse of the *correlation length*.

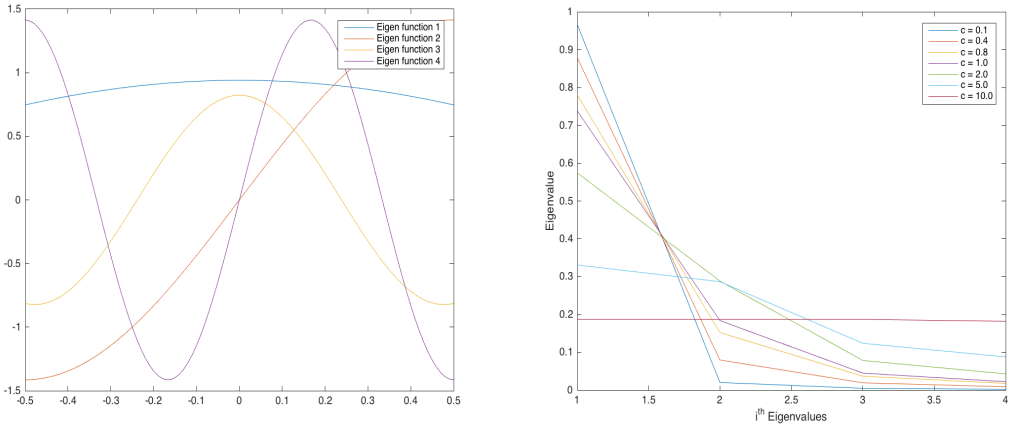


**Figure 3.4: a) First four eigen-functions, b) First four eigen-values for different values of c**

### 3.2.4 Error estimation in input random field

The present section touches upon the utility of the *exponential kernel* for the *Karhunen-Loeve* expansion and the error introduced by truncating higher order terms in the series.

The error referred here is the variance error over the discretization domain and is defined as follows:

$$Var\left[S(x)-\hat{S}(x)\right]=\sigma_S^2(x)-\sum_{i=0}^{M}\lambda_i\phi_i^2(x) \tag{3.25}$$

The more terms in the series the lower the mean error over the support *[-a,a]*. Higher order terms nonetheless come at the cost of more computational power and time. We will later see that the order of expansion of the input variable greatly impacts the size of the global linear system that needs to be solved. The mean error of the input random process is presented below for six orders of expansion.

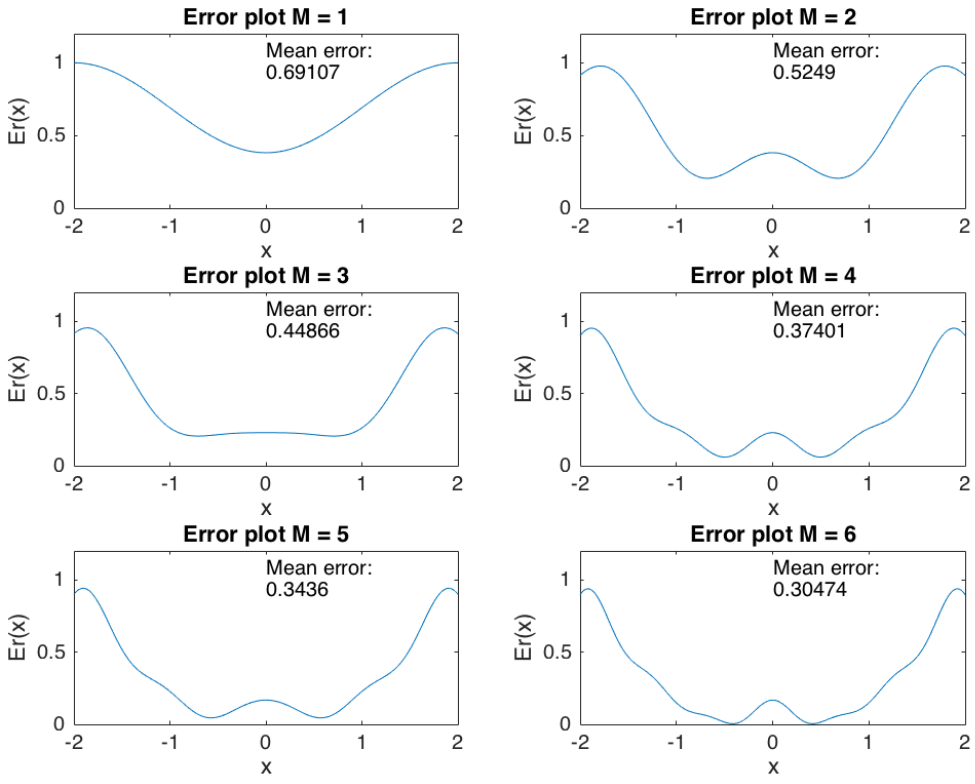


**Figure 3.5: Variance error of input random field for six orders of expansion**

A few observations can be made from the above figure.

- The mean error over the discretization domain decreases with increasing order of expansions.
- The interior points of the discretization domain display a smaller error than points at the boundaries of the domain.
- The error function converges with higher order terms; hence the difference between two consecutive error functions with increasing orders of expansion i.e the $M^{th}$ term decreases. This makes the impact of more terms beyond a certain point negligible.

### 3.2.5 Polynomial Chaos Expansion

Thus far we have provided the mathematical tools to represent the *random processes*, which are the input to our engineering problem using a *Karhunen-Loeve* expansion. We are now interested in representing the response of our problem as a *stochastic process*, which this time, is expanded using a convergent series belonging to the *Hilbert space* of *random functions*. The reasoning behind using a different expansion to represent the response of our computational model is embedded in the fact that it is not evident that the response has the same covariance function as its random input. The absence of this information thereof prompts the need for another representation, one which can do without the knowledge a priori of the covariance function.

Recall our *random process* $S(x)$. We now assume a denumerable set of random variables $\{S_i, i = 1...N\}$ with independent components i.e with joint distribution given by the product of $N$ marginal distributions $\left\{f_{s_i}\right\}_{i=1}^{N}$

$$f_S(x) = \prod_{i=1}^{N} f_{S_i}(x_i) x_i D_{S_i} \tag{3.26}$$

where $D_{S_i}$ is the support of $S_i$.

The set $\{S_i(x)\}$ forms an orthogonal basis in the *Hilbert space* $\boldsymbol{H}$. Since we now operate in the *Hilbert space*; we make use of the notation $Z_j$ to denote the finite set of *random variables*. It is assumed that the response of our computational model has a finite variance and can therefore be expanded as:

$$U = \sum_{J=0}^{\infty} u_j Z_j \tag{3.27}$$

We will use the *Polynomial Chaos Expansion (PCE)* in which the basis terms $\{Z_j\}_{j=0}^{\infty}$ are multivariate orthonormal polynomials in the input vector $S$ such that $Z_j = \psi_j(S)$. To obtain the family of orthogonal polynomials, it is of paramount importance that the inner product of any two orthogonal functions satisfies axioms of orthogonality in the manner presented below.

$$\left\langle \pi_j^{(i)}, \pi_k^{(i)} \right\rangle_i = E\left[\pi_j^{(i)}(S_i)\pi_k^{(i)}(S_i)\right] = \int_{D_{S_i}} \pi_j^{(i)}(x)\pi_k^{(i)}(x) f_{S_i}(x) dx = a_j^i \delta_{jk} \tag{3.28}$$

where subscript *k* denotes the order of the polynomial, $\delta_{jk}$ is the *kronecker* symbol equal to 1 when $j = k$ and 0 otherwise, and $a_j^i$ corresponds to the squared norm of $\pi_j^{(i)}$

$$a_j^i = \left\| \pi_j^{(i)} \right\|_i^2 = \left\langle \pi_j^{(i)}, \pi_j^{(i)} \right\rangle_i \tag{3.29}$$

The *Gram-Schmidt* orthogonalization procedure is then applied to the canonical family of monomials *{1, x, $x^2$,...},* and the orthogonal functions are normalized as follows:

$$\psi_j^{(i)} = \pi_j^{(i)} \Big/ \sqrt{a_j^i} \quad i = 1,\ldots,N, j \in \mathbb{N} \tag{3.30}$$

The family of functions to which the complete set of orthogonal polynomials belongs depends on the distribution of *S*. Table 3.2 provides examples of various distributions of *S* and their corresponding orthogonal functions.

**Table 3.2: Family of Orthogonal functions for different distributions of S**

| Distribution of S | Orthogonal Function family | Support of S |
|---|---|---|
| Gaussian | Hermite polynomials | (-∞, ∞) |
| Uniform | Legendre polynomials | [-1,1] |
| Gamma | Laguerre polynomials | [0,∞) |
| Beta | Jacobi polynomials | [a,b] |

We note that the PC $\psi_j^{(i)}$ constructed thus far is univariate. To obtain multivariate polynomials, one can take the tensor product of univariate orthonormal polynomials in a similar fashion higher order shape functions are built. This is accomplished with the help of tuples $\alpha$ , $\alpha \in \mathbb{N}^M$ also known as multi-indices in which $\alpha$ consists of ordered lists of integers. The definition of $\psi_\alpha$ in terms of the multi-index $\alpha$ is then given by:

$$\psi_{\alpha(x)} = \prod_{i=1}^{N} \psi_{\alpha_i}^{(i)}\left(x_i\right) \tag{3.31}$$

We demonstrate the tensor product of two univariate chaos polynomials and its corresponding *multi-index* $\alpha$ in figure 3.6.

| Basis functions | Multi-index |
|---|---|
| $\Psi_0(\xi_1,\xi_2) = 1$ | $\alpha^0 = (0,0)$ |
| $\Psi_1(\xi_1,\xi_2) = \psi_1(\xi_1)$ | $\alpha^1 = (1,0)$ |
| $\Psi_2(\xi_1,\xi_2) = \psi_1(\xi_2)$ | $\alpha^2 = (0,1)$ |
| $\Psi_3(\xi_1,\xi_2) = \psi_2(\xi_1)$ | $\alpha^3 = (2,0)$ |
| $\Psi_4(\xi_1,\xi_2) = \psi_1(\xi_1)\psi_1(\xi_2)$ | $\alpha^4 = (1,1)$ |
| $\Psi_5(\xi_1,\xi_2) = \psi_2(\xi_2)$ | $\alpha^5 = (0,2)$ |
| $\Psi_6(\xi_1,\xi_2) = \psi_3(\xi_1)$ | $\alpha^6 = (3,0)$ |
| $\Psi_7(\xi_1,\xi_2) = \psi_2(\xi_1)\psi_1(\xi_2)$ | $\alpha^7 = (2,1)$ |
| $\Psi_8(\xi_1,\xi_2) = \psi_1(\xi_1)\psi_2(\xi_2)$ | $\alpha^8 = (1,2)$ |
| $\Psi_9(\xi_1,\xi_2) = \psi_3(\xi_2)$ | $\alpha^9 = (0,3)$ |

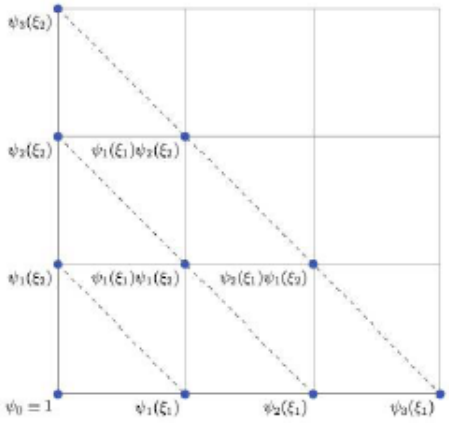


**Figure 3.6: a) Basis of multivariate Polynomial Chaos for M=2, p=3 b) Graphical representation of bivariate tensor product (Source: Alexanderian, A, 2013)**

We can now write our response as follows:

$$U = \sum_{\alpha \in \mathbb{N}^M} u_\alpha \psi_\alpha \left( S \right) \tag{3.32}$$

Figure 3.7 shows the multivariate orthogonal polynomials for a Gaussian distribution.

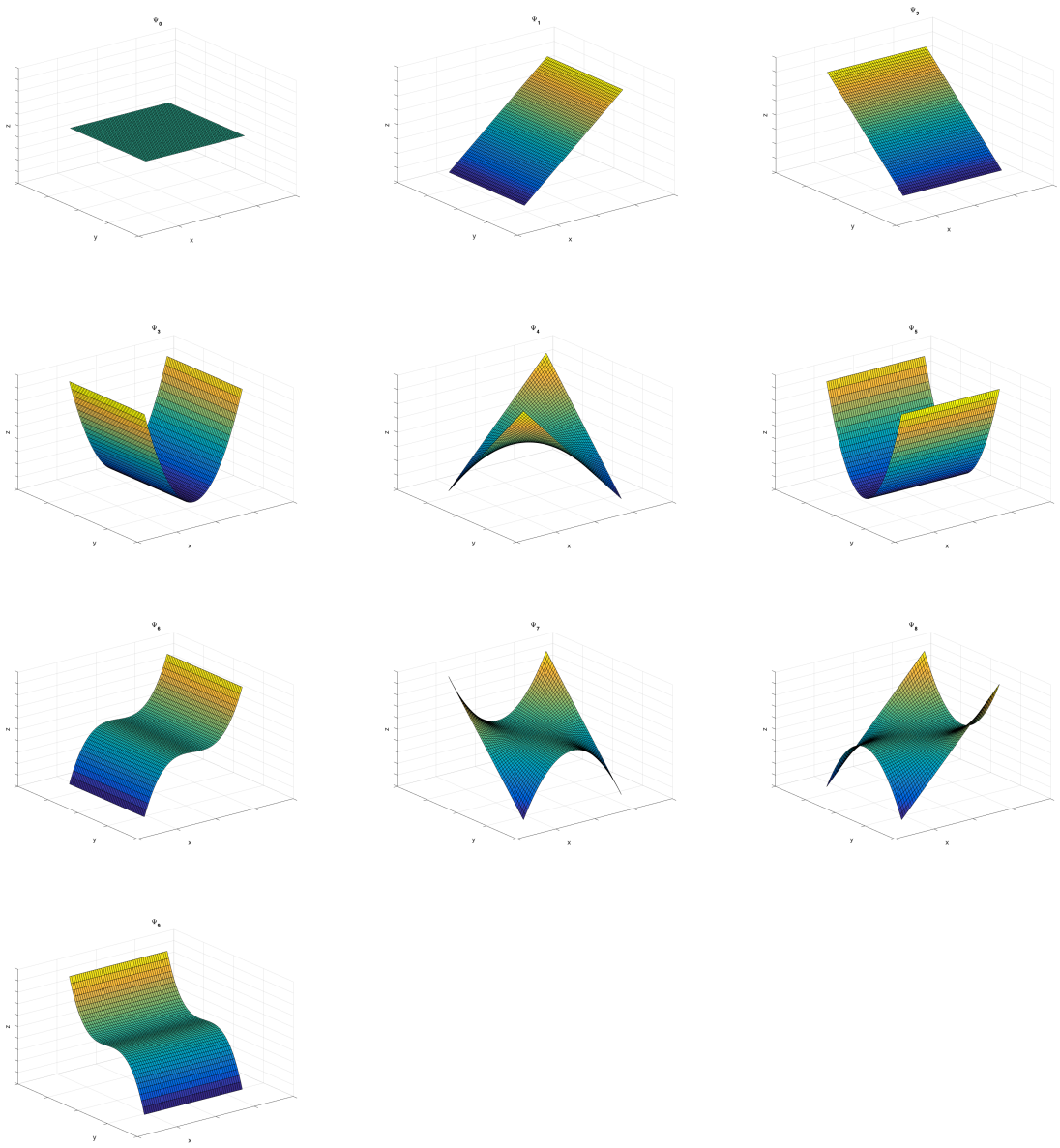

**Figure 3.7: Polynomial Chaos functions (Normalized multivariate Hermite polynomials) of order 3 and dimension 2**

### 3.2.6 Truncation scheme

From the representation of the mechanical response, $U$, it is computationally appealing to truncate the infinite series to a finite number of terms. In this light, the aim is to find an acceptable number of terms such that the representation offers an accurate depiction of the random response. Since we have a series, which consists of polynomials, it is natural

to consider a truncated series of all polynomials up to a specific degree. Let's define the total degree of a multivariate polynomial $\psi_\alpha$ by:

$$|\alpha| = \sum_{i=1}^{M} \alpha_i \tag{3.33}$$

The standard truncation scheme involves choosing all polynomials such that $|\alpha|$ is smaller than a given $p$, which leads us to having a combination of $p$ polynomials chosen from $M+p$ possibilities. $M$ is the number of independent components of the input random vector (number of basis random variables used in higher order terms of the *KL* expansion) and $p$ is the order of the *Polynomial Chaos*. Therefore the number of terms $P$ in the series is given by:

$$P = \begin{pmatrix} M+p \\ p \end{pmatrix} = \frac{(M+p)!}{M!p!} \tag{3.34}$$

In practical applications, the polynomial degree $p$ is in the range of 3-5. Increasing the value of $M$ results in a better resolution of the input random fields. Moreover, due to the rate at which $P$ increases for higher values of $M$, say $M>10$, a new complication known as the curse of dimensionality becomes apparent. Table 3.3 shows the size $P$ of the polynomial basis for different values of $M$ and $p$.

**Table 3.3: Total number of terms in the Polynomial Chaos Expansion for varying values M and p**

| **M** \ **p** | **1** | **2** | **3** |
|---|---|---|---|
| **1** | 2 | 3 | 4 |
| **2** | 3 | 6 | 10 |
| **3** | 4 | 10 | 20 |

### 3.2.7 Stochastic Finite Element Formulation

In this section, we will be following the standard energy formulation introduced by Zienckiewicz and Cheung (1977) applied to a general solid body undergoing deformation. In developing the Finite Element Formulation, we will also account for the variability of the material properties, and the uncertainty in the loads applied. Finally we will represent the random nodal displacement in the $l_2$ space.

Let a solid body with domain $L$ in $R$ have material property $S(x,\xi)$, $x \in L$. Furthermore, let a set $p$ of random external forces be exerted on part of the domain $L_p \subseteq L$. Applying the finite element method and thus discretizing the domain $L$ into "$m$" finite elements of length $l^e$, the internal energy stored in each element is given by:

$$V^e = \frac{1}{2}\int_{l^e} \sigma^e \varepsilon^e \, dl^e \tag{3.35}$$

Where $\sigma^e$ and $\varepsilon^e$ are stress and strain on the element.

Given the constitutive equations dictating the material behaviour, the internal energy stored within an element can be rewritten in terms of the displacement experienced by the element due to an external force.

$$V^e = \frac{1}{2}\left\{u^e\right\}^T \int_{l^e} \left[B^e(x)\right]^T \left[S^e(x,\xi)\right]\left[B^e(x)\right] dx \left\{u^e\right\} \tag{3.36}$$

Where $\{u^e\}$ is the vector of nodal displacements, $[B^e(x)]$ is the strain-displacement matrix, $[S^e(x,\xi)]$ is the random material property and the superscript "*e*" denotes calculations performed over the domain of an element.

Let us now formulate the internal energy of the system as the sum of the contributions of every individual element.

$$V = \sum_{e=1}^{m} V^e = \frac{1}{2} \sum_{e=1}^{m} \{u^e\}^T \int_{l^e} [B^e(x)]^T [S^e(x,\xi)][B^e(x)] dx \{u^e\} \tag{3.37}$$

In line with the standard energy formulation, we now define the external work done on an element as:

$$W^e = \{u^e\}^T \{p\} \tag{3.38}$$

In a similar fashion to obtaining the total internal energy, we seek to obtain the total external work done by summing up the contributions of every element:

$$W = \sum_{e=1}^{m} W^e = \{U\}^T \{P\} \tag{3.39}$$

Using the principle of conservation of energy and minimizing the potential energy leads to:

$$\frac{\partial(V - W)}{\partial\{U\}} = 0 \tag{3.40}$$

Defining the stiffness matrix of an element as:

$$[K^e] = \int_{l^e} [B^e(x)]^T [S^e(x,\xi)][B^e(x)] dx \tag{3.41}$$

We can then define the global stiffness matrix as:

$$\left[K\right]=\oplus\left[K^{e}\right] \tag{3.42}$$

Substituting *[K]* in our expression for the residual of the potential energy, we end up with the famous finite element formulation in its compact form shown below:

$$\left[K\right]\left\{U\right\}=\left\{P\right\}$$

We will now express the random material property as its deterministic and stochastic part.

$$S\left(x,\xi\right)=\overline{S}\cdot X\left(x,\xi\right) \tag{3.43}$$

Where $\overline{S}$ is the deterministic constitutive matrix, $X\left(x,\xi\right)$ is the random field function of the position vector x

We represent $X\left(x,\xi\right)$ using the *Karhunen-Loeve* expansion up to M terms:

$$X\left(x,\xi\right)=1+\sum_{k=1}^{M}t_{k}\sqrt{\lambda_{k}}\phi_{k}\left(x\right) \tag{3.44}$$

where $\lambda_{k}$ and $\phi_{k}$ are real positive *eigen-values* and complete orthogonal *eigen-functions* of the *covariance kernel*.

Substituting equation 3.36, 3.37 and 3.40 into 3.38 yields:

$$\left[K_{0}+\sum_{k=1}^{M}K_{k}t_{k}\left(\xi\right)\right]\cdot U\left(\xi\right)=F_{i} \tag{3.45}$$

where $K_{0}=\oplus\int_{l^{e}}\left[B^{e}\left(x\right)\right]^{T}\left[\overline{S}^{e}\left(x\right)\right]\left[B^{e}\left(x\right)\right]dx$ , and $K_{k}=\oplus\sqrt{\lambda_{k}}\int_{l^{e}}\phi_{k}\left(x\right)\left[B^{e}\left(x\right)\right]^{T}\left[B^{e}\left(x\right)\right]dx$

It is assumed that the force and the nodal displacements are Gaussian processes. Hence $t_k$ is a standard normal variable and the parameter $\xi$ is used to differentiate random parameters from deterministic ones. The subscript "*i*" was also added for instances of non-deterministic forces. $F_i = \vec{0}$ for i > 0 represents the case of deterministic loading.

We proceed by expanding the vector of nodal displacements as follows:

$$U(\xi) = \sum_{j=0}^{P} U_j \psi_j(\xi) \tag{3.46}$$

Recall that $\psi_j(\xi)$ are *Polynomial Chaos* functions also known as *Wiener Chaos* satisfying the following properties:

$$\psi_0 \equiv 1 \tag{3.47-a}$$

$$E[\psi_j] = 0 \tag{3.47-b}$$

$$E[\psi_j(\xi)\psi_k(\xi)] = 0 \tag{3.47-c}$$

Due to the truncation scheme adopted, the residual after substituting equation 3.46 in 3.45 reads:

$$\varepsilon_{M,P} = \sum_{k=0}^{M} \sum_{j=0}^{P-1} K_k \cdot U_j t_k(\xi) \cdot \psi(\xi) - F_i \tag{3.48}$$

In order to find the best approximation of the exact solution $U(\xi)$ in the *Hilbert space* of *random functions*, spanned by the complete set of orthonormal functions $\{\psi_j\}_{j=1}^{P-1}$, the residual is minimized in a *mean square* sense. Such a minimization is akin to having the

residual be orthogonal to the space spanned by the polynomial functions $\left\{\psi_j\right\}_{j=1}^{P-1}$. In other words we have the inner product of the residual and the *Polynomial Chaos* functions satisfy:

$$E\left[\varepsilon_{M,P}\cdot\psi_j\right]=0 \quad \text{j=0,...P-1} \tag{3.49}$$

As a result, equation 3.48 can be rewritten as:

$$\sum_{k=1}^{M}\sum_{j=0}^{P-1}c_{kji}K_k\cdot U_j=F_i \tag{3.50}$$

Where $c_{kji}=E\left[t_k\psi_j\psi_i\right]$ and $F_i=E\left[\psi_i F\right]$

This *mean square* minimization is also known as the *regression method*. Since the computational model i.e the finite element model is essentially unaltered in finding the coefficients $c_{ijk}$, the method is said to be non-intrusive.

The final form of the equation as shown above contains *P-1* vectors of size *N* where *N* is equal to the total number of degrees of freedom of the system (# of nodes x dof/node) for $U_j$ and a stiffness matrix that is cast as a linear system of size $NP\times NP$. A visual representation of the global linear system for *M = 2* and different degrees of the *Polynomial Chaos* is shown in figure 3.8.

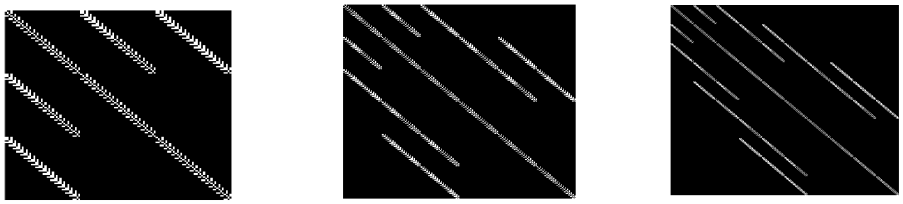

**Figure 3.8: Sparse global linear system for a) M=2, p=1, b) M=2, p=2, c) M=2,p=3**

From the derivation of the mechanical response, it comes to no surprise that the global linear system is symmetric. This is a result of the orthogonal property of the *Polynomial Chaoses*. What is less evident from our system of equations is the resulting sparse matrix. The coefficients formed from the expectation of the product of orthogonal functions effectively yield numerous zero values. We interpret the off-diagonal values of the global stiffness matrix as the white noise introduced in the system. On the other hand, the diagonal values of the matrix represent the mean properties of the system. Increasing the polynomial order "*p*" therefore not only increases the size of the global matrix but also introduces higher order noise terms in our model.

## 3.3 Validation and Results

In the given non-intrusive method, the computational model, and the uncertainty propagation stand alone as individual engines. This implies that the solutions to our problems are highly dependent upon the validity of the computational model regardless of the uncertainties introduced. In this section, the computational model, and the stochastic finite element method is validated for each case.

### 3.3.1 Deterministic Finite Element validation

As a primer, we validate the finite element code developed for the three pile problems. In each case, the pile is idealized using a *Winkler* model, which establishes a linear relationship between the force on the foundation and the resulting deflection. We verify the accuracy of the numerical solution by using the mean parameters as input to our models and we compare the FEM solution of each case to their analytical counterparts where applicable.

**Case 1**:

Case 1 entails a beam resting on an elastic foundation and subjected to a uniform load acting along its entire length. This configuration depicts the well-known uniform beam on *Winkler* foundation whose governing equation is given by:

$$EI\frac{d^4u}{dx^4}+ku=q \tag{3.51}$$

where *EI* is the beam's bending rigidity, *k* is the spring stiffness and *q* is a uniform load. We are now interested in applying the Finite element method to the above equation. This is accomplished by transforming the governing ordinary differential equation (ODE) into its weak form. To obtain the weak form of the above equation, we integrate the weighted residual of equation 3.51 over the domain L as follows:

$$\int_0^L\left(\frac{d^2We}{dx^2}\cdot EI\cdot\frac{d^2u}{dx^2}+We\cdot k\cdot u\right)dx=\int_0^L We\cdot q\,dx+M*\left.\frac{dWe}{dx}\right|_{x=L}+S*We\Big|_{x=L} \tag{3.52}$$

where *We* is a weight function and *M** and *S** are the moment and shear acting at the end of the beam. In case 1, *M* = 0* kNm and *S* = 0 kN*.

Since we are dealing with a beam with free-ends, the boundary conditions are given by:

$$M\Big|_{x=0} = EI\frac{d^2u}{dx^2}\Big|_{x=0} = 0 \tag{3.53-a}$$

$$M\Big|_{x=L} = EI\frac{d^2u}{dx^2}\Big|_{x=L} = 0 \tag{3.53-b}$$

Using Galerkin's method, we substitute the weight function and response function with $C^3$ shape functions and obtain the following system of linear equations:

$$\bigoplus_e \left[ \int_{x_i}^{x_{i+1}} \left( \left[ \left( \frac{d^2N_i(x)}{dx^2} \right) EI \left( \frac{d^2N_j(x)}{dx^2} \right) + N_i(x) k N_j(x) \right] dx \right) u_i \right] = \bigoplus_e \left[ \int_{x_i}^{x_{i+1}} N_i(x) q\, dx \right] \tag{3.54}$$

where the shape functions $N_i$ are cubic Hermite polynomials with $L_e$ representing the length of an element, $x_{i+1}$-$x_i$.

$$N = \begin{Bmatrix} \frac{1}{L_e}\left(2x^3 - 3x^2L_e + L_e^3\right) \\ \frac{1}{L_e^3}\left(x^3L_e - 2x^2L_e^2 + xL_e^3\right) \\ \frac{1}{L_e^3}\left(-2x^3 + 3x^2L_e\right) \\ \frac{1}{L_e^3}\left(x^3L_e - x^2L_e^2\right) \end{Bmatrix} \tag{3.55}$$

To validate the FEA solution to case 1, we use the closed form solution derived by M.Hetenyi in 1946 (Hetenyi, 1946). The particular closed-form used is one which was originally derived for symmetrically placed uniformly distributed loading on free-end beams.

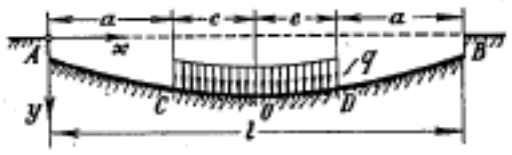


**Figure 3.9: Response of a free-end beam on elastic foundation under a uniformly distributed load (Source: Hetenyi, 1946)**

The deflection line for portion A-C ($x<a$) is given by:

$$y_{A-C}=\frac{q}{k}\frac{1}{\mathrm{Sinh}(\lambda l)+\sin(\lambda l)}\Big[\mathrm{Cosh}(\lambda x)\cos(\lambda x)\Big[\mathrm{Cosh}(\lambda a)\sin\big(\lambda(l-a)\big)$$
$$-\mathrm{Sinh}(\lambda a)\cos\big(\lambda(l-a)\big)+\cos(\lambda a)\mathrm{Sinh}\big(\lambda(l-a)\big)-\sin(\lambda a)\mathrm{Cosh}\big(\lambda(l-a)\big)\Big] \quad (3.56)$$
$$+\big(\mathrm{Cosh}(\lambda x)\sin(\lambda x)+\mathrm{Sinh}(\lambda x)\cos(\lambda x)\big)\Big[\sin(\lambda a)\mathrm{Sinh}\big(\lambda(l-a)\big)-\mathrm{Sinh}(\lambda a)\sin\big(\lambda(l-a)\big)\Big]\Big]$$

The deflection line for portion C-D is given by:

$$y_{C-D}=\Big[y_{A-C}\Big]_{X>0}+\frac{q}{k}\Big[1-\mathrm{Cosh}\big(\lambda(x-a)\big)\cos\big(\lambda(x-a)\big)\Big] \quad (3.57)$$

where $\lambda=\sqrt[4]{\frac{k}{4EI}}$ and to mimic case 1 loading condition, we set *a = 0,* such that *c = l/2*.

The mean parameters used in the deterministic finite element model and Hetenyi's solution are shown in table 3.4.

**Table 3.4: Deterministic properties of soil and beam for validation of case 1**

| **Beam and Soil Parameters for Model Validation** | |
|---|---|
| **EI [Nm$^2$]** | 8.33E+07 |
| **k [N/m$^3$]** | 6.00E+05 |
| **q [N]** | -5.00E+04 |
| **l [m]** | 8 |
| **n** | 200 |

Figure 3.10 shows the displacement of case 1 using the FE solution versus Hetenyi's closed-form solution.

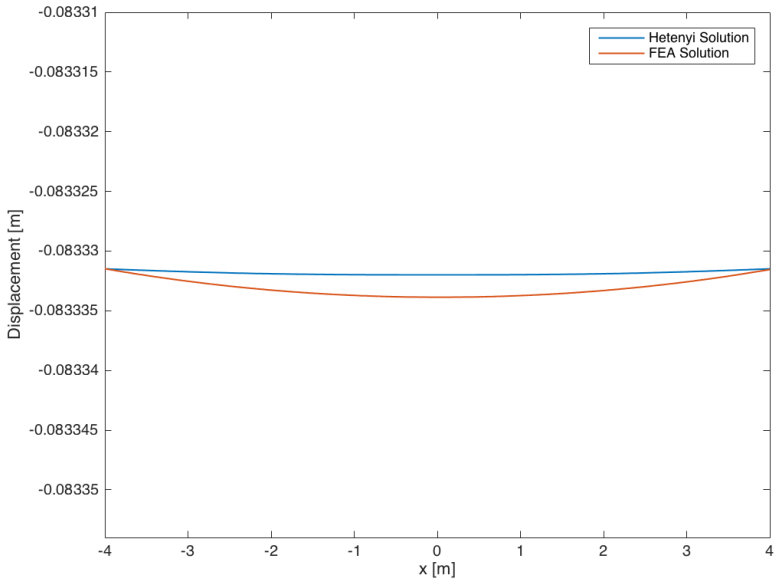


**Figure 3.10: Deterministic deflection of case 1**

It is clear that the FE solution is in good agreement with Hetenyi's solution with *0.000013%* error at the beam's ends and *0.00098%* error at the beam's mid-span.

**Case 2**:

Case 2 is a laterally loaded beam fixed at one end and resting on an elastic foundation. Once more a Winkler model is adopted with the following governing equation:

$$EI\frac{d^4u}{dx^4}+ku=P\delta\left(x\right) \tag{3.58}$$

where δ(x) is the *Kronecker delta* function which assumes a value of 1 *at x = 0* and *P* is a point load applied at the free end of the beam.

Similarly to case 1, the weak form of the governing ODE can be obtained by integrating the weighted-residual of equation 3.58. We note that the stiffness matrix formed from the integration on the left hand side of the discretized weak form remains unchanged from equation 3.54. Only the forcing vector changes as follows:

$$f^e = \int_{x_i}^{x_{i+1}} P\delta(x) N_i(x) dx \tag{3.59-a}$$

$$F = \bigoplus_e f^e \tag{3.59-b}$$

The closed-form solution is taken from Hetenyi's analysis of a cantilever beam resting on elastic foundation.


**Figure 3.11: Response of Cantilevered beam under a point load (Source: Hetenyi, 1946)**

The deflection line is given by:

$$y = \frac{2P\lambda}{k} \frac{\text{Sinh}(\lambda x)\cos(\lambda x')\text{Cosh}(\lambda l) - \sin(\lambda x)\text{Cosh}(\lambda x')\cos(\lambda l)}{\text{Cosh}^2(\lambda l) + \cos^2(\lambda l)} \tag{3.60}$$

The beam and soil parameters used for case 2 are the same as those used in case 1 as shown in table 3.5:

**Table 3.5: Deterministic properties of soil and beam for validation of case 2**

| Beam and Soil Parameters for Model Validation | |
|---|---|
| **EI [Nm$^2$]** | 8.33E+07 |
| **k [N/m$^3$]** | 6.00E+05 |
| **P [N]** | -5.00E+04 |
| **l [m]** | 8 |
| **n** | 200 |

Figure 3.12 shows the deflection of case 2 using the FE solution vs Hetenyi's closed-form solution.

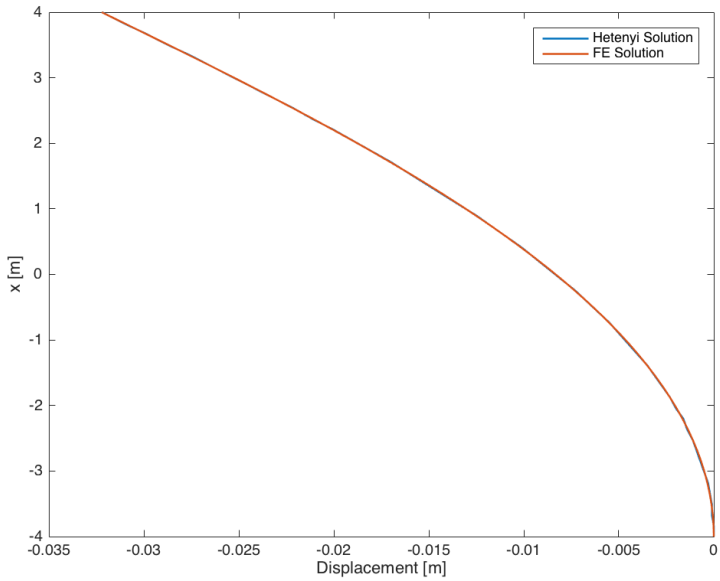


**Figure 3.12: Deterministic deflection of case 2**

The result of the FE solution remains in good agreement with that of Hetenyi's solution with *4.28E-07%* error at the free end.

**Case 3:**

In case 3 we have an axially loaded column fixed at one end and with springs providing resistance against the applied vertical force. The governing equation of case 3 is given by:

$$AE\frac{d^2u}{dx^2}-ku=0 \tag{3.61}$$

with the following boundary conditions:

$$-AE\left.\frac{du}{dx}\right|_{x=0}=P \tag{3.62-a}$$

$$u\big|_{x=L}=u^*=0 \tag{3.62-b}$$

where $AE$ is the axial rigidity of the column, $P$ is a vertical load applied at the free-end and $k$ is still the spring stiffness.

This time the weak form of the governing ODE is given by:

$$-\int_0^L\left[\frac{dWe}{dx}\cdot AE\cdot\frac{du}{dx}+We\cdot k\cdot u+We\cdot p\right]dx+We\cdot P\big|_{x=0}=0 \tag{3.63}$$

where $We$ are weight functions and $p = 0$ when no uniform load is applied.

Using Galerkin's method and substituting the weight and response functions in the equation above with $C^1$ shape functions, we obtain:

$$\bigoplus_e\left[-\left[\int_{x_i}^{x_{i+1}}\left(\frac{dN_i(x)}{dx}AE\frac{dN_j(x)}{dx}+N_i(x)kN_j(x)\right)dx\right]u^e-\int_{x_i}^{x_{i+1}}N_i(x)p\,dx\right]-P=0 \tag{3.64}$$

We choose the shape functions $N_i$ to be linear Lagrange functions with $L_e$ once more representing the length of an element.

$$N = \begin{Bmatrix} 1 - \dfrac{x}{L_e} \\ \dfrac{x}{L_e} \end{Bmatrix} \tag{3.65}$$

For case 3, equation 3.61 was solved analytically and the following deflection was obtained:

$$y = \left( \frac{-P/AE}{\lambda + \lambda e^{2\lambda L}} \right) e^{\lambda x} + \left( \frac{\left(P/AE\right) e^{2\lambda L}}{\lambda + \lambda e^{2\lambda L}} \right) e^{-\lambda x} \tag{3.66}$$

The column and soil parameters used for the validation of case 3 are summarized in the table 3.6:

**Table 3.6: Deterministic properties of soil and beam for validation of case 3**

| **Column and Soil Parameters for Model Validation** | |
|---|---|
| **AE [N]** | 7.45E+08 |
| **k [N/m$^3$]** | 6.00E+04 |
| **P [N]** | -5.00E+05 |
| **l [m]** | 8 |
| **n** | 200 |

Figure 5.13 shows the deflection of case 3 using the FE solution vs the developed analytical solution.

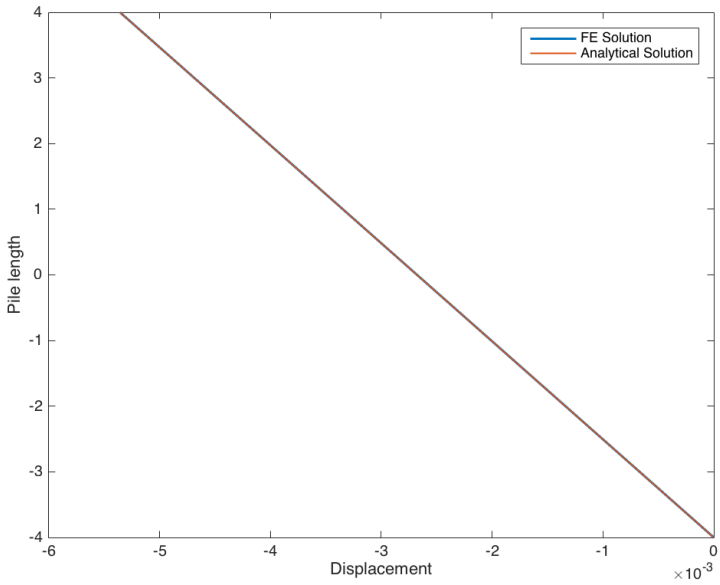


**Figure 3.13: Deterministic deflection of case 3**

The FE solution in case 3 is remarkably close to the exact solution. We note an error of $10^{-8}$ % at the free-end.

### 3.3.2 Solution Algorithm

All the components to solve the three cases with random beam and soil parameters have now been presented. In this section we present a flow diagram of the implementation of the Stochastic Finite Element method. Spatially random parameters in each case have their random fields represented using a *Karhunen-Loeve* expansion and the response function is represented using a *Polynomial Chaos* expansion. For each case, the spatially *random parameters* are assumed to have an *exponential covariance* structure and are assumed to be Gaussian processes. This method originally developed by Ghanem and Spanos, (1991) boasts a fast computational time compared to the *Monte Carlo* method and an accurate probabilistic depiction of simple models.

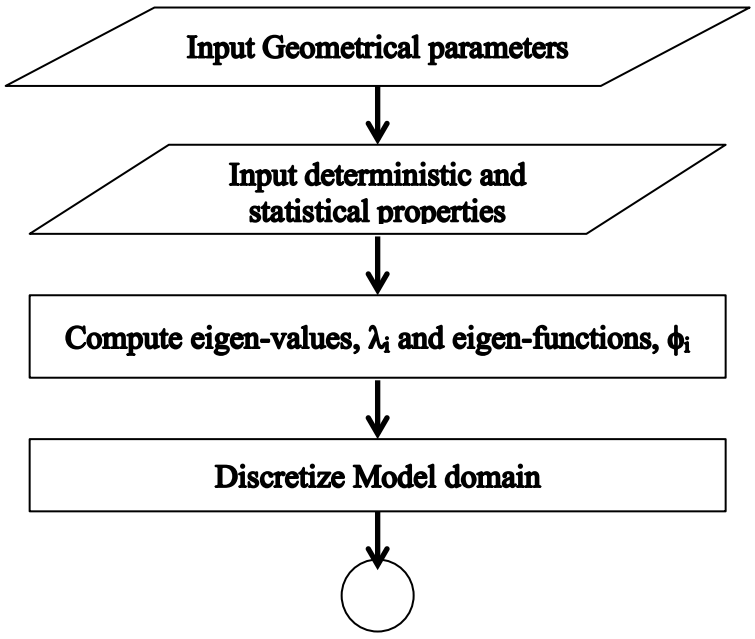


**Figure 3.14: Flowchart of implementation of SFEM**

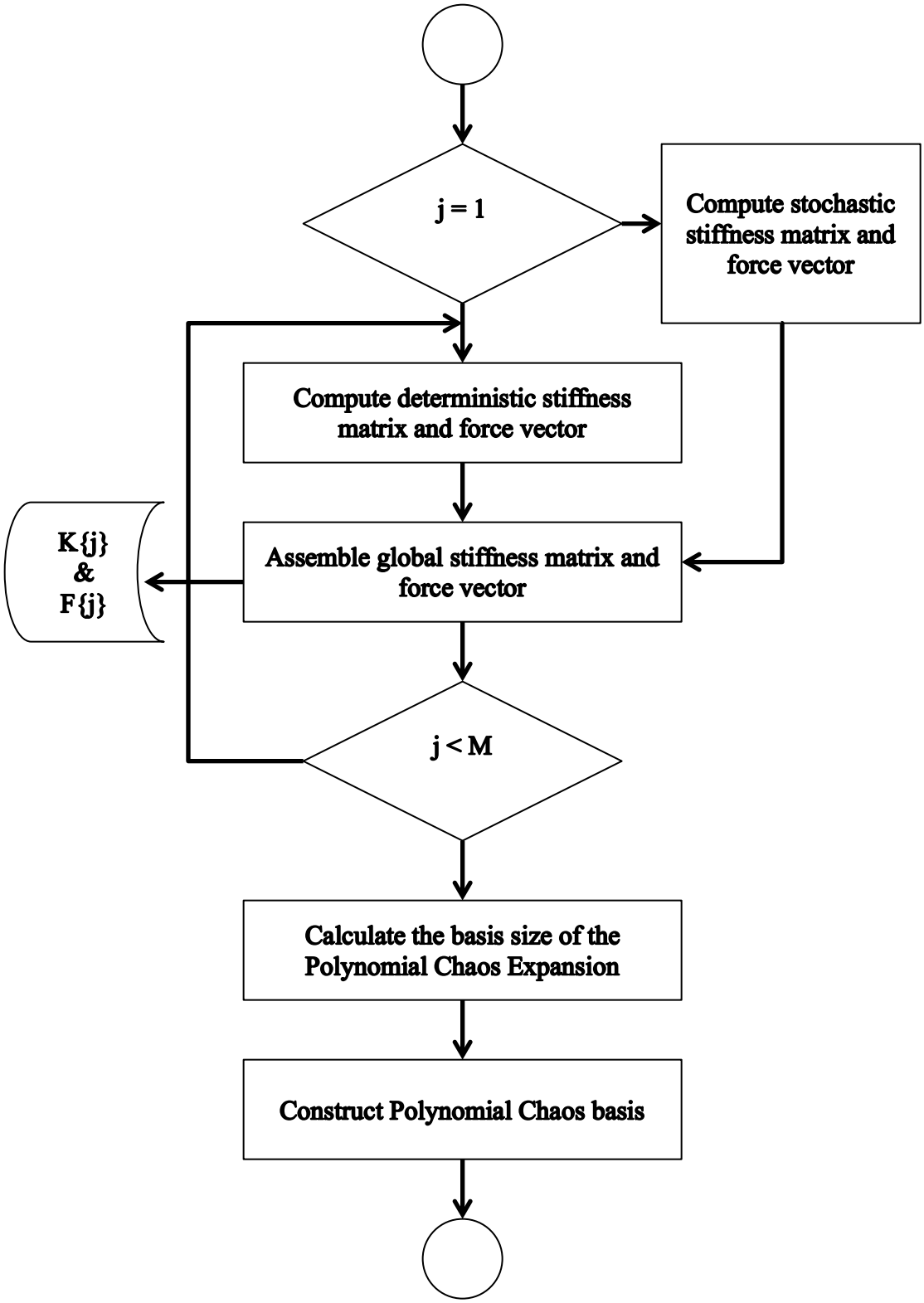


**Figure 3.14: Flowchart of implementation of SFEM (Continued)**

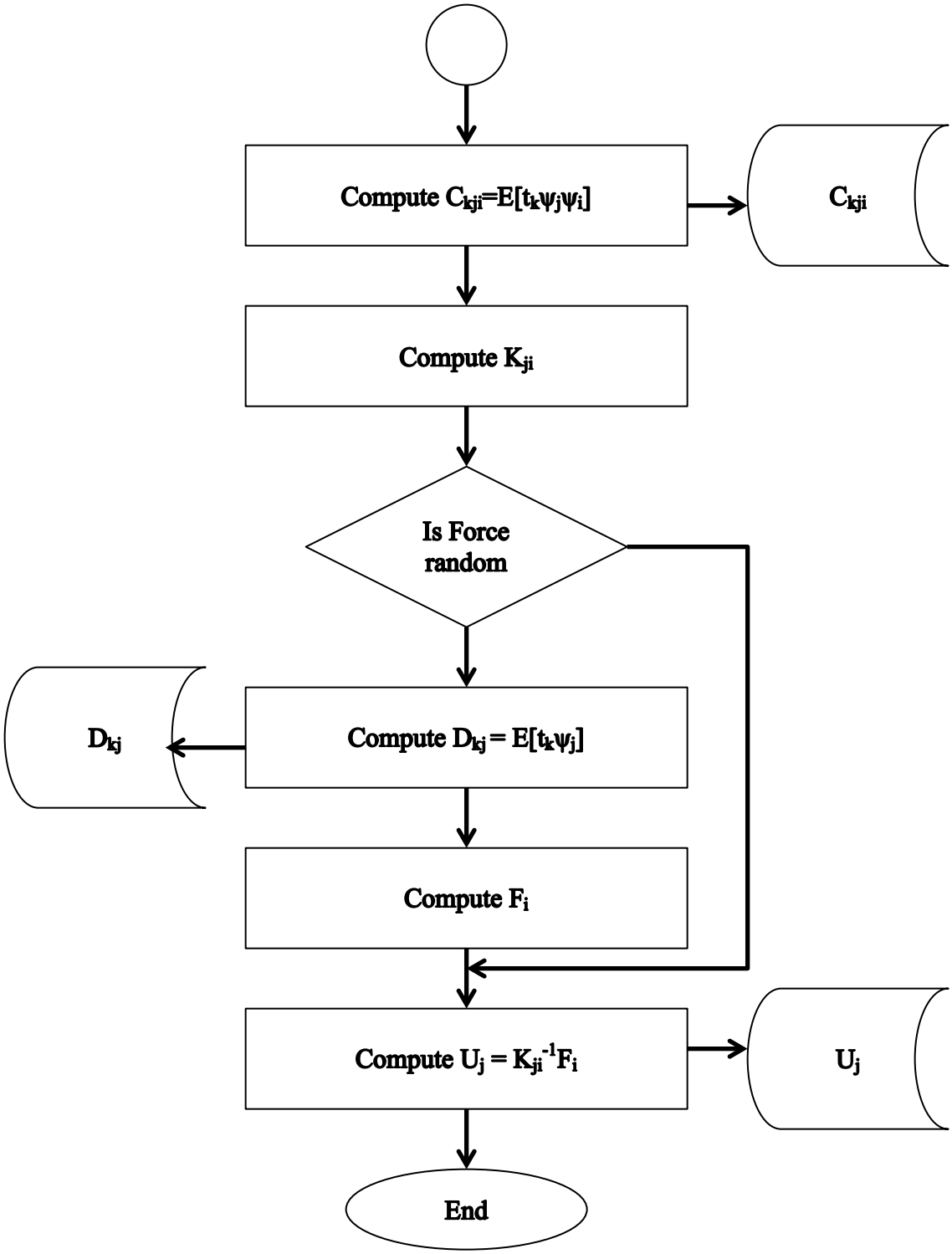


**Figure 3.14: Flowchart of implementation of SFEM (Continued)**

### 3.3.3 Numerical implementation

Having confirmed the validity of the Finite Element code developed, the Stochastic Finite element method laid out previously is now applied to our three cases. The accuracy of the results obtained with the Stochastic Finite Element method for each case is checked against a *Monte Carlo* simulation and the efficiency of each approach compared in terms of their respective runtime.

**Case 1**:

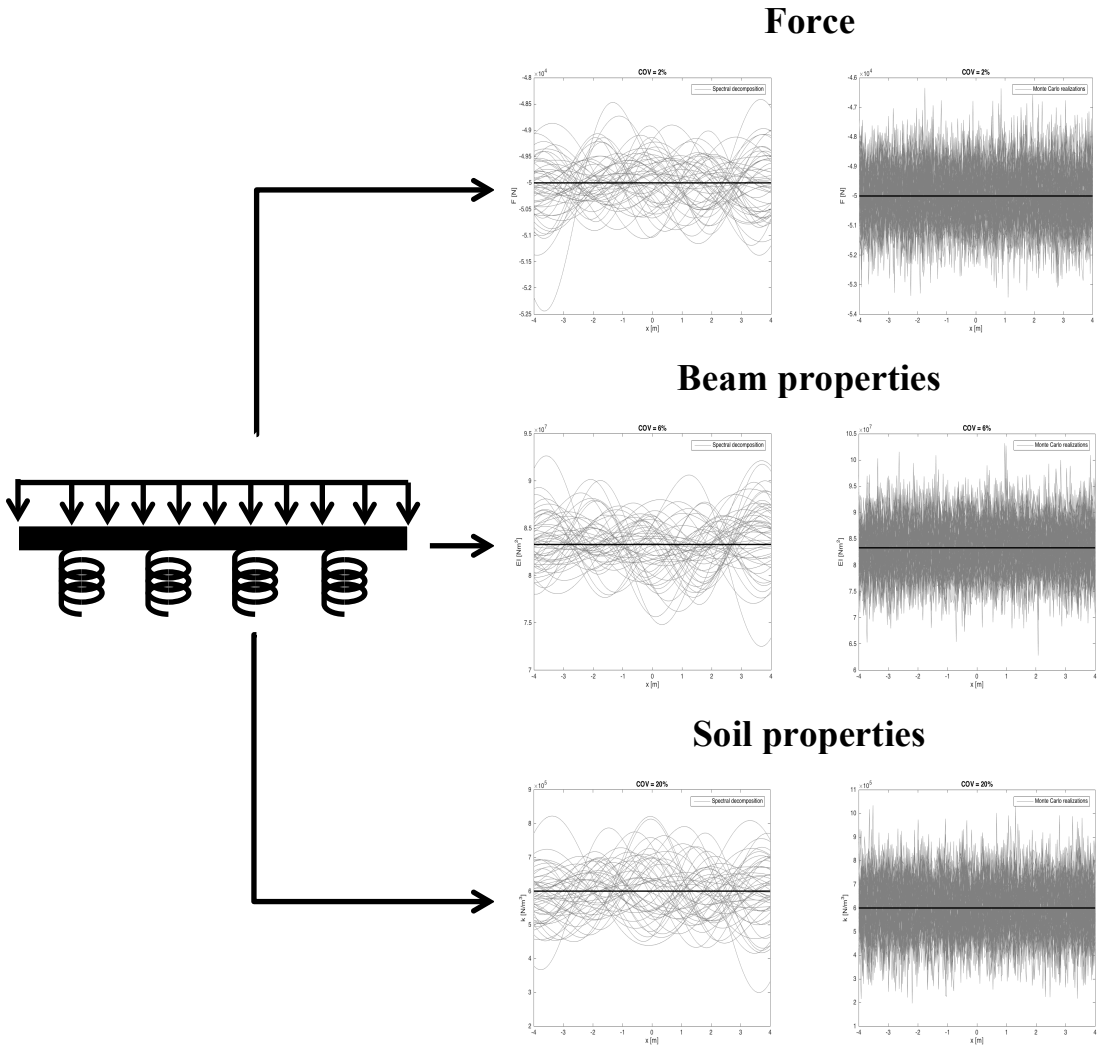


**Figure 3.15: KL expansion of random fields vs random sampling for Monte Carlo for Case 1**

In figure 3.15, we see the *random realizations* of each *random parameters* of case 1 using the *KL* expansion versus using a random sampling method for a *Monte Carlo* simulation. We automatically note the difference in the smoothness of the realizations of each method. The kinks and fluctuations in the *KL* representation are controlled by the order of the expansion and the correlation length. Using a series approximation such as the *KL* expansion, a bandwidth the size of the variance becomes apparent with sufficient number of realizations. On the other hand, a random sampling at each discretized node generates a triangular or saw tooth like realization with more outliers. We draw the reader's attention to the fact that if the material properties and the load are assumed to be ergodic, the mean can be obtained from a single realization. This becomes accurate for a discretized domain with a mesh much smaller than that of the correlation length and with enough terms in the series expansion. The addition of more terms in the series compensate for a larger sample size. Table 3.7 summarizes the statistical properties of each of the random parameters.

**Table 3.7: Statistical moments of soil and pile properties for Case 1**

| **Beam and Soil Statistical parameters** | |
|---|---|
| **COV = 6%** | |
| **<EI> [Nm$^2$]** | 8.33E+07 |
| **Std.dev[EI] [Nm$^2$]** | 4.99E+06 |
| **COV = 20%** | |
| **<k> [N/m$^3$]** | 6.00E+05 |
| **Std.dev[k] [N/m$^3$]** | 1.20E+05 |
| **COV = 2%** | |
| **<q> [N]** | -5.00E+04 |
| **Std.dev[q] [N]** | 1.00E+03 |

**Case 2**:

For case 2, the same assumptions are made with regards to the *KL* expansion and a random sampling method is again used as benchmark for comparison purposes.

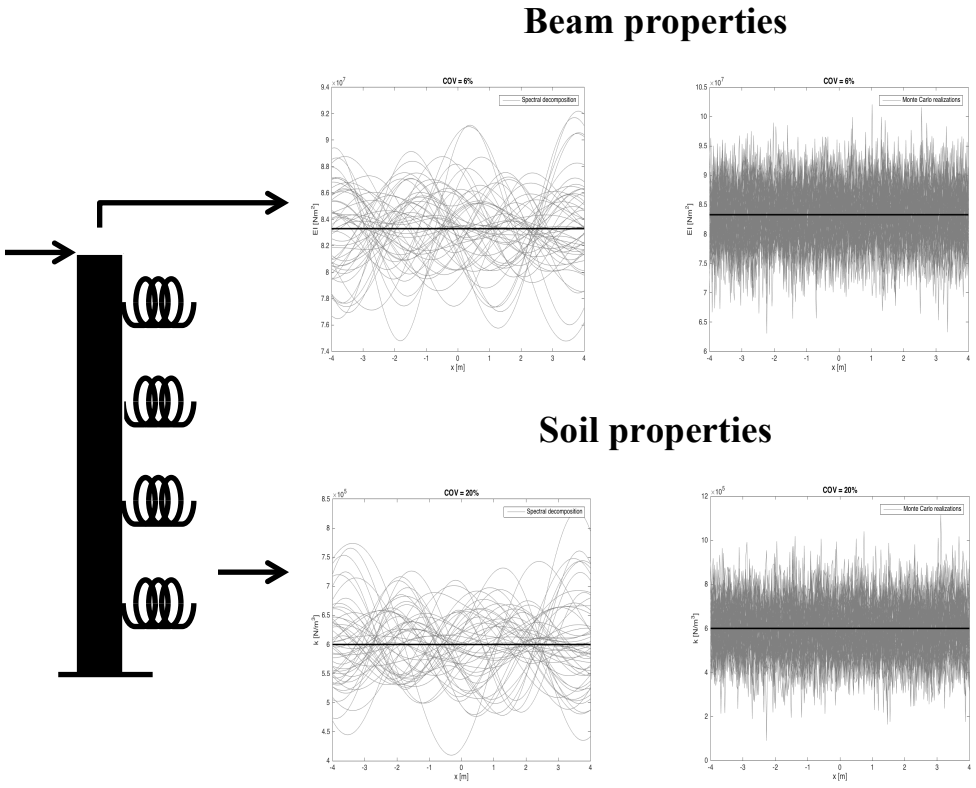


**Figure 3.16: KL expansion of random fields vs random sampling for Monte Carlo for Case 2**

In case 2 since we are dealing with a point load, only the beam properties and the soil properties display spatial variation. Table 3.8 summarizes the statistical properties of each of the random parameters for case 2.

**Table 3.8: Statistical moments of soil and pile properties for Case 2**

| Beam and Soil Statistical parameters | |
|---|---|
| **COV = 6%** | |
| **<EI> [$Nm^2$]** | 8.33E+07 |
| **Std.dev[EI] [$Nm^2$]** | 4.99E+06 |
| **COV = 20%** | |
| **<k> [$N/m^3$]** | 6.00E+05 |
| **Std.dev[k] [$N/m^3$]** | 1.20E+05 |

It should be noted that the *correlation length* of each of the parameters can be accounted for in the random sampling method through the use of an auto-regressive filter.

**Case 3**:

In case 3, it is the column's axial rigidity and the spring's stiffness that exhibit spatial variability. The figure 3.17 shows the random fields of case 3.

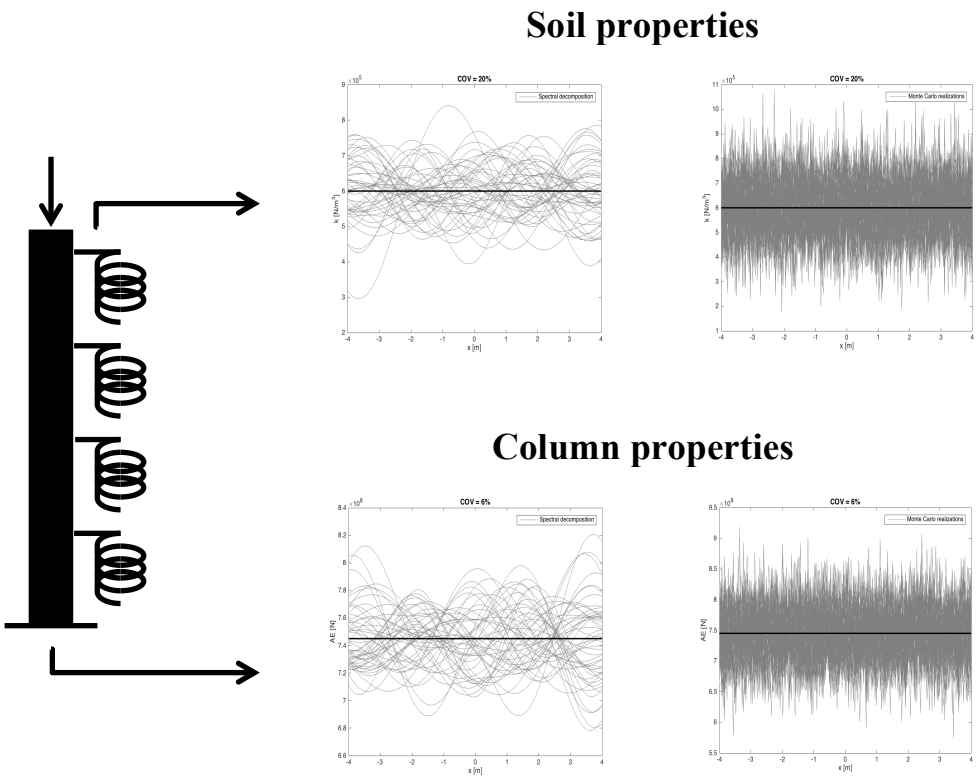


**Figure 3.17: KL expansion of random fields vs random sampling for Monte Carlo for Case 3**

Table 3.9 summarizes the statistical properties of axial rigidity of pile and the soil stiffness for Case 3.

**Table 3.9: Statistical moments of soil and pile properties for Case 3**

| **Column and Soil Statistical parameters** | |
|---|---|
| **COV = 6%** | |
| **<AE> [N]** | 7.45E+08 |
| **Std.dev[EI] [Nm$^2$]** | 4.47E+07 |
| **COV = 20%** | |
| **<k> [N/m$^3$]** | 6.00E+05 |
| **Std.dev[k] [N/m$^3$]** | 1.20E+05 |

### 3.3.4 Response statistics

Using the results of the SFEM, it is now possible to provide a statistical description for the three cases introduced at the beginning of this chapter. The first and second statistical moments, which are the mean and variance, are easily obtained from the orthonormality of the polynomial basis. The mean is in fact the first term of the response expansion:

$$E\left[U\left(\xi\right)\right]=E\left[\sum_{j=0}^{P-1}U_j\psi_j\right]=U_0 \tag{3.67}$$

The variance on the other hand is given by the sum of the squared coefficients of the expansion written as:

$$Var\left[U\left(\xi\right)\right]=E\left[\left(U\left(\xi\right)-U_0\right)^2\right]=\sum_{j=1}^{P-1}U_j^2 \tag{3.68}$$

The applications of SFEM in geotechnical problems are numerous. It gives its user an insight in the fundamental causes of variability in the response of soil-structure interactions and by extension the mechanics at play. But the strength of the SFEM lies in its computational efficiency. With a ten term (*P = 10*) PCE, more specifically a random input expanded up to the second term and Polynomial Chaos of order 3, the SFEM executed at a speed eighteen times (18X) faster than the RFEM for Case 1. The performance of the SFEM was nine times (9X) faster for Case 2 and twenty-seven times (27X) faster for Case 3. The figures below show the statistics of the piles.

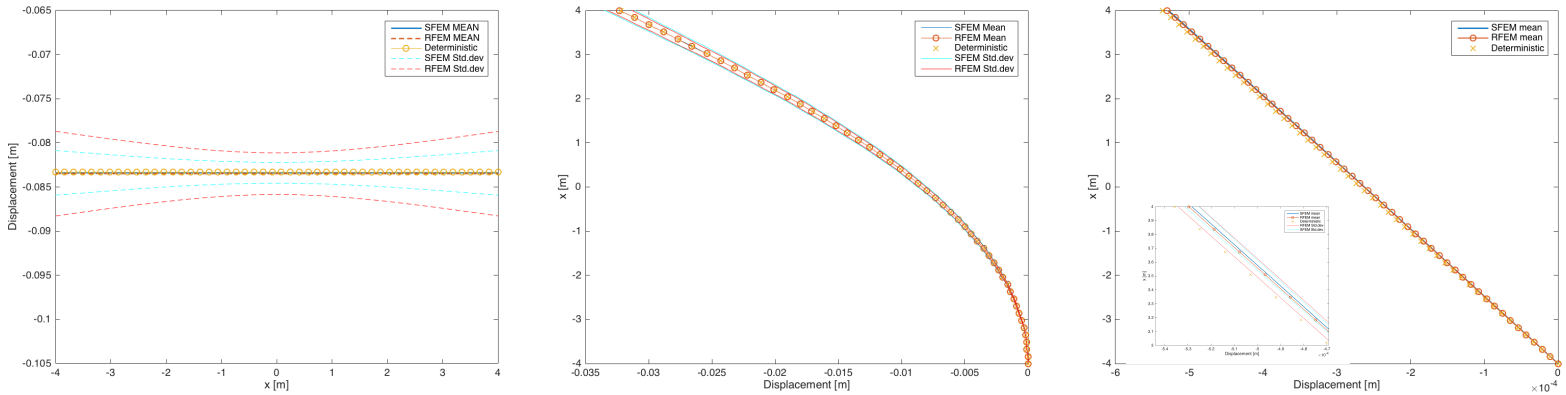


**Figure 3.18: SFEM Mean vs MC Mean for deflection of Case 1, 2 and 3**

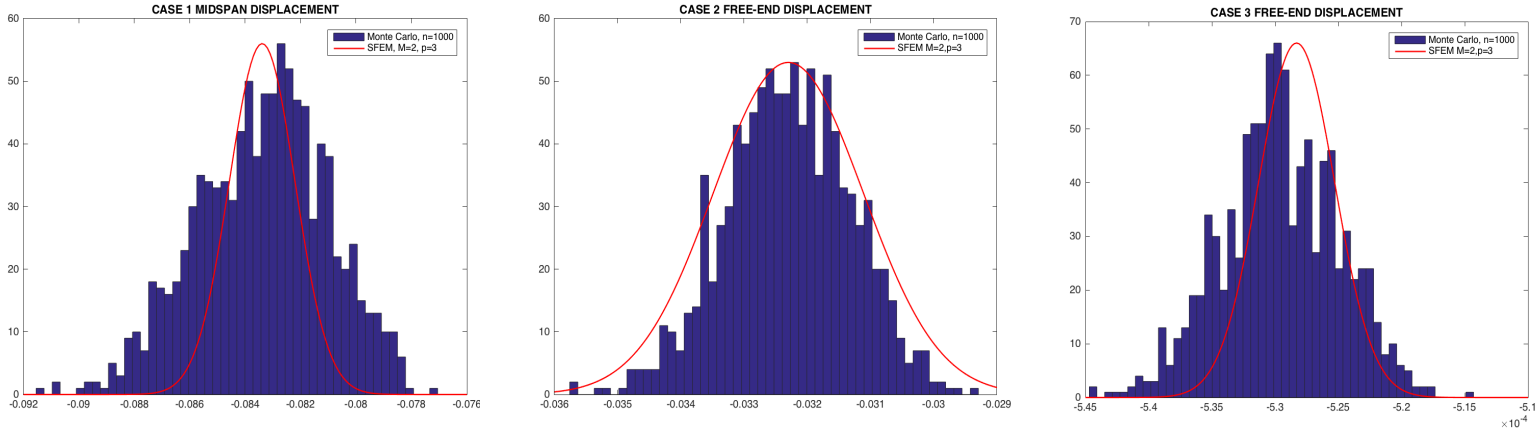


**Figure 3.19: SFEM pdf vs MC pdf of $u_{max}$ for Case 1, 2 and 3**

Looking at the statistics of the response in each case, we note a few noticeable differences. The most prevalent disparity is in the magnitudes of the standard deviation for each case. While it is obvious that the case with the most uncertainty is expected to yield the response with the highest standard deviation, it is not apparent which system would behave more unpredictably if the variance of the input variable were not known a priori. From the results obtained, it is clear that case 1 presents the highest degree of randomness. This can be attributed to the fact that the uniformly distributed load applied along the pile's length is itself spatially random, thus introducing an additional element of variability to the problem. However, investigating case 2 and 3, it is not evident why their standard deviations would differ by magnitudes of the order of $10^2$. In both cases, the same properties were assumed random with the same coefficients of variation. The loading condition for each case, however, differs drastically in that case 2 has a lateral load acting at the pile's head while in case 3, a vertical load is applied at the pile's head. Such behaviour suggests that the orientation of the line of action of the force impacts the variance of the response. This can be explained from the standpoint of the alignment of fibers in a material. Given the slenderness of the body under investigation, it is clear that the action of a force collinear to the longer face of the pile will have a lesser impact on the response's variability. The random material property at each node averages out over longer spans thus making the problem in a way more deterministic.

Also of interest is the accuracy of the mean obtained by the SFEM compared to the RFEM, which relies on *Monte Carlo* simulations with large sample sizes. In each case, the results of the SFEM with inputs expanded up to two terms and chaos polynomial of

order three is in good agreement with results from the *Monte Carlo* simulations. The SFEM mean of each case is within one standard deviation from its RFEM counterpart. Case 2 in particular shows almost identical response statistics as that of the RFEM. Once more, we suspect the mechanics at play affects the statistical behaviour of the system. In both cases 2 and 3 the slight difference in the means could be associated with the number of random nodes under the direct or indirect action of a force. Although this time the orientations of the line of action of the forces are perpendicular to each other, all the "random" nodes are under the direct action of a force. Unlike in case 2 where only the first node is subjected to a force.

We are now interested in knowing the influence of increasing the order of the *Polynomial Chaos* on the mean of the response. Intuitively we expect to see the convergence of the mean function in the *mean square* (Rahman, 2017). The proof is provided below:

**Proof**: Let $\mathbf{X} := (X_1,\ldots,X_N)^T : \left(\Omega,F\right)\to\left(\mathbb{R}^N,B^N\right), N\in\mathbb{N}$, be an $\mathbb{R}^N$-valued Gaussian random vector with zero mean; *symmetric, positive definite covariance matrix* $C_X$ and *multivariate probability density function* $\phi_X(x;C_X)$.

if , $u\left(x\right)\in L^2\left(\mathbb{R}^N,B^N,\phi_X dx\right)$ then the expansion of *u(x)* can be written as:

$$u\left(x\right)\sim\sum_{l\in N_0} proj_l u\left(x\right) \tag{3.69}$$

where $proj_l u\left(x\right): L^2\left(\mathbb{R}^N,B^N,\phi_X dx\right)\to v_l^N$ denotes the projection operator and $v_l^N$ is a polynomial subspace spanned by the multivariate Hermite polynomials $H_j$.

$$v_l^N = span\left\{H_j : |j| = l, j \in \mathbb{N}_0^N\right\}, 0 \le l < \infty \tag{3.70}$$

Since standardization only rescales the Hermite polynomials, the Standardized *Polynomial Chaos* $\Psi_j(x;C_x)$ also spans $v_l^N$. From the definition of the *random vector* $\boldsymbol{X}$, the sequence $\left\{\psi_j\left(X;C_X\right)\right\}_{j\in\mathbb{N}_0^N}$ is a basis of $L^2(\Omega,F,P)$ hence inheriting the properties of the basis of $L^2\left(\mathbb{R}^N, B^N, \phi_x dx\right)$. As a result, the expansion of $u(\boldsymbol{X})$ can be rewritten as:

$$u\left(X\right) \sim \sum_{j\in\mathbb{N}_0^N} a_j \psi_j\left(X;C_X\right) \tag{3.71}$$

where $a_j$ are coefficients to be determined. But from the definition of $\Psi_j(x;C_X)$, the polynomials formed from the orthogonal sum of *Polynomial Chaos*:

$$\bigoplus_{l\in N_0} span\left\{\psi_j\left(x;C_X\right) : |j| = l, j \in \mathbb{N}_0^N\right\} = \Pi^N \tag{3.72}$$

is dense in $L^2\left(\mathbb{R}^N, B^N, \phi_x dx\right)$. Hence the expansion of $u(\boldsymbol{X})$ has Bessel's inequality:

$$E\left[\sum_{j\in\mathbb{N}_0^N} a_j \psi_j\left(X;C_X\right)\right]^2 \le E\left[u^2\left(X\right)\right] \tag{3.73}$$

Thus proving that the *PCE* of $u(\boldsymbol{X})$ converges in the *mean square* or $L^2$.

We can also demonstrate this convergence inductively by varying the order of the *Polynomial Chaos* for the solution of one of the cases. Figure 3.20 shows the mean response of case 1 for increasing order of the *PCE*.

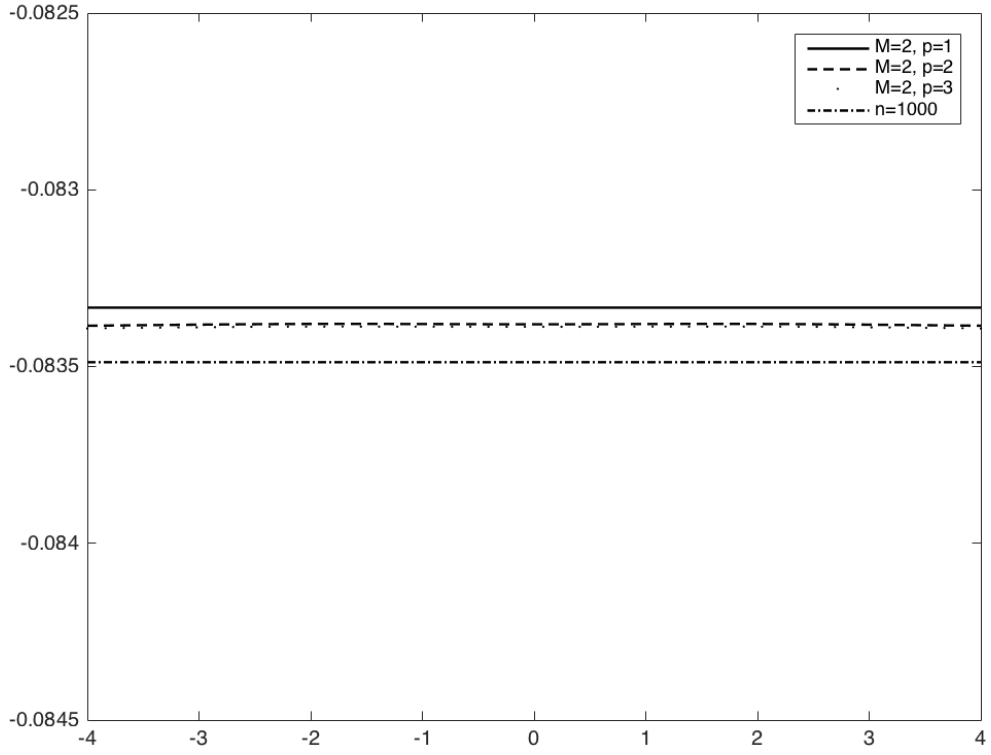


**Figure 3.20: Mean deflection of Case 1 for polynomial order p=1, p=2, and p=3**

From figure 3.20, we can see the mean response of higher order *Polynomial Chaos* converging to the *Monte Carlo* mean. The result of the *Monte Carlo* simulation is regarded as more accurate from the law of large numbers but the computational advantage that the SFEM possesses surmounts this slight discrepancy in accuracy. Nonetheless, the curse of dimensionality remains an issue as the total number of polynomials $P$ rapidly increases with higher values of $M$, and $p$. Interestingly, despite the much larger systems generated from higher order polynomials, the *Monte Carlo* remains the most computationally expensive method.

Furthermore, a sensitivity analysis is carried out by varying the *coefficient of variation* (*COV)* of each *random process* and evaluating the variance of the response at the point of maximum deflection. The initial *COV* of each *random process* is doubled, and then tripled while keeping the *COV*s of the other parameters unchanged. In doing so, we note that in the first two cases, varying the *COV* of the soil stiffness, *k* results in the highest uncertainty in the response. Once more, we are reminded of the importance of treating soil as a stochastic material. In case 3, the variance of the response is the most sensitive to changes in the *COV* of the pile's axial rigidity.

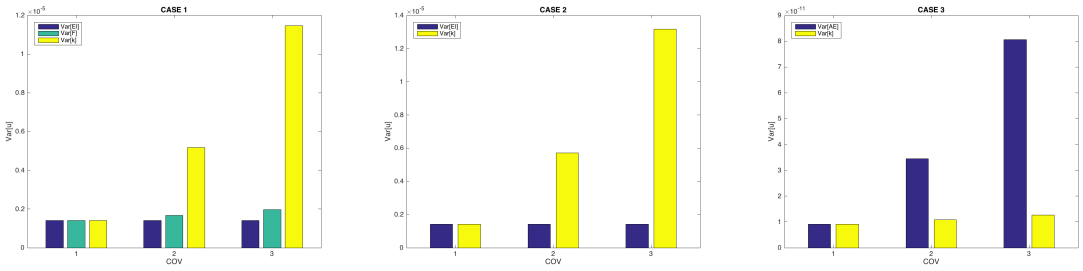


**Figure 3.21: Sensitivity analysis of random parameters for Case 1, 2 and 3**

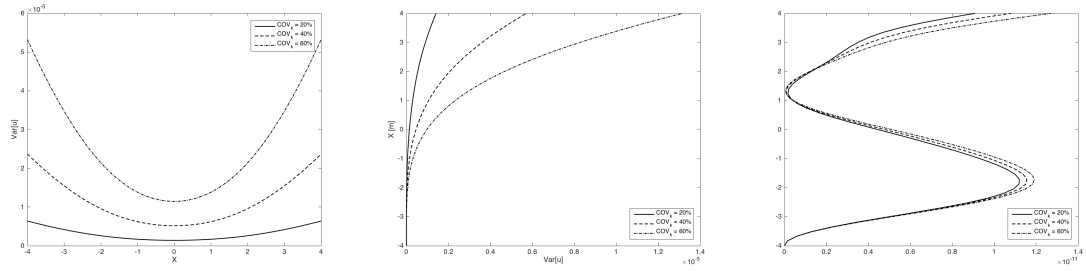


**Figure 3.22: Variance function for increasing COV of k for Case 1, 2 and 3**

Having identified the soil stiffness, *k* as the most sensitive parameter, the variance of the response as a function of the foundation's length is investigated for increasing *COV* of *k*. The results shown in figure 3.22 are remarkably different from each other. Increasing the *COV* of a sensitive parameter significantly impacts the variance of the response. Case 1,

and 2 are prime examples. Case 3 to the contrary shows little variability in its response. What is even more striking is how revelatory the variance functions are in indicating the mechanical behaviour of the system. What the variance function is effectively showing us is an analogous depiction of the pile's potential energy. We note in case 1, that the variance is minimum at the mid-span, while in case 2, the minimum variance is reported at the fixed end of the pile. Case 3, has perhaps the most interesting variance function. It has a minimum at the fixed end and another one approximately 5.2m from the fixed end. Intuitively, the distance between the minima alludes to the effective length of a column. In theory, we can obtain the effective length from the product of the unsupported length of the pile, $L$ and a parameter $K$ whose value depends on the support conditions at both ends of the pile. In practice we assume the pile head to be free, thus $\sqrt{2}/2 \leq K \leq 2$. However, the unsupported distance $L$ is less than the pile's length, and depends on the soil stiffness.

## 3.4 Summary

The Stochastic Finite Element method was used to analyze three piles of different configurations and a statistical description of the three cases was provided. In the first part of the chapter, the mathematical tools required to implement the stochastic finite element method was presented. The derivation of the *Karhunen-Loeve* expansion in one-dimension was shown and its implementation in the representation of pile-soil random fields illustrated. The *PCE* basis used to represent the random response was then constructed and implemented in the Finite Element Method. The results of each case were verified against a *Monte Carlo* simulation. The results in all three cases were in

good agreement with the *Monte Carlo* simulations and the computational efficiency of both schemes in terms of their runtimes was compared. The second part of the chapter presented the results of the statistical moments calculated for each case and provided an interpretation of those results from a mechanical perspective. Two themes in particular were tackled: 1) the impact of the orientation of the loads on the variance of the solution. 2) The impact of the number of nodes under the direct action of a load on the mean of the response. For the purpose of these statistical inferences, the probability distribution functions of the maximum deflection of each case were plotted and compared to histograms generated from the *Monte Carlo* simulations. In addition, the mean, and *standard variations* as functions of the pile's length were generated using both methods after which they were compared to each other. The performance and accuracy of the SFEM was investigated for different orders of *Polynomial Chaos*. We demonstrated via mathematical proof and inductively that with increasing orders of *PCE*, the mean response converges to a unique solution, which seems very close to the *Monte Carlo* mean of a very large sample size. To conclude, a sensitivity analysis was conducted where the variance of the response at the maximum deflection and the variance function of each case were analyzed for different values of *COV*. The analysis showed that the soil parameter, k was the most sensitive for case 1 and 2, and the axial rigidity, *AE* was the most sensitive for case 3. After which, the analysis revealed that the variance function provides insights into a system mechanical behaviour.

# CHAPTER 4.

# STOCHASTIC ANALYSIS OF A TWO-PARAMETER CONTINUUM PILE MODEL USING THE KARHUNEN-LOEVE EXPANSION

## 4.1 Introduction

In the face of considerable limitations, which the one-parameter *Winkler* model (Winkler, 1867) suffers from, a two-parameter model originally developed by Vlasov and Leont'ev (1966) for a beam on elastic foundation and later modified by Vallabhan and Das (1991) is investigated with spatially random parameters. This time around, a two-dimensional random field is generated with random fluctuations about a mean plane in a Cartesian coordinate system. Several accounts of two-parameter continuum models exist in the geomechanic literature, but seldom are of stochastic nature. Griffiths et al (2013) performed a reliability analysis on *Winkler* models, but their analysis was limited to the consideration of only one random parameter represented using a one-dimensional random field. In this chapter, a two-dimensional *KL* expansion developed for plates by Ghanem and Spanos (1990) is used to represent the random processes of a two-parameter continuum pile model.

The biggest drawback of the Winkler model is that the springs used to model the soil are not connected with one another when in reality in a soil continuum, adjacent *REV*'s

interact with each other. This interaction, known as the shear resistance, plays an important role in the mechanical behaviour of laterally loaded piles. It is also the property which typically exhibits the largest coefficient of variation (*COV*). The compressive resistance of the soil on the other hand exhibits variability, but of order significantly lower than the shear resistance as a function of its location. This is the case in general for soil; the horizontal scale of fluctuation is higher than the vertical scale of fluctuation (Phoon and Kulhawy, 1999).

In this chapter we do not use the SFEM method due to the complexity of the problem, effectively making the methodology computationally expensive. Instead, a two dimensional random field for each random parameter is generated with the help of the K-L expansion and the model is solved using an iterative scheme along with a closed-form solution. The governing equation for the two-parameter model is derived using the variational principles of mechanics and the random material properties are introduced in the formulation as series representations (all assumed to have an exponential covariance structure) of two variables $x$, and $y$ using the *KL* expansion.

Haldar and Basu (2013) performed similar analyses on free-end beams on elastic foundations. They discretized the soil in the $x$ and $z$ direction by using a grid with elements of equal lengths and widths. Each element was assigned a value of soil Young's modulus sampled from a distribution. Thereafter, they performed a *Monte Carlo* simulation akin to the analysis done in Chapter 3 and compared their results with the

deterministic solution. In this chapter also, we compare the mean results of our stochastic method to the deterministic solution.

## 4.2 Analysis

### 4.2.1 Problem definition

A pile having a rectangular cross-section and subjected to a horizontal force $F_a$ and a moment $M_a$ at its head is analyzed using a continuum approach. The latter is embedded in a soil deposit of $n$ layers with each layer assumed to span an infinitely large distance in the $x$-$y$ Cartesian coordinate system. The soil medium within each layer is assumed to have random properties mimicking real field conditions.

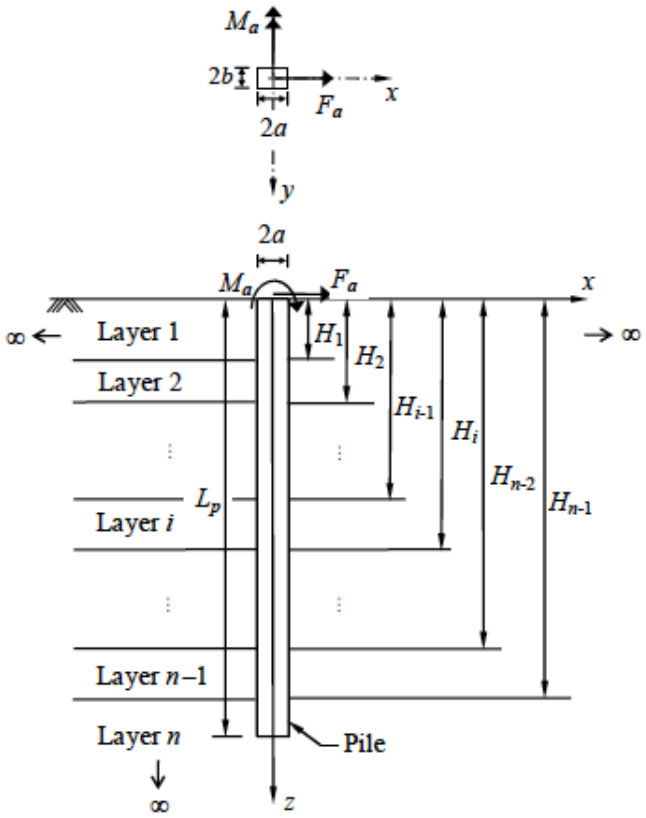


**Figure 4.1: A Laterally loaded rectangular pile in a layered elastic medium (Source: Basu and Salgado, 2008)**

### 4.2.2 Random fields

Recall the integral equation 3.2 for the *eigen-values* and *eigen-functions* problem solved in Chapter 3 for the spectral decomposition of a one-dimensional input random field. Analogously, we now introduce the *covariance function* $C(x_1,x_2;y_1,y_2)$ for the spectral decomposition of a two-dimensional random field.

$$\lambda_n f_n(x_1,y_1) = \int_{\Omega} C(x_1,y_1;x_2,y_2) f_n(x_2,y_2) dx_1 dy_1 \tag{4.1}$$

The kernel of $C(x_1,x_2;y_1,y_2)$ has an *exponential* structure given by:

$$C(x_1,x_2;y_1,y_2) = \sigma_1^2\sigma_2^2 e^{-\frac{|x_1-y_1|}{l_1}-\frac{|x_2-y_2|}{l_2}} \tag{4.2}$$

where $l_1$ and $l_2$ are *correlation lengths* between $x_1$ and $y_1$ and $x_2$ and $y_2$ respectively. $\sigma_1$ and $\sigma_2$ are the standard deviation of the process in the 1 and 2 directions. Once more, $\lambda_n$ and $f_n$ are the *eigen-values* and *eigen-functions* obtained after solving equation 4.1.

Assuming the *eigen-functions* $f_n(x,y)$ can be expressed as the product of separable functions such that:

$$f_n(x_1,x_2) = f_i^{(1)}(x_1) f_j^{(2)}(x_2) \tag{4.3}$$

and the eigenvalues $\lambda_n$ can be expressed in a similar fashion s.t:

$$\lambda_n = \lambda_i^{(1)}\lambda_j^{(2)} \tag{4.4}$$

We can now substitute equations 4.2 through 4.4 into equation 4.1 and obtain:

$$\lambda_i^{(1)}\lambda_j^{(2)} f_i^{(1)}(x_1) f_j^{(2)}(x_2) = \sigma_1^2\sigma_2^2 \int_{-l_{x_1}/2}^{l_{x_1}/2} \int_{-l_{x_2}/2}^{l_{x_2}/2} \left[ e^{-\frac{|x_1-y_1|}{l_1}-\frac{|x_2-y_2|}{l_2}} \right] f_i^{(1)}(y_1) f_j^{(2)}(y_2) dy_1 dy_2 \tag{4.5}$$

The above equation can be re-arranged and split into two equations by comparing the *left-hand side* (*LHS)* to the *right-hand side* (*RHS)* of the equation.

$$\lambda_i^{(1)} f_i^{(1)}\left(x_1\right) = \sigma_1^2 \int_{-l_{x_1}/2}^{l_{x_1}/2} e^{-c_1|x_1-y_1|} f_i^{(1)}\left(y_1\right) dy_1 \tag{4.6}$$

and

$$\lambda_j^{(2)} f_j^{(2)}\left(x_2\right) = \sigma_2^2 \int_{-l_{x_2}/2}^{l_{x_2}/2} e^{-c_2|x_2-y_2|} f_j^{(2)}\left(y_2\right) dy_2 \tag{4.7}$$

where $c_1 = 1/l_1$ and $c_2 = 1/l_2$.

Hence, the solution to equation 4.5 is the product of the individual solutions of the above two equations introduced previously as *Fredholm* integral equations. In order to solve these two integral equations, we repeat the steps taken in section 3.2.3 and obtain two ODEs of the form:

$$\left(-2c + c^2\lambda_k\right) f_k\left(x\right) = \lambda_k f_k{}''\left(x\right) \tag{4.8}$$

Solving the first integral equation, we obtain the following eigenvalues and normalized *eigen-functions*:

$$\lambda_i^{(1)} = \frac{2\sigma_1^2 c_1}{\left(\omega_i^2 + c_1\right)} \tag{4.9}$$

and

$$f_i^{(1)}\left(x\right) = \frac{\cos\left(\omega_i x\right)}{\sqrt{a + \dfrac{\sin\left(2\omega_i a\right)}{2\omega_i}}} \tag{4.10}$$

for i odd, and

$$f_i^{(1)}(x) = \frac{\cos(\omega_i x)}{\sqrt{a - \frac{\sin(2\omega_i a)}{2\omega_i}}} \tag{4.11}$$

for i even.

where $\omega_i$ are solutions to the following transcendental equations:

$$c_1 - \omega_i \tan(\omega_i a) = 0 \quad \text{for i odd} \tag{4.12}$$

and

$$\omega_i + c_1 \tan(\omega_i a) = 0 \quad \text{for i even} \tag{4.13}$$

Note: The domain is *[-a, a]*. Therefore here $a = l_{x1}/2$.

The solution to equation 4.7 is identical to that of equation 4.6 with subscripts and superscripts changed accordingly. We obtain the complete set of normalized *eigen-functions* by permuting the subscripts of equation 4.3 as follows:

$$f_n(x,y) = \frac{1}{\sqrt{2}}\left[ f_i^{(1)}(x) f_j^{(2)}(y) + f_j^{(1)}(x) f_i^{(2)}(y) \right] \tag{4.14}$$

Assuming that within every soil layer, the Young's modulus of soil $E_s$ and the soil's Poisson's ratio $\upsilon_s$ are spatially random, the *KL* representation of these *random processes* can be written as:

$$E_s(x,y) = \bar{E}_s + \sum_{i=1}^{\infty} t_i \sqrt{\lambda_i^{Es}} f_i^{Es}(x,y) \tag{4.15-a}$$

$$\upsilon_s(x,y) = \bar{\upsilon}_s + \sum_{i=1}^{\infty} t_i \sqrt{\lambda_i^{\upsilon s}} f_i^{\upsilon s}(x,y) \tag{4.15-b}$$

where $t_i$ is a standard normal random variable i.e $t_i \sim N(0,1)$, $\lambda_i$'s are the *eigen-values*, $f_i$'s are the *eigen-functions* and the leading term of each of the above equation represents the *random processes'* mean values. Truncating each series after *M* terms produces:

$$E_s(x,y) = \overline{E}_s + \sum_{i=1}^{M} t_i \sqrt{\lambda_i^{Es}} f_i^{Es}(x,y) \tag{4.16-a}$$

$$\upsilon_s(x,y) = \overline{\upsilon}_s + \sum_{i=1}^{M} t_i \sqrt{\lambda_i^{\upsilon s}} f_i^{\upsilon s}(x,y) \tag{4.16-b}$$

As more terms are considered in the expansion, undulations of realizations of $E_s$ and $\upsilon_s$ become more pronounced. These undulations are characterized by the addition of noise more specifically *Gaussian White Noise (GWN*) into the random field. Figure 4.2 shows the realization of a *random process* with increasing orders of expansion.

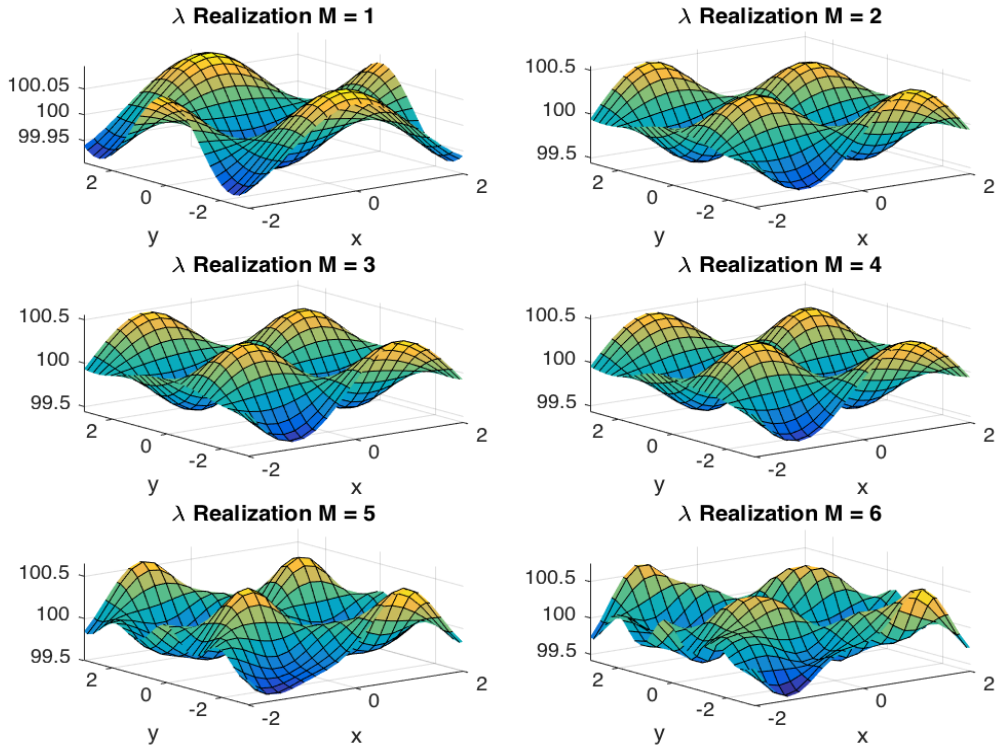


**Figure 4.2: 2-D KL representation of an arbitrary process λ with μ=100, and σ=1 for 6 orders of expansion**

### 4.2.3 Pile-soil potential energy

The governing equation of the pile-soil system is derived using the principle of virtual work. We first obtain the total *potential energy* of the system given by:

$$\Pi = U - V \tag{4.17}$$

where $U$ is the internal energy of the system and $V$ is the external work done on the system. Assuming no work is dissipated, and by considering the strain density energy of the continuous soil medium we get:

$$\Pi = \frac{1}{2} E_p I_p \int_0^{L_p} \left( \frac{d^2 u}{dz^2} \right)^2 dz + \frac{1}{2} \int_\Omega \sigma_{ij} \varepsilon_{ij} \, d\Omega - F_a u \Big|_{z=0} + M_a \frac{du}{dz} \Big|_{z=0} \tag{4.18}$$

where $u$ is the lateral pile displacement; $\sigma_{ij}$ and $\varepsilon_{ij}$ are the stress and strain tensors in the soil; $\Omega$ is the soil domain surrounding the pile (excluding the volume $L_p$ *x 2a x 2b*) and spanning infinitely large distances in the *x*-*y* plane and in the *z*-direction. In the expression for the total potential energy of the pile-soil system, the first term represents the internal *potential energy* of the pile, the second term represents the internal potential energy of the continuous soil medium and the remaining two terms are the sum of the external work done on the system.

### 4.2.4 Stress-strain-displacement relationships

In the derivation of the total potential energy, we note that no constitutive law was assumed. This is made possible due to the fact that the principle of virtual work used to obtain the potential energy applies to any constitutive law. Let us now define a displacement field for the soil continuum.

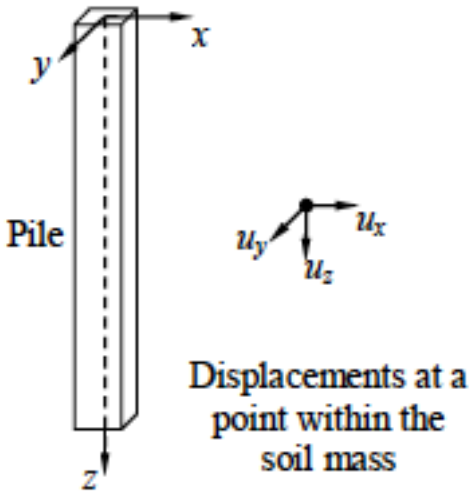


**Figure 4.3: Displacements in soil mass with convention used for positive directions (Source: Basu, 2006)**

$$u_x = u(z)\phi_x(x)\phi_y(y) \tag{4.19-a}$$

$$u_y = 0 \tag{4.19-b}$$

$$u_z = 0 \tag{4.19-c}$$

We introduce the dimensionless soil displacement functions $\phi_x$ and $\phi_y$ each representing the displacement of the soil medium in the x and y direction respectively. We assign a range of values to functions $\phi_x$ and $\phi_y$ such that at the pile interface they assume a value of 1 with a horizontal asymptote at $y = 0$ as the function decays.

We now want to relate the strains to the displacements within our soil continuum. Using the *Cauchy* strain tensor as the measure of strain, the relationship between strain and displacement is given by:

$$\begin{bmatrix} \varepsilon_{xx} \\ \varepsilon_{yy} \\ \varepsilon_{zz} \\ \varepsilon_{xy} \\ \varepsilon_{xz} \\ \varepsilon_{yz} \end{bmatrix} = \begin{bmatrix} -\frac{\partial u_x}{\partial x} \\ -\frac{\partial u_y}{\partial y} \\ -\frac{\partial u_z}{\partial z} \\ -\frac{1}{2}\left(\frac{\partial u_x}{\partial y} + \frac{\partial u_y}{\partial x}\right) \\ -\frac{1}{2}\left(\frac{\partial u_x}{\partial z} + \frac{\partial u_z}{\partial x}\right) \\ -\frac{1}{2}\left(\frac{\partial u_y}{\partial z} + \frac{\partial u_z}{\partial y}\right) \end{bmatrix} = \begin{bmatrix} -u(z)\frac{d\phi_x(x)}{dx}\phi_y(y) \\ 0 \\ 0 \\ -\frac{1}{2}u(z)\phi(x)\frac{d\phi_y(y)}{dx} \\ -\frac{1}{2}\frac{du(z)}{dz}\phi_x(x)\phi_y(y) \\ 0 \end{bmatrix} \tag{4.20}$$

Assuming the elastic constitutive law for plain strain condition, the stress-strain relationship is given by:

$$\begin{bmatrix} \sigma_{xx} \\ \sigma_{yy} \\ \sigma_{zz} \\ \tau_{xy} \\ \tau_{xz} \\ \tau_{yz} \end{bmatrix} = \begin{bmatrix} \lambda_s(x,y,\theta)+2G_s(x,y,\theta) & \lambda_s(x,y,\theta) & \lambda_s(x,y,\theta) & 0 & 0 & 0 \\ \lambda_s(x,y,\theta) & \lambda_s(x,y,\theta)+2G_s(x,y,\theta) & \lambda_s(x,y,\theta) & 0 & 0 & 0 \\ \lambda_s(x,y,\theta) & \lambda_s(x,y,\theta) & \lambda_s(x,y,\theta)+2G_s(x,y,\theta) & 0 & 0 & 0 \\ 0 & 0 & 0 & 2G_s(x,y,\theta) & 0 & 0 \\ 0 & 0 & 0 & 0 & 2G_s(x,y,\theta) & 0 \\ 0 & 0 & 0 & 0 & & 2G_s(x,y,\theta) \end{bmatrix} \cdot \begin{bmatrix} \varepsilon_{xx} \\ \varepsilon_{yy} \\ \varepsilon_{zz} \\ \varepsilon_{xy} \\ \varepsilon_{xz} \\ \varepsilon_{yz} \end{bmatrix}$$

(4.21)

Substituting equation 4.20 and 4.21 in the equation for the strain energy density of soil:

$$U_{D,soil} = \frac{1}{2}\sigma_{ij}\varepsilon_{ij} = \frac{1}{2}\left(\sigma_{xx}\varepsilon_{xx} + \sigma_{yy}\varepsilon_{yy} + 2\tau_{xy}\varepsilon_{xy} + 2\tau_{xz}\varepsilon_{xz} + 2\tau_{yz}\varepsilon_{yz}\right) \qquad (4.22\text{-a})$$

$$= \frac{1}{2}\left[\left(\lambda_s(x,y,\theta)+2G_S(x,y,\theta)\right)u^2\left(\frac{d\phi_x}{dx}\right)^2\phi_y^2 + G_s(x,y,\theta)u^2\phi_x^2\left(\frac{d\phi_y}{dy}\right)^2 + G_s(x,y,\theta)\left(\frac{du}{dz}\right)^2\phi_x^2\phi_y^2\right]$$

(4.22-b)

where $\lambda_s(x,y,\theta)$ and $G_s(x,y,\theta)$ are *Lame*'s constants which are assumed to be spatially *random processes* as a result of their dependency on the Young's modulus and Poisson's ratio of the soil. The random nature of the material properties is denoted by $\theta$, and while this distinction is an important one, for the sake of clarity the $\theta$ will be dropped here onwards. The *Lame*'s constants in terms of the soil's modulus $E_s$ and Poisson's ratio $\upsilon_s$ can be expressed as:

$$\lambda_s(x,y) = \frac{E_s(x,y)\upsilon_s(x,y)}{\left(1+\upsilon_s(x,y)\right)\left(1-2\upsilon_s(x,y)\right)} \qquad (4.23)$$

$$G_s(x,y) = \frac{E_s(x,y)}{2\left(1+\upsilon_s(x,y)\right)} \qquad (4.24)$$

Substituting equation 4.22-b into equation 4.18 we finally get:

$$\Pi = \frac{1}{2}E_p I_p \int_0^{L_p} \left(\frac{d^2u}{dz^2}\right)^2 dz + \frac{1}{2}\int_\Omega \Big[ \left(\lambda_s(x,y) + 2G_s(x,y)\right) u^2 \left(\frac{d\phi_x}{dx}\right)^2 \phi_y^2 + G_s(x,y) u^2 \phi_x^2 \left(\frac{d\phi_y}{dy}\right)^2 + G_s(x,y)\left(\frac{du}{dz}\right)^2 \phi_x^2 \phi_y^2 \Big] d\Omega - F_a u\Big|_{z=0} + M_a \frac{du}{dz}\Big|_{z=0} \tag{4.25}$$

### 4.2.5 Principle of minimum potential energy

The *principle of minimum potential energy* states that a body undergoing deformation reaches equilibrium when its total potential energy minimizes locally (Reddy, 2007). This is derived as a special case of the *principle of virtual work* for an elastic system under the action of conservative forces. This can be mathematically interpreted as $\delta\Pi = 0$. Therefore, taking the first variation of the total potential energy of the pile-soil system gives:

$$\begin{aligned}
&\int_0^{L_p} E_p I_p \frac{d^2u}{dz^2} \delta\left(\frac{d^2u}{dz^2}\right) dz + \int_\Omega \Big[ \left(\lambda_s(x,y) + 2G_s(x,y)\right) u \delta u \left(\frac{d\phi_x}{dx}\right)^2 \phi_y^2 \\
&+ \left(\lambda_s(x,y) + 2G_s(x,y)\right) u^2 \left(\frac{d\phi_x}{dx}\right) \delta\left(\frac{d\phi_x}{dx}\right) \phi_y^2 + \left(\lambda_s(x,y) + 2G_s(x,y)\right) u^2 \left(\frac{d\phi_x}{dx}\right)^2 \phi_y \delta\phi_y \\
&+ G_s(x,y) u \delta u \phi_x^2 \left(\frac{d\phi_y}{dy}\right)^2 + G_s(x,y) u^2 \phi_x \delta\phi_x \left(\frac{d\phi_y}{dy}\right)^2 + G_s(x,y) u^2 \phi_x^2 \left(\frac{d\phi_y}{dy}\right) \delta\left(\frac{d\phi_y}{dy}\right) \\
&+ G_s(x,y)\left(\frac{du}{dz}\right) \delta\left(\frac{du}{dz}\right) \phi_x^2 \phi_y^2 + G_s(x,y)\left(\frac{du}{dz}\right)^2 \phi_x \delta\phi_x \phi_y^2 + G_s(x,y)\left(\frac{du}{dz}\right)^2 \phi_x^2 \phi_y \delta\phi_y \Big] d\Omega \\
&- F_a \delta u\Big|_{z=0} + M_a \delta\left(\frac{du}{dz}\right)\Big|_{z=0} = 0
\end{aligned} \tag{4.26}$$

Since the first variation of $\phi_x$, $\phi_y$ and $u$ are all independent from one another, they must all be individually equal to zero to satisfy the principle of minimum potential energy $\delta\Pi = 0$. We can therefore collect the terms associated with each independent variation over their respective domains to obtain the governing differential equations of the soil-pile system.

### 4.2.6 Soil displacement

First let us consider the variation on $\phi_x$. We collect all the terms associated with $\delta\phi_x$ and $\delta(d\phi_x/dx)$.

$$\int_{\Omega}\left[\left(\lambda_s(x,y)+2G_s(x,y)\right)u^2\frac{d\phi_x}{dx}\phi_y^2\delta\left(\frac{d\phi_x}{dz}\right)+G_s(x,y)u^2\phi_x\left(\frac{d\phi_y}{dy}\right)^2\delta\phi_x \right.$$
$$\left.+G_s(x,y)\left(\frac{du}{dz}\right)^2\phi_x\phi_y^2\delta\phi_x\right]d\Omega=0 \tag{4.27}$$

Equation 4.27 can be rewritten with the soil domain divided into the *X, Y* and *Z* sub-domains as follows:

$$\int_Z u^2\int_Y\phi_y^2\int_X\left(\lambda_s(x,y)+2G_s(x,y)\right)\frac{d\phi_x}{dx}\delta\left(\frac{d\phi_x}{dx}\right)dxdydz$$
$$+\int_Z u^2\int_Y\left(\frac{d\phi_y}{dx}\right)^2\int_X G_s(x,y)\phi_x\delta\phi_x\,dxdydz \tag{4.28}$$
$$+\int_Z\left(\frac{du}{dz}\right)^2\int_Y\phi_y^2\int_X G_s(x,y)\phi_x\delta\phi_x\,dx\,dydz=0$$

Performing integration by parts on the first term and simplifying the above equation we get:

$$\int_X\left(-m_{s_1}\left[p_y^{(1)}(x)\frac{d^2\phi_x}{dx}+p_y^{(2)}(x)\frac{d\phi_x}{dx}\right]+\phi_x\left[m_{s_1}q_y^{(1)}(x)+n_s p_y^{(3)}(x)\right]\right)\delta\phi_x\,dx$$
$$+m_{s_1}p_y^{(1)}(x)\frac{d\phi_x}{dx}\delta\phi_x\Big|_X=0 \tag{4.29}$$

where

$$m_{s_1}=\int_Z u^2\,dz \tag{4.30-a}$$

$$n_s = \int_Z \left( \frac{du}{dz} \right)^2 dz \tag{4.30-a}$$

$$p_y^{(1)}(x) = \int_Y \phi_y^2 \left( \lambda_s(x,y) + 2G_s(x,y) \right) dy \tag{4.30-c}$$

$$p_y^{(2)}(x) = \int_Y \phi_y^2 \frac{d\left( \lambda_s(x,y) + 2G_s(x,y) \right)}{dx} dy \tag{4.30-d}$$

$$p_y^{(3)}(x) = \int_Y \phi_y^2 G_s(x,y) dy \tag{4.30-e}$$

$$q_y^{(3)}(x) = \int_Y \left( \frac{d\phi_y}{dy} \right)^2 G_s(x,y) dy \tag{4.30-f}$$

But since the function $\phi_x$ is known and takes a value of 1 at $x = \pm a$ and 0 at $x = \pm\infty$, the variation at the boundary is zero, $\delta\phi_x = 0$. Incidentally, the integral expression has to equal zero. Since $\delta\phi_x$ is not known a priori for points not located on the boundary, the optimal function $\phi_x$ must be found such that the potential energy is minimized; this is interpreted mathematically as $\delta\phi_x \neq 0$. Hence to satisfy equation 4.29, the following must be true:

$$-m_{s_1} \left[ p_y^{(1)}(x) \frac{d^2\phi_x}{dx^2} + p_y^{(2)}(x) \frac{d\phi_x}{dx} \right] + \phi_x \left[ m_{s_1} q_y^{(1)}(x) + n_s p_y^{(3)}(x) \right] = 0 \tag{4.31}$$

Rearranging and simplifying the above equation, the following governing differential equation is obtained for $\phi_x$:

$$\frac{d^2\phi_x}{dx^2} - \frac{p_y^{(2)}}{p_y^{(1)}} \frac{d\phi_x}{dx} - \frac{1}{m_{s_1} p_y^{(1)}} \left( m_{s_1} q_y^{(1)} + n_s p_y^{(3)} \right) \phi_x = 0 \tag{4.32}$$

Before attempting to solve the differential equation obtained for $\phi_x$, the same procedures are repeated for the unknown displacement $\phi_y$. The variation on $\phi_y$ is considered and all the terms associated with $\delta\phi_y$ and $\delta(d\phi_y/dy)$ are collected:

$$\int_{\Omega}\left[\left(\lambda_s(x,y)+2G_s(x,y)\right)u^2\left(\frac{d\phi_x}{dx}\right)^2\phi_y\delta\phi_y+G_s(x,y)u^2\phi_x^2\left(\frac{d\phi_y}{dy}\right)\delta\left(\frac{d\phi_y}{dy}\right)\right.$$
$$\left.+G_s(x,y)\left(\frac{du}{dz}\right)^2\phi_x^2\phi_y\delta\phi_y\right]d\Omega=0 \tag{4.33}$$

Integrating the first term by parts, and simplifying the above equation yields:

$$\int_{Y}\left(-m_{s_1}\left[p_x^{(1)}(y)\frac{d^2\phi_y}{dy^2}+p_x^{(2)}(y)\frac{d\phi_y}{dy}\right]+\phi_y\left[m_{s_1}q_x^{(1)}(y)+n_s p_x^{(1)}(y)\right]\right)\delta\phi_y\,dy$$
$$+m_{s_1}p_x^{(1)}(y)\left(\frac{d\phi_y}{dy}\right)\delta\phi_y\Big|_Y=0 \tag{4.34}$$

where:

$$p_x^{(1)}(y)=\int_X\phi_x^2G_s(x,y)dx \tag{4.35-a}$$

$$p_x^{(2)}(y)=\int_X\phi_x^2\frac{d\left(G_s(x,y)\right)}{dy}dx \tag{4.35-b}$$

$$q_x^{(1)}(y)=\int_X\left(\frac{d\phi_x}{dx}\right)^2\left(\lambda_s(x,y)+2G_s(x,y)\right)dx \tag{4.35-c}$$

It should be obvious by now that the integral equation obtained for $\phi_x$ and $\phi_y$ are similar but not identical. They are both subjected to the same conditions and are in fact symmetrical functions as a result of the problem's axisymmetric nature. On the other hand, a pile embedded in sloping ground would effectively produce two different

equations for the soil displacement. The governing *ODE* of the soil displacement in the *y*-direction, $\phi_y$ is therefore given by:

$$\frac{d^2\phi_y}{dy^2}+\frac{p_x^{(2)}}{p_x^{(1)}}\frac{d\phi_y}{dy}-\frac{1}{m_{s_1}p_x^{(1)}}\left(m_{s_1}q_y^{(1)}+n_s p_x^{(1)}\right)\phi_y=0 \tag{4.36}$$

Going back to equation 4.32, the finite difference method can be implemented to solve the *ODE*. Discretizing equation 4.32 and using a central difference scheme, the following equation in terms of $\phi_x$ is obtained:

$$\frac{\phi_x^{(i+1)}-2\phi_x^{(i)}+\phi_x^{(i-1)}}{\Delta x^2}-\left(\frac{p_y^{(1)(i+1)}-p_y^{(1)(i-1)}}{2\Delta x p_y^{(1)(i)}}\right)\left(\frac{\phi_x^{(i+1)}-\phi_x^{(i-1)}}{2\Delta x}\right)-\frac{1}{m_{s_1}p_y^{(1)(i)}}\left(m_{s_1}q_y^{(1)(i)}+n_s p_y^{(3)(i)}\right)\phi_x^{(i)}=0 \tag{4.37}$$

Similarly, discretizing equation 4.36 and using a central difference scheme, the following equation in terms of $\phi_y$ is obtained:

$$\frac{\phi_y^{(i+1)}-2\phi_y^{(i)}+\phi_y^{(i-1)}}{\Delta y^2}-\left(\frac{p_x^{(1)(i+1)}-p_x^{(1)(i-1)}}{2\Delta y p_x^{(1)(i)}}\right)\left(\frac{\phi_y^{(i+1)}-\phi_y^{(i-1)}}{2\Delta y}\right)-\frac{1}{m_{s_1}p_x^{(1)(i)}}\left(m_{s_1}q_x^{(1)(i)}+n_s p_x^{(1)(i)}\right)\phi_y^{(i)}=0 \tag{4.38}$$

From equation 4.37, and equation 4.38, a system of *N* simultaneous equations is produced where "*N*" is the number of nodes used in the uniform discretization scheme adopted, "i" represents the $i^{th}$ node and $\Delta x$ and $\Delta y$ are the element lengths in the *x* and *y* direction respectively. Rearranging equations 4.37 and 4.38, we get:

$$\begin{aligned}&\phi_x^{(i-1)}\left[\frac{1}{\Delta x^2}+\frac{1}{2\Delta x}\left(\frac{p_y^{(1)(i+1)}-p_y^{(1)(i-1)}}{2\Delta x p_y^{(1)(i)}}\right)\right]+\phi_x^{(i)}\left[\frac{-2}{\Delta x^2}-\frac{1}{m_{s_1}p_y^{(1)(i)}}\left(m_{s_1}q_y^{(1)(i)}+n_s p_y^{(3)(i)}\right)\right]\\&+\phi_x^{(i+1)}\left[\frac{1}{\Delta x^2}+\frac{1}{2\Delta x}\left(\frac{p_y^{(1)(i+1)}-p_y^{(1)(i-1)}}{2\Delta x p_y^{(1)(i)}}\right)\right]=0\end{aligned} \tag{4.39}$$

and

$$\phi_y^{(i-1)}\left[\frac{1}{\Delta y^2}+\frac{1}{2\Delta y}\left(\frac{p_x^{(1)(i+1)}-p_x^{(1)(i-1)}}{2\Delta y p_x^{(1)(i)}}\right)\right]+\phi_y^{(i)}\left[\frac{-2}{\Delta y^2}-\frac{1}{m_{s_1}p_x^{(1)(i)}}\left(m_{s_1}q_x^{(1)(i)}+n_s p_x^{(1)(i)}\right)\right]$$
$$+\phi_y^{(i+1)}\left[\frac{1}{\Delta y^2}+\frac{1}{2\Delta y}\left(\frac{p_x^{(1)(i+1)}-p_x^{(1)(i-1)}}{2\Delta y p_x^{(1)(i)}}\right)\right]=0 \tag{4.40}$$

which can be recast as matrix equations having the form:

$$\left[K\right]\left\{\phi\right\}=\left\{F\right\} \tag{4.41}$$

where *[K]* is a tri-diagonal matrix of size *(N-2) x (N-2), {ϕ}* is a vector of unknown displacement and *{F}* is the right-hand side vector. The systems of equations have the following boundary conditions:

$$\phi_x^{(1)}=\phi_y^{(1)}=1 \tag{4.42}$$

$$\phi_x^{(N)}=\phi_y^{(N)}=0 \tag{4.43}$$

Hence we have the following *K* and *F* entries for $\phi_x$:

$$K_{j,j-1}=\frac{1}{\Delta x^2}+\frac{1}{2\Delta x}\left(\frac{p_y^{(1)(j+1)}-p_y^{(1)(j-1)}}{2\Delta x p_y^{(1)(j)}}\right) \tag{4.44-a}$$

$$K_{j,j}=-\frac{2}{\Delta x^2}-\frac{1}{m_{s_1}p_y^{(1)(j)}}\left(m_{s_1}q_y^{(1)(j)}+n_s p_y^{(3)(j)}\right) \tag{4.44-b}$$

$$K_{j,j+1}=\frac{1}{\Delta x^2}-\frac{1}{2\Delta x}\left(\frac{p_y^{(1)(j+1)}-p_y^{(1)(j-1)}}{2\Delta x p_y^{(1)(j)}}\right) \tag{4.44-c}$$

$$F_2=-\frac{1}{\Delta x^2}+\left(\frac{p_y^{(1)(3)}-p_y^{(1)(1)}}{2\Delta x p_y^{(1)(2)}}\right) \tag{4.44-d}$$

$$F_j=0 \quad \text{j>2} \tag{4.44-e}$$

and the following $K$ and $F$ entries for $\phi_y$:

$$K_{i,i-1} = \frac{1}{\Delta y^2} - \frac{1}{2\Delta y}\left( \frac{p_x^{(1)(i+1)} - p_x^{(1)(i-1)}}{2\Delta y p_x^{(1)(i)}} \right) \tag{4.45-a}$$

$$K_{i,i} = -\frac{2}{\Delta y^2} - \frac{1}{m_{s_1} p_x^{(1)(j)}}\left( m_{s_1} q_x^{(1)(i)} + n_s p_x^{(1)(i)} \right) \tag{4.45-b}$$

$$K_{i,i+1} = \frac{1}{\Delta y^2} + \frac{1}{2\Delta y}\left( \frac{p_x^{(1)(i+1)} - p_x^{(1)(i-1)}}{2\Delta y p_x^{(1)(i)}} \right) \tag{4.45-c}$$

$$F_2 = -\frac{1}{\Delta y^2} - \left( \frac{p_x^{(1)(3)} - p_x^{(1)(1)}}{2\Delta y p_x^{(1)(2)}} \right) \tag{4.45-d}$$

$$F_i = 0 \quad \text{i>2} \tag{4.45-e}$$

Imposing the essential boundary conditions from equations 4.42 and 4.43, the first and last row of the unknown vector $\phi$ and right-hand side vector $F$ are deleted. Consequently, the first and last row and column of the tri-diagonal matrix are removed hence producing the following matrix equation:

$$\begin{bmatrix} \cancel{K_{11}} & \cancel{K_{12}} & \cancel{0} & . & . & \cancel{0} \\ \cancel{K_{21}} & K_{22} & K_{23} & 0 & . & \cancel{0} \\ . & K_{23} & K_{33} & K_{34} & . & \cancel{0} \\ . & . & . & . & . & . \\ . & . & 0 & K_{N-1N-2} & K_{N-1N-1} & \cancel{K_{N-1N}} \\ \cancel{0} & . & . & \cancel{0} & \cancel{K_{NN-1}} & \cancel{K_{NN}} \end{bmatrix} \begin{Bmatrix} \cancel{\phi^{(1)}} \\ \phi^{(2)} \\ . \\ . \\ \phi^{(N-1)} \\ \cancel{\phi^{(N)}} \end{Bmatrix} = \begin{Bmatrix} \cancel{F^{(1)}} \\ F^{(2)} \\ . \\ . \\ F^{(N-1)} \\ \cancel{F^{(N)}} \end{Bmatrix} \tag{4.46}$$

Since the equations of the soil displacement are coupled with the pile displacement $u$, and its derivative $u'$, an initial guess for the unknown $\phi$'s is necessary. The pile displacement is then solved using the initial guess and the solution of the pile displacement is fed iteratively into the equations of the soil displacement until convergence is observed. The

convergence criteria used are $\frac{1}{N}\sum_{j=1}^{N-1}\left|\phi_x^{j+1}-\phi_x^{j}\right|\le 10^{-5}$ and $\frac{1}{N}\sum_{i=1}^{N-1}\left|\phi_y^{i+1}-\phi_y^{i}\right|\le 10^{-5}$. The rate of convergence is reliant upon the discretization scheme and the choice of $\phi$ as initial guess. Although the functions $\phi_x$ and $\phi_y$ are not known a priori, their behaviour follows a monotonic decreasing curve. A good initial guess could be a linear function with negative slope spanning the *X* or *Y* domain of the problem. As for the discretization scheme, higher accuracy in the solution can be attained with smaller elements at the expense of computational speed. We elaborate on the discretization scheme in section 4.4 when we present the reader with the spectral decomposition of the random processes in two-dimensions in the solution of the continuum pile.

### 4.2.7 Pile deflection

We now turn our attention to the variation of the function *u*. We collect all the terms associated with $\delta u$ and $\delta(du/dx)$ from equation 4.26 and set their sum to zero:

$$\int_0^{L_p} E_p I_p \frac{d^2u}{dz^2}\delta\left(\frac{d^2u}{dz^2}\right)dz+\int_\Omega\Bigg[\left(\lambda_s(x,y)+2G_s(x,y)\right)u\delta u\left(\frac{d\phi_x}{dx}\right)^2\phi_y^2+G_s(x,y)u\delta u\phi_x^2\left(\frac{d\phi_y}{dy}\right)^2 \\ +G_s(x,y)\left(\frac{du}{dz}\right)\delta\left(\frac{du}{dz}\right)\phi_x^2\phi_y^2\Bigg]d\Omega-F_a\delta w\Big|_{z=0}+M_a\delta\left(\frac{du}{dz}\right)\Big|_{z=0}=0 \tag{4.47}$$

Integrating the terms containing $\delta(d^2u/dz^2)$ and $\delta(du/dz)$ we get:

$$
\begin{aligned}
&\int_0^{L_p}\left[E_pI_p\frac{d^4u}{dz^4}-\int_Y\int_X G_s(x,y)\phi_x^2\phi_y^2\frac{d^2u}{dz^2}dx\,dy+\int_Y\int_X\left[\left(\lambda_s(x,y)+2G_s(x,y)\right)\left(\frac{d\phi_x}{dx}\right)^2\phi_y^2+G_s(x,y)\phi_x^2\left(\frac{d\phi_y}{dy}\right)^2\right]u\,dx\,dy\right]\delta u\,dz\\
&+\int_{L_p}^{\infty}\int_Y\int_X\left\{-G_s(x,y)\phi_x^2\phi_y^2\frac{d^2u}{dz^2}+\left[\left(\lambda_s(x,y)+2G_s(x,y)\right)\left(\frac{d\phi_x}{dx}\right)^2\phi_y^2+G_s(x,y)\phi_x^2\left(\frac{d\phi_y}{dy}\right)^2\right]u\right\}\delta u\,dx\,dy\,dz\\
&-\left[E_pI_p\frac{d^2u}{dz^2}-M_a\right]\delta\left(\frac{du}{dz}\right)\Big|_{z=0}+E_pI_p\frac{d^2u}{dz^2}\delta\left(\frac{du}{dz}\right)\Big|_{z=L_p}\\
&+\left[E_pI_p\frac{d^3u}{dz^3}-\int_Y\int_X G_s(x,y)\phi_x^2\phi_y^2\left(\frac{du}{dz}\right)dx\,dy-F_a\right]\delta u\Big|_{z=0}-\left[E_pI_p\frac{d^3u}{dz^3}-\int_Y\int_X G_s(x,y)\phi_x^2\phi_y^2\left(\frac{du}{dz}\right)dx\,dy\right]\delta u\Big|_{z=L_p}\\
&+\int_X\int_Y G_s(x,y)\phi_x^2\phi_y^2\left(\frac{du}{dz}\right)dx\,dy\,\delta u\Big|_{z=\infty}=0
\end{aligned}
\tag{4.48}
$$

Delineating the soil layers with $n$ subdivisions of the pile-length and letting the $(n+1)^{th}$ layer extend to infinity from the bottom of the pile.

$$
\begin{aligned}
&\sum_{i=1}^{n}\int_{H_{i-1}}^{H_i}\left[E_pI_p\frac{d^4u_i}{dz^4}-\int_Y\int_X G_{s_i}(x,y)\phi_x^2\phi_y^2\frac{d^2u_i}{dz^2}dx\,dy+\int_Y\int_X\left[\left(\lambda_{s_i}(x,y)+2G_{s_i}(x,y)\right)\left(\frac{d\phi_x}{dx}\right)^2\phi_y^2+G_{s_i}(x,y)\phi_x^2\left(\frac{d\phi_y}{dy}\right)^2\right]u_i\,dx\,dy\right]\delta u_i\,dz\\
&+\int_{L_p}^{\infty}\int_Y\int_X\left\{-G_{s_{n+1}}(x,y)\phi_x^2\phi_y^2\frac{d^2u_{n+1}}{dz^2}+\left[\left(\lambda_{s_{n+1}}(x,y)+2G_{s_{n+1}}(x,y)\right)\left(\frac{d\phi_x}{dx}\right)^2\phi_y^2+G_{s_{n+1}}(x,y)\phi_x^2\left(\frac{d\phi_y}{dy}\right)^2\right]u_{n+1}\right\}\delta u_{n+1}\,dx\,dy\,dz\\
&-\left[E_pI_p\frac{d^2u_1}{dz^2}-M_a\right]\delta\left(\frac{du_1}{dz}\right)\Big|_{z=0}+E_pI_p\frac{d^2u_n}{dz^2}\delta\left(\frac{du_n}{dz}\right)\Big|_{z=L_p}\\
&+\left[E_pI_p\frac{d^3u_1}{dz^3}-\int_Y\int_X G_{s_1}(x,y)\phi_x^2\phi_y^2\left(\frac{du_1}{dz}\right)dx\,dy-F_a\right]\delta u_1\Big|_{z=0}-\left[E_pI_p\frac{d^3u_n}{dz^3}-\int_Y\int_X G_{s_n}(x,y)\phi_x^2\phi_y^2\left(\frac{du_n}{dz}\right)dx\,dy\right]\delta u\Big|_{z=L_p}\\
&+\int_X\int_Y G_{s_{n+1}}(x,y)\phi_x^2\phi_y^2\left(\frac{du_{n+1}}{dz}\right)dx\,dy\,\delta u_{n+1}\Big|_{z=\infty}=0
\end{aligned}
\tag{4.49}
$$

Considering the function u in the domain $0\le z\le L_p$, the variation $\delta u\neq 0$ since u is not known a priori. Therefore, to satisfy the principle of minimum potential energy $\delta\Pi=0$ we have:

$$
\begin{aligned}
&\sum_{i=1}^{n}\left[E_pI_p\frac{d^4u_i}{dz^4}-\int_Y\int_X G_{s_i}(x,y)\phi_x^2\phi_y^2\frac{d^2u_i}{dz^2}dx\,dy\right.\\
&\left.+\int_Y\int_X\left[\left(\lambda_{s_i}(x,y)+2G_{s_i}(x,y)\right)\left(\frac{d\phi_x}{dx}\right)^2\phi_y^2+G_{s_i}(x,y)\phi_x^2\left(\frac{d\phi_y}{dy}\right)^2\right]u_i\,dx\,dy\right]=0
\end{aligned}
\tag{4.50}
$$

From which the pile's governing *ODE* can be extracted:

$$\frac{d^4 u_i}{dz^4} - 2t_i \frac{d^2 u_i}{dz^2} + k_i u_i = 0 \tag{4.51}$$

where

$$2t_i = \frac{1}{E_p I_p} \int_Y \int_X G_{s_i}(x,y) \phi_x^2 \phi_y^2 \, dx \, dy \tag{4.52-a}$$

$$= \begin{cases} \dfrac{1}{E_p I_p} \left[ \displaystyle\int_{-\infty}^{-b} \phi_y^2 \left[ \int_{-\infty}^{-a} \phi_x^2 G_{s_i}(x,y) dx + \int_{a}^{\infty} \phi_x^2 G_{s_i}(x,y) dx \right] dy \right. \\ \left. + \displaystyle\int_{b}^{\infty} \phi_y^2 \left[ \int_{-\infty}^{-a} \phi_x^2 G_{s_i}(x,y) dx + \int_{a}^{\infty} \phi_x^2 G_{s_i}(x,y) dx \right] dy \right. & \text{for i =1,2...n} \\ \dfrac{1}{E_p I_p} \left[ \displaystyle\int_{-\infty}^{+\infty} \phi_y^2 \int_{-\infty}^{+\infty} \phi_x^2 G_{s_i}(x,y) dx \, dy \right] & \text{for i = n+1} \end{cases} \tag{4.52-b}$$

$$k_i = \frac{1}{E_p I_p} \left[ \int_{-\infty}^{+\infty} \phi_y^2 \int_{-\infty}^{+\infty} \left( \lambda_{s_i}(x,y) + 2G_{s_i}(x,y) \right) \left( \frac{d\phi_x}{dx} \right)^2 dx \, dy + \int_{-\infty}^{+\infty} \left( \frac{d\phi_y}{dy} \right)^2 \int_{-\infty}^{+\infty} G_{s_i}(x,y) \phi_x^2 \, dx \, dy \right] \tag{4.52-c}$$

The terms $t_i$ and $k_i$ encompass the resistance provided by the soil against the motion of the pile subjected to a force and moment at its head. One can recognize the similarities between the parameter $k_i$ in the 2-parameter continuum model and the spring stiffness $k$ in the *Winkler* model. Analogous to the parameter $k$ from the *Winkler* model, $k_i$ accounts for the compressive resistance of the soil. The parameter $t_i$, in contrast accounts for the shear resistance in the soil. It is evident from the above equations that $t_i$ and $k_i$ are scalar values having a representative value at the $i^{th}$ layer. In order to capture the actual

dependency of these parameters with respect to depth, the layers can be further discretized into smaller strips of soil with each strip assigned different mean values of the soil properties with depth.

We now consider the function $u$ in the domain $L_p \leq z < \infty$. Setting all the terms associated with the variation $\delta u$ and $\delta(du/dz)$ in the domain $L_p \leq z < \infty$ to zero to satisfy $\delta\Pi = 0$ yields:

$$\begin{aligned}
&\int_{L_p}^{\infty}\int_{Y}\int_{X}\Bigg\{-G_{s_{n+1}}(x,y)\phi_x^2\phi_y^2\frac{d^2u_{n+1}}{dz^2} \\
&+\left[\left(\lambda_{s_{n+1}}(x,y)+2G_{s_{n+1}}(x,y)\right)\left(\frac{d\phi_x}{dx}\right)^2\phi_y^2+G_{s_{n+1}}(x,y)\phi_x^2\left(\frac{d\phi_y}{dy}\right)^2\right]u_{n+1}\Bigg\}\delta u_{n+1}dz \\
&+\left[\int_{Y}\int_{X}G_{s_{n+1}}(x,y)\phi_x^2\phi_y^2\left(\frac{du_{n+1}}{dz}\right)dx\,dy\right]\delta u_{n+1}\Big|_{z=\infty}=0
\end{aligned} \tag{4.53}$$

Equation 4.53 can be further simplified by incorporating the boundary conditions of the pile such that at $z = \infty$, the displacement due to the pile is zero. This gives the following *ODE* for the displacement due to the pile deflection beyond its base.

$$-2t_{n+1}E_pI_p\frac{d^2u_{n+1}}{dz^2}+k_{n+1}E_pI_pu_{n+1}=0 \tag{4.54}$$

The solution to the *ODE* gives the displacement due to the pile at depths extending beyond the pile length of free-end piles. Alternatively, for piles fixed at the bottom, the displacement $u_n = 0$ can be prescribed at $z = L_p$.

## 4.3 Closed-form solution for pile deflection

Since we are dealing with a fourth order *ODE* for the pile deflection in the domain $0 \leq z \leq L_p$, the following general solution is assumed:

$$u_i(z) = C_1^{(i)}\Phi_1 + C_2^{(i)}\Phi_2 + C_3^{(i)}\Phi_3 + C_4^{(i)}\Phi_4 \tag{4.55}$$

where $C_1^{(i)}$. $C_2^{(i)}$, $C_3^{(i)}$ and $C_4^{(i)}$ are integration constants for the $i^{th}$ layer and $\Phi_1$, $\Phi_2$, $\Phi_3$ and $\Phi_4$ are the individual solutions of the *ODE*. The integration constants can be obtained by ensuring boundary conditions are respected and continuity at every layer interface is maintained. The individual solutions on the other hand can be obtained using conventional methods of solving ordinary differential equations such as the method of initial parameters. In fact Basu (2006) obtained analytical solutions for short piles and long piles embedded in a multi-layered soil deposit. Recall that $t_i$ and $k_i$ are scalar values; hence the *ODE* can be categorized as linear with constant coefficients. This allows us to assume a general solution of the form $u(z) = e^{mz}$. Had we been dealing with variable coefficients, the solution could take the form of Bessel functions or non-exponential functions. Differentiating $u(z)$ and substituting it in the general solution given by equation 4.55, we get the auxiliary equation:

$$m^4 - 2t_i m^2 + k_i = 0 \tag{4.56}$$

whose solution is given by:

$$m = \pm\sqrt{t_i \pm \sqrt{t_i^2 - k_i}} \tag{4.57}$$

Looking at the above equation, three cases are apparent.

1. $k_i > t_i^2$ (4.58-a)

2. $k_i < t_i^2$ (4.58-b)

3. $k_i = t_i^2$ (4.58-c)

We worry about the first two cases, as case 3 occurs under very stringent conditions, which are mostly inconceivable. Case 1 produces complex values for m of the form $a+ib$. Substituting this form back into our solution for m yields the following two equations in terms of the constants a and b: $a^2 + b^2 = t_i$ and $2ab = \sqrt{k_i - t_i^2}$. For $k_i < t_i^2$, $m$ is a real number and can be readily solved using equation 4.57. Table 4.1 below compiled by Basu and Salgado (2008) shows the individual solutions $\Phi_1$, $\Phi_2$, $\Phi_3$ *and* $\Phi_4$.

**Table 4.1: Functions of the general solution given in equation 4.55 (Source: Basu and Salgado, 2008)**

| Relative magnitudes of k and t | Constants | | Derivatives of individual solutions of pile deflection | Individual solutions of pile deflection | | | |
|---|---|---|---|---|---|---|---|
| | a | b | | $\Phi_1$ | $\Phi_2$ | $\Phi_3$ | $\Phi_4$ |
| $k > t^2$ | $\sqrt{[(1/2)(\sqrt{k}+t)]}$ | $\sqrt{[(1/2)(\sqrt{k}-t)]}$ | $\Phi$ | $\text{Sinh}(az)\cos(bz)$ | $\text{Cosh}(az)\cos(bz)$ | $\text{Cosh}(az)\sin(bz)$ | $\text{Sinh}(az)\sin(bz)$ |
| | | | $\Phi'$ | $a\Phi_1 - b\Phi_4$ | $a\Phi_1 - b\Phi_3$ | $a\Phi_4 + b\Phi_2$ | $a\Phi_3 + b\Phi_1$ |
| | | | $\Phi''$ | $(a^2 - b^2)\Phi_1 - 2ab\Phi_3$ | $(a^2 - b^2)\Phi_2 - 2ab\Phi_4$ | $(a^2 - b^2)\Phi_3 + 2ab\Phi_1$ | $(a^2 - b^2)\Phi_4 + 2ab\Phi_2$ |
| | | | $\Phi'''$ | $a(a^2-3b^2)\Phi_2 + b(b^2- 3a^2)\Phi_4$ | $a(a^2-3b^2)\Phi_1 + b(b^2- 3a^2)\Phi_3$ | $a(a^2-3b^2)\Phi_4 - b(b^2- 3a^2)\Phi_2$ | $a(a^2-3b^2)\Phi_3 - b(b^2- 3a^2)\Phi_1$ |
| $k < t^2$ | $\sqrt{[t + \sqrt{(t^2 - k)}]}$ | $\sqrt{[t - \sqrt{(t^2 - k)}]}$ | $\Phi$ | $\text{Sinh}(az)$ | $\text{Cosh}(az)$ | $\text{Sinh}(bz)$ | $\text{Cosh}(bz)$ |
| | | | $\Phi'$ | $a\Phi_2$ | $a\Phi_1$ | $b\Phi_4$ | $b\Phi_3$ |
| | | | $\Phi''$ | $a^2\Phi_1$ | $a^2\Phi_2$ | $b^2\Phi_3$ | $b^2\Phi_4$ |
| | | | $\Phi'''$ | $a^3\Phi_2$ | $a^3\Phi_1$ | $b^3\Phi_4$ | $b^3\Phi_3$ |

Inasmuch as the soil strata are well defined, the unknowns $C_1^{(i)}$, $C_2^{(i)}$, $C_3^{(i)}$ and $C_4^{(i)}$ can be obtained by satisfying the boundary conditions and by ensuring continuity is not violated at every soil layer interface. The reader should be familiar with the different types of boundary conditions; namely Dirichlet, Neumann or Mixed boundary conditions. Starting at the pile's head, two boundary conditions are imposed; firstly the applied load (Neumann), which can also be a prescribed deflection (Dirichlet), and secondly the applied moment (Neumann), which can be given as a prescribed rotation (Dirichlet). At the pile's base, we require the residual shear force exerted by the pile to balance out the shear resistance provided by the $(n+1)^{th}$ soil layer. This is mathematically expressed by equation 4.59-n. Alternatively, the base could be made to replicate a fixed support boundary condition. Good engineering judgment is required before making such an assumption as a fixed-support means that the bottom of the pile now carries moment. We illustrate the system of equations generated from continuity and the boundary conditions at the head and base of the pile for a 3-layered soil deposit.

$$M_1\Big|_{z=H_0} = M_a \;;\; S_1\Big|_{z=H_0} = F_a \tag{4.59-a}$$

$$C_1^{(1)}\Phi_{31}\left(H_0\right)+C_2^{(1)}\Phi_{32}\left(H_0\right)+C_3^{(1)}\Phi_{33}\left(H_0\right)+C_4^{(1)}\Phi_{34}\left(H_0\right)=M_a \tag{4.59-b}$$

$$C_1^{(1)}\Phi_{41}\left(H_0\right)+C_2^{(1)}\Phi_{42}\left(H_0\right)+C_3^{(1)}\Phi_{43}\left(H_0\right)+C_4^{(1)}\Phi_{44}\left(H_0\right)=F_a \tag{4.59-c}$$

$$u_1\Big|_{z=H_1} = u_2\Big|_{z=H_1} \;;\; \theta_1\Big|_{z=H_1} = \theta_2\Big|_{z=H_1} \;;\; M_1\Big|_{z=H_1} = M_2\Big|_{z=H_1} \;;\; S_1\Big|_{z=H_1} = S_2\Big|_{z=H_1} \tag{4.59-d}$$

$$C_1^{(2)}\Phi_{31}\left(H_2\right)+C_2^{(2)}\Phi_{32}\left(H_2\right)+C_3^{(2)}\Phi_{33}\left(H_2\right)+C_4^{(2)}\Phi_{34}\left(H_2\right)-C_1^{(3)}\Phi_{31}\left(H_2\right)-C_2^{(3)}\Phi_{32}\left(H_2\right)-C_3^{(3)}\Phi_{33}\left(H_2\right)-C_4^{(3)}\Phi_{34}\left(H_2\right)=0 \tag{4.59-e}$$

$$C_1^{(1)}\Phi_{21}\left(H_1\right)+C_2^{(1)}\Phi_{22}\left(H_1\right)+C_3^{(1)}\Phi_{23}\left(H_1\right)+C_4^{(1)}\Phi_{24}\left(H_1\right)-C_1^{(2)}\Phi_{21}\left(H_1\right)-C_2^{(2)}\Phi_{22}\left(H_1\right)-C_3^{(2)}\Phi_{23}\left(H_1\right)-C_4^{(2)}\Phi_{24}\left(H_1\right)=0 \tag{4.59-f}$$

$$C_1^{(1)}\Phi_{31}\left(H_1\right)+C_2^{(1)}\Phi_{32}\left(H_1\right)+C_3^{(1)}\Phi_{33}\left(H_1\right)+C_4^{(1)}\Phi_{34}\left(H_1\right)-C_1^{(2)}\Phi_{31}\left(H_1\right)-C_2^{(2)}\Phi_{32}\left(H_1\right)-C_3^{(2)}\Phi_{33}\left(H_1\right)-C_4^{(2)}\Phi_{34}\left(H_1\right)=0 \tag{4.59-g}$$

$$C_1^{(1)}\Phi_{41}(H_1)+C_2^{(1)}\Phi_{42}(H_1)+C_3^{(1)}\Phi_{43}(H_1)+C_4^{(1)}\Phi_{44}(H_1)-C_1^{(2)}\Phi_{41}(H_1)-C_2^{(2)}\Phi_{42}(H_1)-C_3^{(2)}\Phi_{43}(H_1)-C_4^{(2)}\Phi_{44}(H_1)=0 \quad (4.59\text{-h})$$

$$u_2\big|_{z=H_2}=u_3\big|_{z=H_2};\ \theta_2\big|_{z=H_2}=\theta_3\big|_{z=H_2};\ M_2\big|_{z=H_2}=M_3\big|_{z=H_2};\ S_2\big|_{z=H_2}=S_3\big|_{z=H_2} \quad (4.59\text{-i})$$

$$C_1^{(2)}\Phi_{11}(H_2)+C_2^{(2)}\Phi_{12}(H_2)+C_3^{(2)}\Phi_{13}(H_2)+C_4^{(2)}\Phi_{14}(H_2)-C_1^{(3)}\Phi_{11}(H_2)-C_2^{(3)}\Phi_{12}(H_2)-C_3^{(3)}\Phi_{13}(H_2)-C_4^{(3)}\Phi_{14}(H_2)=0 \quad (4.59\text{-j})$$

$$C_1^{(2)}\Phi_{21}(H_2)+C_2^{(2)}\Phi_{22}(H_2)+C_3^{(2)}\Phi_{23}(H_2)+C_4^{(2)}\Phi_{24}(H_2)-C_1^{(3)}\Phi_{21}(H_2)-C_2^{(3)}\Phi_{22}(H_2)-C_3^{(3)}\Phi_{23}(H_2)-C_4^{(3)}\Phi_{24}(H_2)=0 \quad (4.59\text{-k})$$

$$C_1^{(2)}\Phi_{31}(H_2)+C_2^{(2)}\Phi_{32}(H_2)+C_3^{(2)}\Phi_{33}(H_2)+C_4^{(2)}\Phi_{34}(H_2)-C_1^{(3)}\Phi_{31}(H_2)-C_2^{(3)}\Phi_{32}(H_2)-C_3^{(3)}\Phi_{33}(H_2)-C_4^{(3)}\Phi_{34}(H_2)=0 \quad (4.59\text{-l})$$

$$C_1^{(2)}\Phi_{41}(H_2)+C_2^{(2)}\Phi_{42}(H_2)+C_3^{(2)}\Phi_{43}(H_2)+C_4^{(2)}\Phi_{44}(H_2)-C_1^{(3)}\Phi_{41}(H_2)-C_2^{(3)}\Phi_{42}(H_2)-C_3^{(3)}\Phi_{43}(H_2)-C_4^{(3)}\Phi_{44}(H_2)=0 \quad (4.59\text{-m})$$

$$M_3\big|_{z=H_3}=0;\ S_3\big|_{z=H_3}=\sqrt{2k_nt_n\zeta}u_n \quad (4.59\text{-n})$$

$$C_1^{(3)}\Phi_{31}(H_3)+C_2^{(3)}\Phi_{32}(H_3)+C_3^{(3)}\Phi_{33}(H_3)+C_4^{(3)}\Phi_{34}(H_3)=0 \quad (4.59\text{-o})$$

$$C_1^{(3)}\Phi_{31}(H_3)+C_2^{(3)}\Phi_{32}(H_3)+C_3^{(3)}\Phi_{33}(H_3)+C_4^{(3)}\Phi_{34}(H_3)=\sqrt{2k_nt_n\zeta}u_n \quad (4.59\text{-p})$$

The above equations can be recast as a matrix equation and solved simultaneously. The matrix form of the equation is given by:

$$\left[\Phi\right]\left\{C\right\}=\left\{R\right\} \quad (4.60)$$

where the entries of the matrix *[Φ]* are the individual solutions and their derivatives evaluated at the soil interface such that the first subscript '*i*' denoting the $i^{th}$ row of the matrix is also the $(i-1)^{th}$ derivative of the $j^{th}$ individual solution at the $j^{th}$ column i.e

$\Phi_{ij}=\Phi_j^{(i-1)}$ for $i < 4$. For $i = 4$, $\Phi_{4j}=\Phi_j^{(3)}-2t_i\Phi_j^{(1)}$, where "*i*" this time corresponds to the $i^{th}$ *layer*. *{C}* is the vector of unknowns $C_1^{(i)}$. $C_2^{(i)}$, $C_3^{(i)}$ and $C_4^{(i)}$ and *{R}* is the right-hand side vector consisting of mostly zeros. The values $H_i$ corresponds to the depth of the soil interface from the surface, $z = 0$ and $\zeta = t_{n+1}/t_n$.

## 4.4 Solution Algorithm

The solution to this chapter's problem consists of three main parts, notably the pair of soil displacement functions $\phi_x$ and $\phi_y$ and the pile deflection, $u$. Knowledge of at least two out of these three unknown functions is necessary to solve the problem. Since we know approximately the behaviour of the soil profile, we start with initial guesses of $\phi_x$ and $\phi_y$. We assume a linear function starting from a value of 1 at one edge of the pile to zero at some distance x or y sufficiently far such that no boundary effects are taken into consideration. Values of the soil's modulus and Poisson ratio are then generated using the 2D *KL* expansion. From the spectral decomposition of these soil properties we then compute *Lame*'s constants as functions of the space variables $x$ and $y$. The statistical properties of the soil Young's modulus and Poisson's ratio as a function of space for each layer are passed to a subroutine that generates these parameters' random fields. Figure 4.4 shows how the spatially random soil properties map over the soil domain.

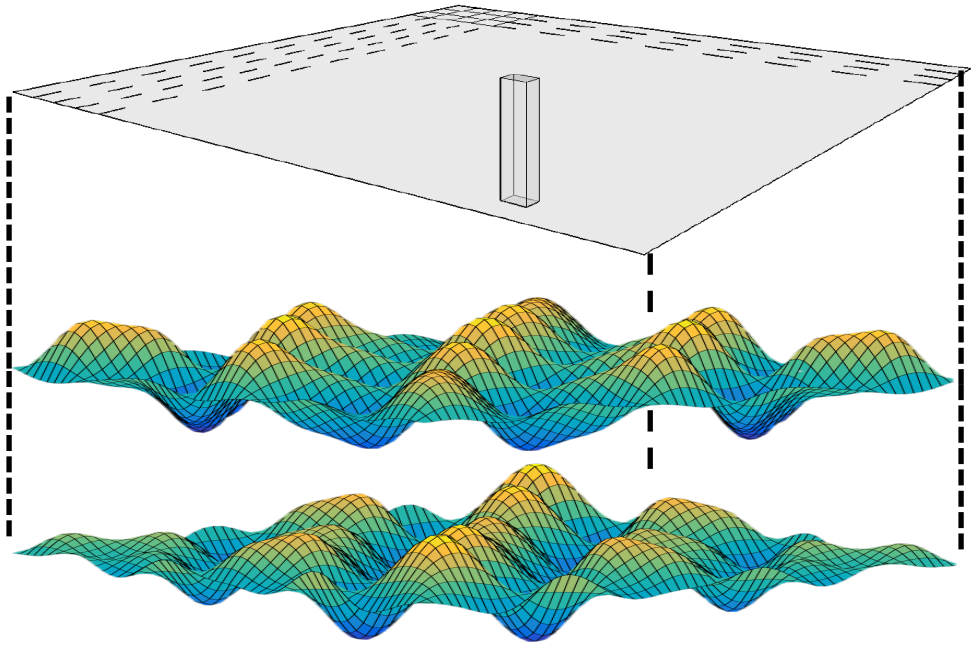

**Figure 4.4: 2-D Random field of soil properties spanning problem domain**

Evidently, several iterations are required, for which the values of $t_i$ and $k_i$ are computed numerically. A trapezoidal rule is used for the numerical integration of $t_i$ and $k_i$. Thereafter, the system of equations formed from the pile differential equation is simultaneously solved. From the pile deflection, the soil-displacement functions can be computed and used as new guesses in the next iteration. The convergence criteria used are $\frac{1}{N}\sum_{j=1}^{N-1}\left|\phi_x^{j+1}-\phi_x^{j}\right| \le 10^{-5}$ and $\frac{1}{N}\sum_{i=1}^{N-1}\left|\phi_y^{i+1}-\phi_y^{i}\right| \le 10^{-5}$ where $N$ is the number of nodes in the discretization scheme of the finite difference method employed to solve the soil displacement functions. The flowchart shown in figure 4.5 lays out the implementation of a two-dimensional *KL* expansion in the analysis of a two-parameter continuum model of a pile.

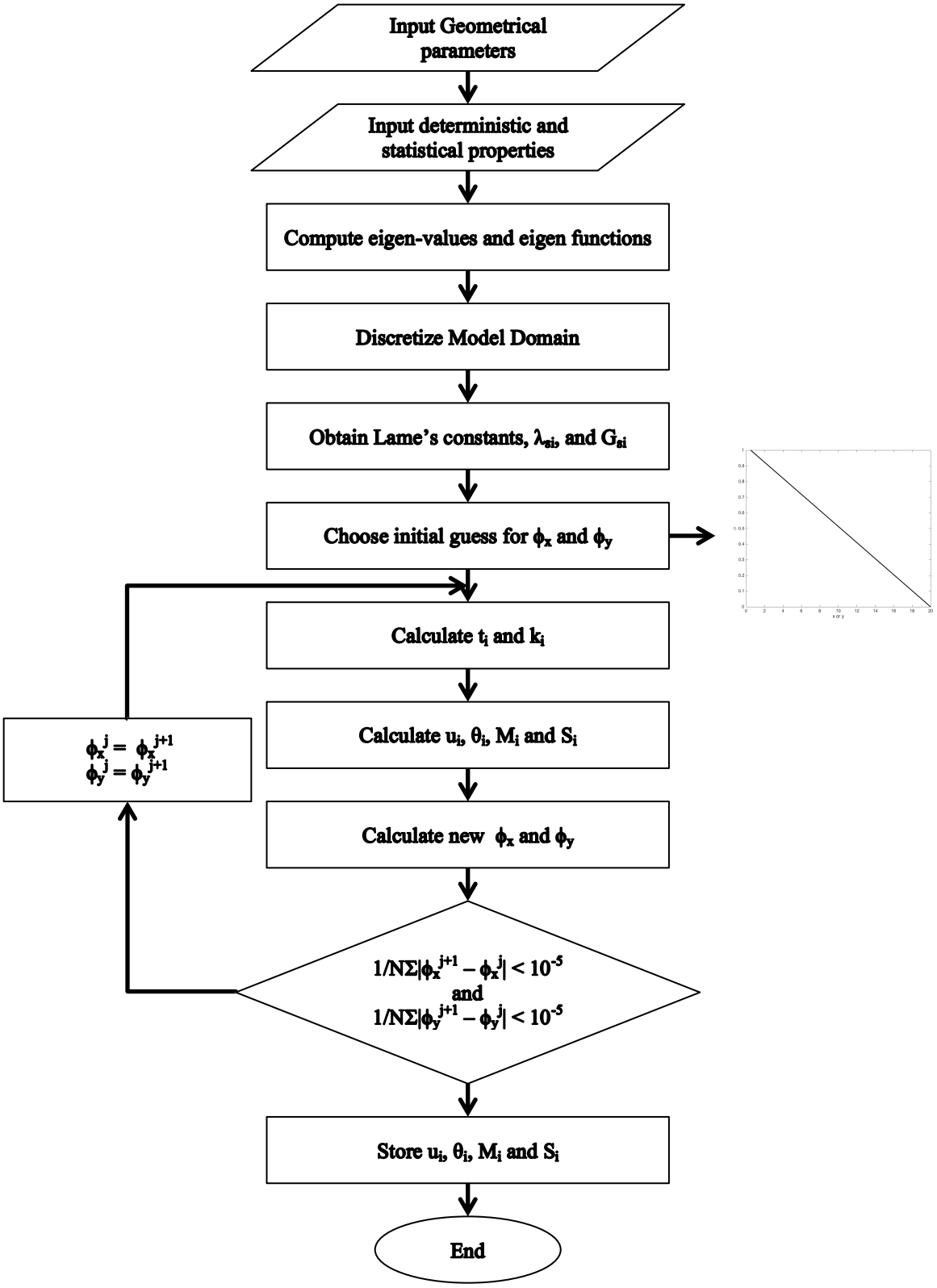


**Figure 4.5: Flowchart of stochastic analysis of 2-parameter continuum pile**

## 4.5 Numerical Examples

In this section, we apply the developed method to two examples of laterally loaded piles embedded in a multilayered soil, which were previously analyzed, by Basu and Salgado (2008). In the first example, we consider a pile subjected to a lateral load of *300kN* embedded in a four-layer soil profile with the thickness of each layer given by $H_i = 2m$, $H_2 = 5m$, $H_3 = 8m$ and the last layer extending to an infinitely large depth. The mean soil's Young's modulus of each layer is: $E_{s1} = 20MPa$, $E_{s2} = 35MPa$, $E_{s3} = 50MPa$ and $E_{s4} = 80Mpa$ respectively. The mean soil's Poisson ratio of each layer is: $\upsilon_{s1} = 0.35$, $\upsilon_{s2} = 0.25$, $\upsilon_{s3} = 0.20$ and $\upsilon_{s4} = 0.15$ respectively. The pile has a cross-sectional area *of 0.5m x 0.5m* and is *25m* long with a Young's modulus, $E_p = 25 \times 10^6 kPa$. The soil's statistical properties are summarized in table 4.2.

**Table 4.2 Statistical moments of soil properties for example 1**

| Soil Layer, i | 1 | 2 | 3 | 4 |
|---|---|---|---|---|
| **Soil Statistical parameters in the x-direction** | | | | |
| $\langle E_{s,i} \rangle$ [kPa] | 2.00E+04 | 3.50E+04 | 5.00E+04 | 8.00E+04 |
| $\sigma_{Es,I}$ [kPa] | 2.20E+02 | 2.30E+02 | 2.00E+02 | 2.10E+02 |
| $\langle v_{s,i} \rangle$ | 0.35 | 0.25 | 0.2 | 0.15 |
| $\sigma_{v,I}$ | 1.10E-02 | 1.20E-02 | 1.10E-02 | 9.50E-03 |
| **Soil Statistical parameters in the y-direction** | | | | |
| $\langle E_{s,i} \rangle$ [kPa] | 2.00E+04 | 3.50E+04 | 5.00E+04 | 8.00E+04 |
| $\sigma_{Es,I}$ [kPa] | 2.50E+02 | 2.40E+02 | 2.30E+02 | 2.20E+02 |
| $\langle v_{s,i} \rangle$ | 0.35 | 0.25 | 0.2 | 0.15 |
| $\sigma_{v,I}$ | 8.00E-03 | 5.00E-03 | 4.50E-03 | 4.00E-03 |

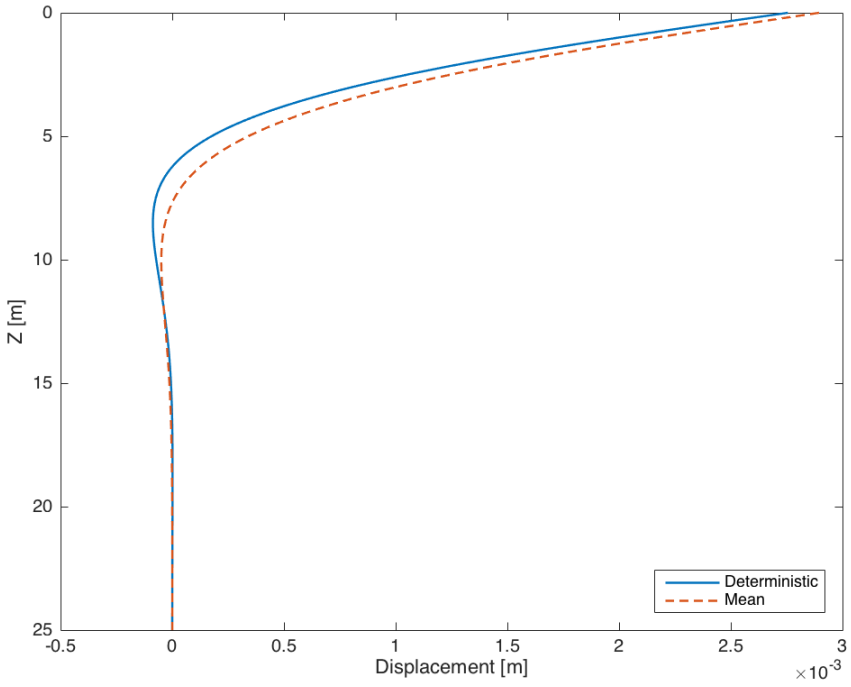


**Figure 4.6: Mean pile deflection for example 1**

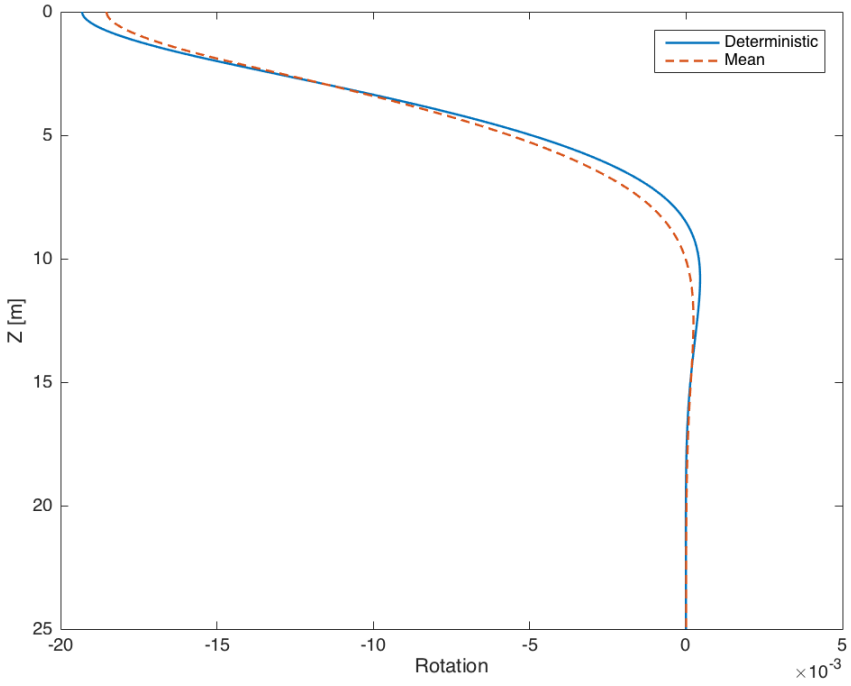


**Figure 4.7: Mean pile rotation for example 1**

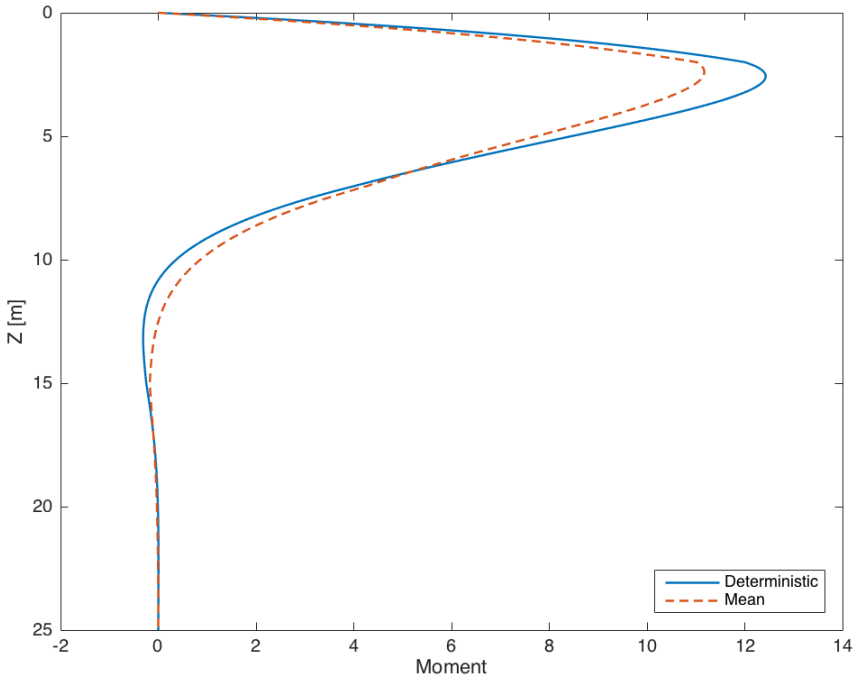


**Figure 4.8: Mean pile moment for example 1**

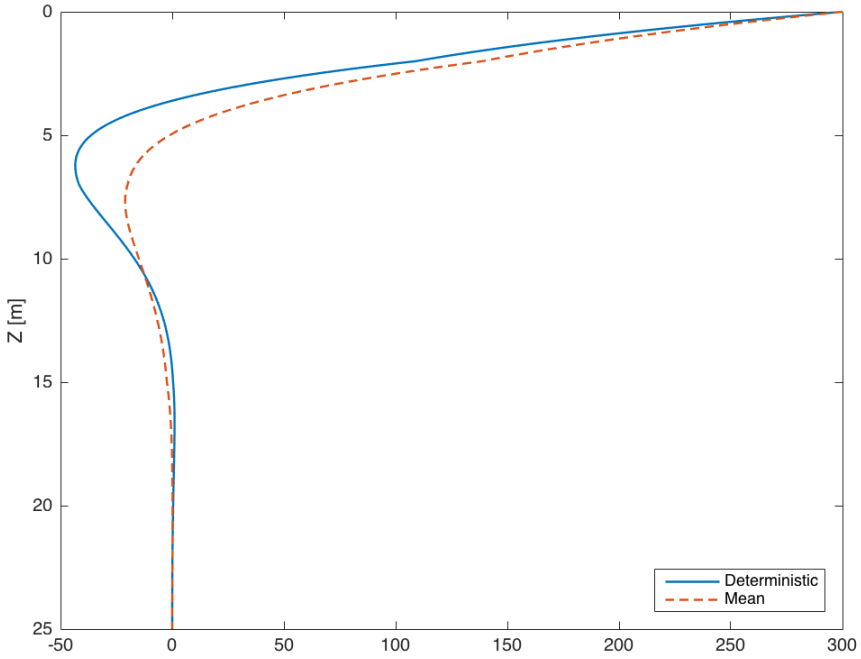


**Figure 4.9: Mean pile shear for example 1**

A few observations can be made from the results: firstly we note that close to points at which boundary conditions are in effect, the mean result converges to the deterministic solution. This makes sense as the boundary conditions are imposed and are thus known (deterministic). Noteworthy also is a deterministic length, $L_{det}$ so to speak in the range $15m<Z<25m$, where the mean response and the deterministic solution are almost identical. We suspect that this deterministic length is in fact, the critical length of the pile. The critical length of a pile is essentially a threshold length such that any additional pile length does not have any impact on the lateral pile response. From this definition, a new definition with respect to the pile's random behaviour can be postulated. If the critical length delineates the pile into two parts, one where the lateral beam response is not impacted and the other where changes in the response do occur; it can be said from a statistical point of view that one part is deterministic, while the other is probabilistic. A better depiction of this phenomenon can be captured looking at the variance of the pile's response with respect to its length.

The second observation, which we can make, is that the difference between the mean response and the deterministic solution of the pile is larger for the moment and shear than the pile deflection and rotation. This is attributed to transformation errors mentioned in Chapter 1 of this thesis. Because the rotation, moment and shear of the pile are obtained from its deflected shape, the accuracy of the former heavily relies on the accuracy of the pile deflection. The reader is therefore advised to tread carefully when reporting the shear or moment of the pile. Higher orders of expansions are recommended and as we will see special care should be given to piles of significant lengths.

In the second example, we consider a much longer pile of length *40m*, with a cross-sectional area of *2.8m x 0.8m* and a Young's modulus, $E_p = 25 \times 10^6 kPa$. The pile is embedded in a four-layer soil deposit having thicknesses, $H_1 = 1.5m$, $H_2 = 3.5m$, $H_3 = 8.5m$ and the last layer extending far beyond the pile's base. The mean soil's Young's modulus are: $E_{s1} = 20MPa$, $E_{s2} = 25MPa$, $E_{s3} = 40MPa$, and $E_{s4} = 80MPa$ respectively. The mean soil's Poisson ratio are: $\upsilon_{s1} = 0.35$, $\upsilon_{s2} = 0.30$, $\upsilon_{s3} = 0.25$ and $\upsilon_{s4} = 0.20$ respectively. A load of *3000kN* is applied at the top of the pile parallel to the *x-axis* along the cross-section longer dimension ($a = 1.4m$). The soil's statistical properties are summarized in table 4.3.

**Table 4.3: Statistical moments of soil properties for example 2**

| Soil Layer, i | 1 | 2 | 3 | 4 |
|---|---|---|---|---|
| **Soil Statistical parameters in the x-direction** | | | | |
| $\langle E_{s,i} \rangle$ [kPa] | 2.00E+04 | 2.50E+04 | 4.00E+04 | 8.00E+04 |
| $\sigma_{Es,I}$ [kPa] | 2.20E+02 | 2.30E+02 | 2.00E+02 | 2.10E+02 |
| $\langle \upsilon_{s,i} \rangle$ | 0.35 | 0.30 | 0.25 | 0.20 |
| $\sigma_{v,I}$ | 1.10E-02 | 1.20E-02 | 1.10E-02 | 9.50E-03 |
| **Soil Statistical parameters in the y-direction** | | | | |
| $\langle E_{s,i} \rangle$ [kPa] | 2.00E+04 | 2.50E+04 | 4.00E+04 | 8.00E+04 |
| $\sigma_{Es,I}$ [kPa] | 2.50E+02 | 2.40E+02 | 2.30E+02 | 2.20E+02 |
| $\langle \upsilon_{s,i} \rangle$ | 0.35 | 0.30 | 0.25 | 0.20 |
| $\sigma_{v,I}$ | 8.00E-03 | 5.00E-03 | 4.50E-03 | 4.00E-03 |

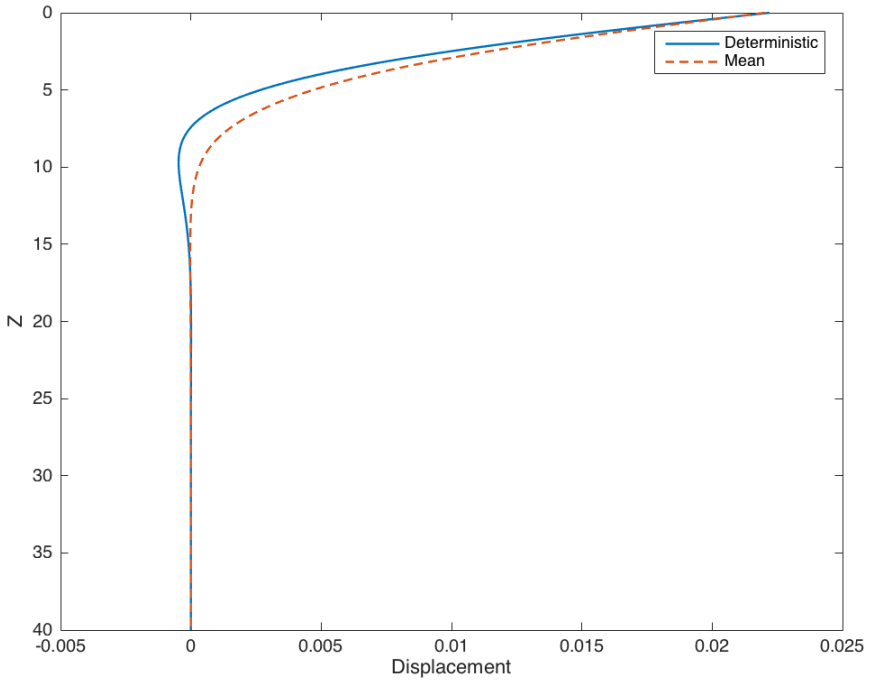


**Figure 4.10: Mean pile deflection for example 2**

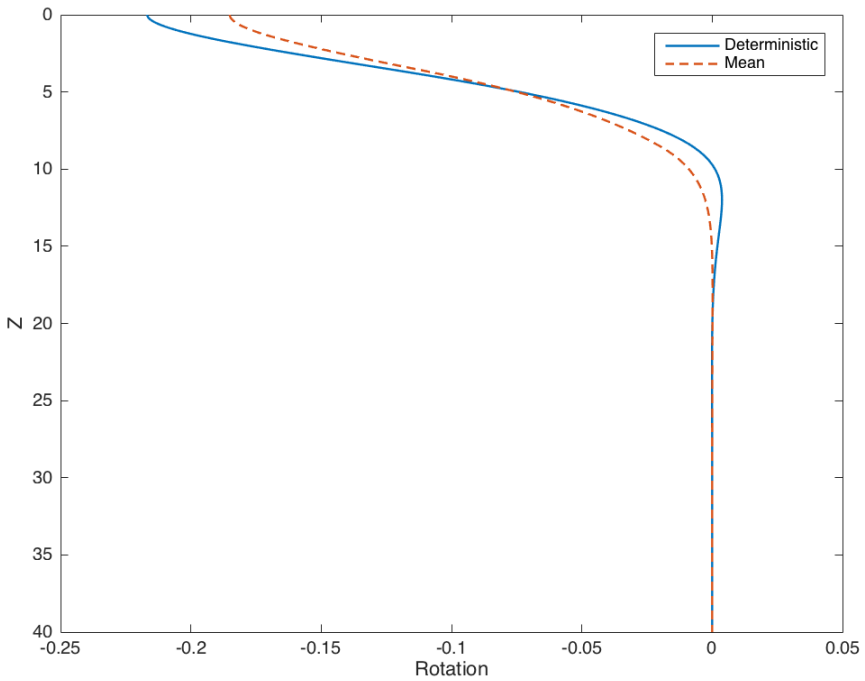


**Figure 4.11: Mean pile rotation for example 2**

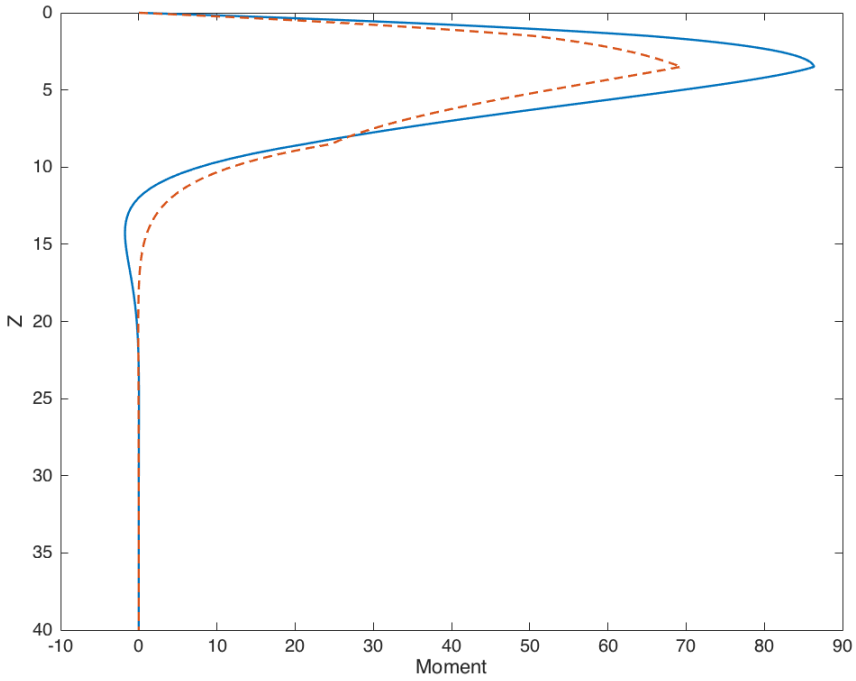


**Figure 4.12: Mean pile moment for example 2**

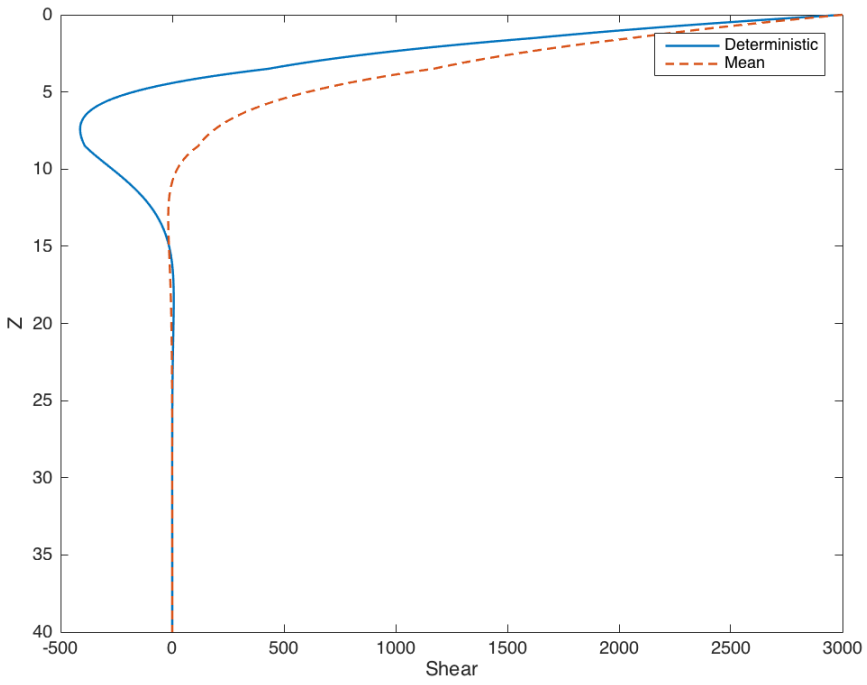


**Figure 4.13: Mean pile shear for example 2**

In the second example, we note a larger difference between the mean responses and the deterministic solutions. This is a result of the higher slenderness ratio of the pile in example 2. When subjected to a constant load, the potential energy of the pile increases with length. From a physical point of view, this makes sense since longer piles take longer to reach equilibrium. This translates to a response having a larger variance, which aligns with the theory of stability for a one-dimensional beam. Hence, the statistical results of our analyses support the mechanical behaviour the system.

## 4.6 Summary

A stochastic method in which a rectangular pile subjected to a lateral force and embedded in multiple soil layers each having spatially random properties is developed in Chapter 4. The random properties of each soil layer are represented using a 2-dimensional *Karhunen-Loeve* expansion. The soil's Young's modulus and the Poisson's ratio are assumed to be spatially random with exponential covariance. Thereafter, an analytical solution for the pile deflection involving the soil displacement is developed using *variational* principles. The random soil properties are introduced in the governing differential equations and an iterative solution is devised. An initial guess for the functions $\phi_x$ and $\phi_y$ is required, after which the pile's deflection is calculated. Using the pile's deflection, new values of $\phi_x$ and $\phi_y$ are calculated. This process is repeated until the absolute sum of the difference between the averages of two consecutive iterations of $\phi_x$ and $\phi_y$ converges. Two examples are considered, from which statistical inferences are made. In the first example a *25m* long pile embedded in four layers of soil is analyzed. The mean deflection is in close agreement with the deterministic solution. The rotation, moment, and shear are also produced. Greater disparities are noted in the mean response

of these values. A second example involving a *40m* long pile embedded in a four-layer soil is analyzed. In this example, the mean response shows less agreement with the deterministic solution. This increase in disparity is attributed to the longer slenderness ratio of the pile.

# CHAPTER 5.

# TIME EVOLUTION OF STOCHASTIC CONSTITUTIVE MODELS

## 5.1 Introduction

In addition to the foregoing analyses, let us now closely examine the evolution of probabilistic constitutive models across time. In this chapter, *elastic* and *elasto-plastic* constitutive models with random material properties are analyzed by way of the Fokker-Plank-Kolmogorov equation (FPKE). This approach, which was inspired by the work of many great scientists on Brownian motion, was first adapted to the field of civil engineering in 2003 by Kavvas (2003) for the purpose of investigating nonlinear hydrologic processes. In his work, Kavvas demonstrated that the conservation equations of hydrologic processes governed by non-linear *PDE*s could be transformed into linear deterministic *PDE*s whose solutions are the probability density functions of the hydrologic systems. Recognizing the similarities between non-linear conservation equations of hydrologic systems and non-linear constitutive equations, Kallol et al (2007) adapted the methodology to the probabilistic study of stress-strain behaviour of elastic and elasto-plastic materials.

Although in practice we could use the *KL* expansion introduced in Chapter 3 to propagate uncertainties in the material properties of non-linear constitutive models, the method suffers from "closure problems", where the computation of higher-order moments are

required to solve for lower-order moments. Moreover, as we have seen, the *KL* expansion, like perturbation methods, tends to underestimate the variability in the response of mechanical systems when large coefficients of variations for the input properties are assumed. And while it is the preferred method over *Monte Carlo* simulations for its computational efficiency, the constitutive model assumed undoubtedly impacts the accuracy of the method.

The goal of introducing uncertainties at the constitutive level is to have the full picture. The influence of material fluctuations on the stress-strain behaviour as we will see cannot be ignored. This is especially true for complicated non-linear material constitutive laws as is the case for soil models. Therefore, to truly encompass all sources of uncertainties, and provide a complete probabilistic framework, the evolution of stress must be treated as a random process.

As we delve into the preliminary work done by Kavvas (2003) on the development of a Eulerian-Lagrangian FPKE for non-linear hydrologic systems, we draw parallels between conservation equations of hydrologic systems and constitutive equations of elastic and elasto-plastic models. The methodology is developed for one-dimensional and three-dimensional classes of problems using Kallol's framework (2007). In the first class of problems, a linear elastic shear constitutive model along with a *Von Mises* model is considered. To conclude, we then apply the methodology to a 3-dimensional hypo-elastic model.

## 5.2 Analysis

In this section, we present the mathematical derivation of the FPKE for a general constitutive law. The equations are derived in a one-dimensional framework and extended to a three-dimension framework with two numerical examples provided for each framework. *Elastic* and *elasto-plastic* constitutive models are considered and their solutions using the FPKE are compared to *Monte Carlo* simulations. The method's performance and limitations are addressed and a discussion of the results is provided at the end of the chapter.

### 5.2.1 Probabilistic constitutive laws in one-dimension

More than a century has passed since Albert Einstein's paper on the theory of Brownian motion, and it has been several decades since the derivation of the Fokker-Planck-Kolmogorov Equation (Fokker, 1914; Planck, 1917; Kolmogorov, 1931), yet here we are still reaping the fruits of the labor of exceptional researchers. In appreciation for their work, a brief historical account is given on the development of the one-dimensional Fokker-Planck equation and how it made its way to Kavvas' analysis of hydrological systems to ultimately be employed by Kallol in the analysis of probabilistic constitutive models.

Starting with the derivation of the Fokker-Plank equation for a Brownian particle, let us consider a general Langevin equation for the dynamics of a particle in a "noisy" surrounding medium.

$$\frac{dX(t)}{dt} = v\left(X(t),t\right) + \Gamma(t) \tag{5.1}$$

which can simply be written as:

$$\frac{dX(t)}{dt} = \eta\left(x,v,t\right) \tag{5.2}$$

where $X(t)$ is the random position of a particle at time *t*, $v\left(X(t),t\right)$ is a general friction term, and $\Gamma(t)$ is the *Gaussian White Noise (GWN*) with the following properties:

$$\left\langle \Gamma(t) \right\rangle = 0 \tag{5.3-a}$$

$$\left\langle \Gamma(t_1)\Gamma(t_2) \right\rangle = a\delta(t_2 - t_1) \tag{5.3-b}$$

Because the *GWN*, $\Gamma(t)$ is a stochastic variable, $\eta\left(x,v,t\right)$ will be different for each realization of $\Gamma(t)$. However, these changes happen almost instantaneously and are very hard to observe. What is in fact observed is the average motion of the particle. We therefore introduce the following probability measure, which is the average of $\eta\left(x,v,t\right)$ over all the realizations of *Γ*.

$$P\left(X(t),t\right) = \left\langle \eta\left(X(t),t\right) \right\rangle_{\Gamma} \tag{5.4}$$

Enforcing continuity in the phase-space of *X(t)* such that probability is conserved, we have the following equation:

$$\frac{\partial}{\partial t}\eta\left(X(t),t\right) + \frac{\partial}{\partial X}\cdot\left[\frac{dX}{dt}\eta\left(X(t),t\right)\right] = 0 \tag{5.5}$$

Substituting the above equation, and the probability density into Langevin's equation yields the second order *PDE* known as the Diffusion equation:

$$\frac{\partial}{\partial t}P\left(X\left(t\right),t\right)=-\frac{\partial}{\partial X}\left(v\left(X\left(t\right)\right)P\left(X\left(t\right),t\right)\right)+\frac{1}{2}\frac{\partial}{\partial X}\cdot a\cdot\frac{\partial}{\partial X}P\left(X\left(t\right),t\right) \tag{5.6}$$

Without going into details, we will now go over Kavvas' derivation of the same equation for a probabilistic hydrologic system. This exercise will bring forth the similarities between the dynamical behaviour of a Brownian particle and an upscaled hydrologic system. It is worth mentioning that the probabilistic nature of Kavvas' problem is rooted in the upscaling of non-linear hydrologic systems. Those problems have been tackled by means of ensemble averaging point-location conservation equations. In his paper, Kavvas' defines a system of point-scale hydrologic conservation equations by the following equation:

$$\frac{\partial \underset{\sim}{H}\left(x,t\right)}{\partial t}=\underset{\sim}{\eta}\left(\underset{\sim}{H},\underset{\sim}{A},\underset{\sim}{f};x,t\right) \tag{5.7}$$

where $\underset{\sim}{H}$ is a state vector containing all the state variables from the hydrologic system, $\underset{\sim}{A}$ is tensor of all other parameters in the hydrologic system and $\underset{\sim}{f}$ is the forcing vector. The resemblance of equation 5.2 with equation 5.7 is flagrant. We note that just like *X, H* can be thought of as a point in a phase-space whose evolution is continuous in time, like the velocity of the Brownian particle. Equation 5.7 is therefore our Langevin's equivalent equation. Since the evolution of $\underset{\sim}{H}$ at large scales entails fluctuations akin to the *GWN*, we can define a *phase density* $\rho$ for the state variables $\underset{\sim}{H}$ after which we can express the continuity mathematically as follows:

$$\frac{\partial \rho\left(\underset{\sim}{H}\left(x,t\right),t\right)}{\partial t}=-\frac{\partial}{\partial H_i}\eta_i\left[\underset{\sim}{H}\left(x,t\right),\underset{\sim}{A}\left(x,t\right),\underset{\sim}{f}\left(x,t\right)\right]\cdot\rho\left[\underset{\sim}{H}\left(x,t\right),t\right] \tag{5.8}$$

The above equation is none but *Kubo's stochastic Liouville* equation (Kubo 1963). Taking the expectation (average) on both sides and using the equivalence $P\left(\underset{\sim}{H}\left(x,t\right),t\right)\equiv\left\langle \rho\left(\underset{\sim}{H}\left(x,t\right),t\right)\right\rangle$, we eventually obtain the FPKE. We will go in more details shortly when deriving the FPKE for a general constitutive law.

From Brownian motion to flow in hydrologic systems, the types of differential equations that we have dealt with thus far all have one thing in common: they represent the evolution of one or more state parameters in a medium of fluctuating variables. Another common denominator among these differential equations is their non-linear characteristics, which as we will see is not a necessary condition for the application of the FPKE but rather an incentive as one of the greatest strength of the FPKE is that it linearizes non-linear *PDE*s. We will also see that the FPKE can be equally applied to linear *ODE*s such as an elastic constitutive rate equation. Having introduced the basic concepts of the FPKE, we shall now take an in-depth look at its derivation with regards to a general constitutive rate equation defined by:

$$\frac{d\sigma_{ij}\left(x_t,t\right)}{dt}=D_{ijkl}\left(x_t,t\right)\frac{d\varepsilon_{kl}\left(x_t,t\right)}{dt} \tag{5.9}$$

where $D_{ijkl}$ represents the material stiffness and can be either elastic, or *elasto-plastic* such that:

$$D_{ijkl}=\left\{\begin{array}{ll} D_{ijkl}^{el}, & \text{when } f<0\vee\left(f=0\wedge df<0\right) \\ D_{ijkl}^{ep}, & \text{when } f=0\vee df=0 \end{array}\right\} \tag{5.10}$$

and $D_{ijkl}^{ep} = D_{ijkl}^{el} - \left\langle D_{ijkl}^{pl} \right\rangle$, where the symbol '$\left\langle \bullet \right\rangle$' in this equation is the *Macauley* bracket (not to be mistaken with the inner product or expectation operator) which takes the value $D_{ijkl}^{pl}$ if plasticity is in effect, and 0 otherwise; *'f'* is the yield function and depends on the stress tensor $\sigma_{ij}$, as well as internal variables $q^*$ and the direction of their evolution $r^*$. Essentially, the mathematical expression on the right representing the conditions for yielding dictates the form of $D_{ijkl}$ (linear or non-linear). In the latter case, $D_{ijkl}$ becomes a function of the plastic surface, and the yield surface, which are themselves functions of the stress tensor, and internal variables. We can therefore amalgamate all the independent variables, which the stiffness tensor $D_{ijkl}$ depends upon into a general tensor $\beta_{ijkl}$ and generalize equation 5.9 further as follows:

$$\frac{d\sigma_{ij}\left(x_t,t\right)}{dt} = \beta_{ijkl}\left(\sigma_{ij}, D_{ijkl}^{el}, q^*, r^*; x_t, t\right)\frac{d\varepsilon_{kl}\left(x_t,t\right)}{dt} \tag{5.11}$$

Evident from the index notation, the above equation is a 3-D description of the material constitutive rate equation. The number of indices denotes the order of each tensor, and the repeated indices on the right-hand side of the equation imply the double summation over the indices $k$ and $l$ respectively. This can be interpreted as a double contraction of the fourth order tensor $\beta_{ijkl}$ with the second-order strain rate tensor. Shifting our view to a one-dimensional framework, we rewrite equation 5.11 in the following manner:

$$\frac{d\sigma\left(x_t,t\right)}{dt} = \beta\left(\sigma, D^{el}, q, r; x_t, t\right)\frac{d\varepsilon\left(x_t,t\right)}{dt} \tag{5.12}$$

It is now a matter of introducing uncertainties into the one-dimensional constitutive rate equation. This can be accomplished in three different ways: the material properties can be assumed to be random; the forcing function can be random, or it can be a combination of

both. Random material properties yield differential equations with stochastic coefficients while random forcing functions yield differential equations with stochastic forcing. Without loss of generality, let us assume the material properties and the forcing function to be random. We are therefore left with an equation whose right hand-side is stochastic, and represented by the function $\eta$:

$$\eta\left(\sigma, D^{el}, q, r, \varepsilon; x_t, t\right) = \beta\left(\sigma, D^{el}, q, r; x_t, t\right)\frac{d\varepsilon\left(x_t, t\right)}{dt} \tag{5.13}$$

such that we now have the following equation:

$$\frac{\partial\sigma\left(x_t, t\right)}{\partial t} = \eta\left(\sigma, D^{el}, q, r, \varepsilon; x_t, t\right) \tag{5.14}$$

with initial conditions:

$$\sigma\left(x, 0\right) = \sigma_0 \tag{5.15}$$

In the above form, the constitutive rate equation bears overwhelming similarity with the conservation equations of hydrologic systems and the equation of the velocity of a Brownian particle. The stress state can therefore be idealized as a point in the *σ-space*, where the above equation represents the velocity of that point provided that at time $t_0$, the point is located at $\sigma_0$ in the *σ-space*. Given the stochastic nature of $\sigma$, several trajectories are possible. These seemingly aleatory trajectories, when analyzed in a unit volume of the phase-space *(σ-space)* give rise to a *phase density* $\rho$ of $\sigma(x,t)$. Enforcing continuity of the phase density, which is tantamount to the conservation of the points $\sigma$ in the phase-space (*σ-space*), the *Kubo's stochastic Liouville* equation is obtained (Kubo, 1963):

$$\frac{\partial\rho\left(\sigma\left(x,t\right),t\right)}{\partial t} = -\frac{\partial}{\partial\sigma}\eta\left[\sigma\left(x,t\right), D^{el}\left(x\right), q\left(x\right), r\left(x\right), \varepsilon\left(x,t\right)\right]\cdot\rho\left[\sigma\left(x,t\right),t\right] \tag{5.16}$$

having initial condition:

$$\rho(\sigma,0)=\delta(\sigma-\sigma_0) \tag{5.17}$$

where δ is the *Dirac delta* function, and the equation above signifies that at time $t_0$, $\sigma$ takes on a "sure" value of $\sigma_0$. This is the probabilistic restatement of the initial condition given in equation 5.15.

Using Van Kampen's Lemma, the probability density function reads:

$$P(\sigma,t)=\langle\rho(\sigma,t)\rangle \tag{5.18}$$

where this time the '$\langle\bullet\rangle$' implies the expectation operation on the *phase density*. Van Kampen's Lemma is reminiscing of the observable probability introduced for the evolution of a Brownian particle. Taking the ensemble average of the stochastic differential equation 5.16 yields:

$$\begin{aligned}
&\frac{\partial\langle\rho(\sigma(x_t,t),t)\rangle}{\partial t}= \\
&-\frac{\partial}{\partial\sigma}\Bigg\{\Bigg[\Big\langle\eta(\sigma(x_t,t),D^{el}(x_t),q(x_t),r(x_t),\varepsilon(x_t,t))\Big\rangle \\
&-\int_0^t d\tau COV_0\Big[\eta(\sigma(x_t,t),D^{el}(x_t),q(x_t),r(x_t),\varepsilon(x_t,t));\\
&\frac{\partial\eta(\sigma(x_{t-\tau},t-\tau),D^{el}(x_{t-\tau}),q(x_{t-\tau}),r(x_{t-\tau})\varepsilon(x_{t-\tau},t-\tau))}{\partial\sigma}\Big]\Bigg]\langle\rho(\sigma(x_t,t),t)\rangle\Bigg\} \\
&+\frac{\partial}{\partial\sigma}\Bigg\{\Bigg[\int_0^t d\tau COV_0\Big[\eta(\sigma(x_t,t),D^{el}(x_t),q(x_t),r(x_t),\varepsilon(x_t,t));\\
&\eta(\sigma(x_{t-\tau},t-\tau),D^{el}(x_{t-\tau}),q(x_{t-\tau}),r(x_{t-\tau}),\varepsilon(x_{t-\tau},t-\tau))\Big]\Bigg]\frac{\partial\langle\rho(\sigma(x_t,t),t)\rangle}{\partial\sigma}\Bigg\}
\end{aligned} \tag{5.19}$$

The derivation follows that of Kavvas and Karakas (Kavvas et al 2003) and is shown in Appendix B of this thesis. Equation 5.19 is exact to second order i.e up to order of the covariance of η in time where $COV_0$ is the time ordered covariance function given by:

$$COV_0\left[\eta\left(x,t_1\right),\eta\left(x,t_2\right)\right]=\left\langle\eta\left(x,t_1\right)\eta\left(x,t_2\right)\right\rangle-\left\langle\eta\left(x,t_1\right)\right\rangle\cdot\left\langle\eta\left(x,t_2\right)\right\rangle \tag{5.20}$$

Substituting the *probability density function* $P\left(\sigma\left(x,t\right),t\right)\equiv\left\langle\rho\left(\sigma\left(x,t\right),t\right)\right\rangle$ into equation 5.19 and rearranging, a linear second order parabolic *PDE* also known as the FPKE is obtained:

$$\begin{aligned}
&\frac{\partial P\left(\sigma\left(x_t,t\right),t\right)}{\partial t}=\\
&-\frac{\partial}{\partial\sigma}\Bigg[\Bigg\{\left\langle\eta\left(\sigma\left(x_t,t\right),D^{el}\left(x_t\right),q\left(x_t\right),r\left(x_t\right),\varepsilon\left(x_t,t\right)\right)\right\rangle\\
&+\int_0^t d\tau COV_0\Bigg[\frac{\partial\eta\left(\sigma\left(x_t,t\right),D^{el}\left(x_t\right),q\left(x_t\right),r\left(x_t\right),\varepsilon\left(x_t,t\right)\right)}{\partial\sigma};\\
&\eta\left(\sigma\left(x_{t-\tau},t-\tau\right),D^{el}\left(x_{t-\tau}\right),q\left(x_{t-\tau}\right),r\left(x_{t-\tau}\right),\varepsilon\left(x_{t-\tau},t-\tau\right)\right)\Bigg]\Bigg\}P\left(\sigma\left(x_t,t\right),t\right)\Bigg]\\
&+\frac{\partial^2}{\partial\sigma^2}\Bigg[\Bigg\{\int_0^t d\tau COV_0\Big[\eta\left(\sigma\left(x_t,t\right),D^{el}\left(x_t\right),q\left(x_t\right),r\left(x_t\right),\varepsilon\left(x_t,t\right)\right);\\
&\eta\left(\sigma\left(x_{t-\tau},t-\tau\right),D^{el}\left(x_{t-\tau}\right),q\left(x_{t-\tau}\right),r\left(x_{t-\tau}\right),\varepsilon\left(x_{t-\tau},t-\tau\right)\right)\Big]\Bigg\}P\left(\sigma\left(x_t,t\right),t\right)\Bigg]
\end{aligned} \tag{5.21}$$

which is exact to second order. Taking a closer look at equation 5.14, we note that the non-linear constitutive rate equation has effectively been transformed into a linear second order *PDE* whose solution is the probability density function of the stress at different times *t*. Specifying the boundary and initial conditions suffice to solve the above linear *PDE* in a straightforward manner.

Another remark worth mentioning is the fact that equation 5.21 is a mixed Eulerian-Lagrangian equation. This comes to no surprise given its origins in hydrological systems describing fluid flow. We can accurately describe the behaviour of the system at a reference position $x_t$ analogous to the visualization of water as it passes a fixed point while the observer sits on the bank of a river. Ideally, we would also like a Lagrangian description, like the motion of water from the perspective of someone sitting and drifting in a boat. In the above equation, using small strain theory, a mixed Eulerian-lagrangian description can be provided. The behaviour of the system at a position $x_{t-\tau}$ can be found using the strain rate through the following relationship:

$$d\varepsilon = \dot{\varepsilon}\tau = \frac{x_t - x_{t-\tau}}{x_t} \tag{5.22}$$

After solving for the probability density function $P(\sigma(t),t)$, the statistical moments can be found by the expectation operation.

- The mean is given by:

$$\left\langle \sigma(t) \right\rangle = \int_{-\infty}^{+\infty} \sigma(t) P\left(\sigma(t)\right) d\sigma(t) \tag{5.23}$$

- The variance is given by:

$$\left\langle \sigma(t)^2 \right\rangle - \left\langle \sigma(t) \right\rangle^2 = \int_{-\infty}^{+\infty} \sigma(t)^2 P\left(\sigma(t)\right) d\sigma(t) - \left( \int_{-\infty}^{+\infty} \sigma(t) P\left(\sigma(t)\right) d\sigma(t) \right)^2 \tag{5.24}$$

- The auto-correlation function is given by:

$$\left\langle \sigma(t_1)\sigma(t_2) \right\rangle = \int_{-\infty}^{+\infty}\int_{-\infty}^{+\infty} \sigma(t_1)\sigma(t_2) P_2\left(\sigma(t_1),t_1;\sigma(t_2),t_2\right) d\sigma(t_1) d\sigma(t_2) \tag{5.25}$$

- The auto-covariance function is given by:

$$\left\langle\left\langle \sigma(t_1)\sigma(t_2)\right\rangle\right\rangle = \left\langle \sigma(t_1)\sigma(t_2)\right\rangle - \left\langle \sigma(t_1)\right\rangle\left\langle \sigma(t_2)\right\rangle \tag{5.26}$$

Note that the stochastic differential equations can be solved by other means, which are not covered in this thesis. One way is to employ Itô or Stratonovich calculus. We mention it here in passing as these methods are the pillars of Stochastic Differential Equations (SDEs). It is in the readers' best interest to refer to Van Kampen's Stochastic Processes in Physics and Chemistry (Kampen, 2011), or Gardiner's Handbook of Stochastic Methods for Physics, Chemistry, and the Natural Sciences (Gardiner, 2004) for more information.

### 5.2.2 Solution Algorithm for 1-D Development

The general solution of linear second-order parabolic *PDE*s are well documented and can be found in any books on *PDE*s. We will use a numerical approximation to solve the FPKE. For the sake of simplicity, we use a finite difference scheme, more specifically the central difference method in which the derivatives of the probability density function are approximated as follows:

$$\frac{\partial P}{\partial \sigma} = \frac{P^{(i+1)} - P^{(i)}}{2\Delta\sigma} \tag{5.27}$$

$$\frac{\partial^2 P}{\partial \sigma^2} = \frac{P^{(i+1)} - 2P^{(i)} + P^{(i-1)}}{\Delta\sigma^2} \tag{5.28}$$

where the superscript represents the location of a node in the discretized *σ-space* and *Δσ* is the distance between two consecutive nodes in an equidistance discretization. We can rewrite equation 5.21 in a more compact form as shown below:

$$\frac{\partial P(\sigma(t),t)}{\partial t} = -\frac{\partial}{\partial \sigma}\left\{P(\sigma(t),t)N_1\right\} + \frac{\partial^2}{\partial \sigma^2}\left\{P(\sigma(t),t)N_2\right\} \tag{5.29}$$

Factoring the above equation further we obtain:

$$\frac{\partial P\left(\sigma\left(t\right),t\right)}{\partial t}=-\frac{\partial}{\partial\sigma}\left[P\left(\sigma\left(t\right),t\right)N_1-\frac{\partial}{\partial\sigma}\left\{P\left(\sigma\left(t\right),t\right)N_2\right\}\right] \tag{5.30-a}$$

$$=-\frac{\partial\zeta}{\partial\sigma} \tag{5.30-b}$$

where $N_1$ and $N_2$ are coefficients of the FPKE having the following equations:

$$\begin{aligned}N_1=&\left\{\left\langle\eta\left(\sigma\left(x_t,t\right),D^{el}\left(x_t\right),q\left(x_t\right),r\left(x_t\right),\varepsilon\left(x_t,t\right)\right)\right\rangle\right.\\&+\int_0^t d\tau COV_0\left[\frac{\partial\eta\left(\sigma\left(x_t,t\right),D^{el}\left(x_t\right),q\left(x_t\right),r\left(x_t\right),\varepsilon\left(x_t,t\right)\right)}{\partial\sigma};\right.\\&\left.\left.\eta\left(\sigma\left(x_{t-\tau},t-\tau\right),D^{el}\left(x_{t-\tau}\right),q\left(x_{t-\tau}\right),r\left(x_{t-\tau}\right),\varepsilon\left(x_{t-\tau},t-\tau\right)\right)\right]\right\}\end{aligned} \tag{5.31-a}$$

$$\begin{aligned}N_2=&\left[\left\{\int_0^t d\tau COV_0\left[\eta\left(\sigma\left(x_t,t\right),D^{el}\left(x_t\right),q\left(x_t\right),r\left(x_t\right),\varepsilon\left(x_t,t\right)\right);\right.\right.\\&\left.\left.\eta\left(\sigma\left(x_{t-\tau},t-\tau\right),D^{el}\left(x_{t-\tau}\right),q\left(x_{t-\tau}\right),r\left(x_{t-\tau}\right),\varepsilon\left(x_{t-\tau},t-\tau\right)\right)\right]\right\}\end{aligned} \tag{5.31-b}$$

Notice the similarity with the Diffusion equation i.e equation 5.6. The coefficients of the equation are analogous to the diffusive and advective coefficients. Furthermore, one can say that $\frac{\partial\zeta}{\partial\sigma}$ is the probability flux. This is because the probability density is the state variable, and equation 5.29 describes the continuity of the probability density. Using the product rule on the right-hand side of equation 5.30-a yields:

$$\frac{\partial P}{\partial t}=-\left[P\frac{\partial N_1}{\partial\sigma}+N_1\frac{\partial P}{\partial\sigma}\right]+\frac{\partial}{\partial\sigma}\left[P\frac{\partial N_2}{\partial\sigma}+N_2\frac{\partial P}{\partial\sigma}\right] \tag{5.32-a}$$

$$=-P\frac{\partial N_1}{\partial\sigma}-N_1\frac{\partial P}{\partial\sigma}+P\frac{\partial^2 N_2}{\partial\sigma^2}+2\frac{\partial P\partial N_2}{\partial\sigma^2}+N_2\frac{\partial^2 p}{\partial\sigma^2} \tag{5.32-b}$$

$$= P\left(\frac{\partial^2 N_2}{\partial \sigma^2} - \frac{\partial N_1}{\partial \sigma}\right) + \frac{\partial P}{\partial \sigma}\left(2\frac{\partial N_2}{\partial \sigma} - N_1\right) + \frac{\partial^2 P}{\partial \sigma^2} N_2 \qquad (5.32\text{-c})$$

Substituting equations 5.27 and 5.28 of the central difference scheme into the above equation we get:

$$\frac{\partial P^{(i)}}{\partial t} = P^{(i-1)}\left(\frac{N_1^{(i)}}{2\Delta\sigma} + \frac{N_2^{(i)}}{\Delta\sigma} - \frac{1}{\Delta\sigma}\frac{\partial N_2^{(i)}}{\partial \sigma}\right) - P^{(i)}\left(\frac{\partial N_1^{(i)}}{\partial \sigma} + \frac{2N_2^{(i)}}{\Delta\sigma^2} - \frac{\partial^2 N_2^{(i)}}{\partial \sigma^2}\right) + P^{(i+1)}\left(-\frac{N_1^{(i)}}{2\Delta\sigma} + \frac{N_2^{(i)}}{\Delta\sigma^2} + \frac{1}{\Delta\sigma}\frac{\partial N_2^{(i)}}{\partial \sigma}\right) \qquad (5.33)$$

The final pieces needed to solve the system of simultaneous equations generated from the finite difference method are the boundary and initial conditions. In order to solve the second order *PDE*, two boundary conditions are necessary. Since the probability density within the system is conserved, we expect no leaking to occur at the boundary and therefore reflective barriers are used as boundary conditions. This is expressed mathematically as follows:

$$\zeta(\sigma, t)\Big|_{\sigma=\pm\infty} = 0 \qquad (5.34)$$

As for the initial condition, the latter can be prescribed deterministically through the use of the *Dirac delta* function or stochastically via a Normal *PDF*. In the former case, the *PDF* assumes the *Dirac Delta* function at time $t = 0$. Therefore, the initial condition (*I.C*) is interpreted as a peak located at a starting value of stress $\sigma_0$ such that $P(\sigma,0) = \delta(\sigma_0)$. Substituting the boundary and initial conditions in the system of simultaneous equations, the probability density will propagate through diffusion and advection controlled by parameters of the constitutive law being used.

### 5.2.3 Probabilistic linear elastic shear constitute law

Using the methodology developed for a general 1-D constitutive law, let's look into the stochastic behaviour of a point being sheared. For linear elastic shear behaviour, the constitutive rate equation reads:

$$\frac{d\sigma_{12}}{dt} = G\frac{d\varepsilon_{12}}{dt} \tag{5.35}$$

where the shear modulus *G,* of the material and the strain rate $d\varepsilon_{12}/dt$ are both assumed to be random. And from our assumption, we can now utilize $\eta$ having the definition:

$$\eta = G\frac{d\varepsilon_{12}}{dt} \tag{5.36}$$

Substituting equation 5.36 into the FPKE given in equation 5.21, the resulting PDE for the probabilistic behaviour of a 1-D point location scale linear elastic shear model is obtained:

$$\begin{aligned}\frac{\partial P\left(\sigma_{12}(t),t\right)}{\partial t} = &-\frac{\partial}{\partial \sigma_{12}}\Bigg[\left\{\left\langle G\frac{d\varepsilon_{12}(t)}{dt}\right\rangle\right. \\ &\left.+\int_0^t d\tau COV_0\left[\frac{\partial}{\partial \sigma_{12}}\left(G\frac{d\varepsilon_{12}(t)}{dt}\right);G\frac{d\varepsilon_{12}(t-\tau)}{dt}\right]\right\}P\left(\sigma_{12}(t),t\right)\Bigg] \\ &+\frac{\partial^2}{\partial \sigma_{12}^2}\Bigg[\left\{\int_0^t d\tau COV_0\left[G\frac{d\varepsilon_{12}(t)}{dt};G\frac{d\varepsilon_{12}(t-\tau)}{dt}\right]\right\}P\left(\sigma_{12}(t),t\right)\Bigg]\end{aligned} \tag{5.37}$$

Turning our attention to the first coefficient, we note that the random process η is independent of the shear stress $\sigma_{12}$. The first term of the covariance is therefore zero, and the covariance of zero with another random process is also zero. Hence, equation 5.37 can be simplified to the following equation:

$$\frac{\partial P\left(\sigma_{12}(t),t\right)}{\partial t} = -\frac{\partial}{\partial \sigma_{12}}\left[\left\langle G\frac{d\varepsilon_{12}(t)}{dt}\right\rangle P\left(\sigma_{12}(t),t\right)\right] + \frac{\partial^2}{\partial \sigma_{12}^2}\left[\left\{\int_0^t d\tau COV_0\left[G\frac{d\varepsilon_{12}(t)}{dt}; G\frac{d\varepsilon_{12}(t-\tau)}{dt}\right]\right\} P\left(\sigma_{12}(t),t\right)\right] \tag{5.38}$$

The above equation can be readily solved under appropriate boundary and initial conditions. If we are given the initial conditions, $P(\sigma_{12},0) = \delta(\sigma_0)$ and assume a reflective barrier at the boundaries such that $\zeta(-\infty,t) = 0$ *and* $\zeta(\infty,t) = 0$, then the derived form of the FPKE will give the time evolution of the probability density function of the shear stress. This is accomplished by substituting in the diffusion and advection coefficient, which is evaluated from the statistical properties of our *random processes*. We shall look into a numerical example to demonstrate the methodology and observe the evolution of shear stress and its probability with time.

### 5.2.4 Numerical example of linear elastic shear behaviour

The following example was taken from Kallol's dissertation (Kallol, 2007) for verification purposes. In this example, a constant strain rate $d\varepsilon_{12}/dt$ of *0.054/s* is assumed hence making the integrals present in the estimation of the diffusive and advective coefficient easy to compute. Moreover, it should be specified that the constant strain rate essentially acts as an intermediate parameter between time and stress, which makes the problem pseudo-time dependent. The selection of the strain rate can be arbitrary, and a relationship between the probability density function of stress and strain can be established; one in which strain is the independent variable. We shall also limit the domain size of the problem to *[-0.1 0.1] MPa* for practical purposes and computational

efficiency. While in reality the domain ranges from -∞ to +∞, for small deformations, the shear stress is not expected to go beyond *[-0.1 0.1]*. Finally, we prescribe a value of $\sigma_{12} = 0$ *at* $t = 0$ as initial condition. The use of the *Dirac delta* function can prove challenging in Matlab©. We therefore approximate the Dirac Delta function using a Gaussian function with zero mean and very small standard deviation of the order of $10^{-4}$*MPa.*

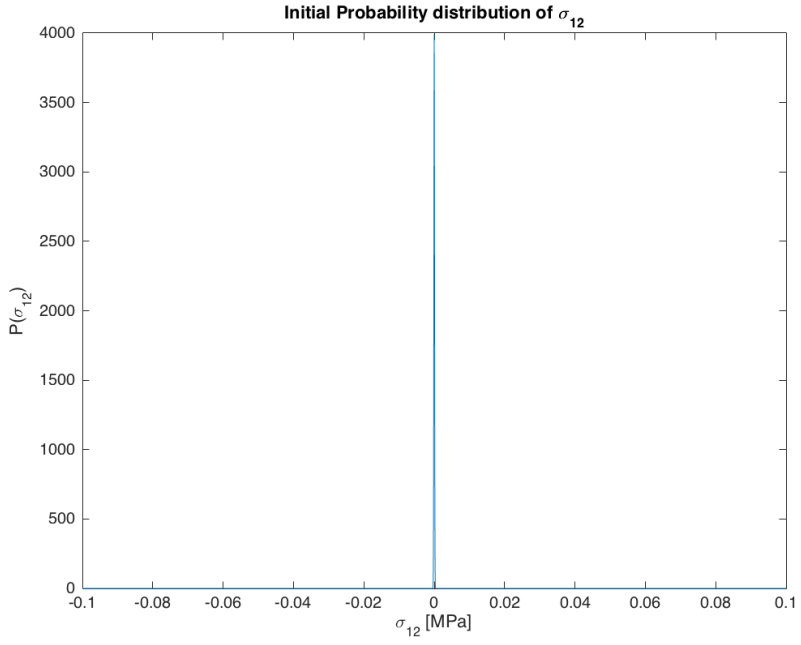


**Figure 5.1: Probability distribution of initial stress at t=0 for linear shear elastic model**

This comes at the cost of introducing a slight error of the magnitude of the variance of the I.C initially, but the error rapidly vanishes as the probability density of stress evolves with time.

Assuming the shear modulus has a mean of *2.5MPa* and a standard deviation of *0.707MPa*, the advection coefficient is calculated as follows:

$$N_1 = \left\langle G\frac{d\varepsilon_{12}}{dt} \right\rangle \tag{5.39}$$

Since the strain-rate is known and deterministic, we can move it out of the expectation operator, and the following equation is obtained:

$$N_1 = \frac{d\varepsilon_{12}}{dt}\left\langle G \right\rangle \tag{5.40-a}$$

$$N_1 = 2\cdot\left(0.054\right)\cdot\left(2.5\right)\text{MPa/s} \tag{5.40-b}$$

where the multiplier of magnitude 2 is from the compatibility of strain. The diffusion coefficient on the other hand is obtained as follows:

$$N_2 = \int_0^t d\tau COV_0\left[ G\frac{d\varepsilon_{12}\left(t\right)}{dt}; G\frac{d\varepsilon_{12}\left(t-\tau\right)}{dt} \right] \tag{5.41}$$

We start by evaluating the covariance term on the right:

$$COV_0\left[ G\frac{d\varepsilon_{12}\left(t\right)}{dt}; G\frac{d\varepsilon_{12}\left(t-\tau\right)}{dt} \right] = \left\langle G\frac{d\varepsilon_{12}\left(t\right)}{dt}\cdot G\frac{d\varepsilon_{12}\left(t-\tau\right)}{dt} \right\rangle - \left\langle G\frac{d\varepsilon_{12}\left(t\right)}{dt} \right\rangle \cdot \left\langle G\frac{d\varepsilon_{12}\left(t-\tau\right)}{dt} \right\rangle \tag{5.42-a}$$

$$\lim_{\tau\to 0}\ COV_0\left[ G\frac{d\varepsilon_{12}\left(t\right)}{dt}; G\frac{d\varepsilon_{12}\left(t-\tau\right)}{dt} \right] = \left\langle \left( G\frac{d\varepsilon_{12}\left(t\right)}{dt} \right)^2 \right\rangle - \left\langle G\frac{d\varepsilon_{12}\left(t\right)}{dt} \right\rangle^2 = Var\left[ G\frac{d\varepsilon_{12}\left(t\right)}{dt} \right] \tag{5.42-b}$$

Once more, because the strain rate is deterministic, it can be moved out of the variance operator such that $N_2$ reads:

$$N_2 = \tau\Big|_0^t \cdot Var\left[ G\frac{d\varepsilon_{12}\left(t\right)}{dt} \right] = t\cdot\left( \frac{d\varepsilon_{12}\left(t\right)}{dt} \right)^2 \cdot Var\left[ G \right] \tag{5.43-a}$$

$$N_2 = t\cdot\left(2\times 0.054\right)^2\left(0.707^2\right) = 0.0058t\ (\text{MPa/s})^2 \tag{5.43-b}$$

The result of the FPKE is shown in figure 5.2. We see from the contours of the probability density function that as time progresses, the *pdf* flattens out while moving at a

slope given by the shear modulus. A *Monte Carlo* simulation is performed with a sample size of n = 1000, and the solution of both approaches are compared.

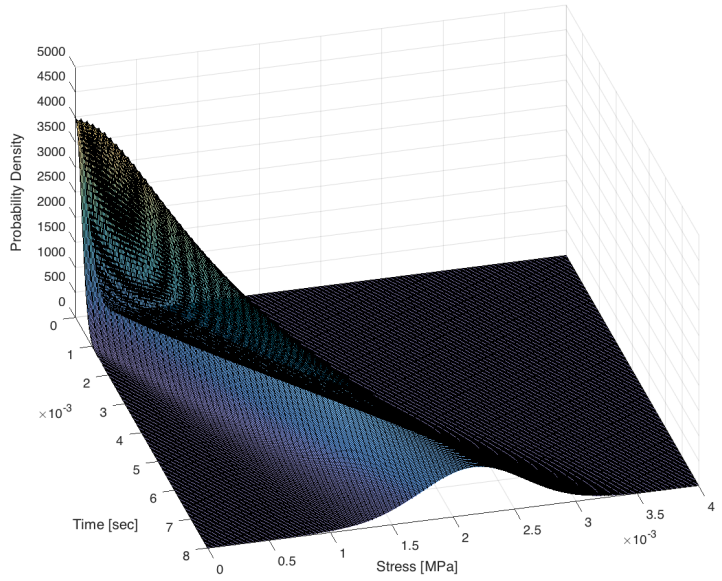


**Figure 5.2: Evolutionary probability distribution of stress for a linear shear elastic model using FPKE**

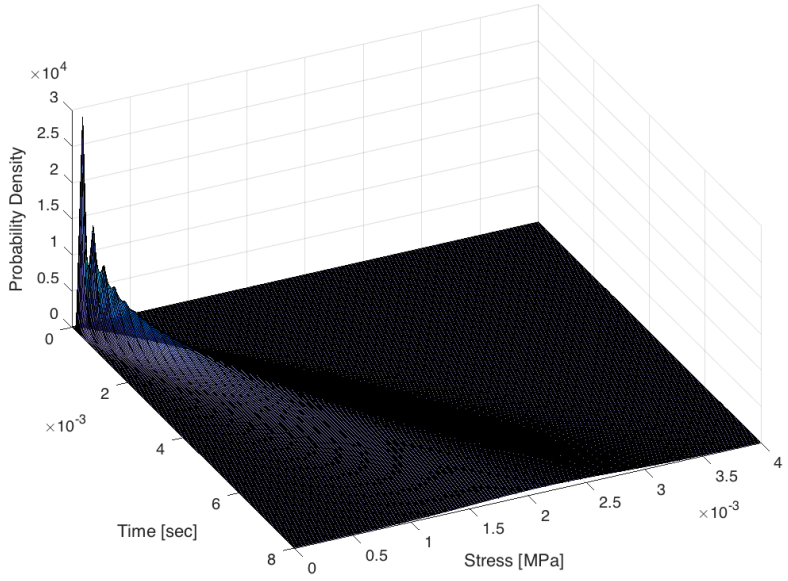


**Figure 5.3: Evolutionary probability distribution of stress for a linear shear elastic model using MC**

At first glance, the *pdf* obtained from the FPKE seems to be in good agreement with the PDF obtained from the *Monte Carlo* simulations. The progression of the *pdf*s follows similar paths and has a similar spread. The difference between both figures can be narrowed down at $t = 0$. This is due to the use of a Gaussian function to approximate the Dirac delta function for the initial condition of the FPKE. This is even more discernable looking at the stress-time plot of the linear elastic shear constitutive model. Figure 5.4 below shows the probabilistic stress-time plot of the linear elastic shear constitutive model using both the FPKE solution and the *Monte Carlo* simulation.

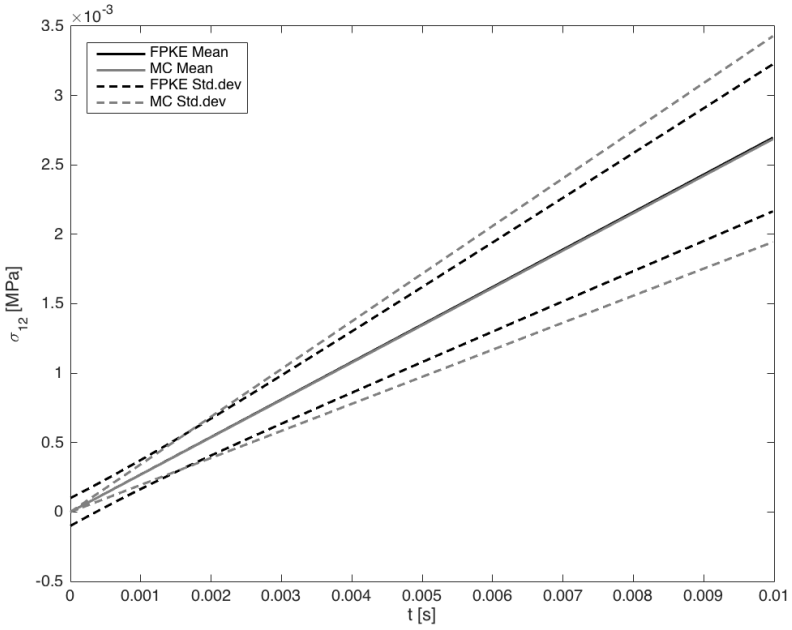


**Figure 5.4: Stress-time plot of linear shear elastic model for FPKE vs MC.**

In figure 5.4, we can see that the mean shear stress produced by both methods are the same. The standard deviation of the shear stress for $t < 0.0.001$ however is slightly over-estimated for the solution of the FPKE. Decreasing the standard deviation of the initial condition, and refining the mesh size of the domain can minimize this error.

### 5.2.5 Probabilistic Von Mises associative elastic-plastic constitutive law

In this section, the FPKE is applied to a linear elastic-plastic constitutive model. *Elastic-plastic* materials require that we define three important parameters:

1. Yield criterion
2. Hardening rule
3. Flow rule

And because we are dealing with random processes, a probabilistic definition of each of these parameters is necessary.

Starting with the yield criterion, a material is said to be within the elastic limit if under the action of external loads, the stress experienced by the material has not exceeded its yield strength. When the stress experienced by the material exceeds its yield strength, the material undergoes permanent deformation, and behaves as a plastic material.

The *Von Mises* constitutive law follows from the *Shear Energy Theory*, which states that a material yields when its distortion energy per unit volume is equal or greater than its distortion energy at yield. This yield criterion can be rewritten for a 1-D Von Mises model as follows:

$$f = \sqrt{J_2} - C_u = 0 \tag{5.44}$$

where $f$ is the yield function or yield surface, $J_2$ is the second invariant of the deviatoric stress tensor $S_{ij}$, and $C_u$ is the shear strength of the material. Figure 5.5 shows the yield surface of a *Von Mises* model.

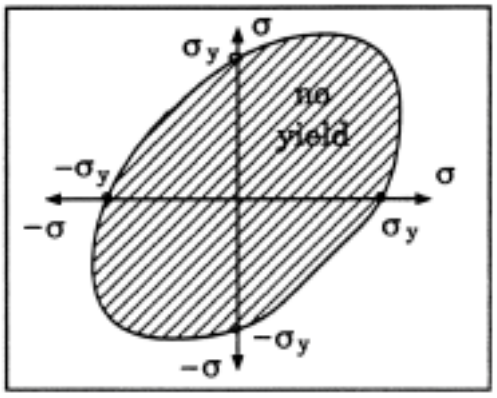


**Figure 5.5: Yield function of Von Mises model (Source: ME 620 course notes)**

Note: The deviatoric stress tensor is the anti-symmetric part of the stress tensor given by:

$S_{ij} = \sigma_{ij} - \frac{\delta_{ij}\sigma_{kk}}{3}$, and the second invariant of $S_{ij}$, $J_2 = \frac{1}{2} S_{ij} S_{ij}$.

Given the yield function we can now write the rate constitutive law for the *Von Mises* shear model:

$$\frac{d\sigma_{12}}{dt} = \left\{ \begin{array}{c} G^{el} \frac{d\varepsilon_{12}}{dt}, \text{when } f < 0 \vee \left( f = 0 \wedge df < 0 \right) \\ G^{ep} \frac{d\varepsilon_{12}}{dt}, \text{when } f = 0 \vee df = 0 \end{array} \right\} \tag{5.45}$$

From the above equation, the *Von Mises* shear constitutive model has two probabilistic equations. The first equation relating the rate of stress to the rate of strain in the pre-yield elastic region i.e $f < 0 \ \vee (f = 0 \wedge df < 0$, and the second equation relating the rate of stress to the rate of strain in the post-yield elastic-plastic region, i.e $f = 0 \ \vee df = 0$. As a result, two FPKEs are generated. In order to solve these two FPKEs, a mean yield criterion must be defined. Recognizing that $f$ is also a random process due to its

dependence on the shear stress, the yield function *f* takes a range of values. This is why it is necessary to restate the above equation in a probabilistic sense by introducing a mean yield criterion. Doing so allows us to know when to use the elastic FPKE and when to use the elastic-plastic FPKE. The constitutive rate equation can now be written as:

$$\frac{d\sigma_{12}}{dt} = \left\{ \begin{array}{c} G^{el}\frac{d\varepsilon_{12}}{dt}, \text{when } \langle f \rangle < 0 \vee \left( \langle f \rangle = 0 \wedge d\langle f \rangle < 0 \right) \\ G^{ep}\frac{d\varepsilon_{12}}{dt}, \text{when } \langle f \rangle = 0 \vee d\langle f \rangle = 0 \end{array} \right\} \tag{5.46}$$

Moving on to the hardening rule, we assume isotropic linear hardening. This necessitates that the yield surface of the material expands linearly as shown in figure 5.6:

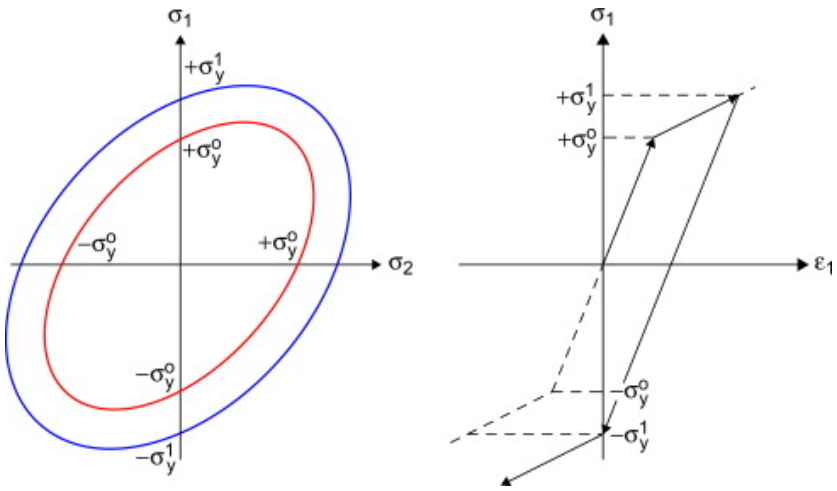


**Figure 5.6: Linear hardening of Von-Mises model (Source: Yung-Li Lee, 2012)**

Last but not least, we assume an *associated flow rule* i.e we assume that the plastic potential function is the same as the yield function. This allows us to write:

$$\frac{\partial f}{\partial \sigma_{ij}} = \frac{\partial U}{\partial \sigma_{ij}} \tag{5.47}$$

where U is the plastic potential.

With this information, we can obtain an equation for the *elasto-plastic* shear modulus $G^{ep}$. The derivation of the shear modulus is not shown here but for the reader's information, because we are dealing with random material properties and random forcing, the stress tensor, its invariants and their derivatives are also random, and any differentiation with respect to a random process as shown in equation 5.47 cannot be carried out in an ordinary sense. To circumvent this issue, differentiation is carried out with respect to deterministic values of $\sigma_{12}$ such that the differentiation is performed in an ordinary sense to obtain an equation for $G^{ep}$. In this respect, the definition of the $G^{ep}$ is not fully probabilistic. Alternatively, the differentiation can be performed using Itô calculus (not covered in this thesis). The equation for the elastic plastic shear modulus for deterministic $\sigma_{12}$ is given by:

$$G^{ep} = G - \frac{G^2}{G + \frac{1}{\sqrt{3}} C_u'} \tag{5.48}$$

where $C_u'$ is the rate of evolution of the shear strength $C_u$.

Putting everything together, and substituting the rate constitutive equation into the general FPK equation we can finally write the two FPKE for a 1-Dimensional *Von Mises* associative shear model.

1. Pre-yield elastic region: when $\langle f \rangle < 0 \vee \left( \langle f \rangle = 0 \wedge d\langle f \rangle < 0 \right)$

$$\begin{aligned} \frac{\partial P\left(\sigma_{12}(t),t\right)}{\partial t} &= -\frac{\partial}{\partial \sigma_{12}}\left[ \left\langle G \frac{d\varepsilon_{12}(t)}{dt} \right\rangle P\left(\sigma_{12}(t),t\right) \right] \\ &+ \frac{\partial^2}{\partial \sigma_{12}^2}\left[ \left\{ \int_0^t d\tau COV_0\left[ G\frac{d\varepsilon_{12}(t)}{dt}; G\frac{d\varepsilon_{12}(t-\tau)}{dt} \right] \right\} P\left(\sigma_{12}(t),t\right) \right] \end{aligned} \tag{5.49}$$

2. Post-yield elastic-plastic region: when $\left\langle f \right\rangle = 0 \vee d\left\langle f \right\rangle = 0$

$$\begin{aligned}\frac{\partial P\left(\sigma_{12}(t),t\right)}{\partial t} &= -\frac{\partial}{\partial \sigma_{12}}\Bigg[\left\{\left\langle G^{ep}(t)\frac{d\varepsilon_{12}(t)}{dt}\right\rangle P\left(\sigma_{12}(t),t\right)\right. \\ &\left.+\int_0^t d\tau COV_0\left[\frac{\partial}{\partial \sigma_{12}}\left(G^{ep}(t)\frac{d\varepsilon_{12}(t)}{dt}\right);G^{ep}(t-\tau)\frac{d\varepsilon(t-\tau)}{dt}\right]\right\}P\left(\sigma_{12}(t),t\right)\Bigg] \\ &+\frac{\partial^2}{\partial \sigma_{12}^2}\left[\left\{\int_0^t d\tau COV_0\left[G^{ep}(t)\frac{d\varepsilon_{12}(t)}{dt};G^{ep}(t-\tau)\frac{d\varepsilon_{12}(t-\tau)}{dt}\right]\right\}P\left(\sigma_{12}(t),t\right)\right]\end{aligned} \quad (5.50)$$

Once more, the above two equations can be readily solved under appropriate boundary and initial conditions. Assuming a similar *I.C* and *B.C* as the linear elastic shear constitutive model, we find the evolution of shear stress and its probability with time by plugging in the diffusion and advection coefficient. A numerical example is presented where the statistical properties of a *Von Mises* constitutive model are provided.

### 5.2.6 Numerical example of linear elastic-plastic shear behaviour

For this example we will use the same strain rate $d\varepsilon_{12}/dt$ of *0.054/s* as the linear elastic shear example. We also impose the same boundary and initial conditions as before with the size of the domain of the problem restricted to *[-0.1 0.1] MPa* for practical purposes and an initial stress of of $\sigma_{12} = 0$ at $t = 0$. The initial condition is approximated using a Gaussian function with zero mean and standard deviation of the order of $10^{-4}$*MPa* as shown in the figure below.

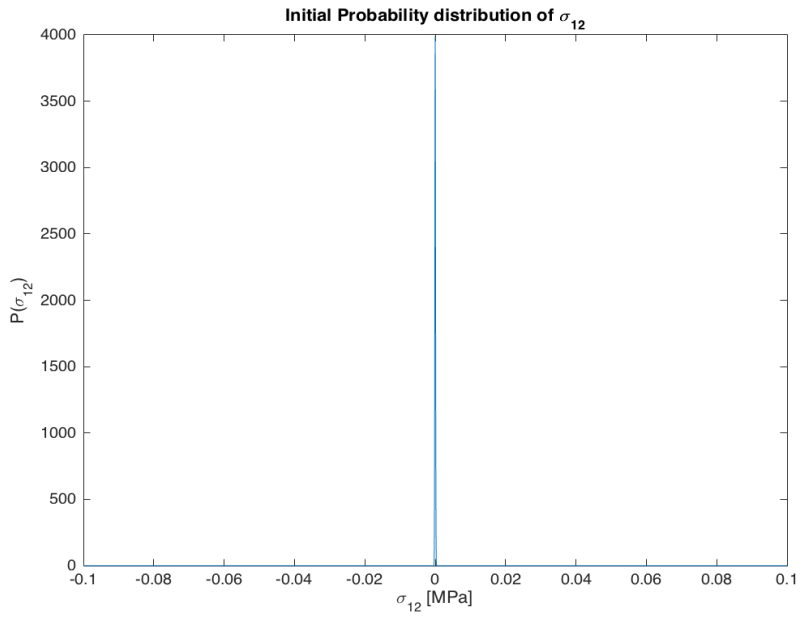


**Figure 5.7: Probability distribution of initial stress at t=0 for linear shear elastic model**

Assuming the shear modulus has a mean of *2.5MPa* and a standard deviation of *0.707MPa*, the advection coefficient for the pre-yield FPKE is calculated as follows:

$$N_1 = \left\langle G \frac{d\varepsilon_{12}}{dt} \right\rangle \tag{5.51}$$

Since the strain-rate is known, we can move it out of the expectation operator, and the following equation is obtained:

$$N_1 = \frac{d\varepsilon_{12}}{dt} \langle G \rangle \tag{5.52-a}$$

$$N_1 = 2 \cdot (0.054) \cdot (2.5) \text{ MPa/s} \tag{5.52-b}$$

where the multiplier of magnitude 2 is from the compatibility of strain. The diffusion coefficient for the pre-yield FPKE on the other hand is obtained as follows:

$$N_2 = \tau\Big|_0^t \cdot Var\left[G\frac{d\varepsilon_{12}(t)}{dt}\right] = t\cdot\left(\frac{d\varepsilon_{12}(t)}{dt}\right)^2 \cdot Var\left[G\right] \tag{5.53-a}$$

$$N_2 = t\cdot\left(2\times 0.054\right)^2\left(0.707^2\right) = 0.0058t \text{ (MPa/s)}^2 \tag{5.53-b}$$

For the post-yield advection coefficient, let's considerer a deterministic shear strength $C_u$ of *6.36 x 10$^{-4}$ MPa* and a rate of evolution of shear strength with plastic strain $C_u'$ having a sure value of *0.5MPa*. The post-yield advection coefficient is given by:

$$N_1 = \left\langle G^{ep}(t)\frac{d\varepsilon_{12}(t)}{dt}\right\rangle + \int_0^t d\tau COV_0\left[\frac{\partial}{\partial\sigma_{12}}\left(G^{ep}(t)\frac{d\varepsilon_{12}(t)}{dt}\right); G^{ep}(t-\tau)\frac{d\varepsilon_{12}(t-\tau)}{dt}\right] \tag{5.54}$$

From equation 5.48, $G^{ep}$ is independent of $\sigma_{12}$, therefore the second term on the right can dropped as a result of the zero covariance term. The post-yield advection coefficient can then be written as:

$$\begin{aligned} N_1 &= \left\langle G^{ep}(t)\frac{d\varepsilon_{12}(t)}{dt}\right\rangle = \frac{d\varepsilon_{12}(t)}{dt}\left\langle G^{ep}(t)\right\rangle \\ &= \frac{d\varepsilon_{12}(t)}{dt}\left\langle G - \frac{G^2}{G+\frac{1}{\sqrt{3}}C_u'}\right\rangle \\ &= \frac{d\varepsilon_{12}(t)}{dt}\left[\left\langle G\right\rangle - \left\langle \frac{G^2}{G+\frac{1}{\sqrt{3}}C_u'}\right\rangle\right] \end{aligned} \tag{5.55-a}$$

$$= \frac{d\varepsilon_{12}(t)}{dt}\left[\left\langle G\right\rangle - \left\langle G^2\right\rangle\left\langle \frac{1}{G+\frac{1}{\sqrt{3}}C_u'}\right\rangle\right] \tag{5.55-b}$$

We can find the second moment of $G$, $\left\langle G^2\right\rangle$ on the right using the equation of the variance as follows:

$$\left\langle G^2\right\rangle = Var\left[G\right] + \left\langle G\right\rangle^2 \tag{5.56}$$

and we can obtain the expectation of a reciprocal process $\left\langle \frac{1}{G+\frac{1}{\sqrt{3}}C_u'}\right\rangle$, using a Taylor series approximation about the mean of the process. The Taylor series of a reciprocal process $E(1/X)$ expanded around $E(X)$ up to second order is given below:

$$\begin{aligned} E\left[\frac{1}{X}\right] &\simeq E\left[\frac{1}{E\left[X\right]} - \frac{1}{E\left[X\right]^2}\left(X - E\left[X\right]\right) + \frac{1}{E\left[X\right]^3}\left(X - E\left[X\right]\right)^2\right] \\ &= \frac{1}{E\left[X\right]} + \frac{1}{E\left[X\right]^3}Var\left[X\right] \end{aligned} \tag{5.57}$$

Substituting the process $X$ by $G + C_u'/\sqrt{3}$, we get:

$$\left\langle \frac{1}{G+\frac{1}{\sqrt{3}}C_u'}\right\rangle = \frac{1}{\left\langle G+\frac{1}{\sqrt{3}}C_u'\right\rangle} + \frac{1}{\left\langle G+\frac{1}{\sqrt{3}}C_u'\right\rangle^3}Var\left[G+\frac{1}{\sqrt{3}}C_u'\right] \tag{5.58}$$

Therefore, the post-yield advection coefficient is given by:

$$N_1 = \frac{d\varepsilon_{12}}{dt}\left[\left\langle G\right\rangle - \left(Var\left[G\right] + \left\langle G\right\rangle^2\right)\left(\frac{1}{\left\langle G + \frac{1}{\sqrt{3}}C_u'\right\rangle} + \frac{1}{\left\langle G + \frac{1}{\sqrt{3}}C_u'\right\rangle^3}Var\left[G + \frac{1}{\sqrt{3}}C_u'\right]\right)\right] \tag{5.59}$$

The post-yield diffusion coefficient on the other hand can be obtained as follows:

$$N_2 = t\left(\frac{d\varepsilon_{12}}{dt}\right)^2 Var\left[G - \frac{G^2}{G + \frac{1}{\sqrt{3}}C_u'}\right] \tag{5.60}$$

The variance term on the right can be further expanded using the same equation as before:

$$Var\left[G - \frac{G^2}{G + \frac{1}{\sqrt{3}}C_u'}\right] = \left\langle\left(G - \frac{G^2}{G + \frac{1}{\sqrt{3}}C_u'}\right)^2\right\rangle - \left\langle G - \frac{G^2}{G + \frac{1}{\sqrt{3}}C_u'}\right\rangle^2 \tag{5.61}$$

We square the bracketed term in the first inner product, and get the following:

$$\left\langle\left(G - \frac{G^2}{G + \frac{1}{\sqrt{3}}C_u'}\right)^2\right\rangle = \left\langle G^2\right\rangle - 2\left\langle G^3\right\rangle\left\langle\frac{1}{G + \frac{1}{\sqrt{3}}C_u'}\right\rangle + \left\langle G^4\right\rangle\left\langle\frac{1}{G^2 + \frac{2GC_u'}{\sqrt{3}} + \frac{C_u'^2}{3}}\right\rangle \tag{5.62}$$

We note that we are now confronted with the evaluation of higher moments to obtain the post-yield diffusion coefficient. To compute these moments, the characteristic function or the moment generating function can be invoked. For Gaussian processes, higher-order moments can be obtained using the following equation:

$$\left\langle X^m\right\rangle = \sum_{l=0}^{\left[\frac{m}{2}\right]} \frac{m!}{\left(m-2l\right)!2^l l!}\mu^{m-2l}\sigma^{2l} \text{ for m even} \tag{5.63}$$

It should be noted that for Gaussian processes, higher order cumulants are described using the first and second cumulants only. This is because $\kappa_m = 0$ for $m \geq 3$. Therefore we have the following equations for the third and forth moment of $G$:

$$\begin{aligned}\left\langle G^3 \right\rangle &= \kappa_3 + 3\mu_2\mu_1 + 2\mu_1^3 \\ &= 3Var\left[G\right]\cdot\left\langle G\right\rangle + 2\left\langle G\right\rangle^3\end{aligned} \tag{5.64}$$

and

$$\begin{aligned}\left\langle G^4 \right\rangle &= \sum_{l=0}^{2} \frac{4!}{\left(4-2l\right)!2^l \cdot l!}\mu^{4-2l}\cdot\sigma^{2l} \\ &= \frac{4!}{4!}\left\langle G\right\rangle^4\left(\sqrt{Var\left[G\right]}\right)^0 + \frac{4!}{2\cdot 2!}\left\langle G\right\rangle^2 Var\left[G\right] + \frac{4!}{4\cdot 2}\left\langle G\right\rangle^0\left(Var\left[G\right]\right)^2\end{aligned} \tag{5.65}$$

The reciprocal processes $\left\langle \frac{1}{G+\frac{1}{\sqrt{3}}C_u'} \right\rangle$ and $\left\langle \frac{1}{G^2+\frac{2GC_u'}{\sqrt{3}}+\frac{C_u'^2}{3}} \right\rangle$ are approximated using a Taylor series expansion about the mean of the process following the same steps undertaken for the evaluation of the post-yield advection coefficient.

Substituting equations 5.61 through 5.65 into the equation for the post-yield diffusion coefficient, we get a value for post-yield $N_2$ after which we can simulate the evolution of stress for a 1-D Von Mises shear model.

The results of the simulation are shown below, and the solution of the FPKE is compared to a *Monte Carlo* simulation with sample size $n = 1000$.

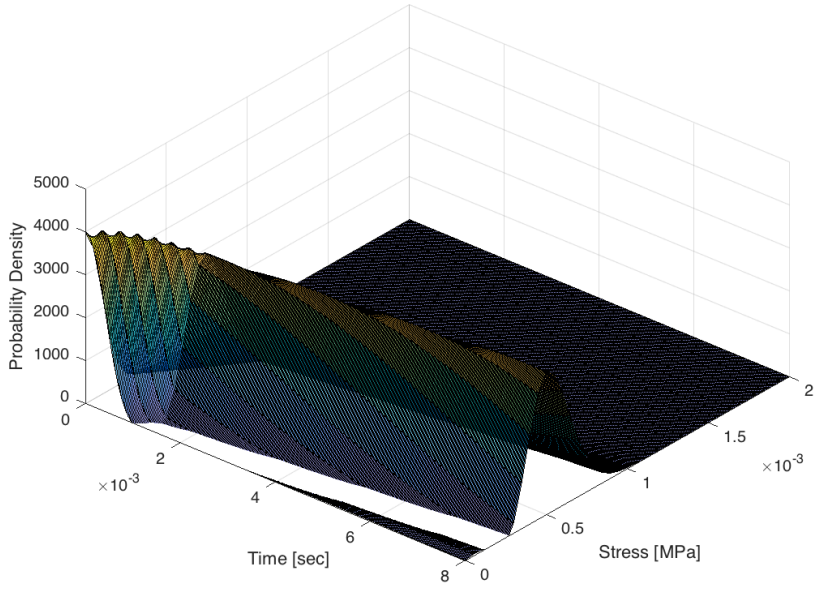


**Figure 5.8: Evolutionary probability distribution of stress for a Von-Mises model using FPKE**

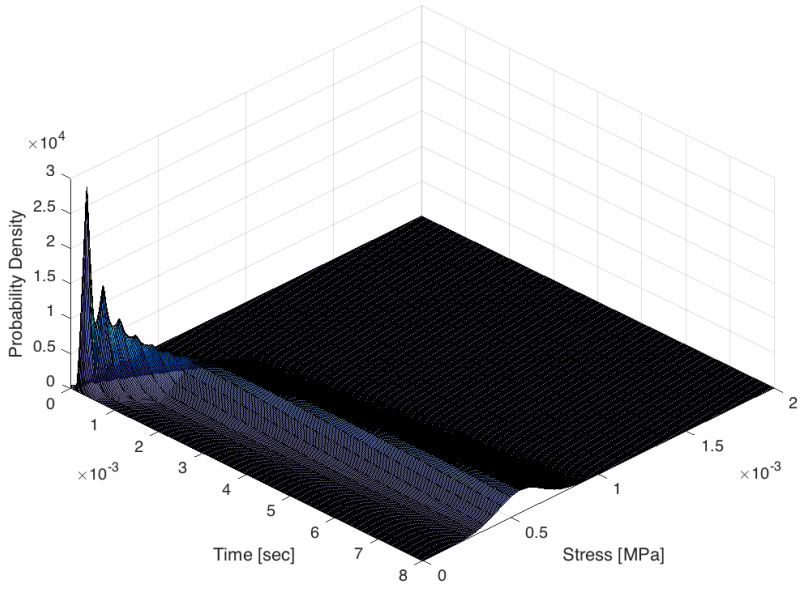


**Figure 5.9: Evolutionary probability distribution of stress for a Von-Mises model using MC**

We note a similar trend where the probability density flattens out as the shear stress progresses. In the solution of the FPKE, an initial error is introduced at time $t = 0$ due to

the approximation of the initial condition by a Gaussian function. The *pdf* obtained from the FPKE is smoother than the *Monte Carlo* simulations, and shows good agreement with its results. This is confirmed by looking at the stress-time plots of the solution of both methods as shown in figure 5.10. Some disparity is visible around the yield stress of the material. We suspect that this difference comes from the fact that in the FPKE, the mean shear stress reaches the mean yield strength a fraction of a millisecond before the *Monte Carlo* simulation. As soon as the post-yield constitutive law is in effect, the error is exaggerated as a result of this lag. Looking at the pre-yield behaviour of the stress-time plot, the disparity between the standard deviation of the FPKE solution and the MC solution decreases up to the yield point. Subsequently it can be seen that the standard deviation of the FPKE stays in good agreement until $t = 0.005$ where the standard deviation of the MC solution starts to increase at a higher rate and diverges from the FPKE solution. There is but a slight overestimation seen in the standard deviation of the MC solution from the time the material yields to $t = 0.006$. Presumably this disparity is again mostly due to the small lag between both methods in shifting from the pre-yield to post-yield constitutive law.

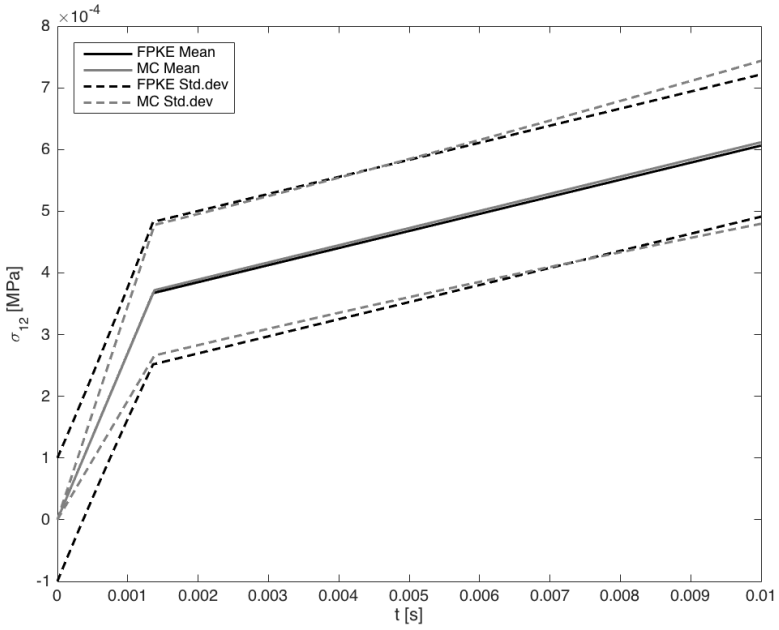


**Figure 5.10: Stress-time plot of Von-Mises model for FPKE vs MC.**

### 5.2.7 Probabilistic constitutive laws in three-dimension

In the previous section, the derived one-dimensional FPKE was applied to two constitutive models. It performed well, and gave results in close agreement with the *Monte Carlo* method. The *Monte Carlo*'s runtime paled in comparison with that of the new probabilistic constitutive framework. In this section, we extend the derivation undertaken in section 5.2.1 to three-dimension. Recall equation 5.11, the general form of a three-dimensional elastic-plastic constitutive rate equation:

$$\frac{d\sigma_{ij}\left(x_t,t\right)}{dt} = D^{ep}_{ijkl}\left(\sigma_{ij},D^{el}_{ijkl},f,U,q^*,r^*;x_t,t\right)\frac{d\varepsilon_{kl}\left(x_t,t\right)}{dt} \tag{5.66}$$

For the sake of simplicity, let $D_{ijkl}$ be a tensor denoting the random material parameters:

$$D_{ijkl} = \left[ D^{el}_{ijkl},f,U,q^*,r^* \right] \tag{5.67}$$

Now let the right-hand side be denoted by the random operator tensor, $\eta_{ij}$

$$\frac{d\sigma_{ij}\left(x,t\right)}{dt}=\eta_{ij}\left(\sigma_{ij},D_{ijkl},\varepsilon_{kl};x,t\right) \tag{5.68}$$

and let the above rate equation have the following initial condition:

$$\sigma_{ij}\left(x,0\right)=\sigma_{ij_0} \tag{5.69}$$

The above mathematical expression can be interpreted as a tensor representing the initial stress state of a point at time $t = 0$. The tensor contains 9 elements, each representing the state of stress on a surface in a given direction. Referring to figure 2.3, the *REV* can be thought of as a point at an initial state, in a 3-D framework and having a trajectory in the *phase-space* constituting all its possible states. Each trajectory corresponds to the transformation of the nine states contained by the stress tensor of a point. If we consider a cloud of points initially concentrated at time $t = 0$, having a phase density $\rho(\sigma_{ij},0)$; the trajectory of the cloud progresses in accordance to some constitutive laws which forms a stochastic differential equation whose ensemble average can be obtained. The conservation of these points in the *σ-space* can be expressed by the continuity of the phase density also known as *Kubo's stochastic Liouville* equation. This stochastic continuity equation for a 3-D stress tensor is given by:

$$\frac{\partial\rho\left(\sigma_{ij}\left(x,t\right),t\right)}{\partial t}=-\frac{\partial}{\partial\sigma_{mn}}\eta_{mn}\left(\sigma_{mn}\left(x,t\right),D_{mnpq}\left(x\right),\varepsilon_{pq}\left(x,t\right)\right)\rho\left(\sigma_{ij}\left(x,t\right),t\right) \tag{5.70}$$

with initial condition,

$$\rho\left(\sigma_{ij},0\right)=\delta\left(\sigma_{ij}-\sigma_{ij_0}\right) \tag{5.71}$$

where equation 5.71 is a probabilistic restatement of the initial condition, with $\delta(.)$ being the Dirac delta function and $\sigma_{ij0}$, the initial stress tensor at time $t = 0$. The linear *PDE* for the ensemble average form of equation 5.70 is then obtained using Van Kampen's Lemma:

$$\left\langle \rho\left(\sigma_{ij},t\right)\right\rangle = P\left(\sigma_{ij},t\right) \tag{5.72}$$

where <.> is the expectation operation, and $P(\sigma_{ij},t)$ is the evolutionary probability density of the stress tensor $\sigma_{ij}$. Therefore performing the expectation operation on both sides of equation 5.70, the ensemble average form of the stochastic continuity equation reads:

$$\begin{aligned}
&\frac{\partial\left\langle \rho\left(\sigma_{ij}\left(x_t,t\right),t\right)\right\rangle}{\partial t} = -\frac{\partial}{\partial\sigma_{mn}}\Bigg[\Bigg\{\left\langle \eta_{mn}\left(\sigma_{mn}\left(x_t,t\right),D_{mnrs}\left(x_t\right),\varepsilon_{rs}\left(x_t,t\right)\right)\right\rangle \\
&-\int_0^t d\tau COV_0\Big[\eta_{mn}\left(\sigma_{mn}\left(x_t,t\right),D_{mnrs}\left(x_t\right),\varepsilon_{rs}\left(x_t,t\right)\right); \\
&\frac{\partial\eta_{ab}\left(\sigma_{ab}\left(x_{t-\tau},t-\tau\right),D_{abcd}\left(x_{t-\tau}\right),\varepsilon_{cd}\left(x_{t-\tau},t-\tau\right)\right)}{\partial\sigma_{ab}}\Big]\Bigg\}\left\langle \rho\left(\sigma_{ij}\left(x_t,t\right),t\right)\right\rangle\Bigg] \\
&+\frac{\partial}{\partial\sigma_{mn}}\Bigg[\Bigg\{\int_0^t d\tau COV_0\Big[\eta_{mn}\left(\sigma_{mn}\left(x_t,t\right),D_{mnrs}\left(x_t\right),\varepsilon_{rs}\left(x_t,t\right)\right); \\
&\eta_{ab}\left(\sigma_{ab}\left(x_{t-\tau},t-\tau\right),D_{abcd}\left(x_{t-\tau}\right),\varepsilon_{cd}\left(x_{t-\tau},t-\tau\right)\right)\Big]\Bigg\}\frac{\partial\left\langle \rho\left(\sigma_{ij}\left(x_t,t\right),t\right)\right\rangle}{\partial\sigma_{ab}}\Bigg]
\end{aligned} \tag{5.73}$$

Equation 5.73 is exact to second order ($\alpha^2\tau_c$) , with the *time ordered covariance function* $COV_0$ given by:

$$COV_0\left[\eta_{mn}\left(x,t_1\right),\eta_{ab}\left(x,t_2\right)\right] = \left\langle \eta_{mn}\left(x,t_1\right)\eta_{ab}\left(x,t_2\right)\right\rangle - \left\langle \eta_{mn}\left(x,t_1\right)\right\rangle\cdot\left\langle \eta_{ab}\left(x,t_2\right)\right\rangle \tag{5.74}$$

Substituting equation 5.72 into equation 5.74, and rearranging the terms of equation 5.73, the three-dimensional Eulerian-Lagrandian form of the Fokker-Plank-Kolmogorov equation (FPKE) is obtained:

$$\begin{aligned}\frac{\partial P\left(\sigma_{ij}\left(x_t,t\right),t\right)}{\partial t}&=\frac{\partial}{\partial\sigma_{mn}}\Bigg[\left\{\left\langle\eta_{mn}\left(\sigma_{mn}\left(x_t,t\right),D_{mnrs}\left(x_t\right),\varepsilon_{rs}\left(x_t,t\right)\right)\right\rangle\right.\\&+\int_0^t d\tau COV_0\Bigg[\frac{\partial\eta_{mn}\left(\sigma_{mn}\left(x_t,t\right),D_{mnrs}\left(x_t\right),\varepsilon_{rs}\left(x_t,t\right)\right)}{\partial\sigma_{ab}};\\&\left.\eta_{ab}\left(\sigma_{ab}\left(x_{t-\tau},t-\tau\right),D_{abcd}\left(x_{t-\tau}\right),\varepsilon_{cd}\left(x_{t-\tau},t-\tau\right)\right)\Bigg]\right\}P\left(\sigma_{ij}\left(x_t,t\right),t\right)\Bigg]\\&+\frac{\partial^2}{\partial\sigma_{mn}\partial\sigma_{ab}}\Bigg[\left\{\int_0^t d\tau COV_0\Big[\eta_{mn}\left(\sigma_{mn}\left(x_{t-\tau},t-\tau\right),D_{abcd}\left(x_{t-\tau}\right),\varepsilon_{cd}\left(x_{t-\tau},t-\tau\right)\right)\Big]\right\}P\left(\sigma_{ij}\left(x_t,t\right),t\right)\Bigg]\end{aligned}\tag{5.75}$$

Equation 5.75 is a second order linear *PDE* whose solution is the tensor-valued *pdf* of the stress tensor $\sigma_{ij}$.

### 5.2.8 Solution Algorithm for 3-D Development

The solution of the 3-D form of the FPKE can be obtained once more by using a numerical approximation. For the sake of practicality, the same central difference scheme used in section 5.2.2 is applied for the approximation of the time-dependent *pdf* of the stress tensor $\sigma_{ij}$. The 3-D form of the FPKE is therefore be written as:

$$\begin{aligned}\frac{\partial P^{(i)}}{\partial t}&=P^{(i-1)}\left(\frac{N_{mn}^{(2),i}}{\Delta\sigma_{mn}^2}+\frac{N_{mn}^{(1),i}}{\Delta\sigma_{mn}}-\frac{1}{\Delta\sigma_{mn}}\frac{\partial N_{mn}^{(2),i}}{\partial\sigma_{ab}}\right)-P^{(i)}\left(-\frac{\partial^2 N_{mn}^{(2),i}}{\partial\sigma_{mn}\partial\sigma_{ab}}+\frac{2N_{mn}^{(2),i}}{\Delta\sigma_{mn}^2}+\frac{\partial N_{mn}^{(1),i}}{\partial\sigma_{mn}}\right)\\&+P^{(i+1)}\left(\frac{N_{mn}^{(2),i}}{\Delta\sigma_{mn}^2}-\frac{N_{mn}^{(1),i}}{\Delta\sigma_{mn}}+\frac{1}{\Delta\sigma_{mn}}\frac{\partial N_{mn}^{(2),i}}{\partial\sigma_{ab}}\right)\end{aligned}\tag{5.76}$$

where $N^{(1)}{}_{mn}$ and $N^{(2)}{}_{mn}$ are the advective and diffusive tensors given by:

$$N_{mn}^{(1)} = \left\langle \eta_{mn}\left(\sigma_{mn}\left(x_t,t\right),D_{mnrs}\left(x_t\right),\varepsilon_{rs}\left(x_t,t\right)\right)\right\rangle + \int_0^t d\tau COV_0\left[\frac{\partial \eta_{mn}\left(\sigma_{mn}\left(x_t,t\right),D_{mnrs}\left(x_t\right),\varepsilon_{rs}\left(x_t,t\right)\right)}{\partial \sigma_{ab}};\right. \\ \left.\eta_{ab}\left(\sigma_{ab}\left(x_{t-\tau},t-\tau\right),D_{abcd}\left(x_{t-\tau}\right),\varepsilon_{cd}\left(x_{t-\tau},t-\tau\right)\right)\right] \tag{5.77-a}$$

$$N_{mn}^{(2)} = \int_0^t d\tau COV_0\left[\eta_{mn}\left(\sigma_{mn}\left(x_t,t\right),D_{mnrs}\left(x_t\right),\varepsilon_{rs}\left(x_t,t\right)\right);\eta_{ab}\left(\sigma_{ab}\left(x_{t-\tau},t-\tau\right),D_{abcd}\left(x_{t-\tau}\right),\varepsilon_{cd}\left(x_{t-\tau},t-\tau\right)\right)\right] \tag{5.77-b}$$

### 5.2.9 Three-dimensional probabilistic linear elastic constitutive law

In the following subsection, we shall apply the FPKE to a 3-D linear elastic constitutive rate equation. The latter is defined by:

$$\frac{d\sigma_{ij}}{dt} = L_{ijkl} : \frac{d\varepsilon_{kl}}{dt} \tag{5.78}$$

where $L_{ijkl}$ is the fourth order linear elastic tensor given by:

$$L_{ijkl} \equiv L^{el} = \lambda\left(\delta \otimes \delta\right) + 2G1^{(4s)} \tag{5.79}$$

and

$$\delta = \begin{bmatrix} 1 & 0 & 0 \\ 0 & 1 & 0 \\ 0 & 0 & 1 \end{bmatrix} \tag{5.80}$$

Given the Young's modulus $E$, and Poisson's ratio, $v$, the shear modulus, $G$, bulk modulus, $K$ and *Lame*'s constant $\lambda$ can be obtained:

$$G = \frac{E}{2\left(1+v\right)} \tag{5.81-a}$$

$$K = \frac{E}{3\left(1-2\nu\right)} \tag{5.81-b}$$

$$\lambda = K - \frac{2G}{3} \tag{5.81-c}$$

In the above definition, the shear modulus $G$ is again assumed to be random. Rewriting the right-hand side using the stochastic operator $\eta_{ij}$, the stochastic differential equation describing the evolution of the stress tensor $\sigma_{ij}$ reads:

$$\frac{d\sigma_{ij}}{dt} = \eta_{ij}\left(\sigma_{ij}, L_{ijkl}, \varepsilon_{kl}; x, t\right) \tag{5.82}$$

where $\eta_{ij}$ is given by:

$$\eta_{ij}\left(\sigma_{ij}, L_{ijkl}, \varepsilon_{kl}; x, t\right) = L_{ijkl} : \frac{d\varepsilon_{kl}}{dt} \tag{5.83}$$

Substituting $\eta_{ij}$ explicitly from equation 5.83, the advective and diffusive tensor can be computed at every time-step. The advective and diffusive coefficients have 9 components in a three-dimensional framework. These components can be computed in a straightforward manner using equation 5.77-a and 5.77-b. For deterministic strain rate, $d\varepsilon_{kl}/dt$ we have:

$$\begin{aligned} N_{ij}^{(1)} &= \left\langle L_{ijkl} : \frac{d\varepsilon_{kl}}{dt} \right\rangle = \left[ \left\langle L_{ijkl} \right\rangle : \frac{d\varepsilon_{kl}}{dt} \right] \\ &= \left[ \left\langle \lambda\left(\delta \otimes \delta\right) + 2G1^{(4s)} \right\rangle : \frac{d\varepsilon_{kl}}{dt} \right] \\ &= \left[ \lambda\left(\delta \otimes \delta\right) + 2\left\langle G \right\rangle 1^{(4s)} \right] : \frac{d\varepsilon_{kl}}{dt} \end{aligned} \tag{5.84}$$

$$N_{ij}^{(2)} = \int_0^t d\tau VAR\left[ L_{ijkl} : \frac{d\varepsilon_{kl}}{dt} \right]$$
$$= t\left[ \left\langle \left( L_{ijkl} : \frac{d\varepsilon_{kl}}{dt} \right)^2 \right\rangle - \left\langle L_{ijkl} : \frac{d\varepsilon_{kl}}{dt} \right\rangle^2 \right] \tag{5.85}$$

Fortunately, for the linear elastic constitutive model, only three cases need to be considered, since all the other combinations yield 0.

Case 1: i=j=k=l

$$L_{ijkl} = \frac{4G}{3} + K \tag{5.86-a}$$

Case 2: i=j∧k=l

$$L_{ijkl} = K - \frac{2G}{3} \tag{5.86-b}$$

Case 3: i=k∧j=l

$$L_{ijkl} = 2G \tag{5.87-c}$$

### 5.2.10 Numerical example for 3-D linear elastic behaviour

To validate the 3-D linear elastic constitutive model, an element is stretched in the *33* direction such that the deformation gradient *F* is given by:

$$F(t) = \begin{bmatrix} 1 & 0 & 0 \\ 0 & 1 & 0 \\ 0 & 0 & 1+\alpha(t) \end{bmatrix}, \ \dot{\alpha} = cons\tan t \tag{5-88}$$

The constitutive model is given by the following stress-strain relationship:

$$\sigma_{ij} = L_{ijkl} : \varepsilon_{kl} \tag{5-89}$$

where $L_{ijkl}$ is the fourth order elastic tensor, σ is the true or *Cauchy* stress tensor, and ε is the true strain tensor. The fourth order elastic tensor can be computed for given values of the Young's modulus *E*, and Poisson's ratio, *v* as shown in equation 5.79. Alternatively, $L_{ijkl}$ can be computed from the shear modulus, *G*, and the bulk modulus, *K*. Assuming a mean shear modulus, $<G> = 82{,}000MPa$, and a *COV* of *5%,* the uncertainty in the shear modulus can be propagated at the constitutive level using the FPKE. It should be mentioned that in theory, the method requires that the stress domain spans $[-\infty, +\infty]$, but for a much faster execution, the stress domain is limited to $[-200\ +200]MPa$. The domain boundaries were chosen after performing a deterministic stress-strain integration of the constitutive model.

An important part of constitutive rate equations is the objectivity of the stress tensor. Objective rates are used to keep the stress objective under rotation, as is the case when integrating stress within a hypo-elastic framework (simple shear). For such cases, the Hughes-Winget algorithm (Hughes and Winget, 1980) with the Jaumann rate can be used. A better objective rate for hypo-elastic constitutive models is the Logarithmic rate. For the Jaumann rate, the equation of the rotation tensor is given by:

$$\Lambda_{\Delta}^{HW} = \Lambda_{n+1}\Lambda_{n}^{T} \approx \left( I - \frac{1}{2} W_{n+\frac{1}{2}} \right)^{-1} \left( I + \frac{1}{2} W_{n+\frac{1}{2}} \right) \tag{5-90}$$

The objective stress update then reads:

$$\sigma_{n+1} = \Lambda_{\Delta}^{HW} \sigma_{n} \left( \Lambda_{\Delta}^{HW} \right)^{T} + L : D_{n+\frac{1}{2}} \tag{5-91}$$

where $D$, and $W$ are the symmetric and anti-symmetric part of the deformation gradient F. The solution is second order accurate. Assuming a constant increment $\dot{\alpha} = \Delta t/200$, and a time-step, $\Delta t = 5 \times 10^{-5} s$, the evolution of the mean stress tensor $\sigma_{ij}$ is calculated and compared to the deterministic solution shown in figure 5.11.

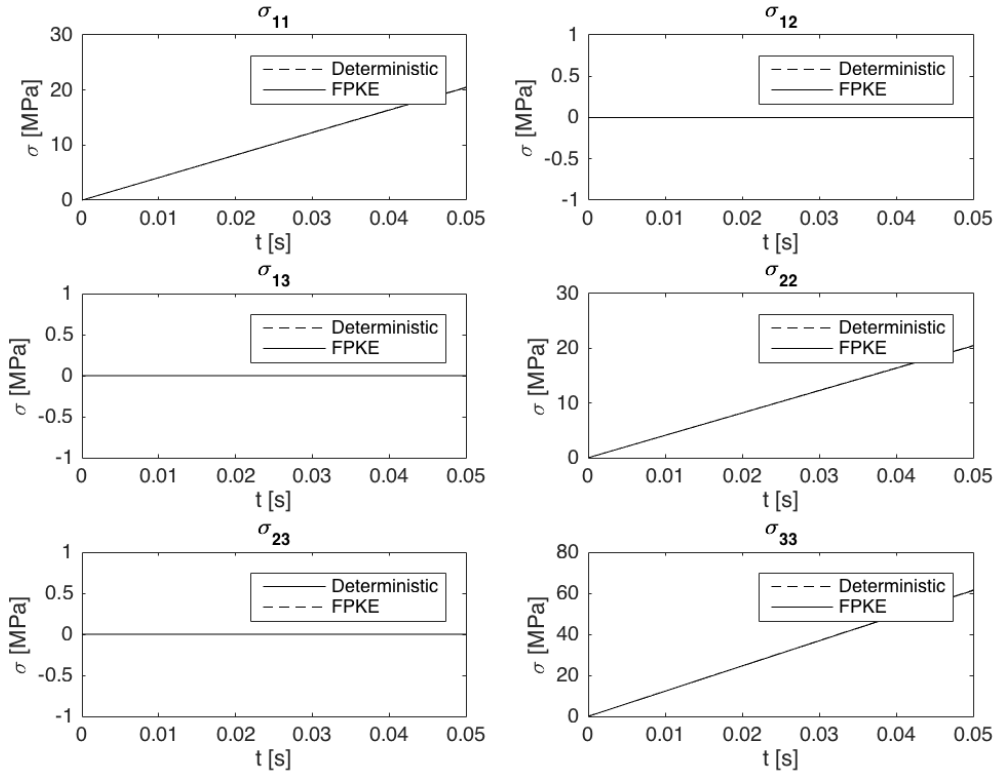


**Figure 5.11: Stress-time plots of 3-D linear elastic model for deterministic vs FPKE solution**

## 5.3 Summary

A methodology for introducing uncertainty at the constitutive scale is developed for a general non-linear constitutive rate equation with random material properties and random forcing. In this new method, the stochastic differential equation describing the evolution of stress of a material is transformed from a non-linear stochastic *PDE* to a linear second

order deterministic *PDE*. This linear second order *PDE* known as the Fokker-Plank-Equation is then solved using a numerical approximation to obtain the evolutionary probability density function of the stress. The advantage of the FPKE is that it linearizes the non-linear *PDE* of the constitutive rate equation. Moreover when compared to the *Monte Carlo* method, the application of the FPKE is computationally more efficient. The method however requires appropriate boundary conditions and that the initial condition be stated from a probabilistic point of view. This is accomplished through the use of the *Dirac delta* function. However, to avoid singularity at the initial time $t_0$, a Gaussian function must be used to approximate the *Dirac delta* function. This approximation introduces an error of the order of the Gaussian function's standard deviation. Therefore, to minimize this initial error, a very small standard deviation should be used. In doing so, special care should be taken in discretizing the stress domain. To capture this sharp value of the probability density at time $t_0$, the discretization of stress should be extremely fine. This can as a result increase the runtime of the numerical approximation. It is therefore up to the user to choose an adequate step size $\Delta\sigma$ such that the initial error is within reason, and the runtime remains faster than the *Monte Carlo* method. It should also be mentioned that that the time-step $\Delta t$ must change according to the step size $\Delta\sigma$ to ensure convergence. A convergence study is not carried out in this work, and is left to the reader to accomplish. The methodology is developed for one-dimensional and three-dimensional constitutive laws. Two examples are provided for the 1-D development. A linear shear elastic model and a linear elastic-plastic shear model are analyzed. Both examples show good agreement with the *Monte Carlo* simulation. The contours of the evolutionary *pdf* for both examples are provided. Finally, a 3-D linear elastic constitutive example is

provided in which the mean solution of the stress states is compared to the deterministic solution.

# CHAPTER 6.

# CONCLUSIONS AND FUTURE WORK

This thesis and the work it contains can be summed up by quoting Carl Freidrich Gauss who said, “I have had my result a long time: but I do not yet know how I am to arrive to them”. As per the introductory chapter, over the years, the statistical treatment of engineering problems has gained more popularity. This trend began as a result of increased computational power but also in an attempt to make risk-averse decisions. In the geotechnical engineering field especially, a probabilistic framework in which uncertainties can be accounted for accurately can prove valuable. The goal of this research was therefore to provide a framework in which better reliability-based designs were possible at no extra computational cost. In addition, a probabilistic description of soil-structure interactions could more realistically unveil the mechanics at play. To this end, the work undertaken by researchers over the past decades in the geotechnical engineering field, and the work done by mathematicians in statistics over the past century was dissected.

In Chapter 1, a background of the research is provided. The literature on descriptive techniques for estimating random properties and inferential techniques for propagating these random properties is reviewed. The motivation for the study and an outline of the thesis is also presented. The reader is exposed from the beginning to the various challenges faced by geotechnical engineers due to the inherent variability of soil

properties. This variability is categorized based on a scale of description. Two cases are presented: in the first case the soil properties are considered piece-wise homogeneous and in the second case the soil properties are considered spatially random. For spatially random properties, the notion of random fields is introduced. It is revealed that the major sources, which contribute to soil's heterogeneity, are measurement errors and transformation uncertainties. One issue, which arises as a result of these sources of uncertainty, is aliasing.

In Chapter 2, a review of numerous concepts ranging from the theory of probability and *stochastic processes*, to the theory of plasticity and continuum mechanics is provided. Starting with a review of *random variables*, a formal definition for a *probabilistic experiment*, and a *random variable* is given. From these definitions and more, the *probability density function* of a *random variable* is formulated. The mathematical operations involving the *probability density function* are also described in the same sub-section. The use of the *Dirac delta* function for the representation of deterministic parameters is shown and several examples of random variables with application in geotechnical engineering are given. Furthermore, the computation of statistical moments is exemplified. Thereafter, a review of *stochastic processes* is offered. A statistical ensemble is defined and operations related to the *pdf* of a *sp* is shown. Continuity, differentiability, and integrability of a *sp* are defined before finally introducing the Fokker-Plank-Kolmogorov equation. Chapter 2 concludes with a review of continuum mechanics and the theory of plasticity. The yield function, *hardening rule*, and *flow rule* are explained with the help of various idealizations of stress-strain curves.

The mathematical tools learned in Chapter 2 are utilized in Chapter 3 for the implementation of the Stochastic Finite Element method in the analysis of three different foundations. The derivation of the *Karhunen-Loeve* expansion in one-dimension is shown and its implementation in the representation of random fields is illustrated. Subsequently the *PCE* basis is constructed to represent the random response of each foundation. A different series representation (*PCE*) is used for the response since the covariance structure of the response is not known a priori. A solution algorithm for the one-dimensional analysis of piles using the SFEM is devised and the methodology is applied to three cases: 1) A uniformly loaded beam on an elastic foundation with free ends; 2) A laterally loaded pile on an elastic foundation that is fixed at one end; 3) An axially loaded pile on an elastic foundation that is fixed at one end. The results of each case were verified against a *Monte Carlo* simulation. The results showed good agreement with the *Monte Carlo* simulations. The performance of the SFEM, however, proved more computationally efficient with little disparity in its statistical moments compared to the *Monte Carlo* method. It is determined that the orientation of the load has an impact on the variance of the response. The rationale given is that for a slender object, as is the case for a pile, the action of a force collinear to the longer face of the object has a lesser impact on the response's variability. In other words, the random material properties at each node average out over longer spans. The convergence of the SFEM method is shown mathematically and inductively. A sensitivity analysis is also carried out and reveals that the soil stiffness is the most sensitive parameter for the first two cases. In the third case, it is revealed that axial rigidity of the column is the most sensitive parameter.

The variance function of each case is generated at the end of the chapter and reveals similarities with a pile's potential energy function.

The successful implementation of the SFEM for the one-dimensional analysis of foundations prompted the development of an analogous method, which would effectively integrate the representation of random fields with the analytical solution of a 2-parameter continuum pile. In Chapter 4, a pile having a rectangular cross-section and subjected to a horizontal force $F_a$ and a moment $M_a$ at its head is analyzed using a continuum approach. The pile is embedded in a multi-layered soil whose properties are modeled using a two-dimensional *Karhunen-Loeve* expansion. Because of the analytical nature of the solution, and due to the non-linearity that arises as a result of the spectral representation of the soil properties, the representation of the response using the *PCE* is dropped to give way to an iterative solution. Two numerical examples taken from Basu and Salgado (2008) are presented, and the results of the stochastic analysis of these two problems with spatially random soil Young's modulus and Poisson's ratio are compared with their respective deterministic solution. In the first example, a *25m* long pile embedded in four soil layers is laterally loaded with a force of magnitude *300kN*. Two observations are made: Firstly, a portion of the response, starting from the pile's base to some length $L_{det}$ converges to the deterministic response. This is referred in Chapter 4 as a deterministic length analogous to a pile's critical length. The second observation that is made is that the disparity between the mean and deterministic solution for the shear and bending moment of the pile is greater. This is attributed to transformation errors. A second example is presented in which a *40m* long pile embedded in four layers and laterally loaded with a

force of magnitude *3000kN* is analyzed. It is shown that the length of the pile significantly impacts the mean response. The disparity between the mean and the deterministic solution increases. It is therefore concluded that longer flexible piles have more unpredictable responses.

In Chapter 5, a new methodology, where uncertainties are propagated at the constitutive level, is investigated. This new methodology, the FPKE, transforms the stochastic continuity equation of a constitutive rate equation into a linear second-order PDE whose solution is the time-dependent probability density function of the stress tensor. The solution for a general one-dimensional constitutive rate equation is derived and two numerical examples are given. In the first numerical example, a linear shear elastic model is analyzed using the FPKE and the results are compared to *Monte Carlo* simulations. The results showed good agreement with the *Monte Carlo* simulations, and with the maximum difference in the two methods being at $t = 0$ due to the approximation of the initial conditions using a Gaussian function. Once more, the *Monte Carlo* simulation is outperformed by the candidate method in terms of computational efficiency and hence in terms of run-time. The evolution of the *pdf* of stress is shown to widen, suggesting that the resulting stress becomes more unpredictable over time. In the second numerical example, a linear elastic-plastic shear constitutive model is analyzed using the *Von Mises* yield criterion. A similar progression is observed within the elastic region. In the plastic region however, the variance appears to remain constant over time. This suggests that with plastic deformation, less uncertainty is introduced in the stress tensor. Finally, the methodology is extended to a 3-D framework, and a linear elastic constitutive model is

analyzed. For the 3-D example, the result of the FPKE is compared to the deterministic solution.

The problems tackled in this thesis are solved in order of difficulty with the aim of improving on existing methods and integrating them together to obtain a complete probabilistic framework for geotechnical problems. The development of the one-dimensional SFEM for foundation problems is used as a starting point to describe the statistical behaviour of a problem at a local scale, where spatial variability exists. A similar problem is tackled with the added difficulty of having a two-dimensional random field. We note that compared to the SFEM, the use of the *KL* expansion alone yields results in good agreement with the analytical deterministic solution. However, further validations are required for such problems. A *Monte Carlo* simulation was not conducted due to time constraints and should be performed to verify the accuracy of the mean response for the 2-parameter continuum pile. Moreover, the future work should verify the results of the proposed method with a two-dimensional SFEM of the 2-parameter continuum pile. As a final comparison, the responses of the proposed method for both the one-dimensional SFEM of piles and the stochastic analysis of a 2-parameter continuum pile should be checked against experimental results. Another aspect that is not explored in this thesis is the response for random fields having different covariance structures. Future work should investigate covariance structures to see how it compares with experimental results and the deterministic solution. A parametric study could also be carried out, where the effects of varying the correlation length of the input variables could be studied. The final layer of complexity added to the probabilistic framework

proposed in this thesis is the propagation of uncertainty at the constitutive level. This is accomplished using the FPKE and verified for two simple models: a linear shear elastic model, and a linear *elastic-plastic Von Mises* model. The FPKE remains to be tested on more complicated three-dimensional constitutive models of soil, such as the *Modified Cam-Clay* model. It is therefore a good candidate for future research. Finally it is my hope to integrate a general two-dimensional SFEM with the FPKE of a two-dimensional or three-dimensional plane-strain soil constitutive model. Such a complete framework has been used for one-dimensional problems with one-dimensional constitutive models such as the *Von Mises* and Drucker-Prager model by Kallol (Kallol, 2007), but has yet been implemented in a two-dimensional or even three-dimensional setting. There are many more avenues to explore such as the applicability of such methods for large deformation problems, which remain to be verified. The challenges are endless and the opportunities are bestowed upon all of us to seize.

# REFERENCES


1. Fenton, G. A. (1999). Estimation for Stochastic Soil Models. *Journal of Geotechnical and Geoenvironmental Engineering*.
2. Phoon, K., & Kulhawy, F. H. (1999). Characterization of geotechnical variability. *Canadian Geotechnical Journal,36*(4), 612-624. doi:10.1139/cgj-36-4-612
3. Kulhawy, F. H. (1992). On evaluation of static soil properties. In *Stability and performance of slopes and embankments 2*. New York, New York: American Society of Civil Engineers.
4. Sudret, B. (2014) Polynomial chaos expansions and stochastic finite element methods, In: Risk and Reliability in Geotechnical Engineering (Chap. 6), K.-K. Phoon & J. Ching (Eds.), pp. 265-300, CRC Press.
5. Jaksa, M. B., Brooker, P. I., & Kaggwa, W. S. (1997). Inaccuracies Associated with Estimating Random Measurement Errors. *Journal of Geotechnical and Geoenvironmental Engineering*.
6. Vanmarcke, E. (1983). *Random Fields*. Cambridge, Massachusetts: The MIT Press.
7. *CPT Data*. (n.d.). Retrieved from https://earthquake.usgs.gov/research/cpt/.
8. Vanmarcke, E.H. (1977). Probabilistic Modeling of Soil Profiles.
9. Beacher, G.B., & Ingra, T.S. (1981). STOCHASTIC FEM IN SETTLEMENT PREDICTIONS.

10. Rackwitz, R. (2001). Reliability analysis—a review and some perspectives. *Structural Safety,23*(4), 365-395. doi:10.1016/s0167-4730(02)00009-7
11. Popescu, R., Deodatis, G., & Nobahar, A. (2005). Effects of random heterogeneity of soil properties on bearing capacity. *Probabilistic Engineering Mechanics,20*(4), 324-341. doi:10.1016/j.probengmech.2005.06.003
12. Monte Carlo method. (2019, March 16). Retrieved from https://en.wikipedia.org/wiki/Monte_Carlo_method
13. Fenton, G. A., & Griffiths, D. V. (2002). Probabilistic Foundation Settlement on Spatially Random Soil. *Journal of Geotechnical and Geoenvironmental Engineering,128*(5), 381-390. doi:10.1061/(asce)1090-0241(2002)128:5(381)
14. Griffiths, D. V., Fenton, G. A., & Manoharan, N. (2002). Bearing Capacity of Rough Rigid Strip Footing on Cohesive Soil: Probabilistic Study. *Journal of Geotechnical and Geoenvironmental Engineering,128*(9), 743-755. doi:10.1061/(asce)1090-0241(2002)128:9(743)
15. Fenton, G. A., & Vanmarcke, E. H. (1990). Simulation of Random Fields via Local Average Subdivision. *Journal of Engineering Mechanics,116*(8), 1733-1749. doi:10.1061/(asce)0733-9399(1990)116:8(1733)
16. Sudret, B., & Kiureghian, A. D. (2000). *Stochastic finite element methods and reliability: A state-of-the-art report*. Berkeley: Dept. of Civil and Environmental Engineering, University of California.
17. DeGroot, D. J., & Baecher, G. B. (1993). Estimating autocovariance of in-situ soil properties. *Journal of Geotechnical Engineering,119*(1).

18. Phoon, K., S. Quek, Y. Chow, and S. Lee. (1990). Reliability analysis of pile settlements. J. Geotech. Eng. 116(11), 1717–1735.
19. Mellah, R., Auvinet, G, and Masrouri, F. (2000). Stochastic finite element method applied to non-linear analysis of embankments, Probabilistic Engineering Mechanics, Vol. 15, pp. 251-259.
20. Eloseily, K., Ayyub, B and Patev, R. (2002). Reliability assessment of pile groups in sands. Journal of Structural Engineering, ASCE, 128(10), 1346-53.
21. Ghanem, R. G., & Spanos, P. D. (1991). *Stochastic finite elements: A spectral approach*. New York, NY: Springer.
22. Sett, Kallol & Jeremić, Boris & Kavvas, M. (2007). Probabilistic elasto-plasticity: Solution and verification in 1D. Acta Geotechnica. 2. 211-220. 10.1007/s11440-007-0037-9.
23. Kavvas, M. (2003). Nonlinear Hydrologic Processes: Conservation Equations for Determining Their Means and Probability Distributions. Journal of Hydrologic Engineering - J HYDROL ENG. 8. 10.1061/(ASCE)1084-0699(2003)8:2(44).
24. Miskovic, Z. (n.d.). *Stochastic Processes in the Physical Sciences*. Lecture. In *Course Notes for Amath 777*. WATERLOO, Ontario: University of Waterloo.
25. Worswick, M. (n.d.). *Mechanics of Continua*. Lecture. In *Course Notes for ME 620*. WATERLOO, ON: University of Waterloo.
26. Butcher, C. (n.d.). *Computational Mechanics of Materials*. Lecture, Waterloo.
27. Maity, R. (n.d.). *Probability method in Civil Engineering*. Lecture. Retrieved from https://nptel.ac.in/

28. Central limit theorem. (2019, April 08). Retrieved from https://en.wikipedia.org/wiki/Central_limit_theorem
29. Warren, P., Ball, R., & Goldstrein, R. (n.d.). *Electron microscope image of cotton sewing thread* [Photograph]. Phys. Rec. Lett.
30. GIBBS, J. W. (2015). *ELEMENTARY PRINCIPLES IN STATISTICAL MECHANICS: Developed with special reference to the ... rational foundations of thermodynamics*. Place of publication not identified: FORGOTTEN Books.
31. Brown, Robert (1828). "A brief account of microscopical observations made in the months of June, July and August, 1827, on the particles contained in the pollen of plants; and on the general existence of active molecules in organic and inorganic bodies" (PDF). *Philosophical Magazine*. 4 (21): 161–173.
32. Einstein, A. (1905). Über die von der molekularkinetischen Theorie der Wärme geforderte Bewegung von in ruhenden Flüssigkeiten suspendierten Teilchen. *Annalen Der Physik,322*(8), 549-560. doi:10.1002/andp.19053220806
33. *Langevin, P. (1908). "Sur la théorie du mouvement brownien [On the Theory of Brownian Motion]". C. R. Acad. Sci. Paris. 146: 530–533.*; reviewed by D. S. Lemons & A. Gythiel: *Paul Langevin's 1908 paper "On the Theory of Brownian Motion" [...]*, Am. J. Phys. 65, 1079 (1997), doi:10.1119/1.18725
34. Basu, D. (2006). Analysis of Laterally Loaded Piles in Layered Soil (Unpublished doctoral dissertation). Purdue University
35. Davis, R. O. & Selvadurai, A. P. S. (1996). Elasticity and geomechanics. Cambridge Univ. Press.
36. Kampen, N. G. (2011). *Stochastic processes in physics and chemistry*. Place of

publication not identified: North Holland.

37. Gardiner, C. W. (2004). *Handbook of stochastic methods for physics, chemistry and the natural sciences*. Berlin: Springer.
38. Ditlevsen, O. and H. Madsen (1996). Structural reliability methods. J. Wiley and Sons, Chichester.
39. Ghanem, R. and V. Brzkala (1996). Stochastic finite element analysis of randomly layered media. J. Eng. Mech. 122 (4), 361–369.
40. Ghiocel, D. and R. Ghanem (2002). Stochastic finite element analysis of seismic soil structure interaction. J. Eng. Mech. 128, 66–77.
41. Clouteau, D. and R. Lafargue (2003). An iterative solver for stochastic soil-structure interaction. In P. Spanos and G. Deodatis (Eds.), Proc. 4th Int. Conf. on Comp. Stoch. Mech (CSM4), pp. 119–124. Corfu.
42. Sudret, B., M. Berveiller, and M. Lemaire (2004). A stochastic finite element method in linear mechanics. Comptes Rendus M´ecanique 332, 531–537.
43. Sudret, B., M. Berveiller, and M. Lemaire (2006). A stochastic finite element procedure for moment and reliability analysis. Eur. J. Comput. Mech. 15 (7-8), 825–866.
44. Berveiller, M., B. Sudret, and M. Lemaire (2006). Stochastic finite elements: a non intrusive approach by regression. Eur. J. Comput. Mech. 15 (1-3), 81–92.
45. Spanos, P. D., & Ghanem, R. (1989). Stochastic Finite Element Expansion for Random Media. Journal of Engineering Mechanics,115(5), 1035-1053. doi:10.1061/(asce)0733-9399(1989)115:5(1035)
46. Wiener, N. (1964). *Extrapolation, interpolation and smoothing of stationary time*

*series: With engineering applications*. Cambridge, Mass: M.I.T. Press.

47. Loève, M. M. (1977). *Probability theory I*. New York: Springer-Verlag.
48. L., V. T. (1968). Detection, estimation and modulation theory. New York: Wiley.
49. Alexanderian, A. (2013). On spectral methods for variance based sensitivity analysis. Probability Surveys,10(0), 51-68. doi:10.1214/13-ps219
50. Zienkiewicz, O. C., & Cheung, Y. K. (1977). *The finite element method in structural and continuum mechanics: Numerical solution of problems in structural and continuum mechanics*. 3rd ed.rev and enl. London: McGraw-Hill.
51. Hetenyi, M. (1946). Beams on Elastic Foundation. Place of publication not identified: University of Michigan Press.
52. Rahman, S. (2017). Wiener–Hermite polynomial expansion for multivariate Gaussian probability measures. *Journal of Mathematical Analysis and Applications,454*(1), 303-334. doi:10.1016/j.jmaa.2017.04.062
53. Winkler, E. (1867). Die Lehre von der Elasticitaet und Festigkeit
54. Vlasov, V. Z., & Leontev, U. N. (1966). *Beams, plates and shells on elastic foundations*. Jerusalem.
55. Vallabhan, C. V., & Das, Y. C. (1991). Modified Vlasov Model for Beams on Elastic Foundations. *Journal of Geotechnical Engineering,117*(6), 956-966. doi:10.1061/(asce)0733-9410(1991)117:6(956)
56. Griffiths, D. V., Paiboon, J., Huang, J., & Fenton, G. A. (2013). Reliability analysis of beams on random elastic foundations. *Geotechnique*, *63*(2), 180.
57. Haldar, S., & Basu, D. (2013). Response of Euler–Bernoulli beam on spatially random elastic soil. *Computers and Geotechnics,50*, 110-128.

doi:10.1016/j.compgeo.2013.01.002

58. Basu, D., & Salgado, R. (2008). Analysis of laterally loaded piles with rectangular cross sections embedded in layered soil. *International Journal for Numerical and Analytical Methods in Geomechanics,32*(7), 721-744. doi:10.1002/nag.639

59. Reddy, J. N. (2007). *Theory and analysis of elastic plates and shells*. Boca Raton: CRC Press.

60. Sett, K., Jeremić, B., & Kavvas, M. L. (2007). The role of nonlinear hardening/softening in probabilistic elasto-plasticity. *International Journal for Numerical and Analytical Methods in Geomechanics,31*(7), 953-975. doi:10.1002/nag.571

61. Fokker, A. D. (1914). Die mittlere Energie rotierender elektrischer Dipole im Strahlungsfeld. *Annalen Der Physik,348*(5), 810-820. doi:10.1002/andp.19143480507

62. Kavvas, M., & Karakas, A. (1996). On the stochastic theory of solute transport by unsteady and steady groundwater flow in heterogeneous aquifers. *Journal of Hydrology,179*(1-4), 321-351. doi:10.1016/0022-1694(95)02835-8

63. Kubo, R. (1963). Stochastic Liouville Equations. *Journal of Mathematical Physics,4*(2), 174-183. doi:10.1063/1.1703941

64. Lacasse, S., and Nadim, F. (1996). Uncertainties in characterizing soil properties. In Uncertainty in Geologic Environment: From Theory to Practice, Proceedings of Uncertainty ’96, July 31-August 3, 1996, Madison, Wisconsin, C. D. Shackelford and P. P. Nelson, Eds., vol. 1 of Geotechnical Special Publication No. 58, ASCE, New York, pp. 49–75.

65. Sudret, B. (2008). Global sensitivity analysis using polynomial chaos expansions. Reliab. Eng. Sys. Safety 93, 964–979.

66. MATLAB. (n.d.). Retrieved from https://www.mathworks.com/help/matlab/

67. Maple online Help. (n.d.). Retrieved from https://www.maplesoft.com/support/help/maple/view.aspx?path=UserManual/Contents

68. Lagrangian and Eulerian specification of the flow field. (2019, May 06). Retrieved from https://en.wikipedia.org/wiki/Lagrangian_and_Eulerian_specification_of_the_flow_field

69. Kallol, S. (2007). Probabilistic Elasto-Plasticity and its Application in Finite Element Simulations of Stochastic Elastic-Plastic boundary Value Problems (Unpublished doctoral dissertation). University of California, Davis

70. Undefined, U. U. (2012). Metal fatigue analysis handbook: Practical problem-solving techniques for computer-aided engineering(Y. Lee, M. E. Barkey, & H. Kang, Authors). Waltham, MA: Butterworth-Heinemann.

71. Kolmogoroff, A. (1931). Über die analytischen Methoden in der Wahrscheinlichkeitsrechnung. *Mathematische Annalen*, *104*(1), 415–458. doi: 10.1007/bf01457949

72. Planck, M. (1917). *Über einen Satz der statistischen Dynamik und seine Erweiterung in der Quantentheorie*. Berlin: Reimer.

73. Ghanem, R., & Spanos, P. D. (1990). Polynomial Chaos in Stochastic Finite Elements. *Journal of Applied Mechanics*, *57*(1), 197. doi: 10.1115/1.2888303

74. Hughes, T. J. R., & Winget, J. (1980). Finite rotation effects in numerical integration of rate constitutive equations arising in large-deformation analysis. *International Journal for Numerical Methods in Engineering*, *15*(12), 1862–1867. doi: 10.1002/nme.1620151210

# APPENDIX A

## The Stieltjes Integral

Let $\Delta$ be a partition of an interval [a,b] by a set $\{x_0, x_1,\ldots, x_n\}$ with $a=x_0 < x_1 < \ldots < x_n = b$ and let $||\Delta||=\max(x_1-x_0,\ldots, x_n - x_{n-1})$.

We define the Stieltjes integral of $\phi(x)$ with respect to F(x) from a to b as follows::

$$\int_a^b \phi(x).dF(x) = \lim_{\substack{||\Delta||\to 0 \\ n\to\infty}} \sum_{i=1}^{n} \phi(x_i^*).\left[F(x_i) - F(x_{i-1})\right] \qquad \text{(A1.1)}$$

where $x_{i-1} \le x^*_i \le x_i$ for I = 1, 2,…,n

Given the above the definition, we have the following corollaries:

- If $\phi(x)$ is continuous and F(x) is non-decreasing (or non-increasing) on [a,b] then the Stieltjes integral exist.
- If $\phi(x)$ and F'(x) are continuous on [a,b] then we have an equivalency with the Riemann integral:

$$\int_a^b \phi(x).dF(x) = \int_a^b \phi(x).F'(x)dx \quad (\leftarrow \text{Ordinary Riemann}) \qquad \text{(A1.2)}$$

- If F(x) is a step function with jumps $h_j$ at points $l_j$, $l_j \in [a,b]$ and $\phi(x)$ is continuous on [a,b] then we have:

$$\int_a^b \phi(x).dF(x) = \sum_j h_j.\phi(l_j) \qquad \text{(A1.3)}$$

Note that some properties of the Stieltjes integrals are analogous to those of Riemann integrals for example the integration by parts:

$$\int_a^b \phi(x)dF(x) = \phi(b).F(b) - \phi(a).F(a) - \int_a^b F(x).d\phi(x) \qquad \text{(A1.4)}$$

# APPENDIX B

## Derivation of FPKE: Ensemble average form of Kubo Stochastic Liouville Equation

The derivation of the FPKE for constitutive rate equations follows Kallol's derivation (2007), which was adapted from Kavvas and Karakas (Kavvas and Karakas, 1996) derivation of the same equation for hydrologic processes.

Starting with Kubo's stochastic Liouville equation, we have:

$$\frac{\partial \rho\left(\sigma\left(x,t\right),t\right)}{\partial t} = -\frac{\partial}{\partial \sigma}\eta\left[\sigma\left(x,t\right),D^{el}\left(x\right),q\left(x\right),r\left(x\right),\varepsilon\left(x,t\right)\right]\cdot\rho\left[\sigma\left(x,t\right),t\right] \quad \text{(A2.1)}$$

Rewriting the above equation in the operator form leads to the following equation:

$$\frac{\partial \rho}{\partial t} = \left(-\nabla\cdot\eta - \eta\cdot\nabla\right)\rho \quad \text{(A2.2)}$$

where $\nabla\cdot\eta$ is the divergence of $\eta$, and the above equation is a result of the product rule.

Let us now introduce a time-space varying sure operator, $A_0(\sigma(x,t),t)$ given by:

$$A_0\left(\sigma\left(x,t\right),t\right) = -\left\langle\eta\right\rangle\cdot\nabla - \nabla\cdot\left\langle\eta\right\rangle \quad \text{(A2.3)}$$

and a time-space non-stationary stochastic operator, $\alpha A_1(x,t)$ given by:

$$\alpha A_1\left(\sigma\left(x,t\right),t\right) = \left(-\eta + \left\langle\eta\right\rangle\right)\cdot\nabla + \nabla\cdot\left(-\eta + \left\langle\eta\right\rangle\right) \quad \text{(A2.4)}$$

where $\langle \bullet \rangle$ is the expectation (average) operator and α is the root mean square of the fluctuations of the random operator on the right-hand side of equation A2.1. Substituting equations A2.3 and A2.4 into A2.2 gives:

$$\frac{\partial \rho}{\partial t} = \left[ A_0\left(\sigma\left(x,t\right),t\right) + \alpha A_1\left(\sigma\left(x,t\right),t\right) \right] \rho \tag{A2.5}$$

The above equation represents the stochastic differential equation of a general constitutive rate equation in the operator form. Using Van Kampen's approach, we can obtain the deterministic operator differential equation for the mean of the phase density. This is achieved by making interaction substitution. However to do so, we must first define the chronologically ordered exponential, $\overleftarrow{\exp}$ of an integral equation.

$$\overleftarrow{\exp}\left( \int_0^t B\left(\tau\right) d\tau \right) = 1 + \sum_1^\infty \int_0^t d\tau_1 \int_0^{\tau_1} d\tau_2 \ldots \int_0^{\tau_{m-1}} d\tau_m B\left(\tau_1\right) B\left(\tau_2\right) \ldots B\left(\tau_m\right) \tag{A2.6}$$

where B(τ) is an arbitrary time-dependent function, and in the exponential series above, the arguments within each integral are ordered in time. Hence, we can rewrite the phase density as follows:

$$\rho\left(\sigma\left(x,t\right),t\right) = \overleftarrow{\exp}\left( \int_0^t A_0\left(\sigma\left(x,\tau\right),\tau\right) d\tau \right) \rho_1\left(\sigma\left(x,t\right)\right) \tag{A2.7}$$

Substituting equation xx.xx into yy.yy, the following equation is obtained:

$$\frac{d\rho_1\left(\sigma\left(x,t\right),t\right)}{dt} =$$
$$\left[ \overleftarrow{\exp}\left( \int_0^t A_0\left(\sigma\left(x,\tau\right)\tau\right) d\tau \right) \right]^{-1} \alpha A_1\left(\sigma\left(x,t\right),t\right) \overleftarrow{\exp}\left( \int_0^t A_0\left(\sigma\left(x,\tau\right),\tau\right) d\tau \right) \rho_1\left(\sigma\left(x,t\right),t\right) \tag{A2.8}$$

where the inverse in the above equation is simply:

$$\left[\overleftarrow{\exp}\left(\int_0^t A_0\left(\sigma\left(x,\tau\right),\tau\right)d\tau\right)\right]^{-1}=\overrightarrow{\exp}\left(-\int_0^t A_0\left(\sigma\left(x,\tau\right),\tau\right)d\tau\right) \tag{A2.9}$$

Equation A2.8 can be further simplified by representing the non-commutative operator inside the bracket using θ. Therefore equation A2.8 becomes:

$$\frac{d\rho_1\left(\sigma\left(x,t\right),t\right)}{dt}=\alpha\theta\left(\sigma\left(x,t\right),t\right)\rho_1\left(\sigma\left(x,t\right),t\right) \tag{A2.10}$$

In the literature, Van Kampen obtained the following ensemble average form for the stochastic continuity equation:

$$\frac{d\left\langle\rho_1\left(\sigma\left(x,t\right),t\right)\right\rangle}{dt}=$$
$$\left[\alpha\left\langle\theta\left(\sigma\left(x,t\right),t\right)\right\rangle+\alpha^2\int_0^t d\tau\left\langle\left\langle\left\langle\theta\left(\sigma\left(x,t\right),t\right)\cdot\theta\left(\sigma\left(x,t-\tau\right),t-\tau\right)\right\rangle\right\rangle\right\rangle\right]\left\langle\rho_1\left(\sigma\left(x,t\right),t\right)\right\rangle \tag{A2.11}$$

where $\left\langle\left\langle\left\langle\bullet\right\rangle\right\rangle\right\rangle$ is the time-ordered second cumulant. By comparing equation A2.8 to A2.10, θ can be expressed explicitly as follows:

$$\theta=\overleftarrow{\exp}\left(-\int_0^t A_0\left(\sigma\left(x,\tau\right),\tau\right)d\tau\right)A_1\left(\sigma\left(x,t\right),t\right)\overleftarrow{\exp}\left(\int_0^t A_0\left(\sigma\left(x,\tau\right),\tau\right)d\tau\right) \tag{A2.12}$$

Substituting equation A2.12 into A2.11 produces:

$$\frac{d}{dt}\left[\overrightarrow{\exp}\left(-\int_0^t A_0\left(\sigma\left(x,\tau\right),\tau\right)d\tau\right)\left\langle\rho\left(\sigma\left(x,t\right),t\right)\right\rangle\right]=$$
$$\left[\alpha\overrightarrow{\exp}\left(-\int_0^t A_0\left(\sigma\left(x,\tau\right),\tau\right)d\tau\right)\left\langle A_1\left(\sigma\left(x,t\right),t\right)\right\rangle\overleftarrow{\exp}\left(\int_0^t A_0\left(\sigma\left(x,\tau\right),\tau\right)d\tau\right)\right.$$
$$+\alpha^2\int_0^t ds\left\langle\left\langle\left\langle\overrightarrow{\exp}\left(-\int_0^t A_0\left(\sigma\left(x,\tau\right),\tau\right)d\tau\right)A_1\left(\sigma\left(x,t\right),t\right)\right.\right.\right. \tag{A2.13}$$
$$\overleftarrow{\exp}\left(\int_0^t A_0\left(\sigma\left(x,\tau\right),\tau\right)d\tau\right)\overrightarrow{\exp}\left(-\int_0^{t-s} A_0\left(\sigma\left(x,\tau\right),\tau\right)d\tau\right)$$
$$\left.\left.\left.A_1\left(\sigma\left(x,t-s\right),t-s\right)\overleftarrow{\exp}\left(\int_0^{t-s} A_0\left(\sigma\left(x,\tau\right),\tau\right)d\tau\right)\right\rangle\right\rangle\right\rangle\left.\right]\left\langle\rho_1\left(\sigma\left(x,t\right),t\right)\right\rangle$$

Working out the above and making use of the time-ordered exponential characteristics, equation A2.13 reduces to:

$$\frac{\partial\left\langle\rho\left(\sigma\left(x,t\right),t\right)\right\rangle}{\partial t}=A_0\left(\sigma\left(x,t\right),t\right)\left\langle\rho\left(\sigma\left(x,t\right),t\right)\right\rangle+\alpha^2\int_0^t ds\left\langle\left\langle\left\langle A_1\left(\sigma\left(x,t\right),t\right)\right.\right.\right.$$
$$\left.\left.\left.\overleftarrow{\exp}\left(\int_{t-s}^t A_0\left(\sigma\left(x,\tau\right),\tau\right)d\tau\right)A_1\left(\sigma\left(x,t-s\right),t-s\right)\right\rangle\right\rangle\right\rangle \tag{A2.14}$$
$$\overrightarrow{\exp}\left(-\int_{t-s}^t A_0\left(\sigma\left(x,\tau\right),\tau\right)d\tau\right)\left\langle\rho\left(\sigma\left(x,t\right),t\right)\right\rangle$$

We shall now focus on the last term of the right-hand side of equation A2.14. Substituting $A_0$ from equation A2.3 into the latter, we obtain:

$$\overrightarrow{\exp}\left(-\int_{t-s}^t A_0\left(\sigma\left(x,\tau\right),\tau\right)\right)\left\langle\rho\left(\sigma\left(x,t\right),t\right)\right\rangle=$$
$$\overrightarrow{\exp}\left(-\int_{t-s}^t d\tau\left[-\frac{\partial\left\langle\eta\left(\sigma\left(x,\tau\right),\tau\right)\right\rangle}{\partial\sigma}-\left\langle\eta\left(\sigma\left(x,\tau\right),\tau\right)\right\rangle\frac{\partial}{\partial\sigma}\right]\right)\left\langle\rho\left(\sigma\left(x,t\right),t\right)\right\rangle \tag{A2.15}$$

Recognizing that the time ordered exponential of two time dependent functions has the following property:

$$\begin{aligned}&\overrightarrow{\exp}\left(\int_0^t d\tau\left(Z(\tau)+Y(\tau)\right)\right)=\\&\overrightarrow{\exp}\left(\int_0^t d\tau\overrightarrow{\exp}\left[\int_0^t dsZ(s)\right]Y(\tau)\overleftarrow{\exp}\left[-\int_0^\tau dsZ(s)\right]\right)\overrightarrow{\exp}\left[\int_0^t d\tau Z(\tau)\right]\end{aligned} \tag{A2.16}$$

We can rewrite equation A2.15 using the above property:

$$\begin{aligned}&\overrightarrow{\exp}\left(-\int_{t-s}^t A_0\left(\sigma(x,\tau),\tau\right)\right)\left\langle\rho\left(\sigma(x,t),t\right)\right\rangle=\\&\overrightarrow{\exp}\left(\int_{t-s}^t d\tau\left\langle\eta\left(\sigma(x,\tau),\tau\right)\right\rangle\frac{\partial}{\partial\sigma}\right)\overrightarrow{\exp}\left(\int_{t-s}^t d\tau\frac{\partial\left\langle\eta\left(\sigma(x,\tau),\tau\right)\right\rangle}{\partial\sigma}\right)\left\langle\rho\left(\sigma(x,t),t\right)\right\rangle\end{aligned} \tag{A2.17}$$

Now shifting our focus to the non-stationary stochastic operator, $\alpha A_1(x,t)$ given in equation A2.4, one can write:

$$\alpha A_1\left(\sigma(x,t),t\right)=\frac{\partial\left\langle\eta\left(\sigma(x,t),t\right)\right\rangle-\eta\left(\sigma(x,t),t\right)}{\partial\sigma}+\left[\left\langle\eta\left(\sigma(x,t),t\right)\right\rangle-\eta\left(\sigma(x,t),t\right)\right]\frac{\partial}{\partial\sigma} \tag{A2.18}$$

Making use of the commutation and product properties of the Lie operator in equation A2.14, the following equation is obtained:

$$
\begin{aligned}
&\overleftarrow{\exp}\left(\int_{t-s}^{t} A_0\left(\sigma\left(x,\tau\right),\tau\right)d\tau\right)\alpha A_1\left(\sigma\left(x,t-s\right),t-s\right)\overrightarrow{\exp}\left(-\int_{t-s}^{t} A_0\left(\sigma\left(x,\tau\right),\tau\right)d\tau\right)\left\langle\rho\left(\sigma\left(x,t\right),t\right)\right\rangle\\
&=\left[\frac{\partial\left\langle\eta\left(\overleftarrow{\exp}\left[\sigma\left(x,t\right),t\right]x;t-s\right)\right\rangle-\eta\left(\overleftarrow{\exp}\left[\sigma\left(x,t\right),t\right]x;t-s\right)}{\partial\sigma}\right]\left\langle\rho\left(\sigma\left(x,t\right),t\right)\right\rangle\\
&+\left[\left\langle\eta\left(\overleftarrow{\exp}\left[\sigma\left(x,t\right),t\right]x;t-s\right)\right\rangle-\eta\left(\overleftarrow{\exp}\left[\sigma\left(x,t\right),t\right]x;t-s\right)\right]\\
&\overleftarrow{\exp}\left(-\int_{t-s}^{t} d\tau\frac{\partial\left\langle\eta\left(\sigma\left(x,\tau\right),\tau\right)\right\rangle}{\partial\sigma}\right)\left[\frac{\partial}{\partial\sigma}\overrightarrow{\exp}\left(\int_{t-s}^{t} d\tau\frac{\partial\eta\left(\sigma\left(x,\tau\right),\tau\right)}{\partial\sigma}\right)\right]\left\langle\rho\left(\sigma\left(x,t\right),t\right)\right\rangle\\
&+\left[\left\langle\eta\left(\overleftarrow{\exp}\left[\sigma\left(x,t\right),t\right]x;t-s\right)\right\rangle-\eta\left(\overleftarrow{\exp}\left[\sigma\left(x,t\right),t\right]x,t-s\right)\right]\frac{\left\langle\rho\left(\sigma\left(x,t\right),t\right)\right\rangle}{\partial\sigma}
\end{aligned}
\tag{A2.19}
$$

where,

$$
\overleftarrow{\exp}\left[\sigma\left(x,t\right),t\right]x=\overleftarrow{\exp}\left[-\int_{t-s}^{t} d\tau\left\langle\eta\left(\sigma\left(x,t\right),t\right)\right\rangle\frac{\partial}{\partial x}\right]x \tag{A2.20}
$$

Now focusing on the operand related to $\alpha A_1(\sigma(x,t),t)$ in the second additive term of equation A2.19, the following equation is obtained:

$$
\begin{aligned}
&\alpha^2\int_0^t ds\left\langle\left\langle\left\langle A_1\left(\sigma\left(x,t\right),t\right)\overleftarrow{\exp}\left(\int_{t-s}^{t} A_0\left(\sigma\left(x,\tau\right),\tau\right)d\tau\right)\right.\right.\right.\\
&\left.\left.\left.A_1\left(\sigma\left(x,t-s\right),t-s\right)\right\rangle\right\rangle\right\rangle\overrightarrow{\exp}\left(-\int_{t-s}^{t} A_0\left(\sigma\left(x,\tau\right),\tau\right)d\tau\right)\left\langle\rho\left(\sigma\left(x,t\right),t\right)\right\rangle\\
&=\int_0^t ds\left\langle\left\langle\left\langle\alpha A_1\left(\sigma\left(x,t\right),t\right)\overleftarrow{\exp}\left(\int_{t-s}^{t} A_0\left(\sigma\left(x,\tau\right),\tau\right)d\tau\right)\right.\right.\right.\\
&\left.\left.\left.\alpha A_1\left(\sigma\left(x,t-s\right),t-s\right)\right\rangle\right\rangle\right\rangle\overrightarrow{\exp}\left(-\int_{t-s}^{t} A_0\left(\sigma\left(x,\tau\right),\tau\right)d\tau\right)\left\langle\rho\left(\sigma\left(x,t\right),t\right)\right\rangle
\end{aligned}
\tag{A2.21}
$$

Performing the inner products within the integral on the right-hand side of the above equation produces:

$$
\begin{aligned}
&= \int_0^t ds \left\{ COV_0 \left[ \frac{\partial \eta\left(\sigma\left(x,t\right),t\right)}{\partial \sigma}; \frac{\partial \eta\left(\overleftarrow{\exp}\left[\sigma\left(x,t\right),t\right]x;t-s\right)}{\partial \sigma} \right] \right. \\
&\left. + COV_0 \left[ \eta\left(\sigma\left(x,t\right),t\right); \frac{\partial^2 \eta\left(\overleftarrow{\exp}\left[\sigma\left(x,t\right),t\right]x;t-s\right)}{\partial \sigma^2} \right] \right\} \left\langle \rho\left(\sigma\left(x,t\right),t\right) \right\rangle \\
&+ \int_0^t ds \left\{ COV_0 \left[ \frac{\partial \eta\left(\sigma\left(x,t\right),t\right)}{\partial \sigma}; \eta\left(\overleftarrow{\exp}\left[\sigma\left(x,t\right),t\right]x;t-s\right) \right] \right. \\
&\left. + COV_0 \left[ \eta\left(\sigma\left(x,t\right),t\right); \frac{\partial \eta\left(\overleftarrow{\exp}\left[\sigma\left(x,t\right),t\right]x;t-s\right)}{\partial \sigma} \right] \right\} \cdot \\
&\overleftarrow{\exp}\left( -\int_{t-s}^t d\tau \frac{\partial \left\langle \eta\left(\sigma\left(x,\tau\right),\tau\right) \right\rangle}{\partial \sigma} \right) \left( \frac{\partial}{\partial \sigma} \overrightarrow{\exp}\left[ \int_{t-s}^t d\tau \frac{\partial \left\langle \eta\left(\sigma\left(x,\tau\right),\tau\right) \right\rangle}{\partial \sigma} \right] \right) \left\langle \rho\left(\sigma\left(x,t\right),t\right) \right\rangle \\
&+ \int_0^t COV_0 \left[ \eta\left(\sigma\left(x,t\right),t\right); \eta\left(\overleftarrow{\exp}\left[\sigma\left(x,t\right),t\right]x;t-s\right) \right] \cdot \\
&\left\{ \left( \frac{\partial}{\partial \sigma} \overleftarrow{\exp}\left[ -\int_{t-s}^t d\tau \frac{\partial \left\langle \eta\left(\sigma\left(x,\tau\right),\tau\right) \right\rangle}{\partial \sigma} \right] \right) \left( \frac{\partial}{\partial \sigma} \overrightarrow{\exp}\left[ \int_{t-s}^t d\tau \frac{\partial \left\langle \eta\left(\sigma\left(x,\tau\right),\tau\right) \right\rangle}{\partial \sigma} \right] \right) \right. \\
&\left. + \overleftarrow{\exp}\left( -\int_{t-s}^t d\tau \frac{\partial \left\langle \eta\left(\sigma\left(x,\tau\right),\tau\right) \right\rangle}{\partial \sigma} \right) \left( \frac{\partial^2}{\partial \sigma^2} \overrightarrow{\exp}\left[ \int_{t-s}^t d\tau \frac{\partial \left\langle \eta\left(\sigma\left(x,\tau\right),\tau\right) \right\rangle}{\partial \sigma} \right] \right) \right\} \left\langle \rho\left(\sigma\left(x,t\right),t\right) \right\rangle \\
&+ \int_0^t ds \left\{ COV_0 \left[ \frac{\partial \eta\left(\sigma\left(x,t\right),t\right)}{\partial \sigma}; \eta\left(\overleftarrow{\exp}\left[\sigma\left(x,t\right),t\right]x;t-s\right) \right] \right. \\
&\left. + COV_0 \left[ \eta\left(\sigma\left(x,t\right),t\right); \frac{\partial \eta\left(\overleftarrow{\exp}\left[\sigma\left(x,t\right),t\right]x;t-s\right)}{\partial \sigma} \right] \right\} \frac{\partial \left\langle \rho\left(\sigma\left(x,t\right),t\right) \right\rangle}{\partial \sigma} \\
&+ \int_0^t ds COV_0 \left[ \eta\left(\sigma\left(x,t\right),t\right); \frac{\partial \eta\left(\overleftarrow{\exp}\left[\sigma\left(x,t\right),t\right]x;t-s\right)}{\partial \sigma} \right] \frac{\partial \left\langle \rho\left(\sigma\left(x,t\right),t\right) \right\rangle}{\partial \sigma} \\
&+ \int_0^t ds COV_0 \left[ \eta\left(\sigma\left(x,t\right),t\right); \eta\left(\overleftarrow{\exp}\left[\sigma\left(x,t\right),t\right]x,t-s\right) \right] \cdot \\
&\overleftarrow{\exp}\left( -\int_{t-s}^t d\tau \frac{\partial \sigma \left\langle \eta\left(\sigma\left(x,\tau\right),\tau\right) \right\rangle}{\partial \sigma} \right) \overrightarrow{\exp}\left( \int_{t-s}^t d\tau \frac{\partial \sigma \left\langle \eta\left(\sigma\left(x,\tau\right),\tau\right) \right\rangle}{\partial \sigma} \right) \frac{\partial \left\langle \rho\left(\sigma\left(x,t\right),t\right) \right\rangle}{\partial \sigma} \\
&+ \int_0^t ds COV_0 \left[ \eta\left(\sigma\left(x,t\right),t\right); \eta\left(\overleftarrow{\exp}\left[\sigma\left(x,t\right),t\right]x;t-s\right) \right] \frac{\partial^2 \left\langle \rho\left(\sigma\left(x,t\right),t\right) \right\rangle}{\partial \sigma^2}
\end{aligned}
\tag{A2.22}
$$

In general, the value of the root mean square, α is very small (α<<1). We can therefore neglect higher order terms whose magnitude is of the order of $\alpha^2\tau_c$, where $\tau_c$ is the correlation length of the stochastic operator $A_1(\sigma(x,t),t)$. Furthermore, the first additive term on the right-hand side of equation A.2.21 can be written as follows:

$$A_0\left(\sigma\left(x,t\right),t\right)\left\langle \rho\left(x,t\right),t\right\rangle = -\frac{\partial\left\langle \eta\left(\sigma\left(x,t\right),t\right)\right\rangle\left\langle \rho\left(\sigma\left(x,t\right),t\right)\right\rangle}{\partial\sigma} \tag{A2.23}$$

Eliminating higher order terms found in the second, and third integral, along with arguments of the sixth integral of equation A2.22 and substituting the additive term given in equation A2.23, we finally obtain the deterministic PDE representing the ensemble average of the stochastic continuity equation for a general constitutive rate equation.

$$\frac{\partial\left\langle \rho\left(\sigma\left(x,t\right),t\right)\right\rangle}{\partial t} =$$
$$\frac{\partial}{\partial\sigma}\left\{\left[\left\langle \eta\left(\sigma\left(x,t\right),t\right)\right\rangle + \int_0^t COV_0\left[\eta\left(\sigma\left(x,t\right),t\right);\frac{\partial\eta\left(\sigma\left(x,t-\tau\right),t-\tau\right)}{\partial\sigma}\right]\right]\left\langle \rho\left(\sigma\left(x,t\right),t\right)\right\rangle\right\}$$
$$+\frac{\partial}{\partial\sigma}\left\{\left[\int_{00}^{t} d\tau COV_0\left[\eta\left(\sigma\left(x,t\right),t\right);\eta\left(\sigma\left(x,t-\tau\right),t-\tau\right)\right]\right]\frac{\partial\left\langle \rho\left(\sigma\left(x,t\right),t\right)\right\rangle}{\partial\sigma}\right\}$$

(A2.24)